NASA CONTRACTOR REPORT

NASA CR-2793

COMPARISON OF DYNAMIC STALL PHENOMENA FOR PITCHING AND VERTICAL TRANSLATION MOTIONS

T. Fukushima and L. U. Dadone

Prepared by
BOEING VERTOL COMPANY
Philadelphia, Pa. 19142
for Langley Research Center

NATIONAL AERONAUTICS AND SPACE ADMINISTRATION • WASHINGTON, D. C. • JULY 1977

1. Report No.	2. Government Accession No.	3. Recipient's Catalog No.
NASA CR-2793		

4. Title and Subtitle	5. Report Date
COMPARISON OF DYNAMIC STALL PHENOMENA FOR PITCHING AND VERTICAL TRANSLATION MOTIONS	July 1977
	6. Performing Organization Code

7. Author(s)	8. Performing Organization Report No.
T. Fukushima and L. U. Dadone	D238-10007-1
	10. Work Unit No.
	505-10-21-01

9. Performing Organization Name and Address	11. Contract or Grant No.
Boeing Vertol Company Boeing Center P. O. Box 16858 Philadelphia, PA 19142	NAS1-14056
	13. Type of Report and Period Covered
	Contractor Report

12. Sponsoring Agency Name and Address	14. Sponsoring Agency Code
National Aeronautics & Space Administration Washington, DC 20546	

15. Supplementary Notes

The contract research effort which has led to the results in this report was financially supported by USAAMRDL (Langley Directorate).
Langley Technical Monitor: Warren H. Young, Jr. Final report

16. Abstract

Test data for vertical translation motions of the V0012 and V23010-1.58 airfoils have been compared with force pitch and oscillation data to determine qualitative differences in dynamic stall behavior. Chordwise differential pressure variations were examined in detail for the test conditions displaying dynamic stall. The comparison revealed a number of differences both in the onset of stall and in the progression of separation as a function of the type of motion. The evidence of secondary stall events following the recovery from initial stall were found to be dependent on the type of motion, but additional data will be needed to incorporate vertical translation effects into the empirical approximation of dynamic stall.

17. Key Words (Suggested by Author(s))	18. Distribution Statement
Airfoils Rotors Unsteady aerodynamics	Unclassified - Unlimited Subject Category 02

19. Security Classif. (of this report)	20. Security Classif. (of this page)	21. No. of Pages	22. Price*
Unclassified	Unclassified	183	$7.50

*For sale by the National Technical Information Service, Springfield, Virginia 22161

COMPARISON OF DYNAMIC STALL PHENOMENA FOR PITCHING AND VERTICAL TRANSLATION MOTIONS

By

T. Fukushima
L. U. Dadone

Boeing Vertol Company

SUMMARY

All comparable dynamic stall data for vertical translation and forced pitch oscillation of the V0012 and V23010-1.58 airfoils, acquired in a previous wind tunnel investigation[1], have been reconstituted from tabulated harmonic coefficients. The reconstituted data, in the form of chordwise differential pressure coefficients, ΔC_p, and integrated normal force and pitching moment coefficients, were plotted against reference angle (time) and airfoil model position at various reference angles. Pitch and translation conditions were matched as closely as possible for comparison.

Stall is presently defined as an event characterized by a large increase in nose-down pitching moments and a reduction in normal force coefficients as the angle of attack is increased. Pitching moment stall generally precedes normal force (or lift) stall. Other events, such as "intermittent turbulent separation" which in themselves do not significantly alter the free stream flow, are not classified as stall, although such events initiate the stall at the leading edge as pointed out by McCroskey, et al[2]. The comparison showed differences in the onset of stall as a function of the type of motion particularly for the progression in the collapse of leading edge pressures. Differences in the chordwise progression of separation were also evident from the pressure distributions.

No apparent differences in the recovery from stall were observed either in the normal force and pitching moment coefficients or in the chordwise pressure distributions. Little evidence was found of secondary stall events following the recovery from the initial stall for both modes of oscillation.

A set of dynamic stall parameters, "gamma functions", was calculated from the vertical translation data. Such parameters were found to be different from the values derived for the pitch data. Dynamic C_n and C_m loops for both pitch and translation motions were synthesized with existing empirical methods derived from the pitch data. The synthesized loops for the two modes were different but both compared poorly with test data. The existing

equivalent angle of attack approach should be used until additional data becomes available to provide the basis for an analytical representation of the dynamic stall for vertical translation motions.

INTRODUCTION

Several series of tests of airfoils undergoing dynamic pitch motions have been carried out in two-dimensional wind tunnels. The resulting data have been applied to helicopter rotor analyses by methods such as the semi-empirical curve fitting of lift and moment coefficients or by the synthesis of characteristics from quasi-steady data by means of stall delay parameters derived from dynamic stall data.

One test was run with airfoils undergoing vertical translation (plunging) as well as pitching motions (reference 1), but the data was not reduced to a form suitable for direct comparison of the two motions or for application to a rotor analysis. Although a helicopter rotor blade experiences larger excursions in angle of attack due to vertical translation than due to pitching as a result of blade flapping and flap bending motions, no effort has been made to apply any vertical translation data to a rotor analysis. Rather, the dynamic stall behavior has been approximated first by reducing all motions to equivalent angle of attack excursions and then by utilizing forced pitch oscillation data to identify and approximate stall.

This study was undertaken to determine whether there are significant differences between the dynamic stall behavior of pitching and translating airfoils. Specifically, the objectives were to delineate differences in

(1) the progression of changes in chordwise pressure distributions, particularly at the leading and trailing edges, and in the progression of the separation along the chord.

(2) the onset of stall and stall recovery.

(3) The dependence on the Mach number, reduced frequency k, and the mean angle of attack, α_o.

(4) The stall delay parameter, "gamma function", and in the synthesis of oscillating airfoil data from quasi-steady data as presently carried out in rotor performance and loads programs.

SYMBOLS AND ABBREVIATIONS

c airfoil chord, m

ΔC_p differential pressure coefficient - $(C_{p\ lower} - C_{p\ upper})$

C_n	airfoil normal force coefficient
$C_{n_{max}}$	maximum value of C_n attained during a cycle of oscillation
f_D	drive frequency of airfoil motion in pitch or translation oscillation, Hz
h	instantaneous translation position, semichords
$\dot{h}$	velocity of vertical translation, dh/dt
Δh	magnitude of forced translation, semichords
k	reduced frequency parameter, $\frac{\pi fc}{V}$
M	Mach number
V	freestream velocity, m/sec
x	airfoil chordwise location measured from the leading edge, m
y	airfoil surface location measured perpendicular to the chordline, m
α	angle of attack (also referred to as "instantaneous" angle of attack), deg
$\dot{\alpha}$	rate of change of angle of attack with time, $d\alpha/dt$
α_o	mean angle of attack, deg
$\Delta\alpha$	magnitude of the forced pitching motion, deg
α_{STALL}	angle of attack corresponding to $C_{n_{max}}$, deg
γ	stall delay function ("gamma function")
θ	pitch and translation motion reference angle, deg
$\dot{\theta}$	rate of change with time of the reference angle, $d\theta/dt$
α_{DS}	angle of attack at which dynamic stall occurs, for either the normal force or the pitching moment (figure 17), rad
$\Delta\alpha_{EQ}$	equivalent amplitude of pitching motion for translation, deg
ΔC_n	increment in normal force coefficients

TP test point identification number

p pressure, Pa

ρ density, kg/m^3

TECHNICAL DISCUSSION

The two-dimensional tests of the V0012 and V23010-1.58 airfoil oscillating near and through stall, reference 1, were conducted for both forced pitch and vertical translation motions. The forced pitch oscillations were about the quarter chord. The contour coordinates of these airfoils are presented in Table II. Test and data reduction methods are fully described in reference 1; however, a brief summary of pertinent points will be presented.

The primary aerodynamic data obtained were chordwise differential pressures. From on-line magnetic tape records five to ten consecutive cycles of data were digitized for each test condition after examining the stripouts of the tapes to verify that all pressures and tunnel information (1/rev, frequency, tunnel conditions) had been properly recorded. Each group of digitized data were averaged and each averaged cycle was then harmonically analyzed.

The airfoil coefficient C_n and C_m were obtained by integrating the chordwise pressures reconstituted from digitized and harmonically analyzed data. The calculated C_n and C_m values were then also harmonically analyzed to obtain the corresponding harmonic coefficients. All harmonic coefficients and phase angles through the ninth harmonic are available in reference 1.

The reconstitution of the data for this study was carried out on a computer. The data points for pitch and translation presented in this report were chosen on the basis of the best match possible of test parameters. Data from the selected test points were plotted as follows:

(1) ΔC_p vs reference angle θ for all available pressure transducers

(2) ΔC_p vs chordwise station at reference angles from 0° to 360° at 20° increments

(3) C_n vs reference angle θ

C_m vs reference angle θ

(4) C_n vs net angle of attack

C_m vs net angle of attack

The variation in reference angle θ is equivalent to a time variation. The airfoil motions in the test can be expressed as:

$$\alpha = \alpha_o + \Delta\alpha \sin \theta \quad \text{(pitching)}$$

$$h = - \Delta h \sin \theta \quad \text{(translation)}$$

The net (or instantaneous) angle of attack was not a primary parameter during the vertical translation tests. Net angle of attack values have been calculated from the velocity of translation as derived from the expression for vertical displacement given above. Comparison of angles of attack between pitch and translation are therefore not exact and the mean angles are also not exactly matched.

The synthesis of dynamic stall data from the quasi-steady airfoil characteristics for performance and loads predictions has been carried out by the "gamma function" method developed by Gross and Harris[3], and incorporated into a number of rotor analysis programs, e.g., reference 4. This method has also been incorporated in the Rotorcraft Flight Simulation Program C-81 (AGAJ71), reference 5, version by Gormont, reference 6. Another technique for synthesizing unsteady aerodynamic data is presented by Bielawa in reference 7.

The synthesis method discussed in this report makes use of quasi-steady airfoil data up to a Mach number of 1.0 and it requires the generation of stall delay parameters, "gamma functions". Reference 3 describes the method by which the "gamma functions" have been generated from forced pitch oscillation data. The "gamma function" approximation has been applied to rotor analysis methods in which the angle of attack along a rotor blade results from blade pitch variations in the downwash and blade flapping motions. The underlying assumption of these methods has been that the effect of all blade motions could be adequately represented by an equivalent angle of attack variation. However, since the largest portion of the angle of attack changes result from blade flapping, both rigid and elastic, if the dynamic stall behavior in translation were significantly different from the behavior in pitch oscillation, the present rotor analysis methodology would not adequately account for the aerodynamic forces.

The data for comparable pitching and translation test conditions will be discussed in the following sequence:

1) Chordwise pressure distributions, particularly at the leading edge and trailing edge, and the progression of the loss in pressure and of locally separated flow along the chord; i.e., the mechanism for the onset of stall and stall recovery.

2) Differences in the dynamic stall behavior of the normal force and pitching moment coefficients C_n and C_m.

3) Dependence of the dynamic stall and reattachment on the mean angle of attack α_o, Mach number M, and the reduced frequency, k.

4) Variation of the dynamic stall delay parameter, γ.

The oscillating airfoil data analyzed for this study have been reconstituted from the harmonic coefficients tabulated in reference 1, using the 0th to 9th harmonics.

Although the chordwise load distributions have been reconstituted in a similar manner, the evaluation of chordwise pressure variations to identify specific stall events is limited by the fact that absolute pressure measurements were not taken, and only differential pressures between the upper and lower surfaces are available, so that any event occurring on the upper surface cannot be separated from whatever is taking place on the lower surface. However, the chordwise propagation of pressure waves at low free-stream velocities has been shown to be primarily an upper surface phenomena by Carta, reference 8, so that differential pressure measurements may be sufficient, as long as it is remembered that the breakdown of the leading edge suction pressure indicated by the differential pressure may be affected by the chordwise movement of the stagnation point. For leading edge pressure measurements absolute gages would have been preferable.

Initially, a total of 48 test points in pitch oscillation and 48 in vertical translation oscillation were evaluated to assess their suitability for this study. These evaluations included close matching of test conditions and the availability of chordwise pressure data. Of these 96 test points, 13 pairs of test points were finally selected for detailed analysis. The test points selected and the principal test parameters are shown in Table I.

CHORDWISE PRESSURE DISTRIBUTIONS

The pressures on the two airfoils were measured by means of differential pressure transducers. The chordwise locations of the pressure ports varied slightly from model to model; in all, four models were used for these tests as pitching and vertical translation required a different test setup.

Significant variations in chordwise pressures are evident between pitch and translation, as will be discussed in the following sections. The difference in chordwise loading between the V0012 and the V23010-1.58 airfoils is also a result of camber (the

V23010-1.58 airfoil was developed from the V0012 by the addition of a drooped nose). For a given angle of attack at quasi-steady conditions the leading edge pressures for the two airfoils differ as shown in figure 1. Both airfoils are stalled at the conditions shown, however, at comparable lift levels, the V0012 airfoil displays a much sharper leading edge suction peak than the V23010-1.58.

Leading Edge Pressures

A comparison of the variation with time (reference angle θ) of the surface pressures shows that for the V23010-1.58 airfoil the loss in leading edge suction is more pronounced in pitch oscillation than for the vertical translation motions, figures 2 and 3 . The leading edge pressures up to $x/c = 0.10$ are sustained to high levels in translation while, by comparison, the pressure at $x/c = 0.10$ in pitch is significantly reduced.

This trend is less pronounced for the V0012 airfoil, figures 4 and 5. The decrease in leading edge suction during translation is more evident since pressure at $x/c = 0.025$ is available, however, figure 1 shows that compared to the V23010-1.58, the leading edge suction for V0012 is significantly lower, and the reduction in leading edge pressures as a function of the type of motion is also less pronounced.

Separation Phenomena

The chordwise progression of the pressure wave following the collapse of leading edge pressures is different for pitch and translation oscillations. The comparison of test points 4041.2 (translation) and 1156.1 (pitch) for the V23010-1.58 airfoil, figures 2 and 3 respectively, shows a possible laminar separation bubble in translation ($\theta = 120°$) and not in pitch, but the breakdown in suction pressures forward of $x/c = 0.1$ is more severe in pitch.

The V0012 airfoil in vertical translation, figures 4 and 5, displays a loss in leading suction and separation bubbles ($\theta = 160°$) similar to the ones observed on the V23010-1.58. The large loss in suction at $x/c = 0.025$ between 140° to 200° observed for the translation data, figure 4b, cannot be verified in pitch because of an instrumentation failure at the $x/c = 0.025$ station for the latter.

Trailing Edge Pressure

A review of the trailing edge pressures for the V23010-1.58 and V0012 airfoils did not show large differences which could be attributed to the change from pitch to translation motions. In examining the separation phenomena which occur at the trailing edge of the V0012 and V23010-1.58 airfoils, it should be remembered that both are front loaded sections for which stall is generally

due to separation at the leading edge. McCroskey, reference 2, has shown that the stall is precipitated by the rapid growth of a turbulent flow reversal region in the flow adjacent to the trailing edge and was measured by hot wire probes.

The pressures over the aft 50% of chord of V23010-1.58 airfoil reach a lower level in pitch than in translation, as shown in figures 2a and 3a. Such a trend was not observed on the V0012 airfoil, figures 4a and 5a.

Stall Delay Effects on C_n and C_m

For both airfoils, the rate of decay of the normal force coefficient C_n after $C_{n_{MAX}}$ (i.e., $dC_n/d\theta = 0.0$) has been attained is greater in translation than in pitch oscillation. However, the rate of change in C_n, $dC_n/d\theta > 0.0$, when approaching $C_{n_{MAX}}$ is larger for the pitch oscillation motion, as schematically illustrated below by superimposing at θ_{STALL} two typical C_n time histories.

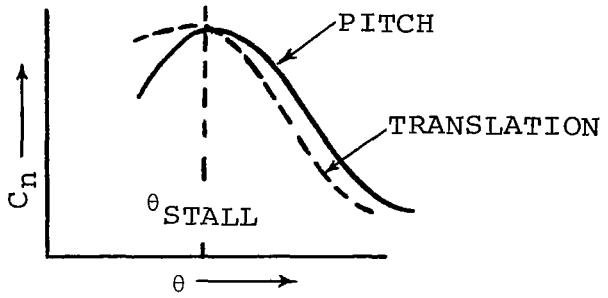

The net loss in C_n, ΔC_n (peak to peak), is substantially the same for pitch or translation independently of differences in the development of stall. The differences in stall behavior can be best appreciated when the normal force and pitching moment coefficients are plotted against the angle of attack, (the equivalent angle of attack,

$$\alpha = \alpha_o - \tan^{-1} \frac{c\Delta h\ \theta\ \cos\ \theta}{2V}, \text{ in translation).}$$

At least a part of the differences observed can be attributed to some mismatch in the mean angle of attack, α_o, and some inaccuracy in the effective amplitude of oscillation, $\Delta\alpha$, which is only estimated for the translation conditions.

For the V23010-1.58 airfoil at Mach number M = 0.4, figure 10a, the normal force loops for translation display larger C_n excursions than the corresponding loops for pitch, i.e.,

$\Delta C_{n_{TRANS}} > \Delta C_{n_{PITCH}}$ while in terms of equivalent angles of attack

$\Delta\alpha_{PITCH} > \Delta\alpha_{TRANS}$. The latter difference is not exact because the angle of attack excursion for translation was estimated from the freestream velocity and from the approximate motions of the airfoil model.

Stall and Multiple Stall from Pressure Time Histories

The development of stall, as seen in pressure time history plots, figures 4a and 5a, is characterized by the progressive attainment and collapse of the maximum suction at each of the chordwise stations where pressures were measured. For the airfoils in this test the collapse in pressure occurs first near the leading edge and it spreads downstream toward the trailing edge. This stall pattern is true generally for dynamic stall at subcritical flow conditions, except for airfoils which are unusually sensitive to trailing edge separation.

The progressive movement of the pressure peak from the leading edge to the trailing edge can be clearly observed in any of the pressure time history plots from test conditions for which the airfoils were driven in and out of stall within each cycle of oscillation. This pattern is not clear at the leading edge because the airfoil models were instrumented with differential pressure transducers making it impossible to separate upper from lower surface pressures. Except for this instance, Carta, reference 8, has shown that the pressure fluctuations on the upper surface can be adequately represented by differential pressure measurements, implying that the lower surface pressures do not fluctuate significantly.

Figure 6 shows an example of the time variation (in terms of reference angle θ) in the position of the pressure peak during comparable dynamic stall events in pitch and translation. Even though the total time required by the pressure peak to travel from the leading edge to the trailing edge is approximately the same for the two types of motion, in most (but not all) cases the pressure peak appears to travel faster over the front 1/3 of the upper surface during translation than during pitch.

Within the test data available at this time the occurrences of a second pressure peak moving along the airfoil within a cycle of oscillation are not consistent, and when there is some evidence of such events the phenomena appear to be very weak. However, for the V0012 and V23010-1.58, vertical translation seems to be more conducive to this development as illustrated in figures 7 and 8 for test points 4028.4 (translation) and 1062.3 (pitch). Differently from the main stall, which causes a pressure disturbance to travel over the entire distance from the leading edge to the trailing

edge, the second pressure wave appears to be restricted to a region between the leading edge and approximately 10% of chord.

Figure 9 shows pressure distributions for comparable pitch and translation cases for conditions ranging from attached flow, prior to stall inception, through stall. The translation data shows signs of a short laminar separation bubble at the leading edge. No judgment can be made as to the presence of a similar bubble for the pitching case because of differences in pressure instrumentation. The only quantitative observation that can be made is that, during the development of stall, pitching is associated with lower leading edge and trailing edge pressures than the corresponding vertical translation case.

Stall Recovery

Figure 10 compares the C_n loops for pitching and translation for several V23010-1.58 and V0012 test conditions which include stall and reattachment within each cycle. The loops, plots of C_n vs α, were generated using the mechanically input angle of attack for the pitch oscillation data, and the equivalent angle of attack for translation. The same loops for the pitching moment, C_m vs α, show no significant trends and therefore have been omitted. No substantial differences were observed in the mode of stall recovery which could be attributed to the different types of motion, although some differences could be observed in the onset of dynamic stall. It can be concluded that normal force and pitching moment stall recovery in vertical translation can be approximated by making use of an equivalent angle of attack in conjunction with existing pitch oscillation data.

EFFECT OF TEST PARAMETERS

There is only a limited number of test points available to make an assessment of the effect of variations in Mach number, frequency, mean angle and $\Delta\alpha$. As shown in the data summary in Table I, most of the data available is at a Mach number of 0.4, with only one test point at M = 0.2 for the V23010-1.58 and V0012 sections. Three test points at M = 0.6 are available, two of which are the V0012 at a frequency of 33 Hz with mean angles α_o = 12.5° and α_o = 14.5°. However, some limited conclusions can still be derived from the data.

Mach Number

Since the V23010-1.58 was tested at mean angles up to 20° at M = 0.2 and at angles up to 15° at M = 0.4, see Table I, a direct comparison cannot be made. However, the lower Mach number pressure data display some evidence of the presence of a separation bubble downstream of the leading edge suction peak. Such separation bubble occurs on both airfoils, and it is more pronounced on the V0012.

The two airfoils used in this study start to show compressibility effects (i.e., they display local regions of supersonic flow over most of the lift range) at M = 0.6. When the incidence or free-stream Mach number is increased after a local supersonic flow is first established, the growth of the velocities (and pressures) about an airfoil section becomes limited by the formation of shock waves. When the lifting capability of an airfoil is restricted by shock-induced separation, unsteady aerodynamic effects no longer produce a delay in stall.

Figures 11 and 12 show pressure distributions for the V23010-1.58 airfoil in translation and pitch, respectively, at M = 0.6. A comparison of the leading-edge pressures at $\theta = 180°$ for translation, and at $\theta = 80°$ and $\theta = 100°$ for pitch, shows that the flow experiences recompression closer to the leading edge during translation.

Frequency

The only data available to examine the effect of variation of frequency is for the V23010-1.58 airfoil at M = 0.4 with an angle of attack excursion $\Delta\alpha \approx 2.5°$, at a mean angle of attack $\alpha_o = 12.5°$. Figures 13 and 14, (test points 4032.3 [15 Hz] and 4028.3 [30 Hz] for translation, and 1058.2 [17 Hz], 1062.2 [33 Hz] for pitch). However, the conditions at which these test points were acquired place stall inception very close to $\dot{\alpha} = 0$ and stall development at $\dot{\alpha} < 0$, while the most useful dynamic stall data is normally acquired with $\dot{\alpha} > 0$ over most if not all the duration of the stall event. The data for pitch (TP 1058.2 and 1062.2 in the appendix) show very limited signs of separation in the integrated loads and just some indication of a collapse in pressures at the leading edge, so that no meaningful comparison can be made with the translation data, except for taking notice of the fact that at $\alpha_o = 12.5°$ and $\Delta\alpha_{equivalent} = 2.5°$ pitching oscillations seem to be somewhat less susceptible to stall.

The translation data (TP 4032.3 and 4028.3 in Figures 13 and 14) show a weak collapse in pressures which spreads along the entire upper surface. Quite predictably the intensity of the stall is reduced as the drive frequency is increased from 15 Hz to 30 Hz.

Mean Angle

Comparison of TP 4041.1, Figure 15, and TP 4041.2, Figure 16, shows that an increase in the mean angle α_o from 12.45° to 14.88° results in the stall occurring earlier in the cycle and that the stall persists over a longer period of time.

Comparison of TP 4041.1 (Figure 15) with TP 4032.3 (Figure 13) shows that a combined increase in frequency and effective $\Delta\alpha$ results in a significant variation in the chordwise pressure propagation. The pressure at x/c = 0.050 in Figure 15 undergoes considerable fluctuations and the first stall event,

characterized by the attainment and collapse of the maximum local ΔC_p, propagates like a pressure wave along the chord.

STALL DELAY PARAMETER - GAMMA FUNCTION

In conjunction with the study to determine the differences in dynamic stall behavior between vertical translation and pitch oscillations, a qualitative evaluation of one method of synthesizing dynamic stall coefficients, reference 3, was undertaken. Although the number of data points available is not sufficient to draw definite conclusions, trends are noted which bear consideration in analyzing the combined pitch and vertical translation oscillations occurring on the rotor blade.

Gamma Function

Using the method outlined by Gross, reference 3, and Gormont, reference 6, gamma functions for pitch and for vertical translation oscillations were constructed. At M = .0.4, figures 17 and 18 show plots of dynamic stall angles vs $\frac{\alpha c}{2V}$ for the V23010-1.58 and V0012 airfoils respectively. The slope of the linear fit to the data has been defined as the "gamma function". The gamma functions from the plots are:

	V0012 (at Mach Number = 0.4)	V23010-1.58 (at Mach Number = 0.4)
$\gamma_{L)PITCH}$	.995	1.03
$\gamma_{L)TRANSL}$	1.040	.75
$\gamma_{L)COMBINED}$	.980	.85
$\gamma_{M)PITCH}$	.730	.79
$\gamma_{M)TRANSL}$	.955	.06
$\gamma_{M)COMBINED}$	.807	.48

The line marked "combined" is the linear fit to both sets (pitch and translation) of data.

DYNAMIC STALL LOOPS SYNTHESIZED FROM QUASI-STEADY DATA

The computation of the aerodynamic coefficients for the approximation of the unsteady flow environment experienced by a helicopter rotor blade requires taking into account dynamic stall extension and stall recovery considerations. The empirical methods to account for unsteady aerodynamic effects can be easily tested by using such methods to reconstruct the lift and pitching moment loops as measured by Liiva et al[1]. These empirical methods are in addition to the effects already accounted for in classical thin oscillating airfoils (i.e., the Theodorsen functions: amplitude reduction, F(k), and phase shift, G(k)).

The gamma function method is one of the techniques which have been used to synthesize the dynamic stall effects from the quasi-steady aerodynamic coefficients. This methodology is built into existing rotor performance and loads programs. One such method available is a version of the unsteady aerodynamic analysis developed by Gormont, reference 6, for the C-81 analysis (Rotorcraft Analysis Program).

The use of the C-60 program, reference 4, to simulate the two-dimensional dynamic stall characteristic requires inputing a value of zero for the thrust and not iterating between the thrust and downwash and loads. The analysis is done at hover for a rigid rotor using either pure flapping to simulate vertical translation or pure cyclic for pitch oscillation simulation. The rotor is operated in the hover mode and the conditions at a specific radial station can be used for comparison with the two-dimensional dynamic data.

The zero thrust input ensures that the initial (and only) pass through the thrust, downwash and airloads calculation is done without the induced downwash adding to the velocity due to rotation. A typical comparison of the lift stall loops for the V0012 airfoil at M = 0.4 is shown in figure 19. The correlation between the synthesized loops and the test data is poor. The synthesis method predicts too rapid a rise in the C_n as the angle of attack begins to increase. This effect is more pronounced in the vertical translation prediction than for pitch.

The correlation between synthesized pitching moment data and test data is very poor. Such data is not shown.

CONCLUSIONS AND RECOMMENDATIONS

A comparison of the experimental data obtained for two airfoils (V0012 and V23010-1.58) in vertical translation and pitch oscillation has been made. The following differences in the onset of stall between the two modes of oscillation have been observed:

1. Leading edge and trailing edge pressures (suction) during stall are generally lower in pitch than in translation.

2. In general, the rate at which stall propagates chordwise is initially greater in vertical translation.

3. Only weak secondary stall phenomena have been observed; vertical translation appears to be somewhat more conducive to secondary stall events.

4. For pitch and translation oscillations similar changes occur in the chordwise progression of stall with variations in frequency and mean angle of attack.

5. Within the limitations of the available data, no significant differences have been observed in the mechanism of stall recovery with respect to effect on the normal force.

6. Stall delay parameters were evaluated from the translation data with the same methods used in estimating stall delay from pitch data. Significant differences were observed between the pitch and translation stall parameters (gamma functions) but not enough translation data is available to provide a meaningful sample.

7. Neither the lift nor the pitching moment loops are reproduced in a completely satisfactory way using the current reconstitution methodology and the stall delay parameters.

8. Until a better dynamic stall representation is formulated and a better definition of the translation phenomena is possible, there is no reason to include an explicit description of translation in the empirical approximation of dynamic stall.

9. The measurement of absolute pressures, particularly at the leading edge, should be superior to the measurement of differential pressures for both vertical translation and pitch oscillations.

10. Flow visualization studies of the dynamic stall phenomena for both pitch and vertical translation can supplement the chordwise pressure measurements.

REFERENCES

1 Liiva, J., Davenport, F.J., Gray, L. and Walton, I.C.; "Two-Dimensional Tests of Airfoils Oscillating Near Stall", Vol. I and II, USAAVLABS Technical Report 68-13, 1968.

2 McCroskey, W.J., Carr, L.W., and McAlister, K.W., "Dynamic Stall Experiments on Oscillating Airfoils", AIAA Journal, Vol. 14, No.1, January 1976, p 57-63.

3 Gross, D.W. and Harris, F.D.; "Prediction of Inflight Stalled Airloads from Oscillating Airfoil Data", 25th Annual National Forum of the American Helicopter Society, Washington, D.C., May 1969.

4 Tarzanin, F.J., Jr., "Prediction of Control Loads due to Blade Stall", 27th Annual National V/STOL Forum of the AHS, Preprint No.513, May 1971.

5 Davis, J.M., Bennett, R.L., and Blankenship, B.L., "Rotorcraft Flight Simulation with Aeroelastic Rotor and Improved Aerodynamic Representation", USAAMRDL-TR 74-10, June 1974.

6 Gormont, R.E.; "A Mathematical Model of Unsteady Aerodynamics and Radial Flow for Application to Helicopter Rotors", USAAMRDL Technical Report 72-67, May 1973.

7 Bielawa, R.L.; "Synthesized Unsteady Airfoil Data with Applications to Stall Flutter Calculations", Preprint No.935, 31st Annual National Forum of the American Helicopter Society, May 1975.

8 Carta, F.O., Commerford, G.L., Carlson, R.G. and Blackwell, R.H.; "Investigation of Airfoil Dynamic Stall and Its Influence on Helicopter Control Loads", USAAMRDL TR72-6, September 1972.

TABLE 1

TEST CONDITIONS FOR VERTICAL TRANSLATION
AND PITCH OSCILLATION - V0012 & V23010-1.58 AIRFOILS

AIRFOIL	T.P. TRANSL.	T.P. PITCH	MACH NO.	FREQ. f_D HZ	α_o DEG	$\Delta\alpha$ OR $\Delta\alpha$ EQ. DEG.	Δh	VEL. m/SEC	REDUCED FREQ k
V23010-1.58	4033.4		.2	15.90	20.14	4.28	.618	66.90	.121
		5036.4	.2	15.11	19.78	4.80		66.96	.115
	4032.3		.4	15.13	12.53	2.05	.616	132.31	.058
		1058.2	.4	17.32	12.36	2.41		135.36	.065
	4041.2		.4	32.79	14.88	3.40	.472	132.44	.126
		1156.1	.4	32.36	15.07	4.99		134.11	.122
	4041.1		.4	30.12	12.45	3.12	.472	132.74	.116
		1088.4	.4	32.89	12.29	4.94		134.11	.124
	4028.4		.4	32.89	14.88	2.25	.306	130.36	.128
		1062.3	.4	33.24	14.59	2.46		135.30	.125
	4028.3		.4	30.96	12.46	2.12	.306	130.48	.121
		1062.2	.4	33.22	12.37	2.50		135.30	.125
	4040.1		.6	32.68	12.38	2.30	.468	194.13	.086
		1061.2	.6	33.22	12.45	2.39		199.10	.085
	4040.2		.6	33.00	14.80	2.35	.473	193.88	.087
		1061.3	.6	33.18	14.62	2.38		199.10	.085
V0012	3085.3		.2	16.37	14.62	2.13	.305	68.37	.122
		3133.3	.2	16.84	14.65	2.49		67.03	.128
	3114.2		.4	16.45	9.71	2.23	.607	130.48	.064
		3135.1	.4	16.50	9.94	2.49		131.61	.064
	3091.2		.4	34.61	12.34	2.31	.305	132.56	.131
		3136.2	.4	33.56	12.10	2.56		131.89	.130
	3091.3		.4	34.48	14.64	2.35	.305	132.37	.133
		3136.3	.4	33.56	14.45	2.56		131.86	.130
	3108.3		.6	25.84	7.17	1.76	.458	196.20	.067
		3139.2	.6	33.22	7.47	2.58		194.61	.087

V0012

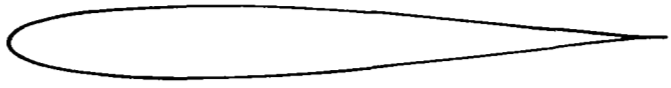

x/c	y/c
0	0
0.0110	0.0170
0.0220	0.0230
0.0330	0.0270
0.0540	0.0340
0.0760	0.0390
0.1087	0.0445
0.1521	0.0493
0.2065	0.0527
0.2500	0.0542
0.3043	0.0547
0.3478	0.0541
0.4130	0.0520

x/c	y/c
0.4564	0.0499
0.5000	0.0472
0.5434	0.0439
0.6086	0.0383
0.6521	0.0343
0.6955	0.0300
0.7607	0.0230
0.8042	0.0181
0.8477	0.0127
0.8911	0.0070
0.9346	0.0011
1.000	0.0011

LEADING EDGE RADIUS = 0.0143
x = 0.0143
y = 0.0

V23010-1.58 with 0° T.E. Tab

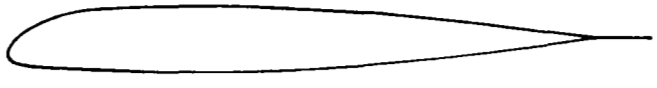

x/c	y/c_U	y/c_L
0	-0.0251	0.0215
0.0056	-0.0070	0.0336
0.0096	-0.0028	0.0361
0.0135	0.0008	0.0374
0.0254	0.0097	0.0394
0.0333	0.0145	0.0401
0.0571	0.0253	0.0419
0.0967	0.0369	0.0443
0.1462	0.0451	0.0471
0.1957	0.0489	0.0497

x/c	y/c_U	y/c_L
0.2452	0.0499	0.0517
0.2848	0.0499	0.0523
0.3937	0.0479	0.0503
0.4729	0.0444	0.0464
0.5521	0.0396	0.0412
0.6313	0.0335	0.0346
0.7502	0.0223	0.0228
0.8293	0.0137	0.0139
0.9086	0.0046	0.0047
1.000	0.0010	0.0011

LEADING EDGE RADIUS = 0.0158
x = 0.0158
y = -0.0215

Table II Airfoil Coordinates

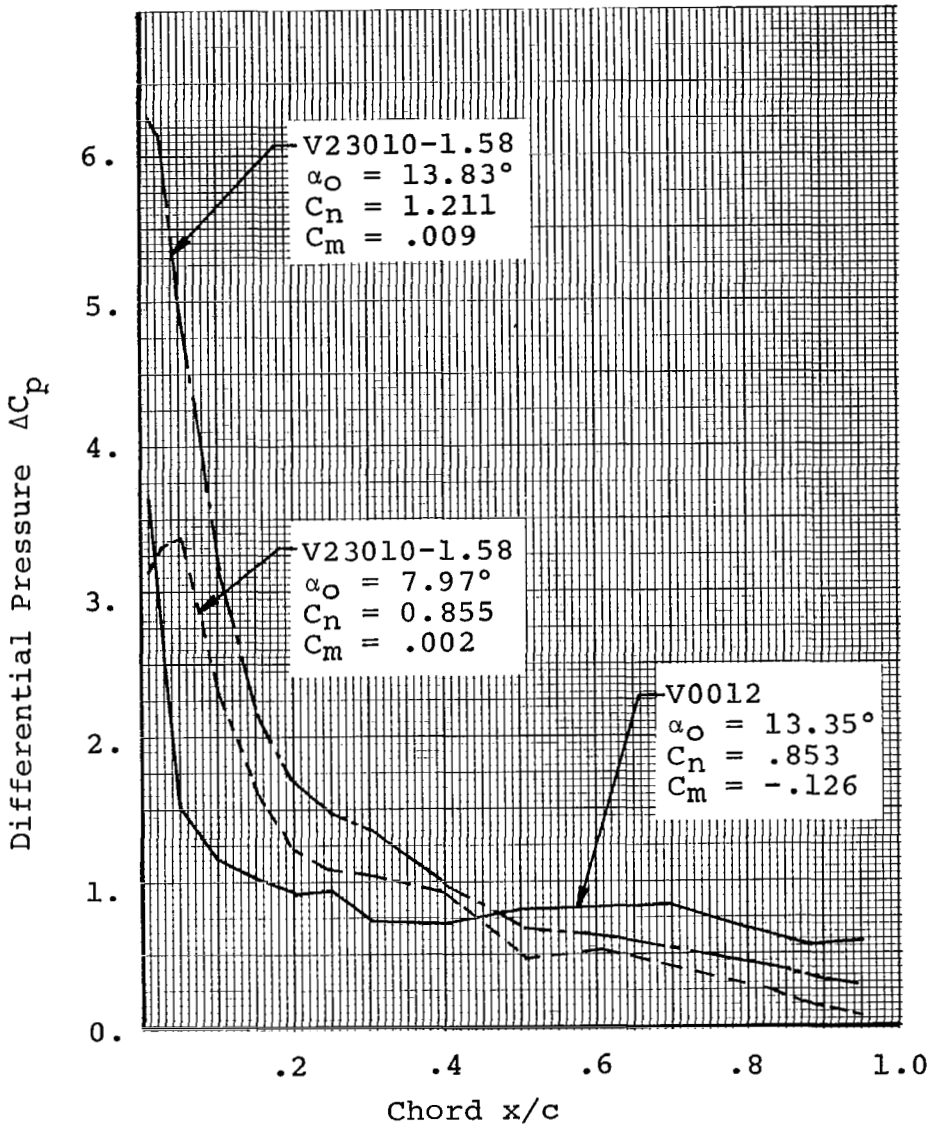

Figure 1. Quasi-Steady Chordwise Loading on the V0012 and V23010-1.58 Airfoils M = 0.4

AIRFOIL V23010-1.58 (0 DEG TE TAB)

TP	FD	MACH	α_o	$\Delta\alpha$	Δh	k	VEL
4041.2	32.79	0.400	14.88	0.00	0.472	0.126	434.5

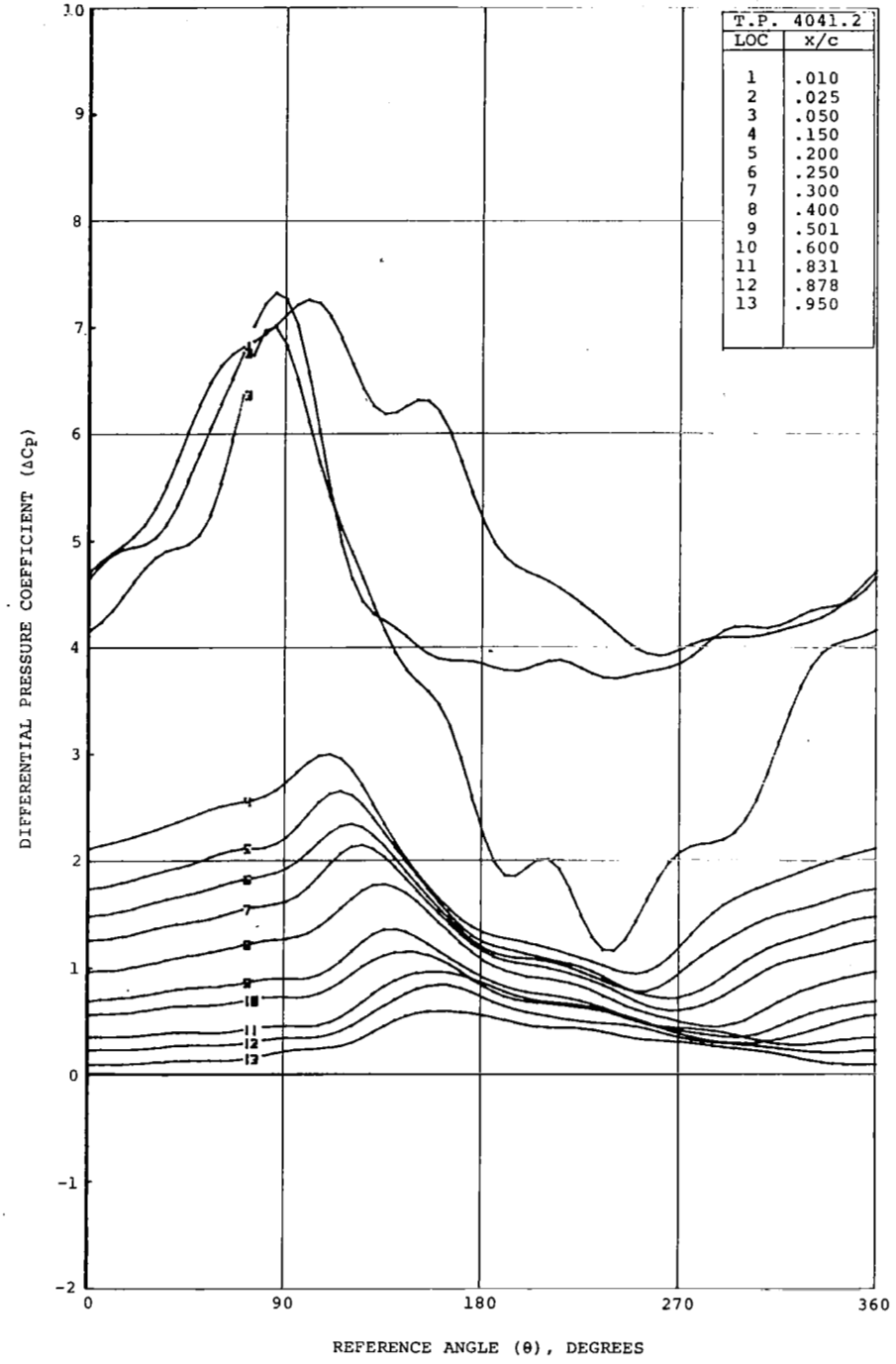

Figure 2a. Airfoil V23010-1.58 in Vertical Translation

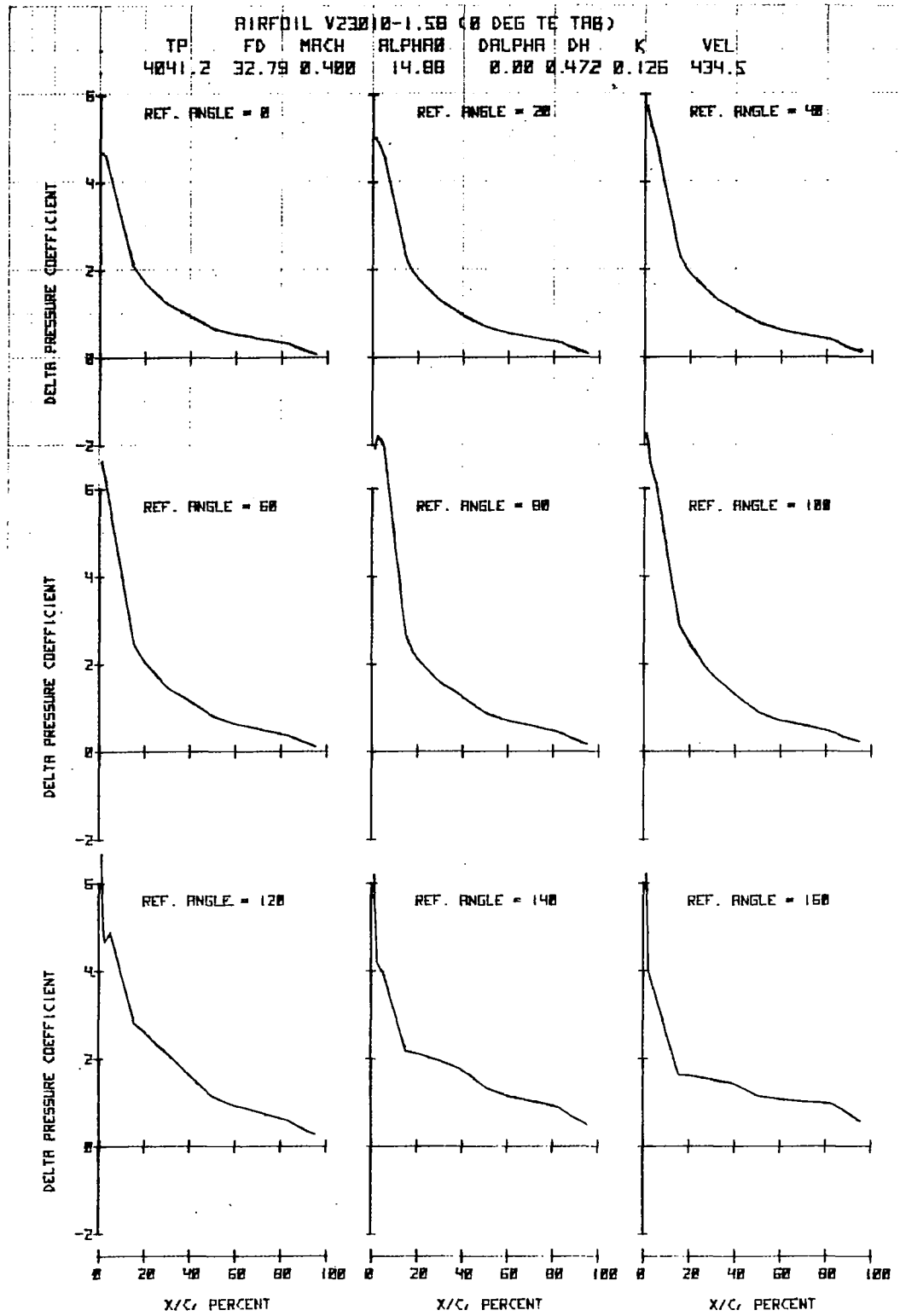

Figure 2b. Airfoil V23010-1.58 in Vertical Translation

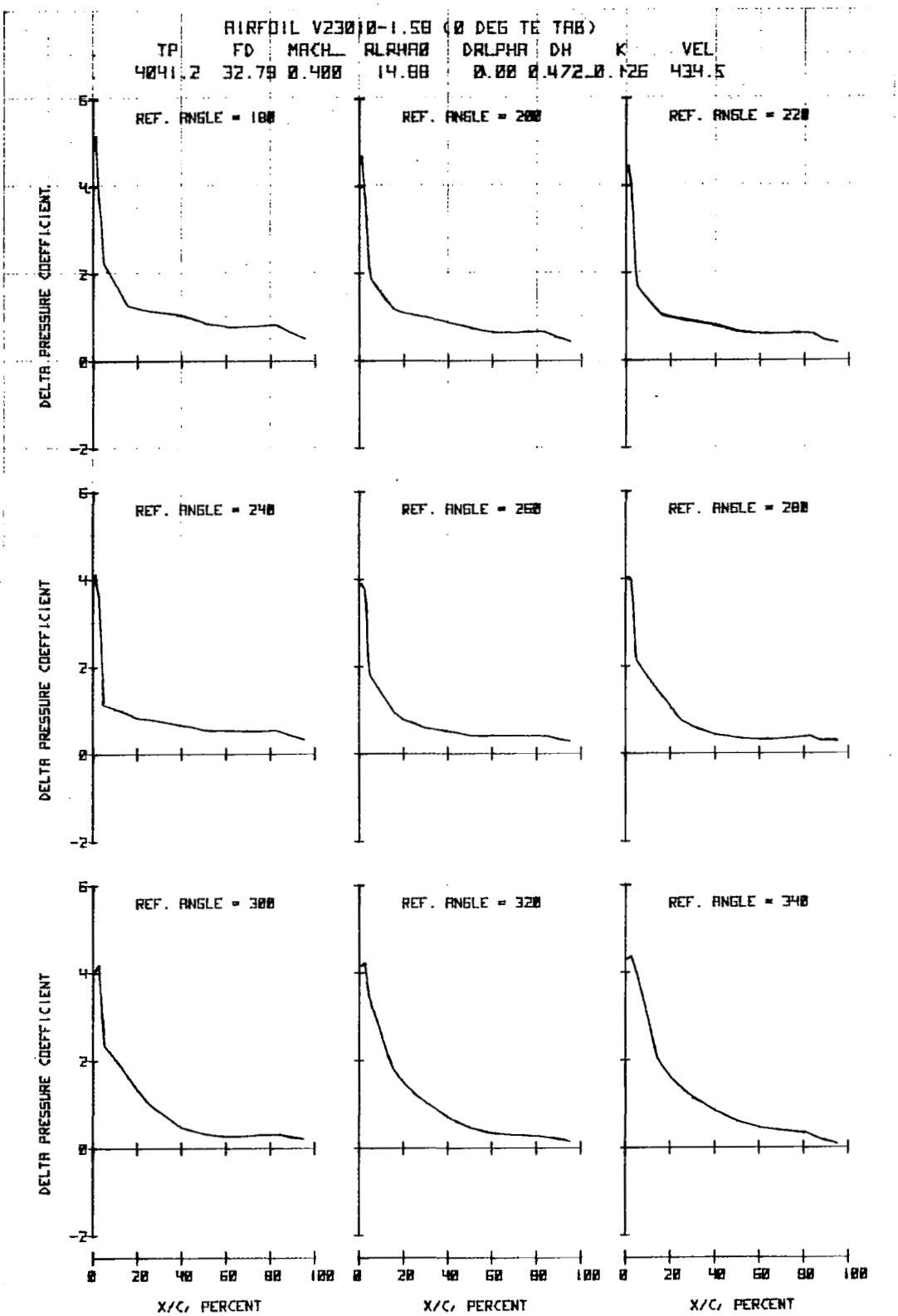

Figure 2c. Airfoil V23010-1.58 in Vertical Translation

AIRFOIL V23010-1.58 (0 DEG TE TAB)

TP	FD	MACH	α_o	$\Delta\alpha$	Δh	k	VEL
1156.1	32.36	0.400	15.07	4.99	0.000	0.122	444.0

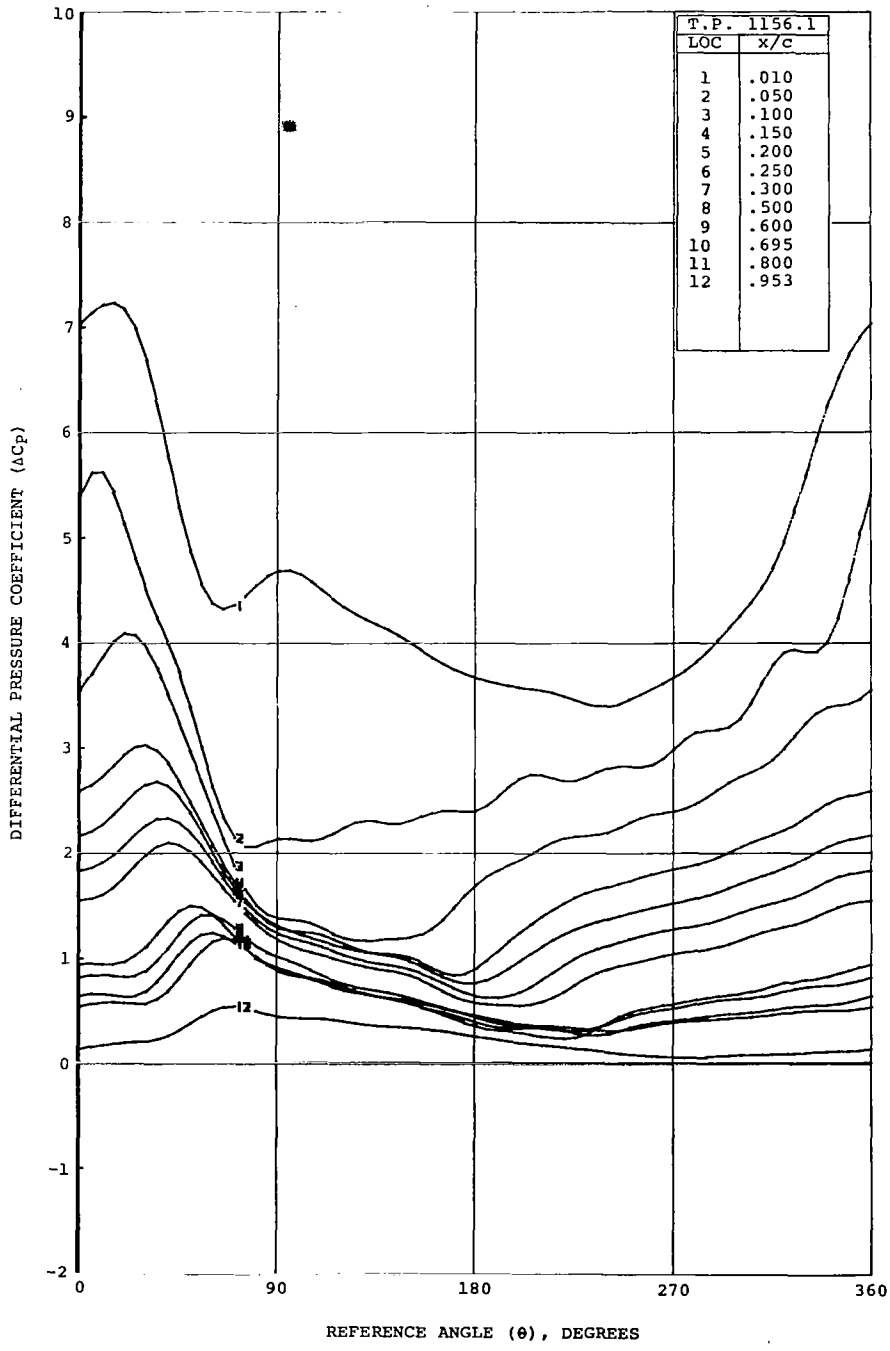

Figure 3a. Airfoil V23010-1.58 in Forced Pitch Oscillation

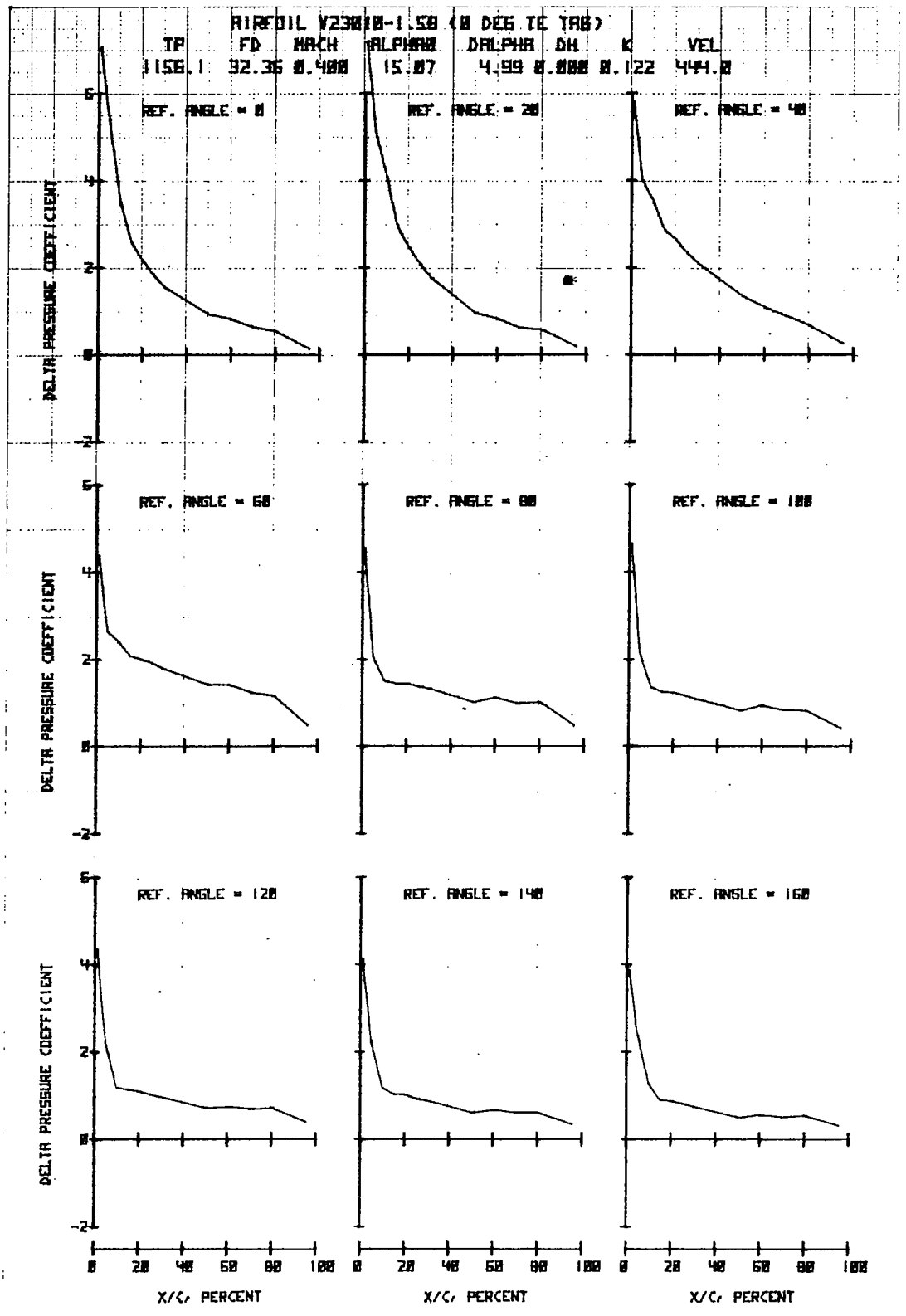

Figure 3b. Airfoil V23010-1.58 in Forced Pitch Oscillation

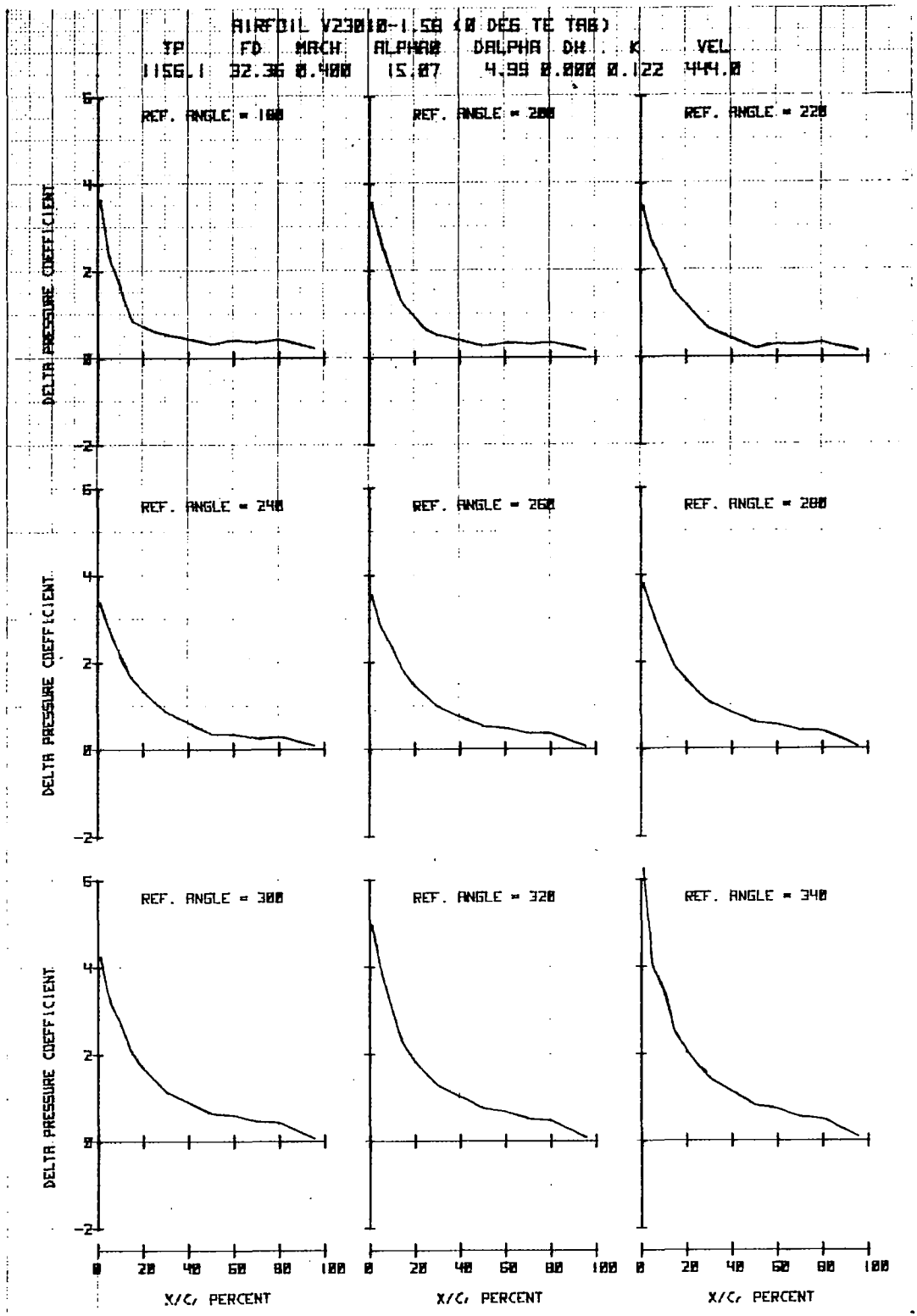

Figure 3c. Airfoil V23010-1.58 in Forced Pitch Oscillation

AIRFOIL V0012

TP	FD	MACH	α_o	$\Delta\alpha$	Δh	k	VEL
3114.2	16.45	0.400	9.71	0.00	0.607	0.064	428.1

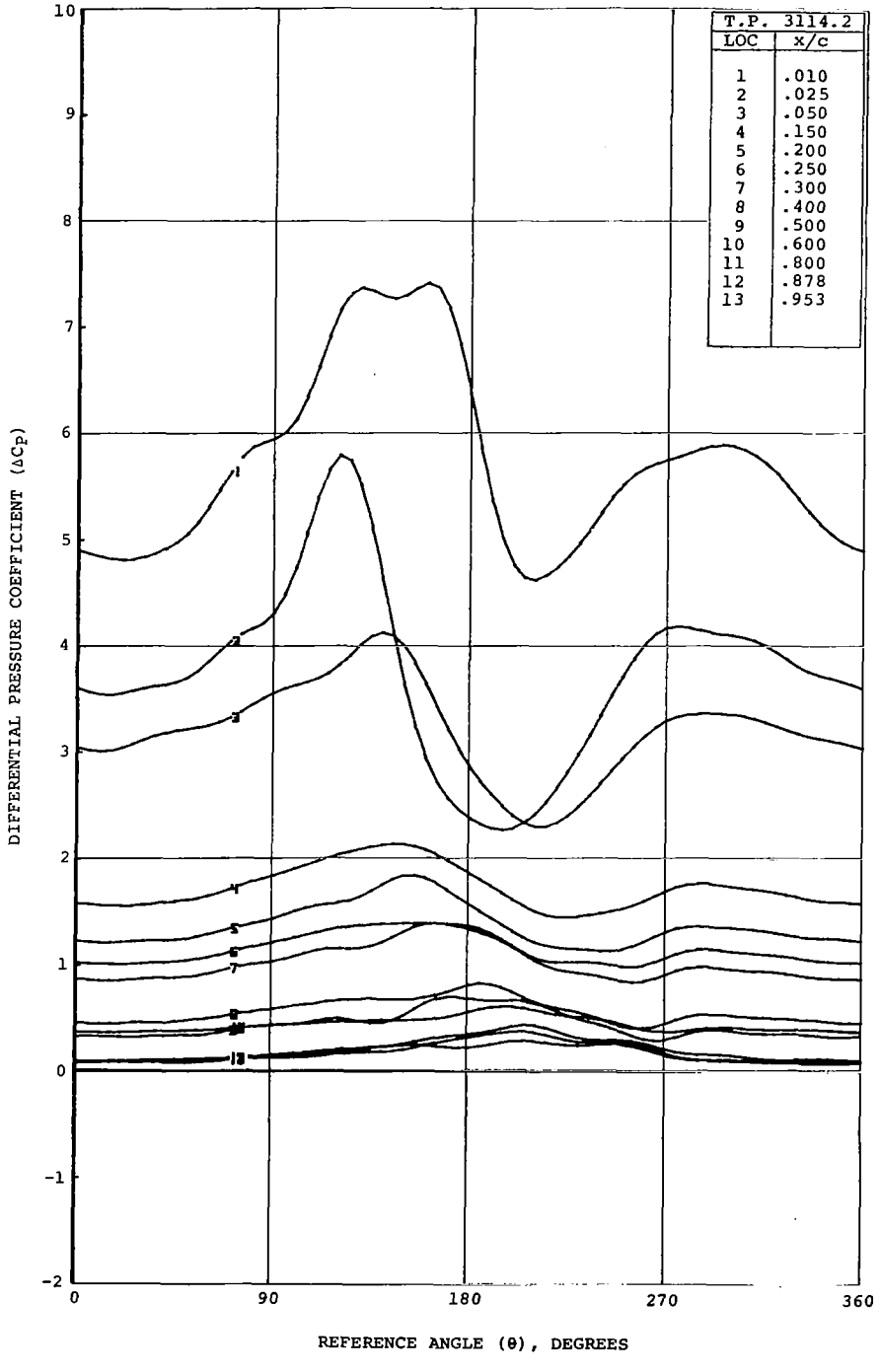

Figure 4a. Airfoil V0012 in Vertical Translation

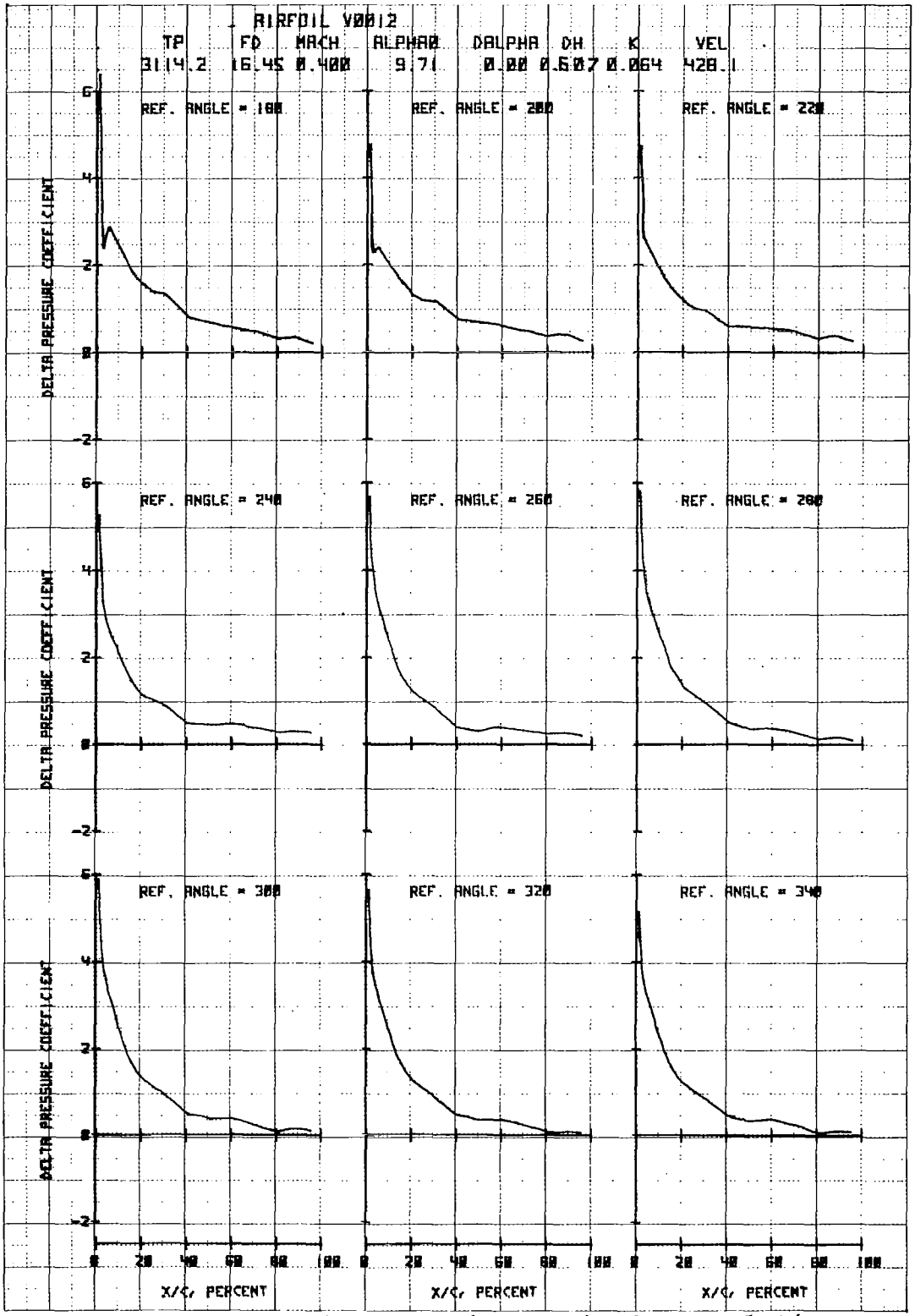

Figure 4b. Airfoil V0012 in Vertical Translation

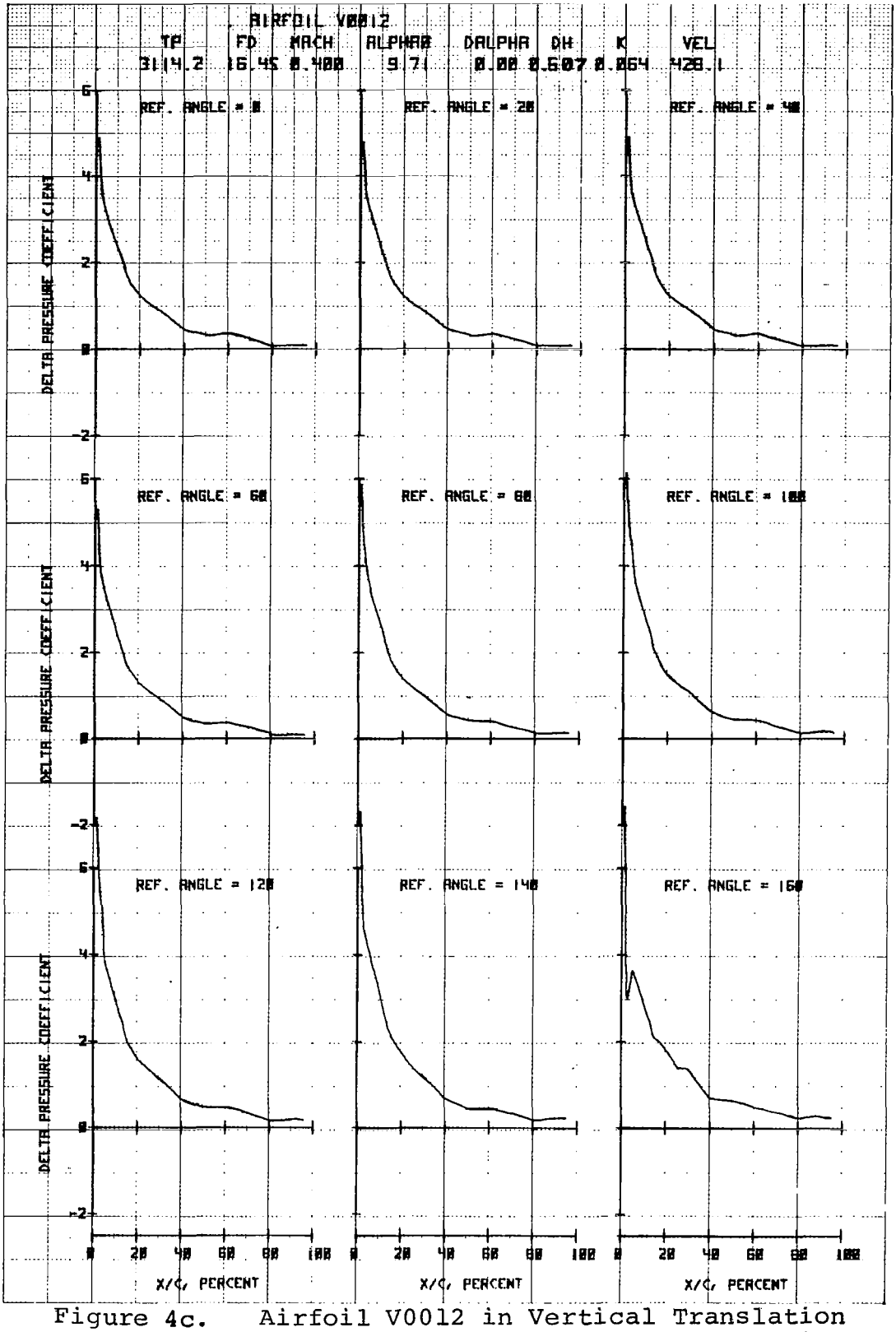

Figure 4c. Airfoil V0012 in Vertical Translation

AIRFOIL V0012

TP	FD	MACH	α_o	$\Delta\alpha$	Δh	k	VEL
3135.1	16.50	0.400	9.94	2.49	0.000	0.064	431.8

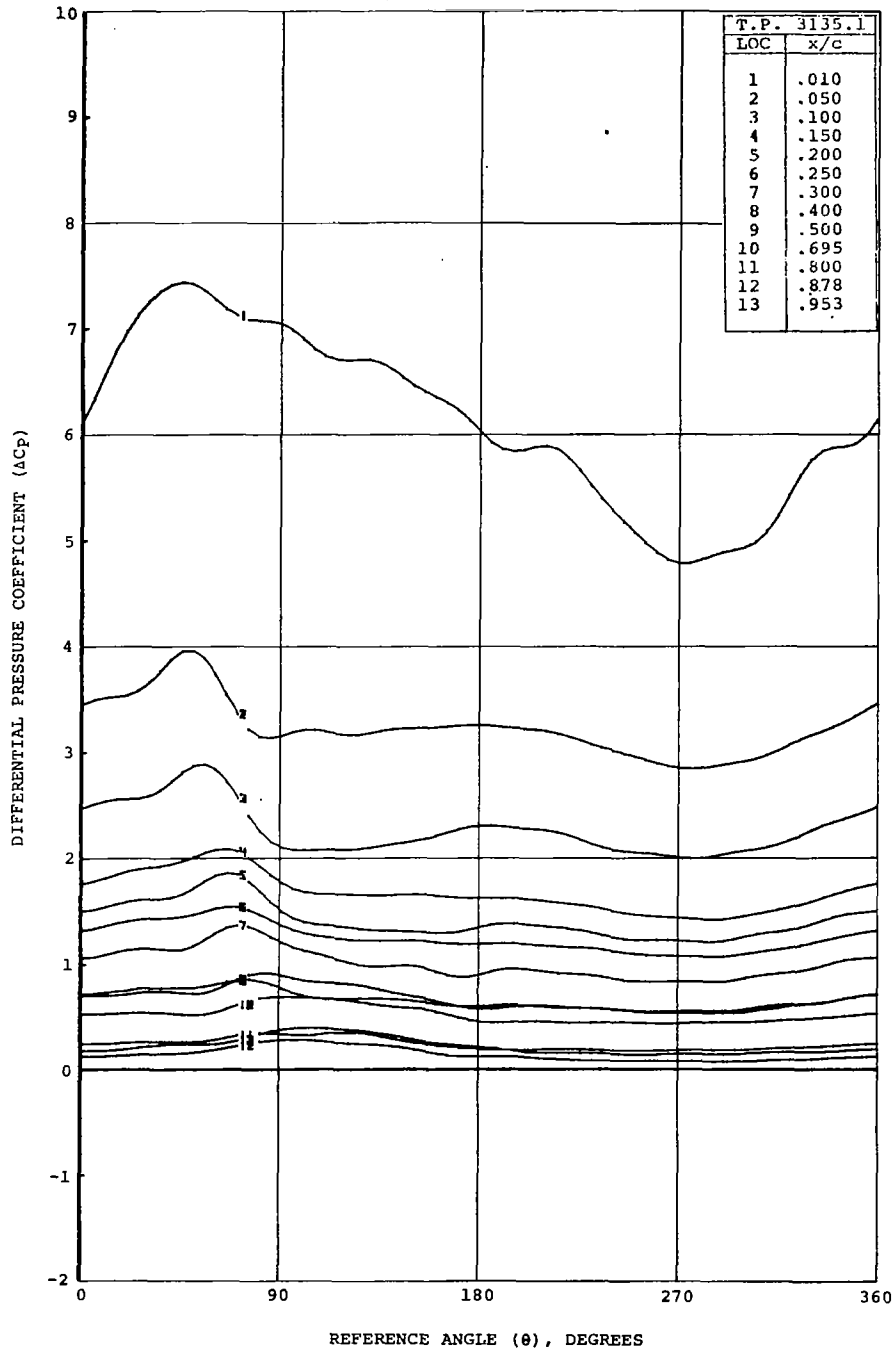

Figure 5a. Airfoil V0012 in Forced Pitch Oscillation

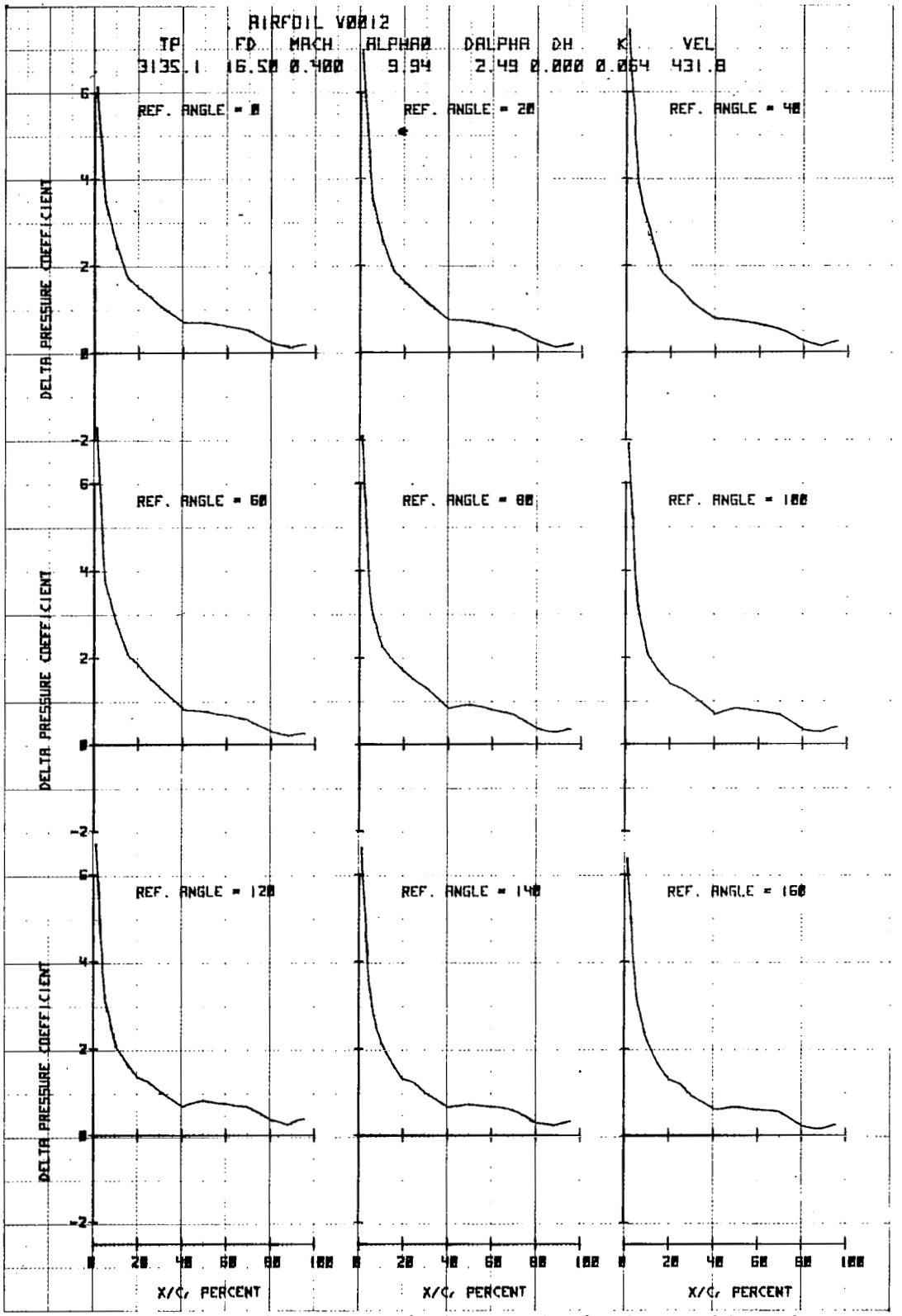

Figure 5b. Airfoil V0012 in Forced Pitch Oscillation

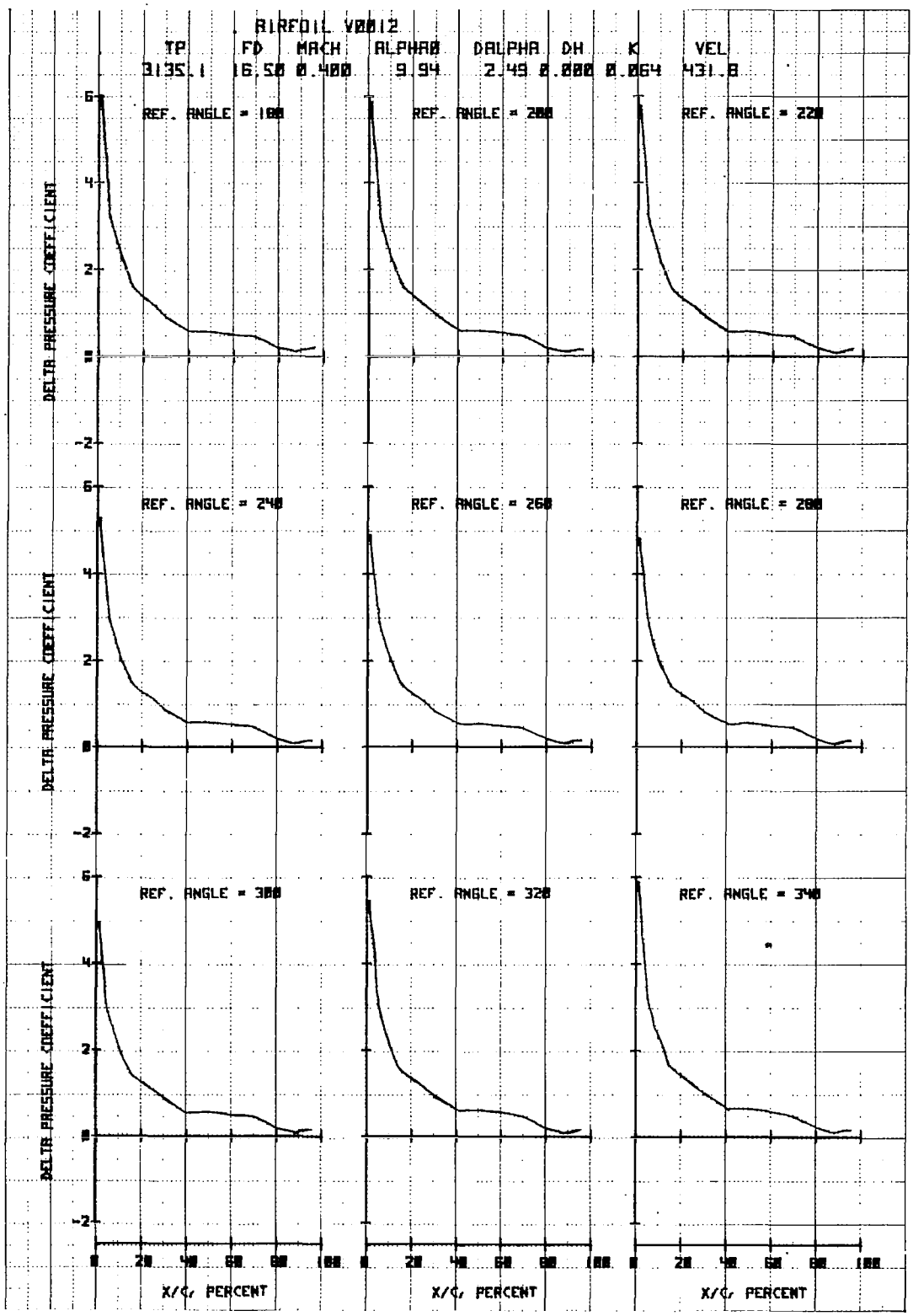

Figure 5c. Airfoil V0012 in Forced Pitch Oscillation

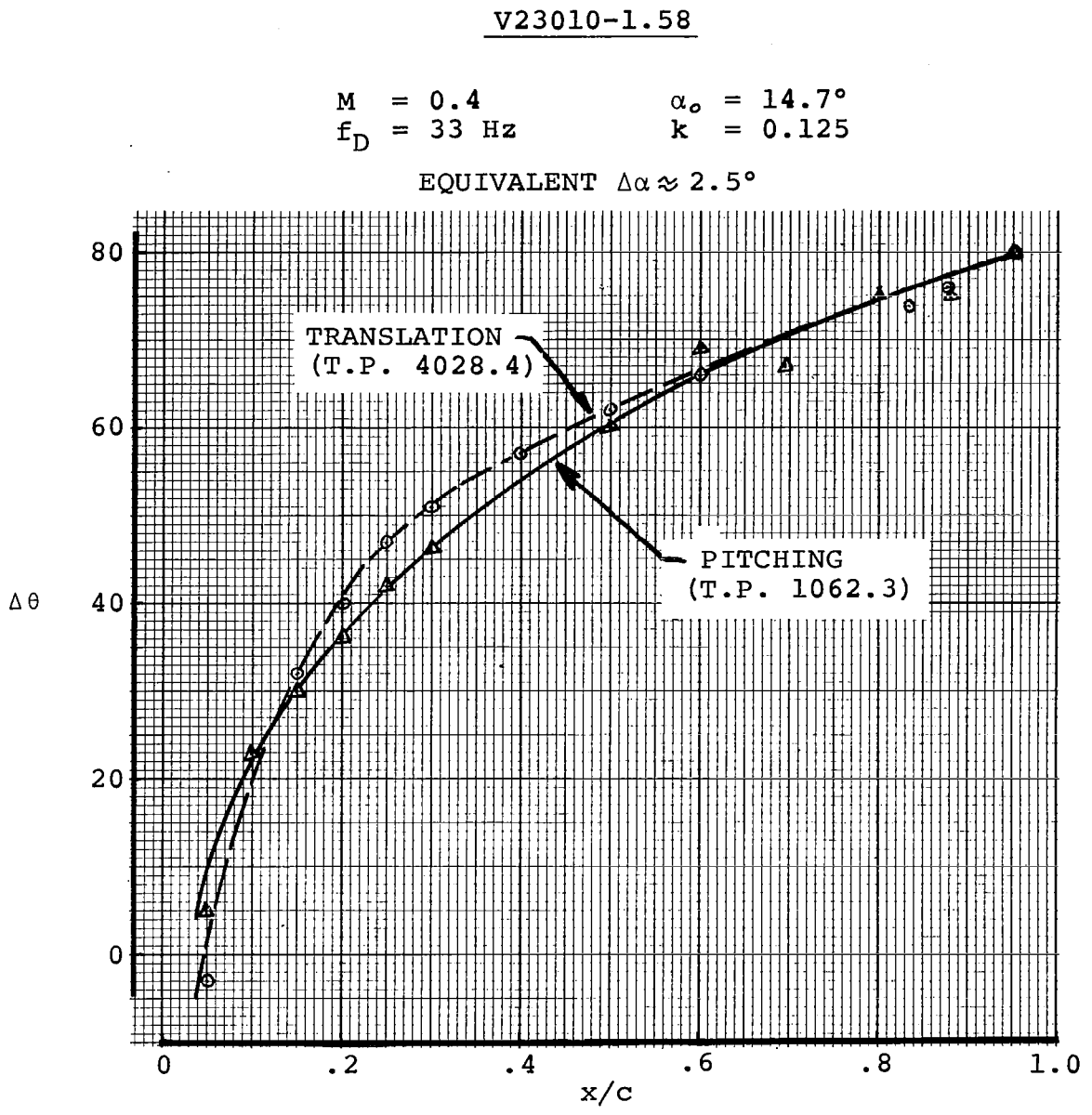

Figure 6. Time Variation in the Position of Pressure Peaks

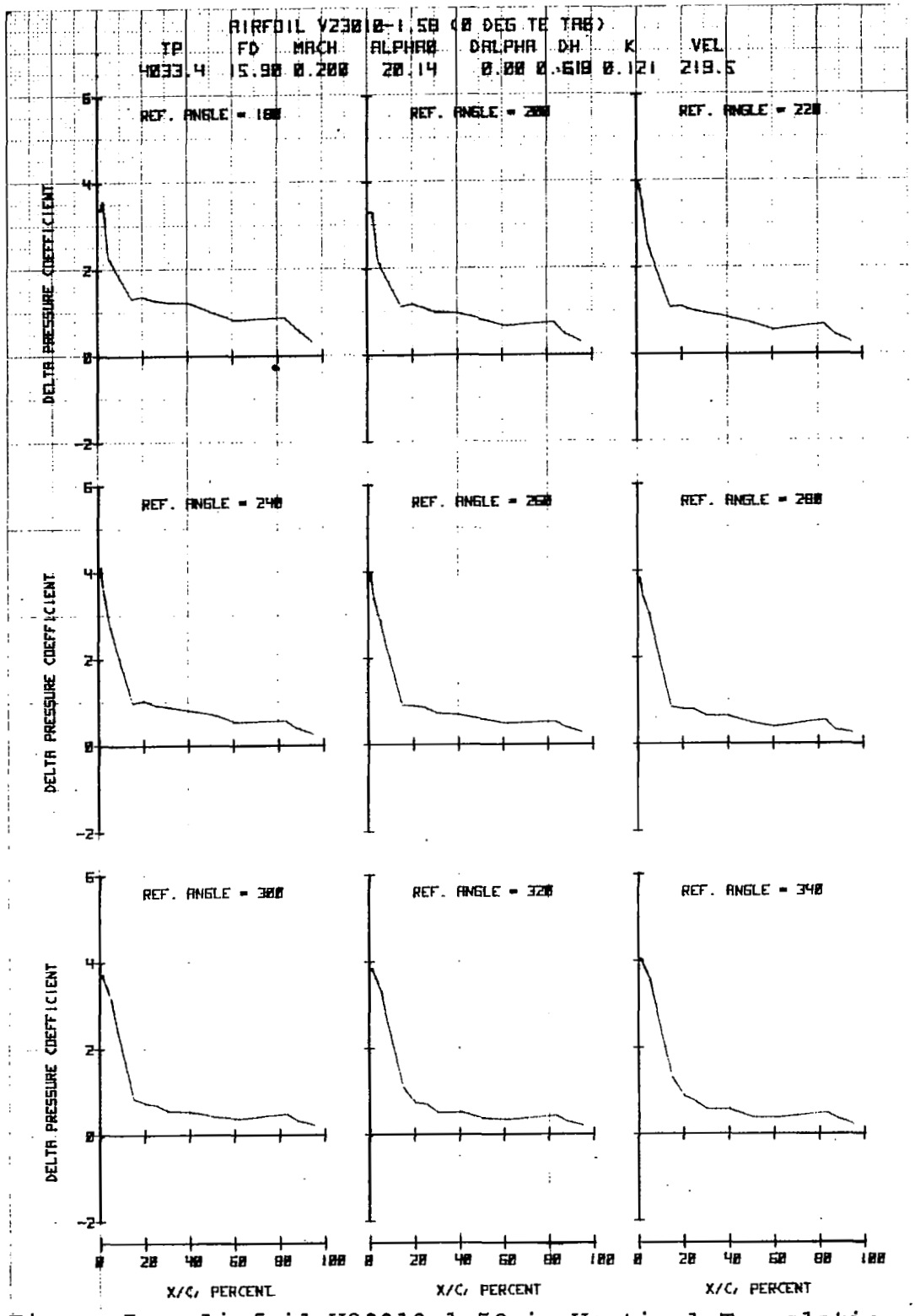

Figure 7a. Airfoil V23010-1.58 in Vertical Translation

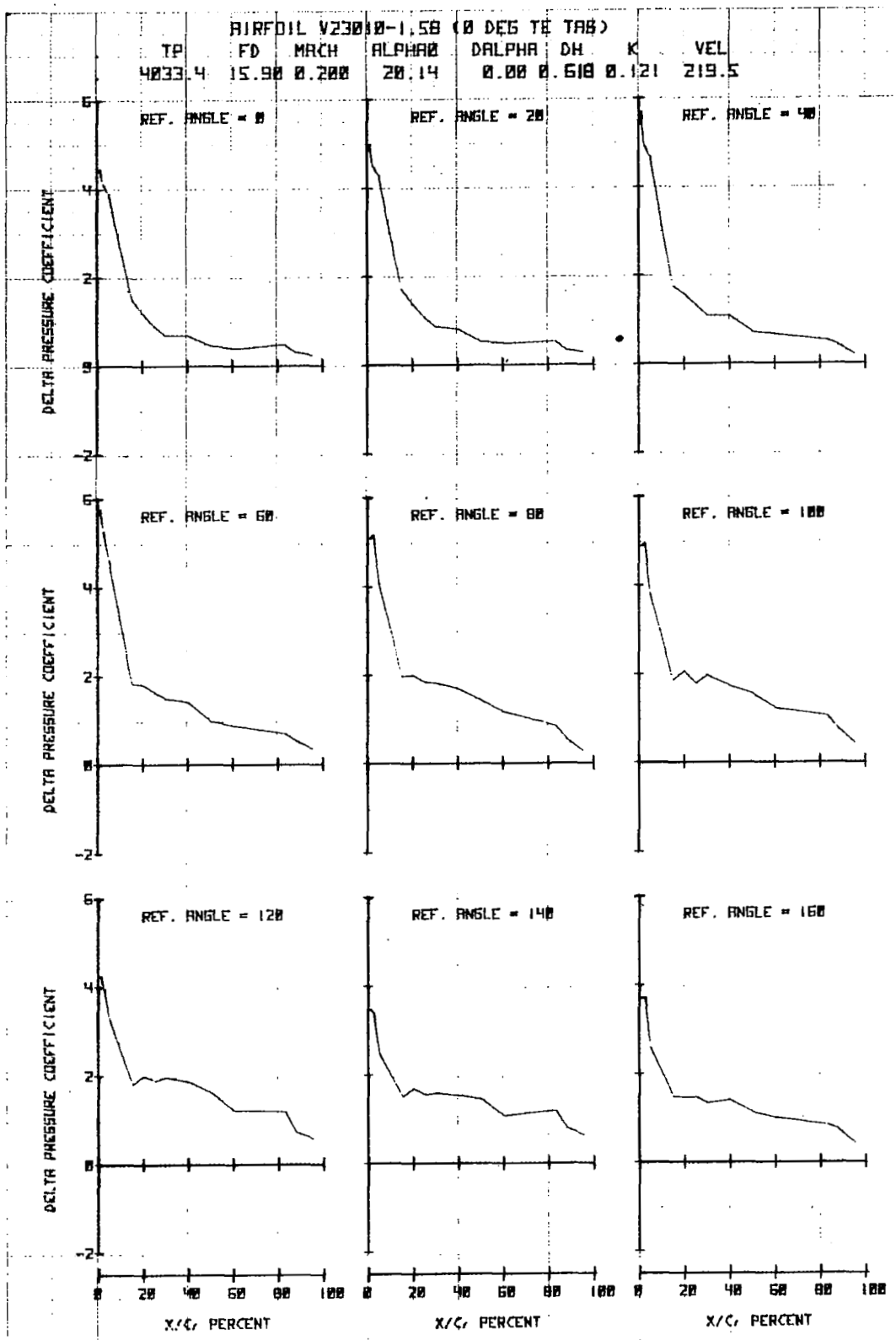

Figure 7b. Airfoil V23010-1.58 in Vertical Translation

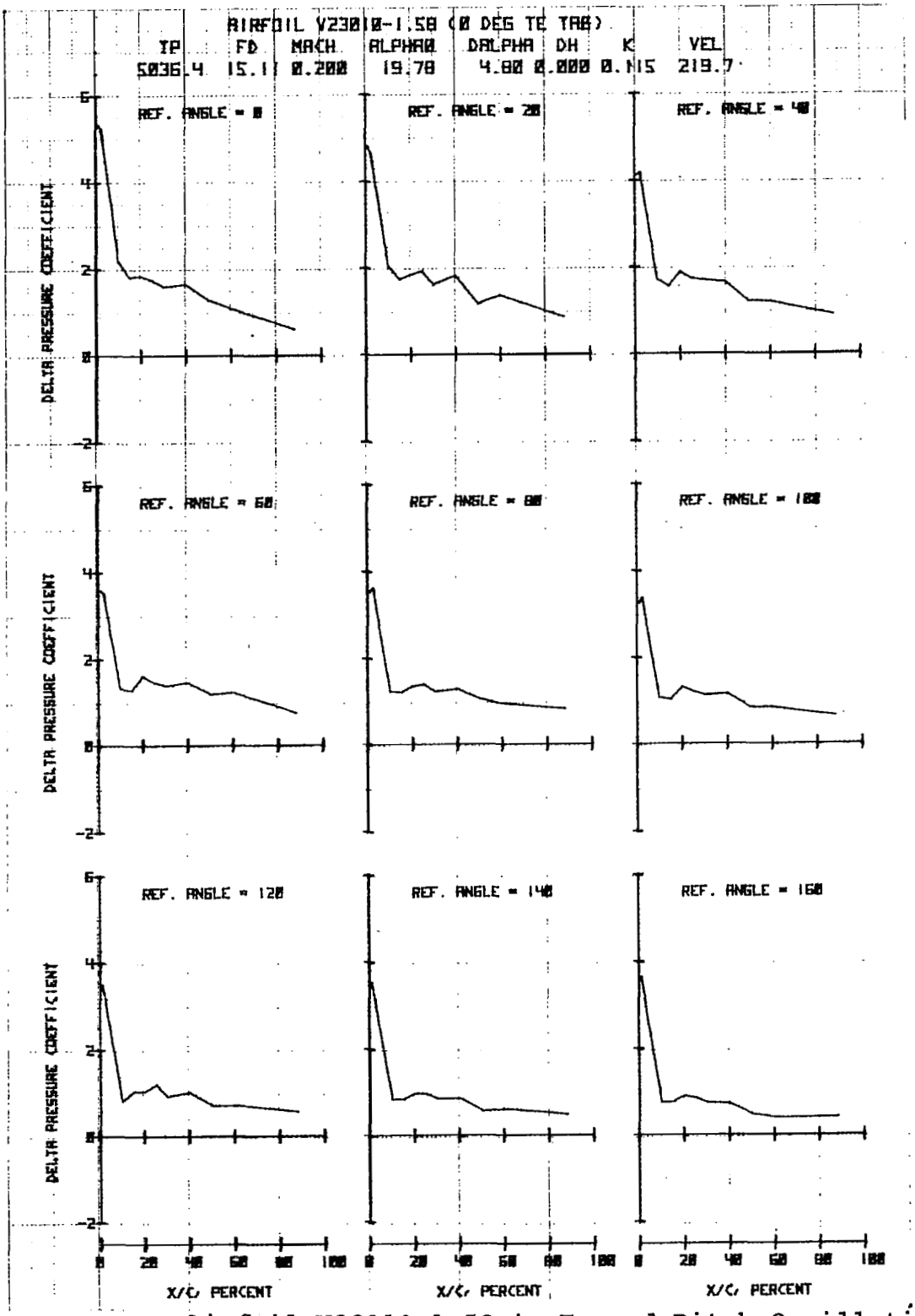

Figure 8a. Airfoil V23010-1.58 in Forced Pitch Oscillation

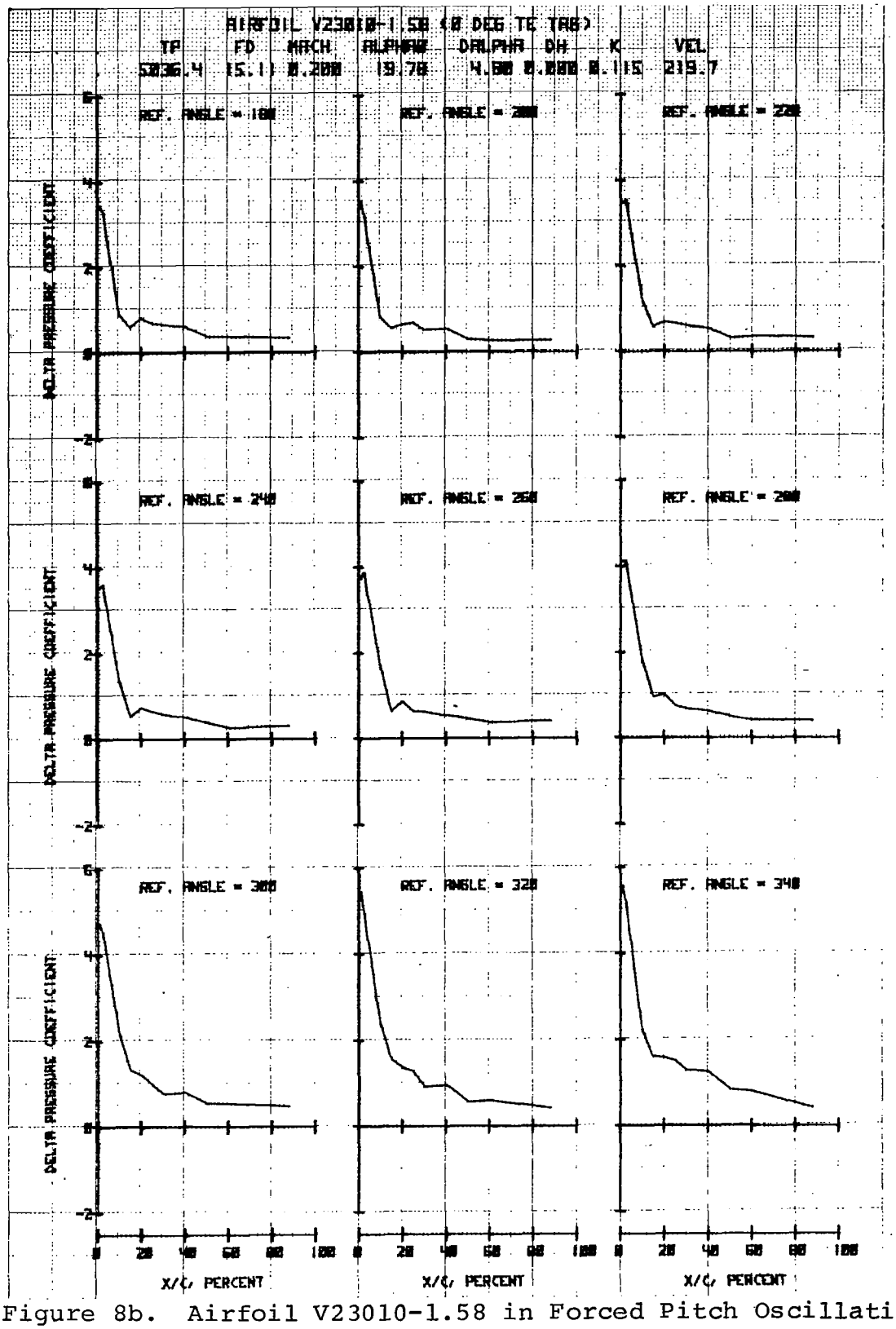

Figure 8b. Airfoil V23010-1.58 in Forced Pitch Oscillation

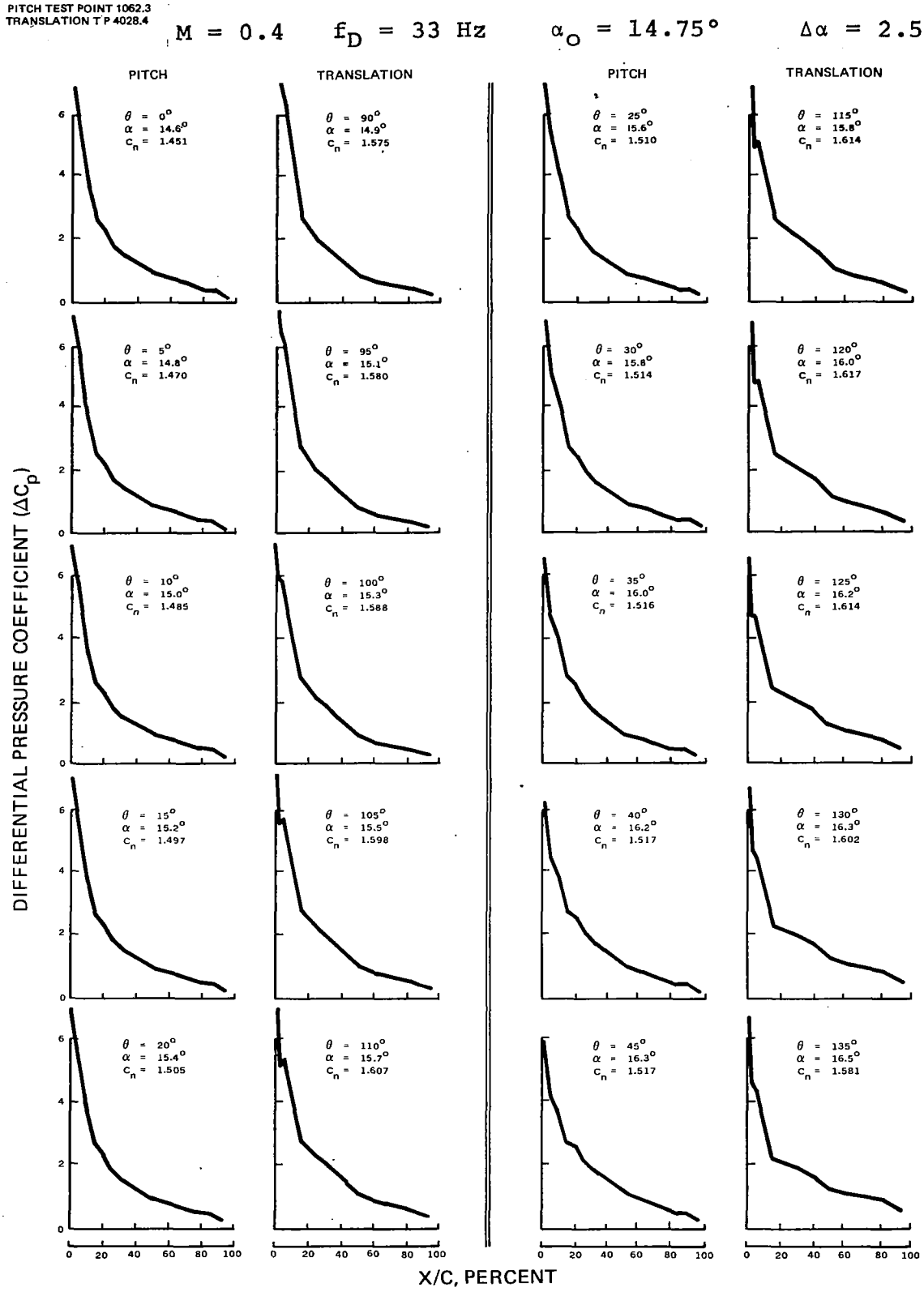

Figure 9a Pressure Distributions for Comparable Pitch and Translation Test Conditions for the V23010-1.58 Airfoil

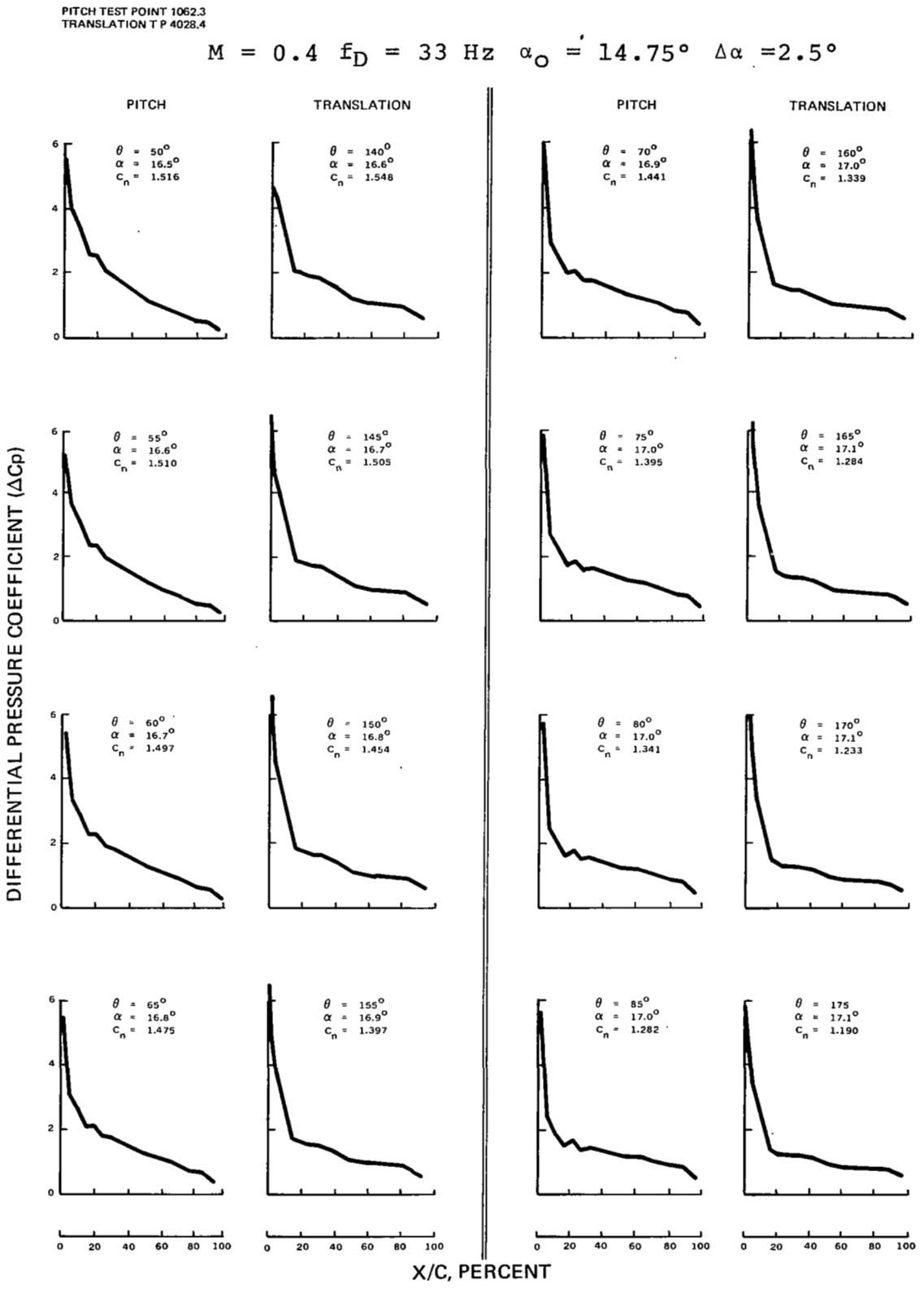

Figure 9b Pressure Distributions for Comparable Pitch and Translation Test Conditions for the V23010-1.58 Airfoil

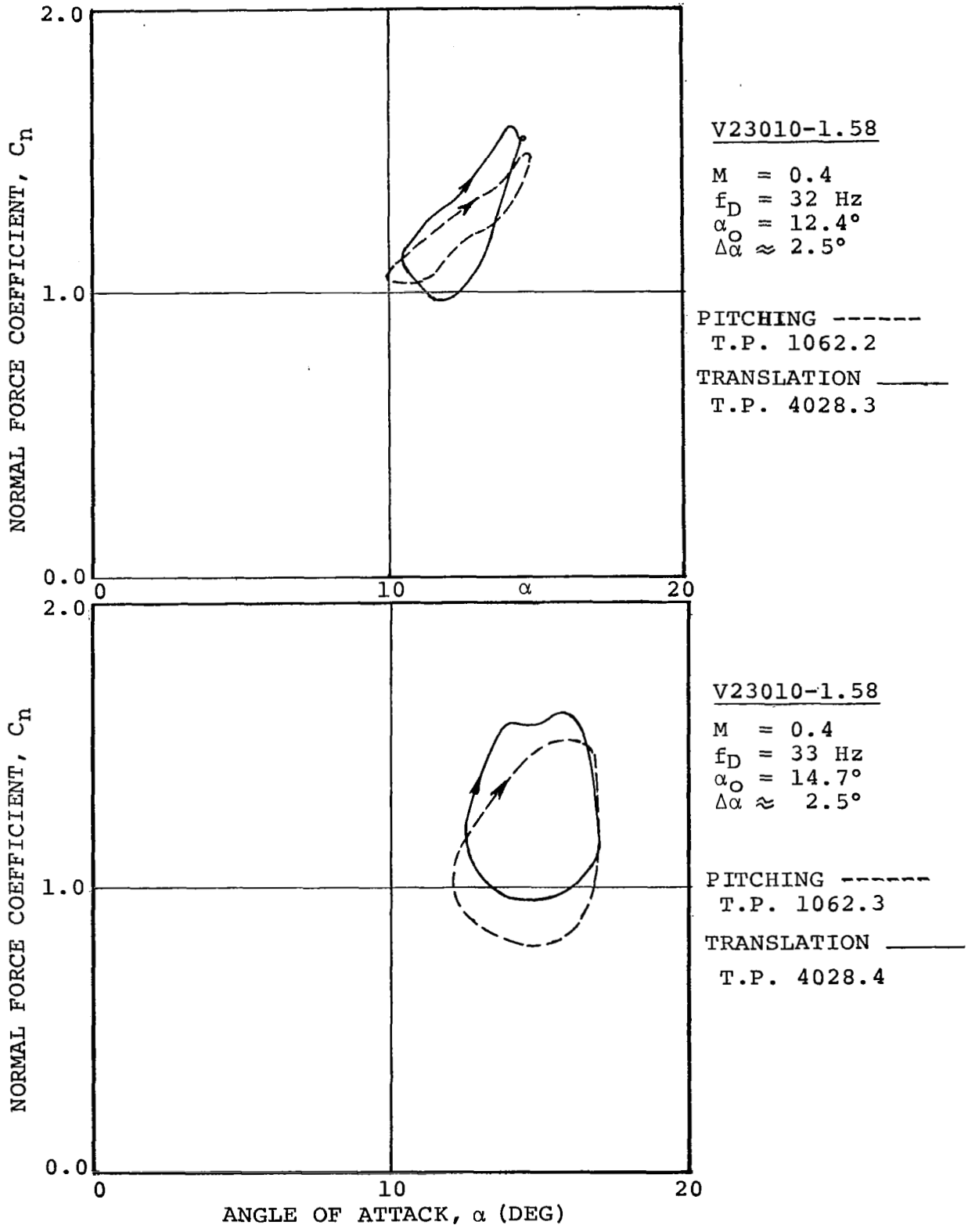

Figure 10 (a) Comparison of Normal Force Loops in Pitching and Translation

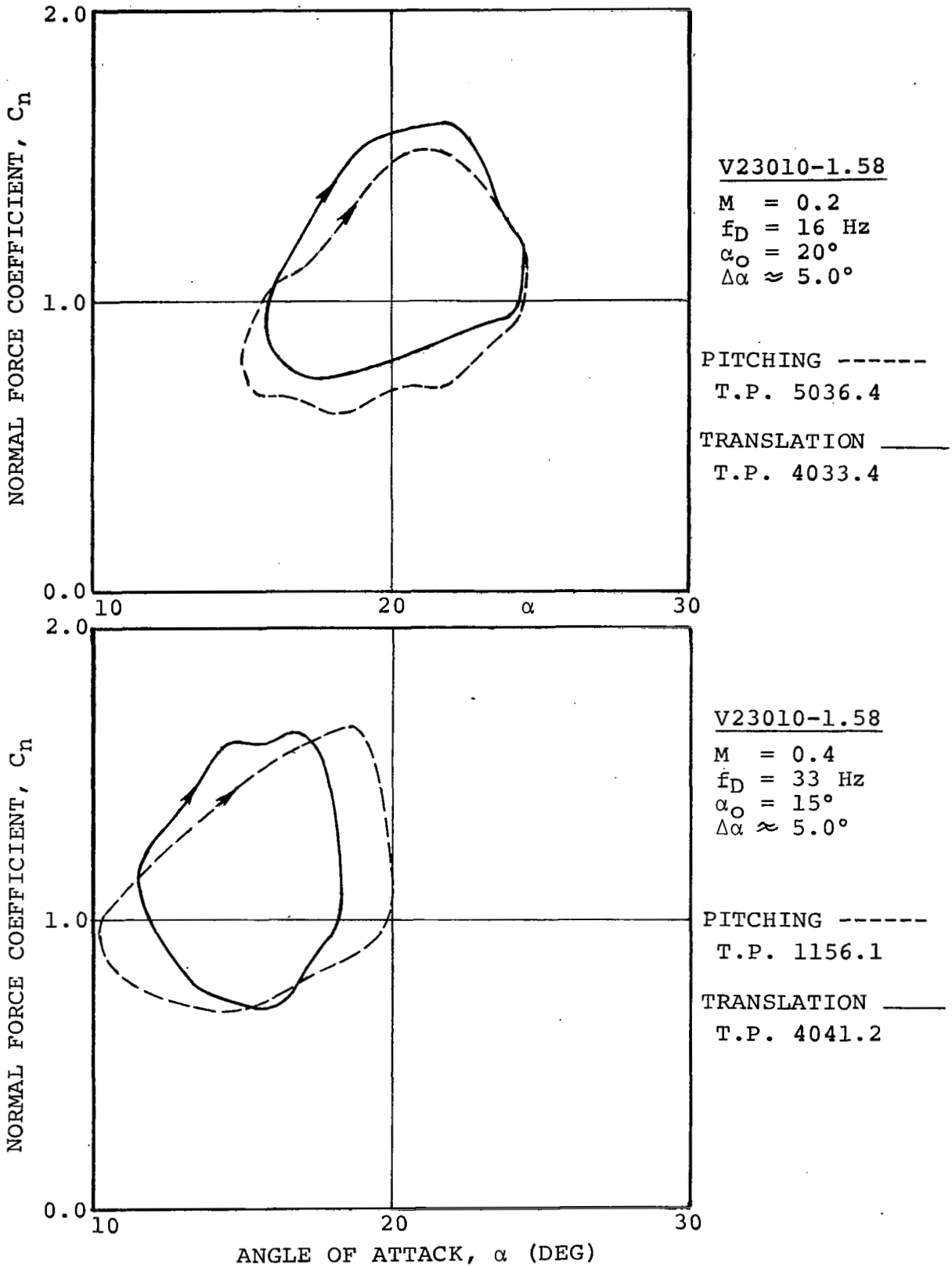

Figure 10 (b) Comparison of Normal Force Loops in Pitching and Translation

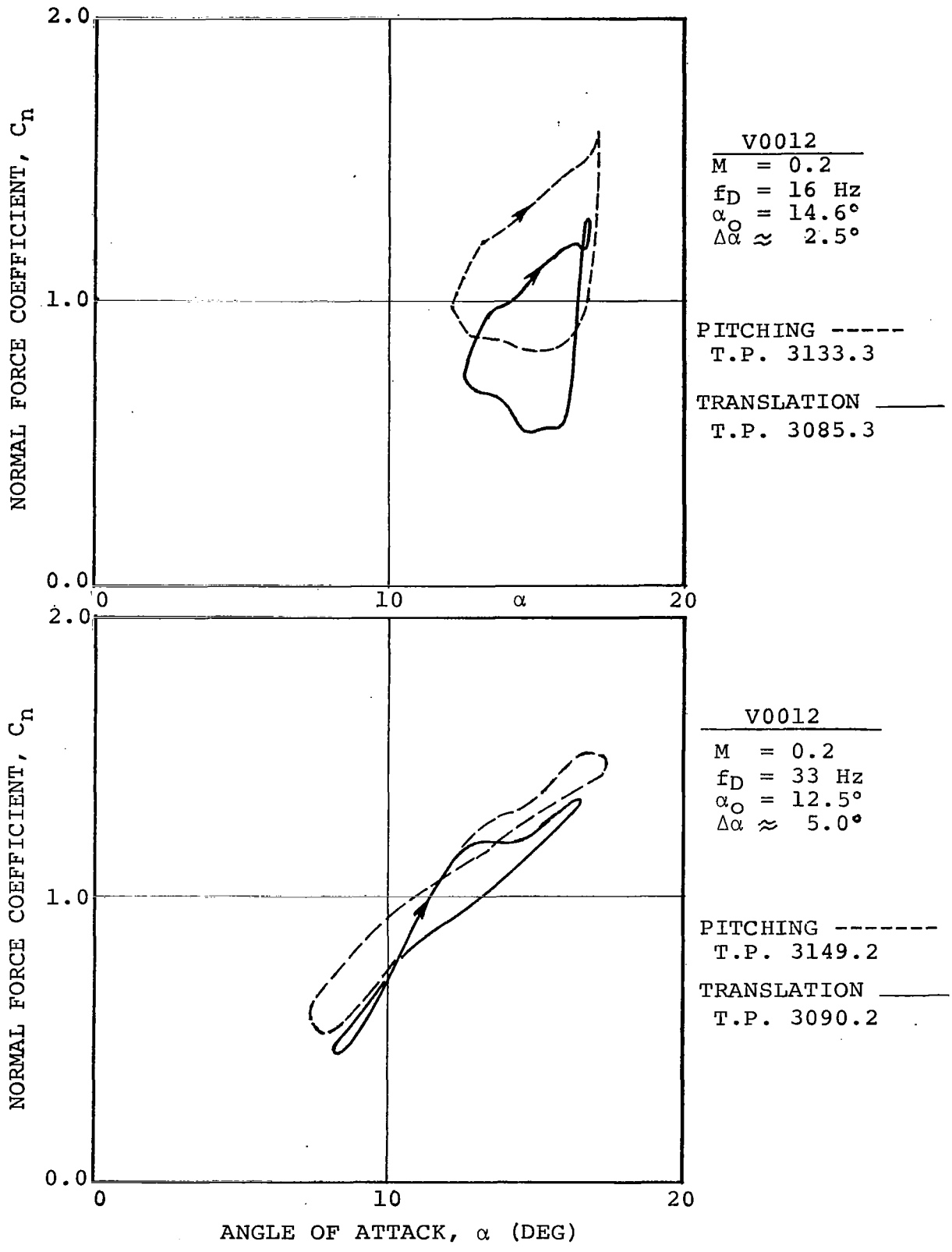

Figure 10 (c) Comparison of Normal Force Loops in Pitching and Translation

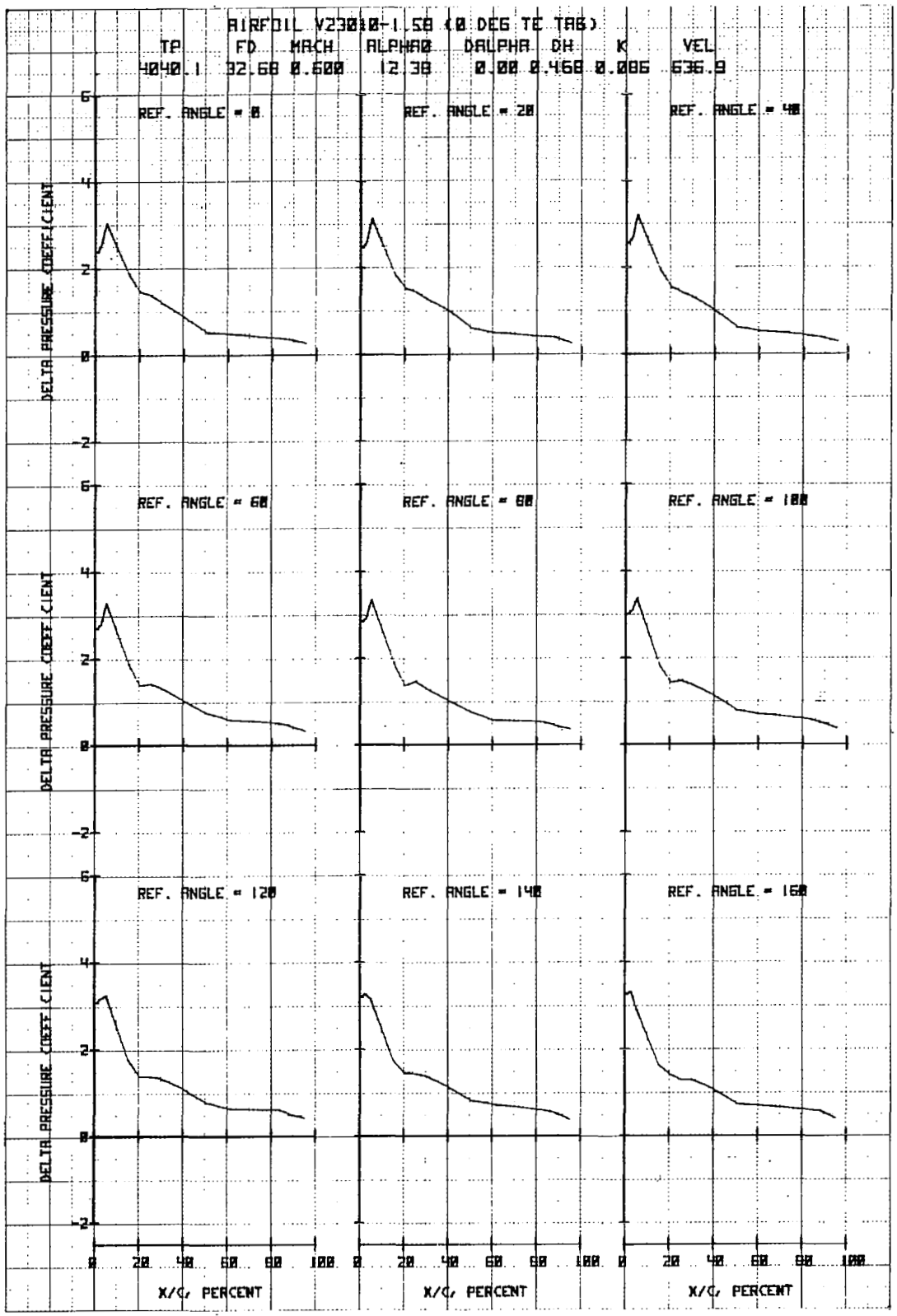

Figure 11a. Airfoil V23010-1.58 in Vertical Translation

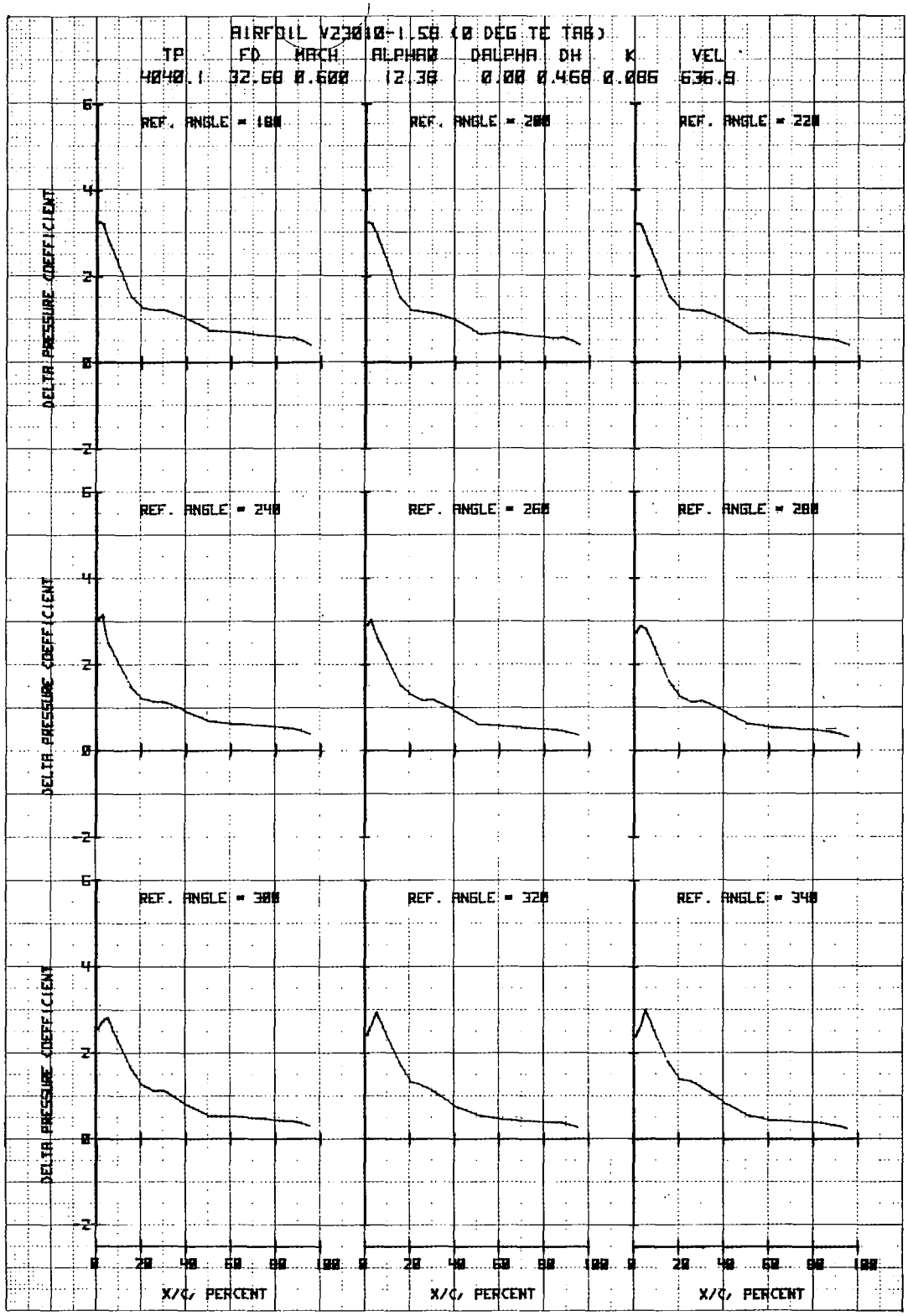

Figure 11b. Airfoil V23010-1.58 in Vertical Translation

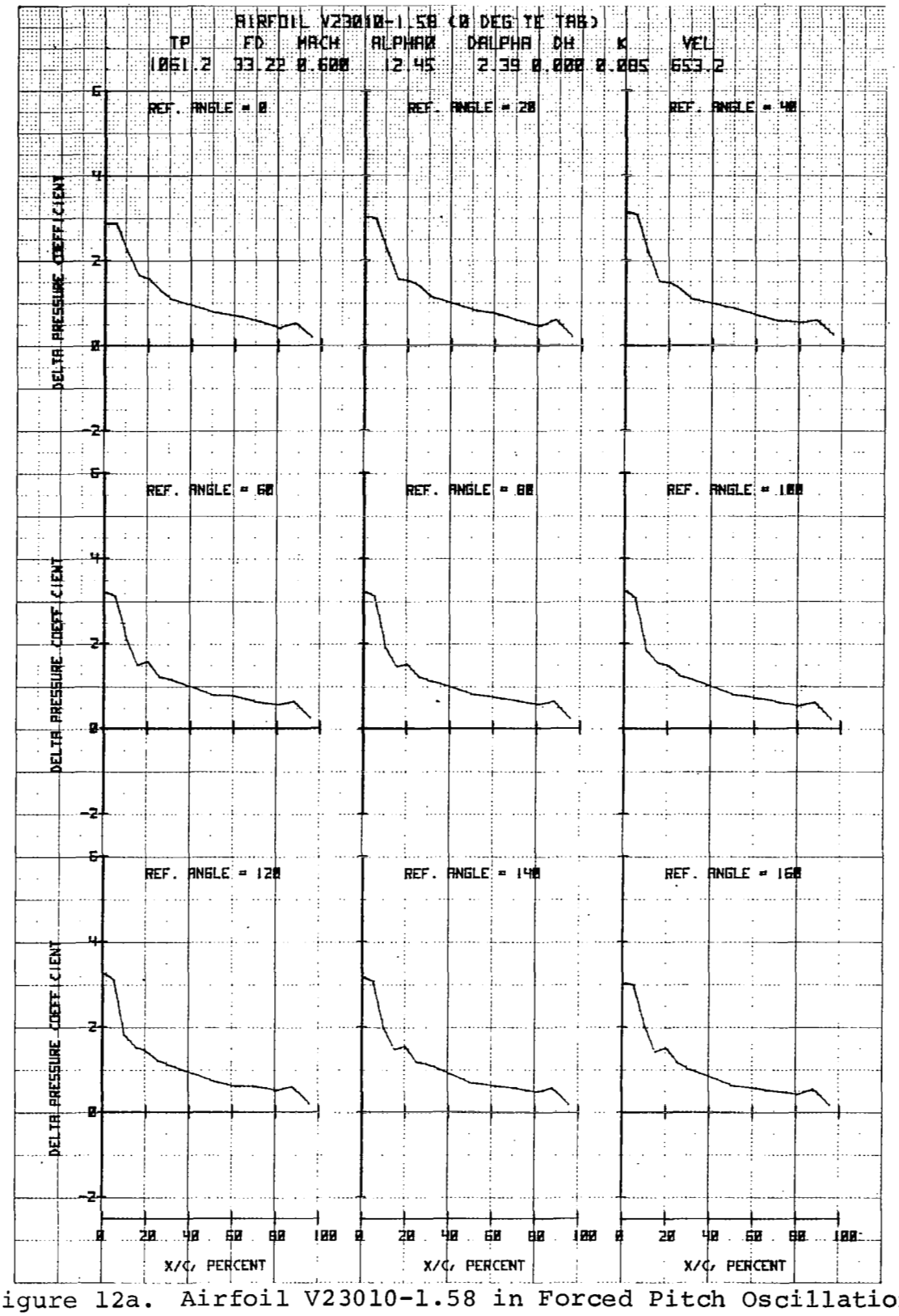

Figure 12a. Airfoil V23010-1.58 in Forced Pitch Oscillation

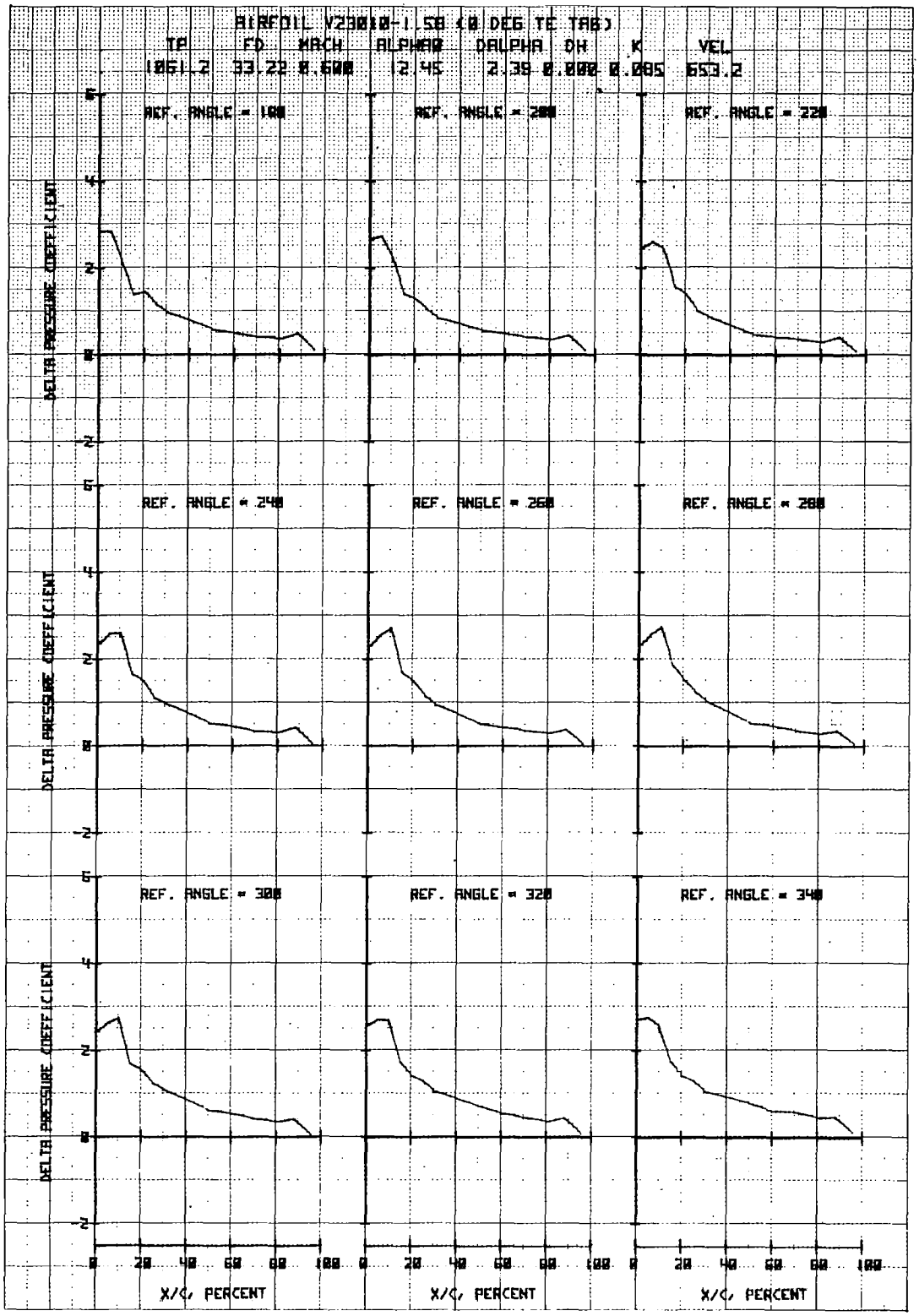

Figure 12b. Airfoil V23010-1.58 in Forced Pitch Oscillation

AIRFOIL V23010-1.58 (0 DEG TE TAB)

TP	FD	MACH	α_o	$\Delta\alpha$	Δh	k	VEL
4032.3	15.13	0.400	12.53	0.00	0.616	0.058	434.1

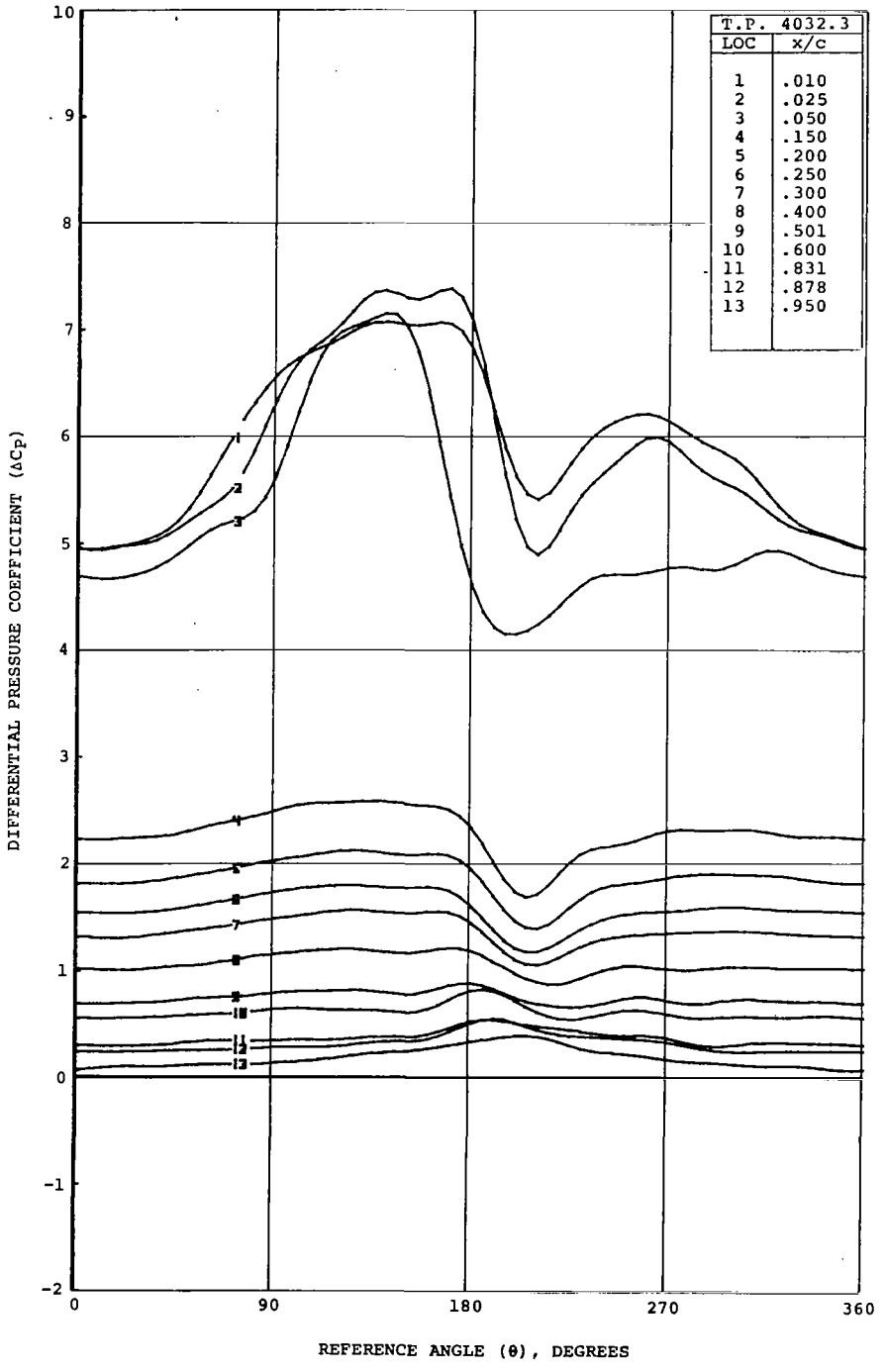

Figure 13. Airfoil V23010-1.58 in Vertical Translation at M = 0.4, Δh = 0.616, α_o = 12.5°, and f_D = 15.0 Hz

AIRFOIL V23010-1.58 (0 DEG TE TAB)

TP	FD	MACH	α_o	$\Delta\alpha$	Δh	k	VEL
4028.3	30.96	0.400	12.46	0.00	0.306	0.121	428.1

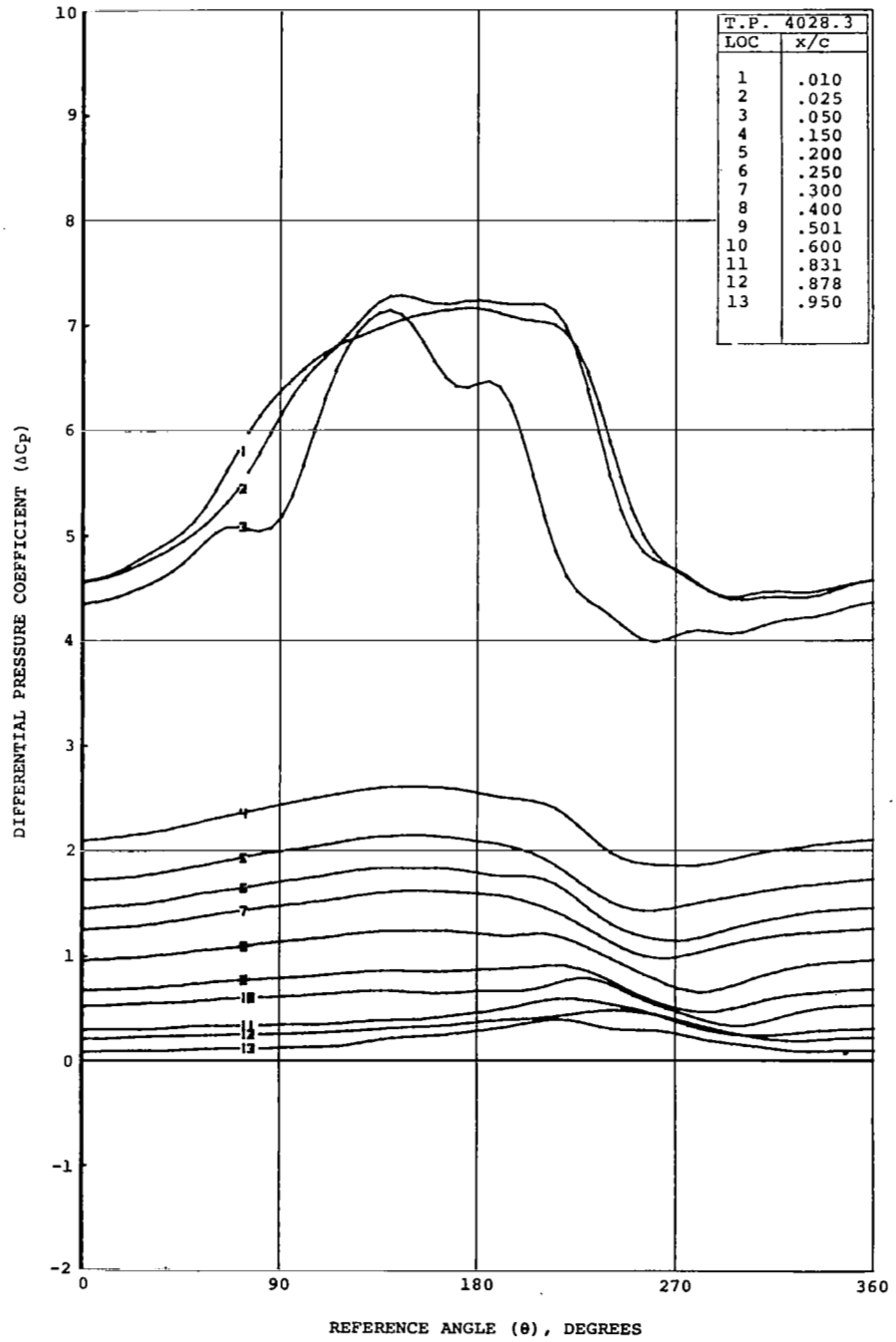

Figure 14. Airfoil V23010-1.58 in Vertical Translation at M = 0.4, Δh = 0.306, α_o = 12.5°, and f_D = 31.0 Hz

AIRFOIL V23010-1.58 (0 DEG TE TAB)

TP	FD	MACH	α_o	$\Delta\alpha$	Δh	k	VEL
4041.1	30.12	0.400	12.45	0.00	0.472	0.116	435.5

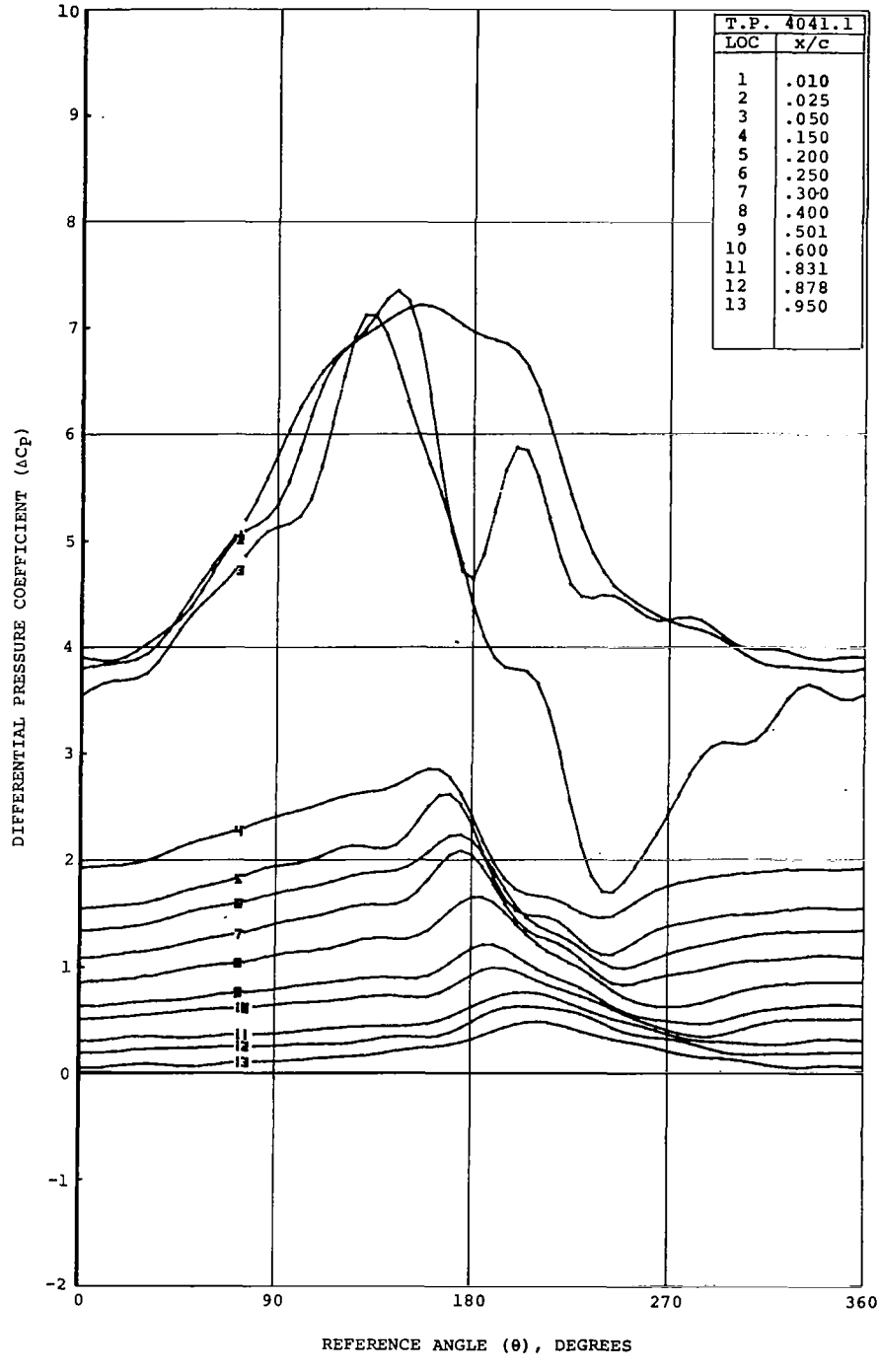

Figure 15. Airfoil V23010-1.58 in Vertical Translation at M = 0.4, Δh = 0.472, α_o = 12.5°, and f_D = 30.0 Hz

AIRFOIL V23010-1.58 (0 DEG TE TAB)

TP	FD	MACH	α_o	$\Delta\alpha$	Δh	k	VEL
4041.2	32.79	0.400	14.88	0.00	0.472	0.126	434.5

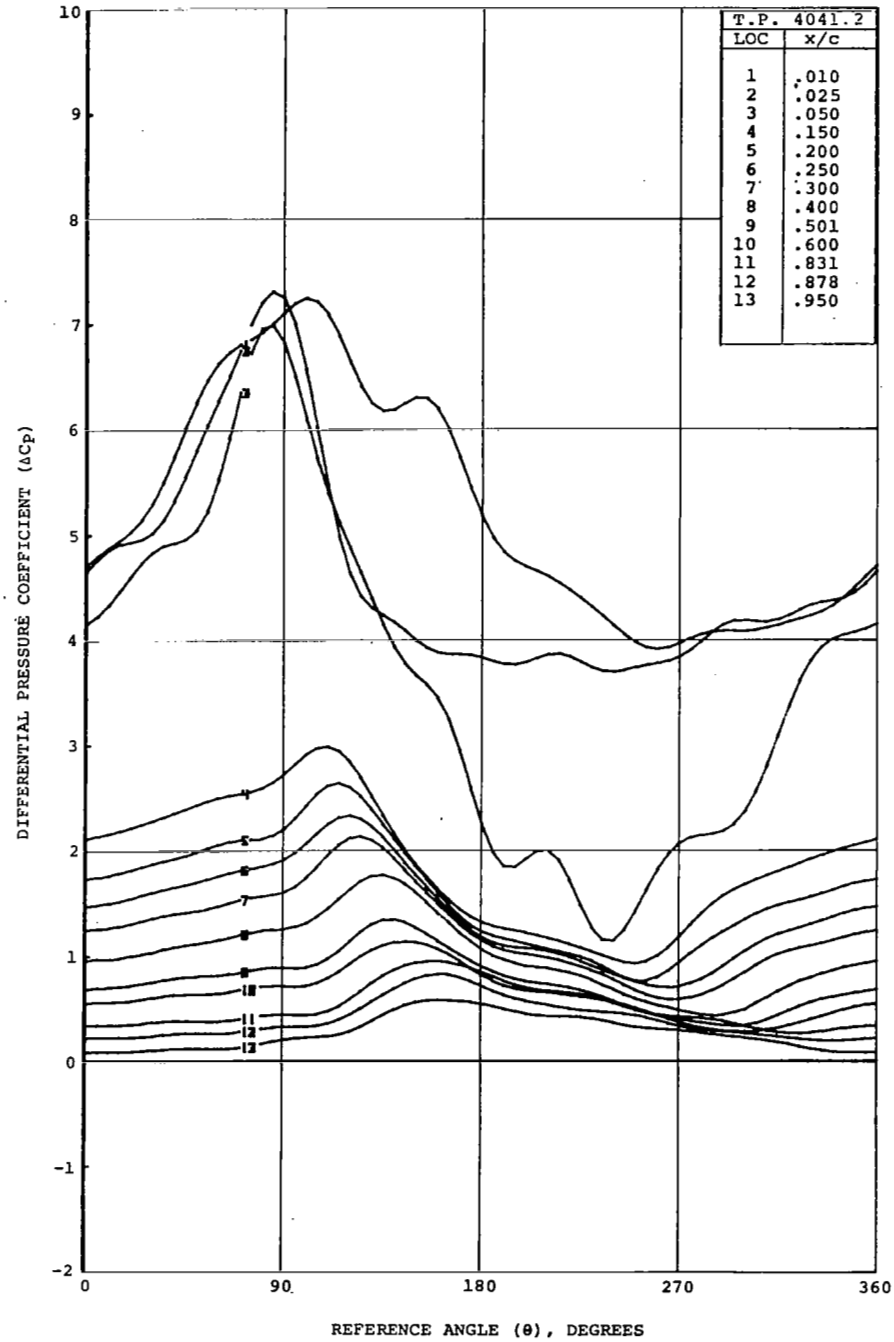

Figure 16. Airfoil V23010-1.58 in Vertical Translation at M = 0.4, Δh = 0.472, α_o = 15.0°, and f_D = 33.0 Hz

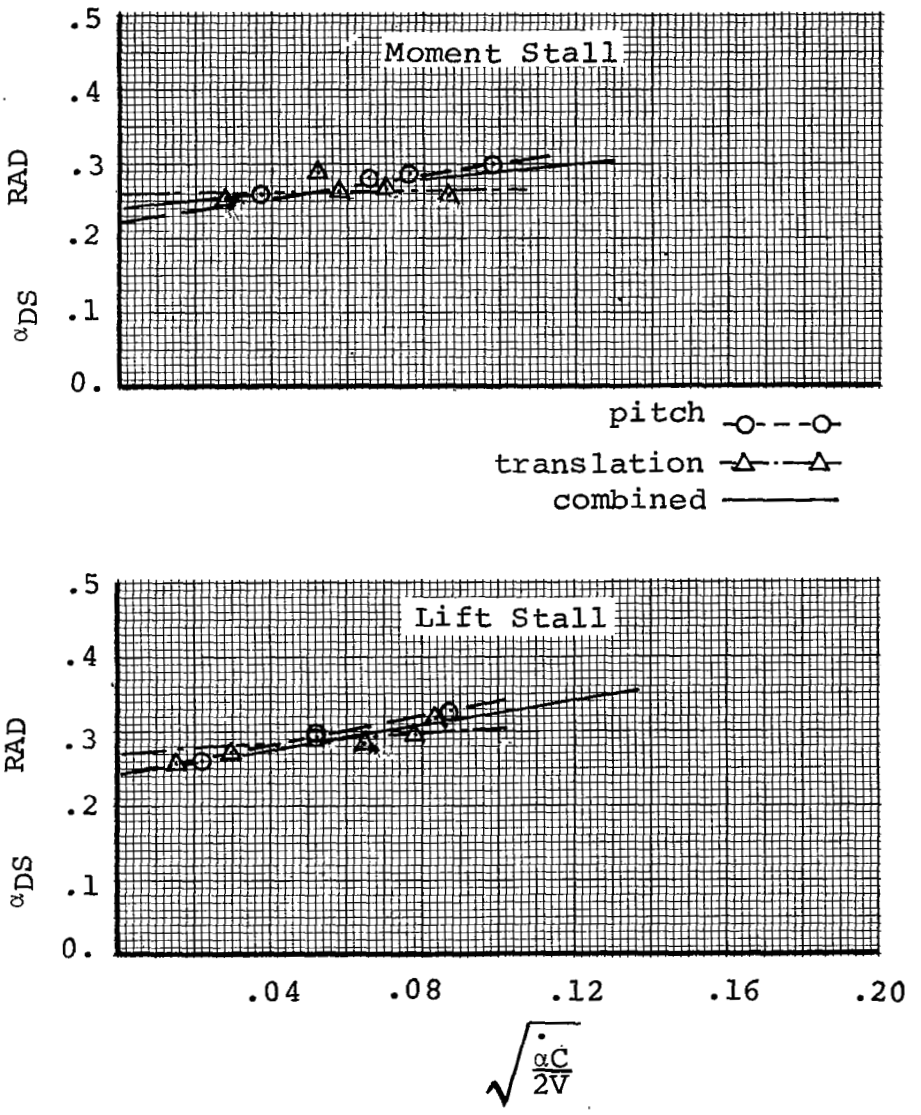

Figure 17. Dynamic Stall Boundaries V23010-1.58 Airfoil Mach No. = 0.4

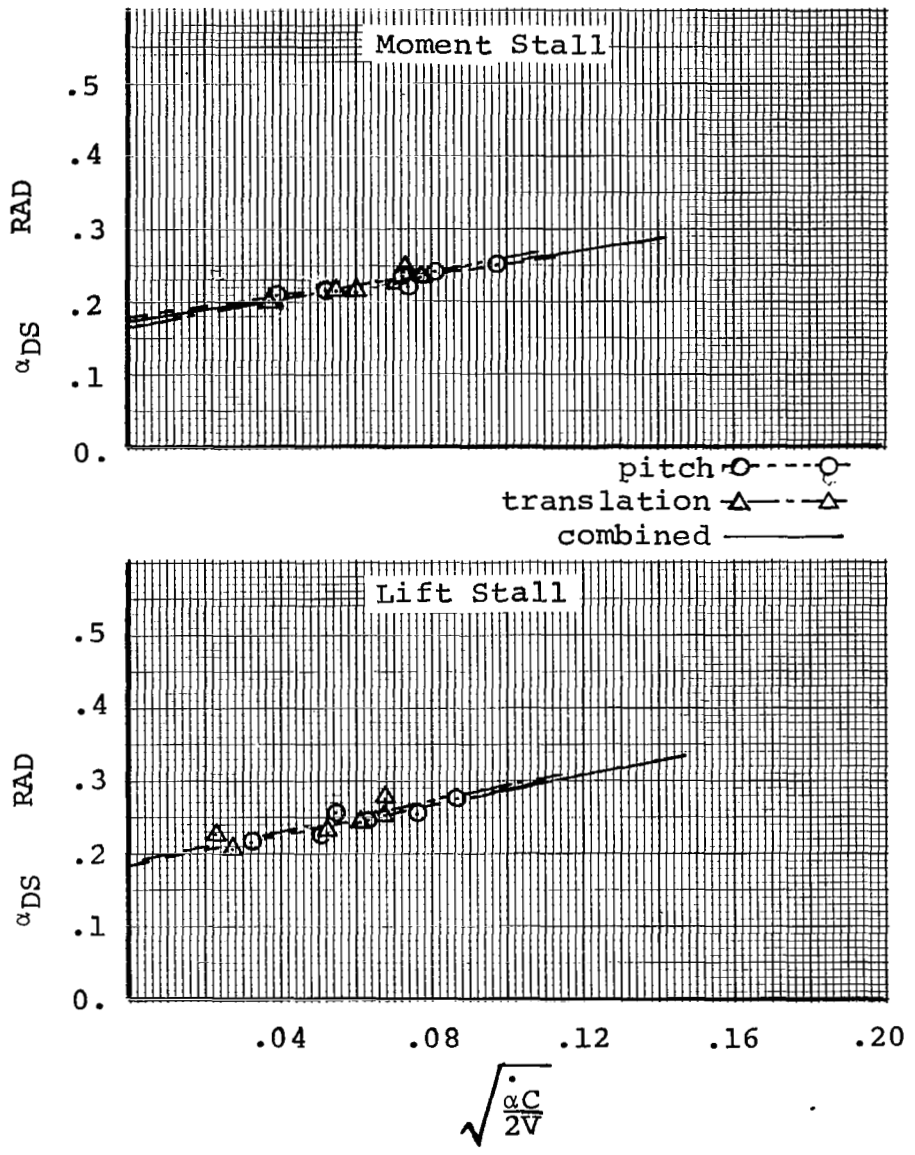

Figure 18. Dynamic Stall Boundaries V0012 Airfoil Mach No. = 0.4

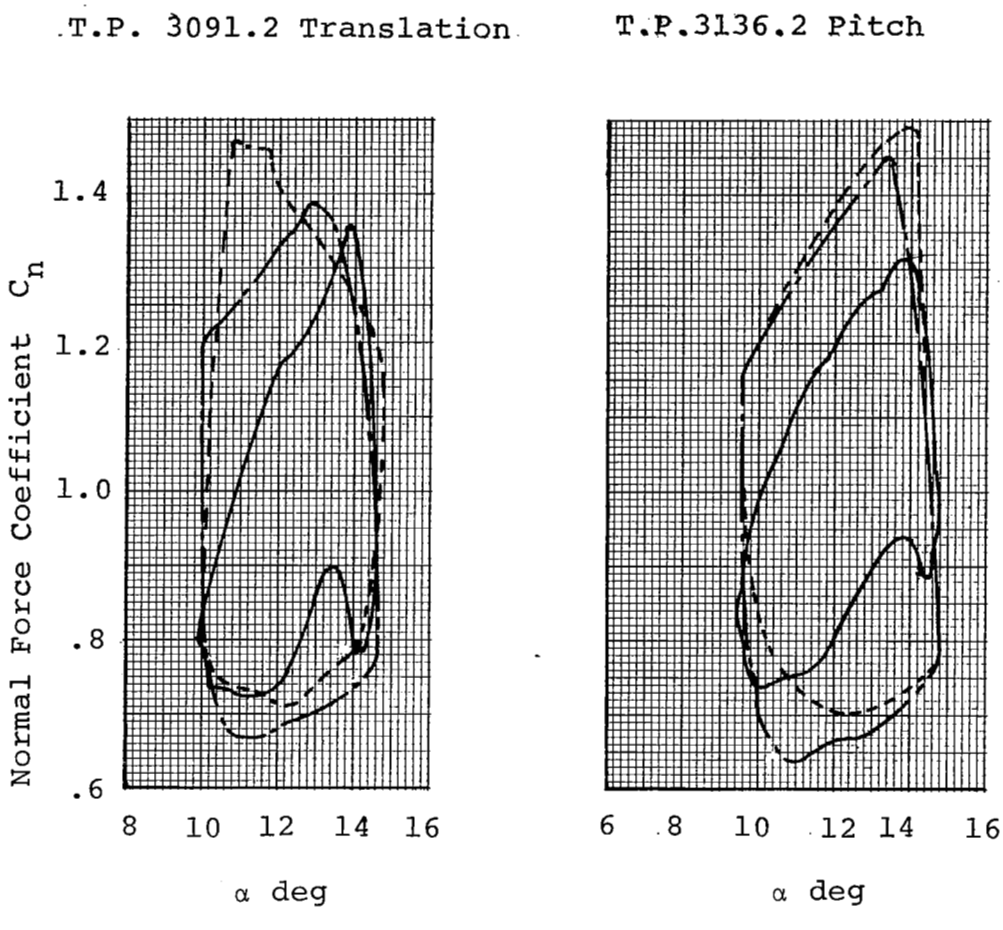

Figure 19. Comparison of Synthesized Lift Stall Loops for V0012 Airfoil M= 0.4

APPENDIX

1. Time histories of C_n and C_m
2. C_n and C_m vs angle of attack (loops)
3. Pressure time histories
4. Pressure distributions at $\Delta\theta = 20°$

SYMBOLS

TP	test point number
FD	drive frequency, Hz
MACH	Mach number
ALPHAO	mean angle of attack (α_o), deg
DALPHA	magnitude of the forced pitching motion ($\Delta\alpha$), deg
DH	magnitude of forced translation, feet
K	reduced frequency
VEL	freestream velocity, ft/sec

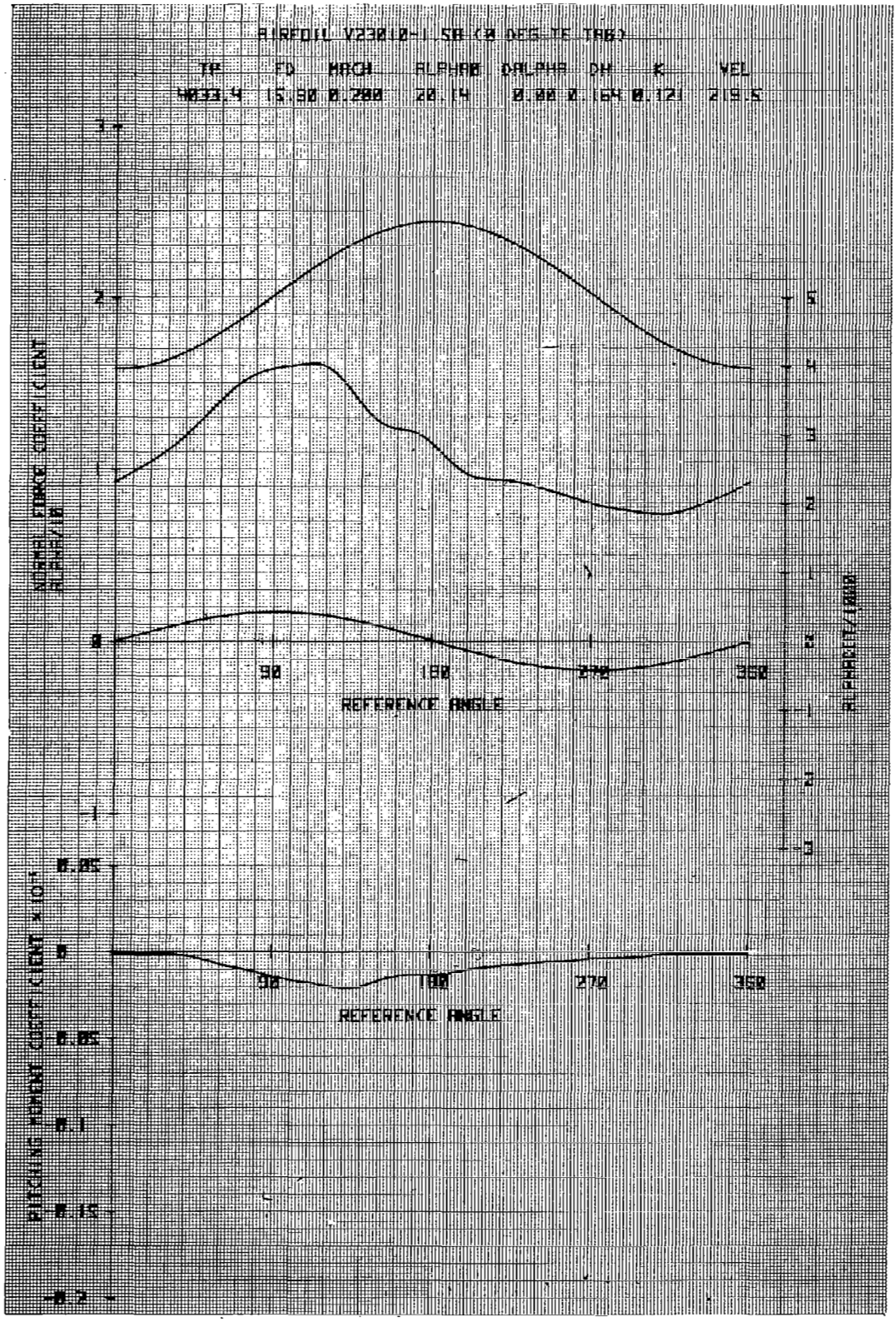

Figure 20a. Airfoil V23010-1.58 in Vertical Translation

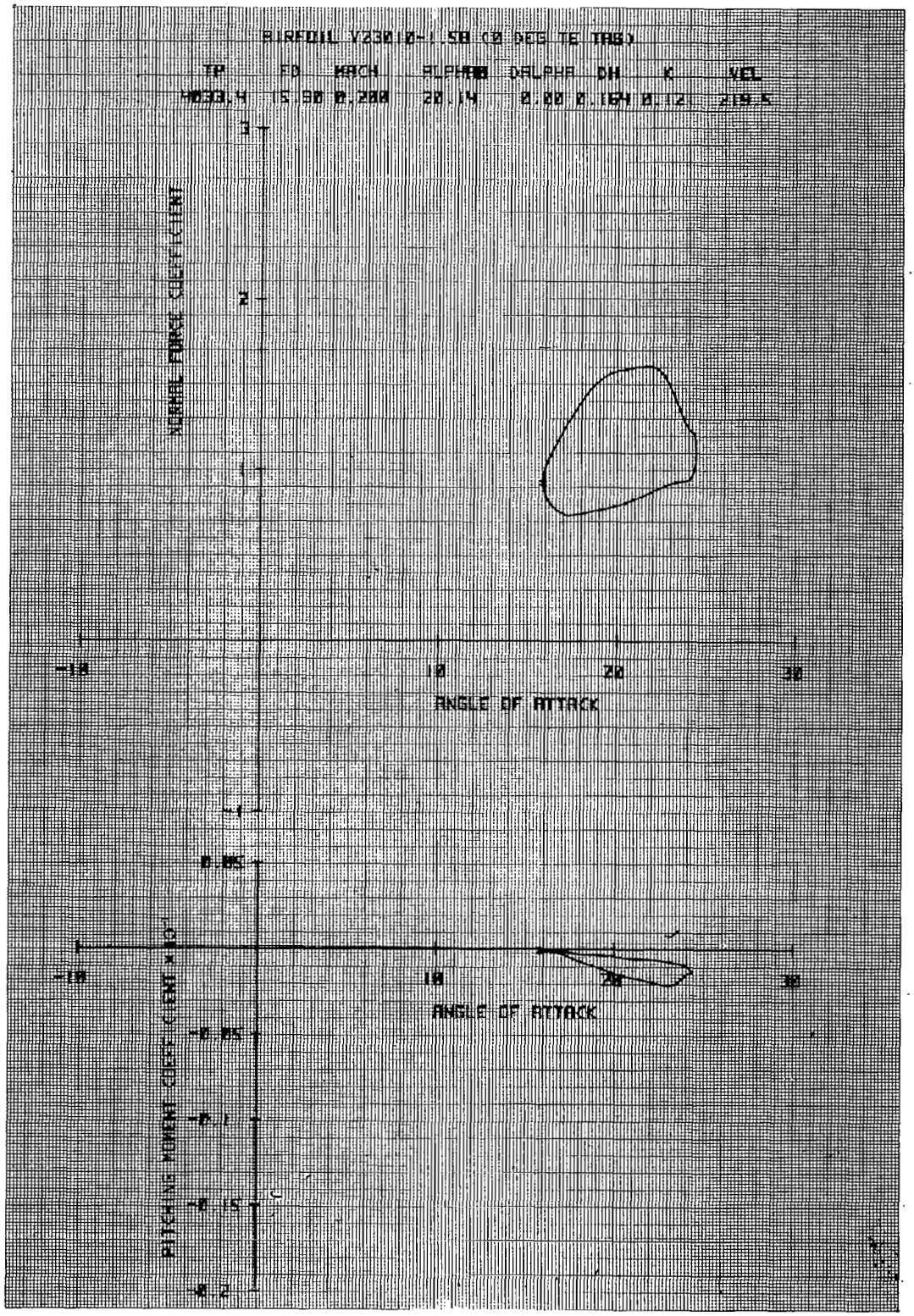

Figure 20b. Airfoil V23010-1.58 in Vertical Translation

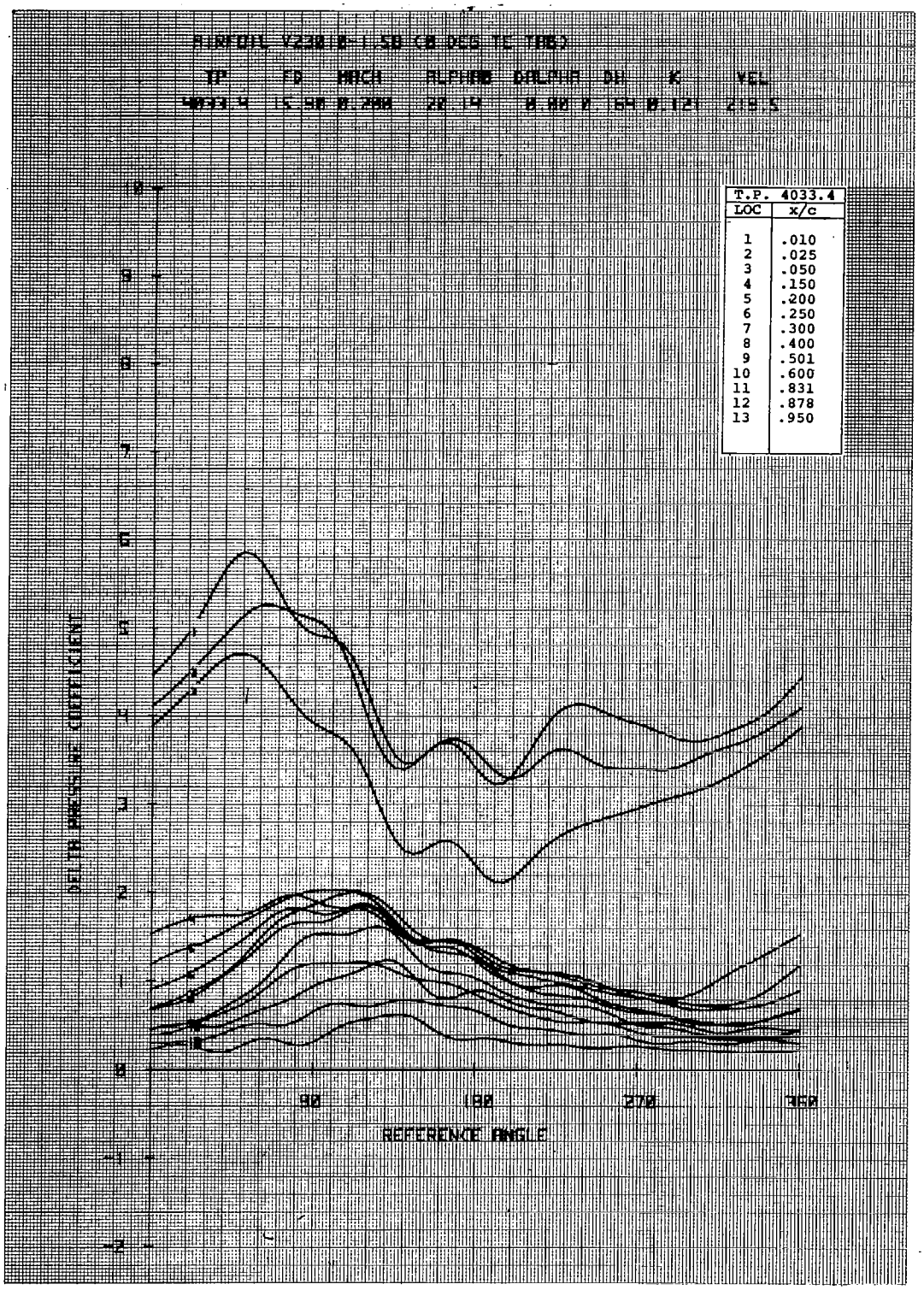

Figure 20c. Airfoil V23010-1.58 in Vertical Translation

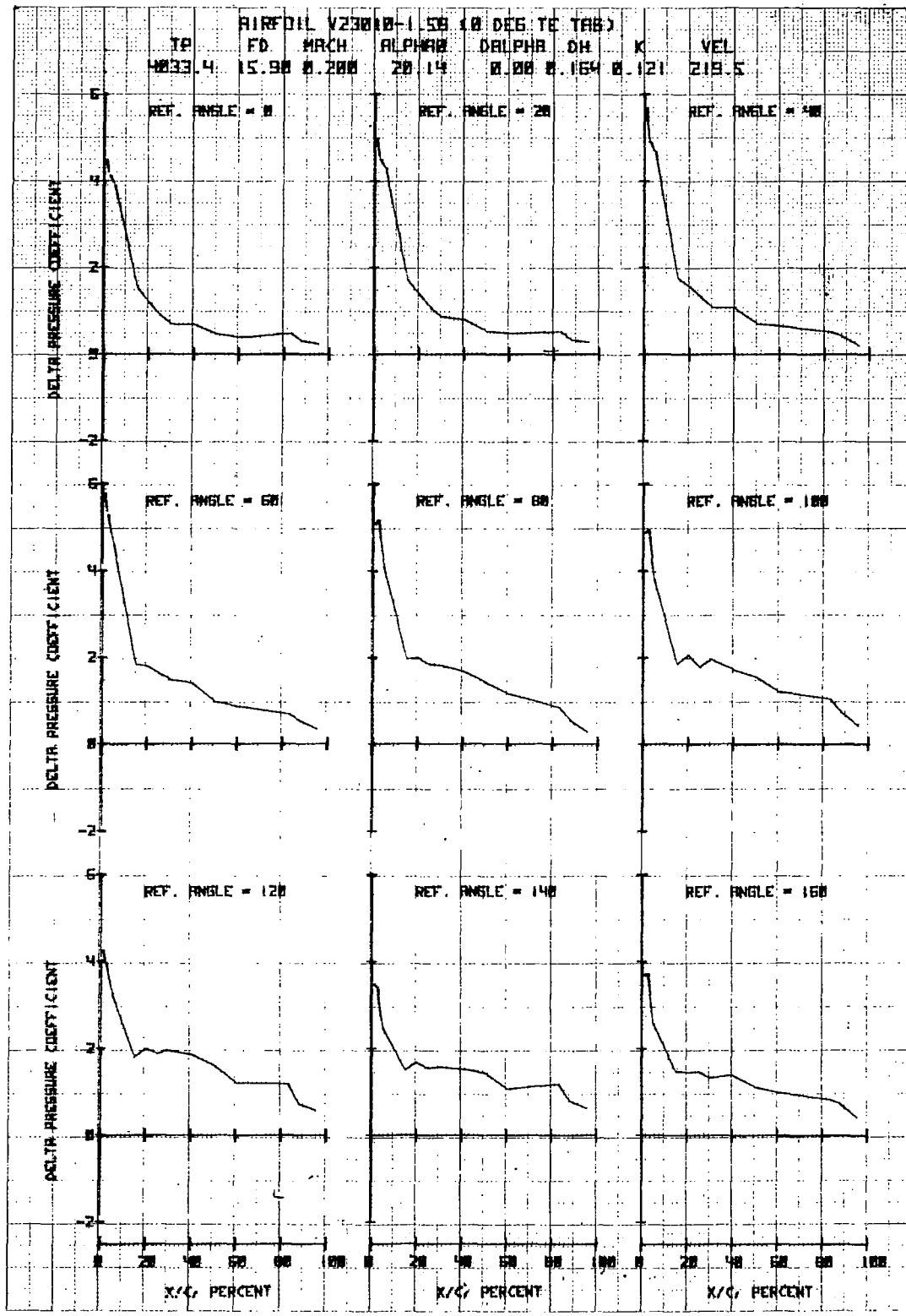

Figure 20d. Airfoil V23010-1.58 in Vertical Translation

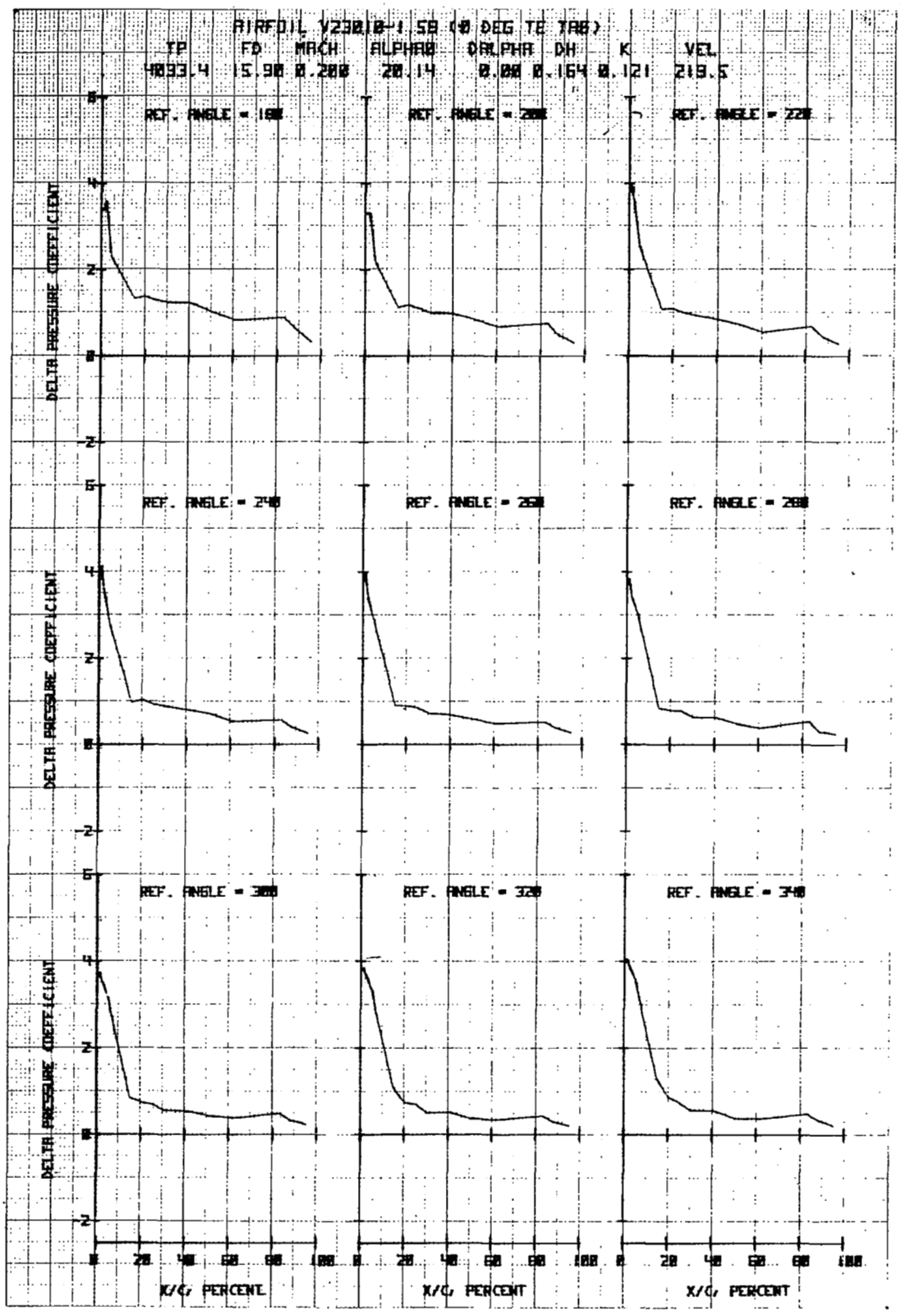

Figure 20e. Airfoil V23010-1.58 in Vertical Translation

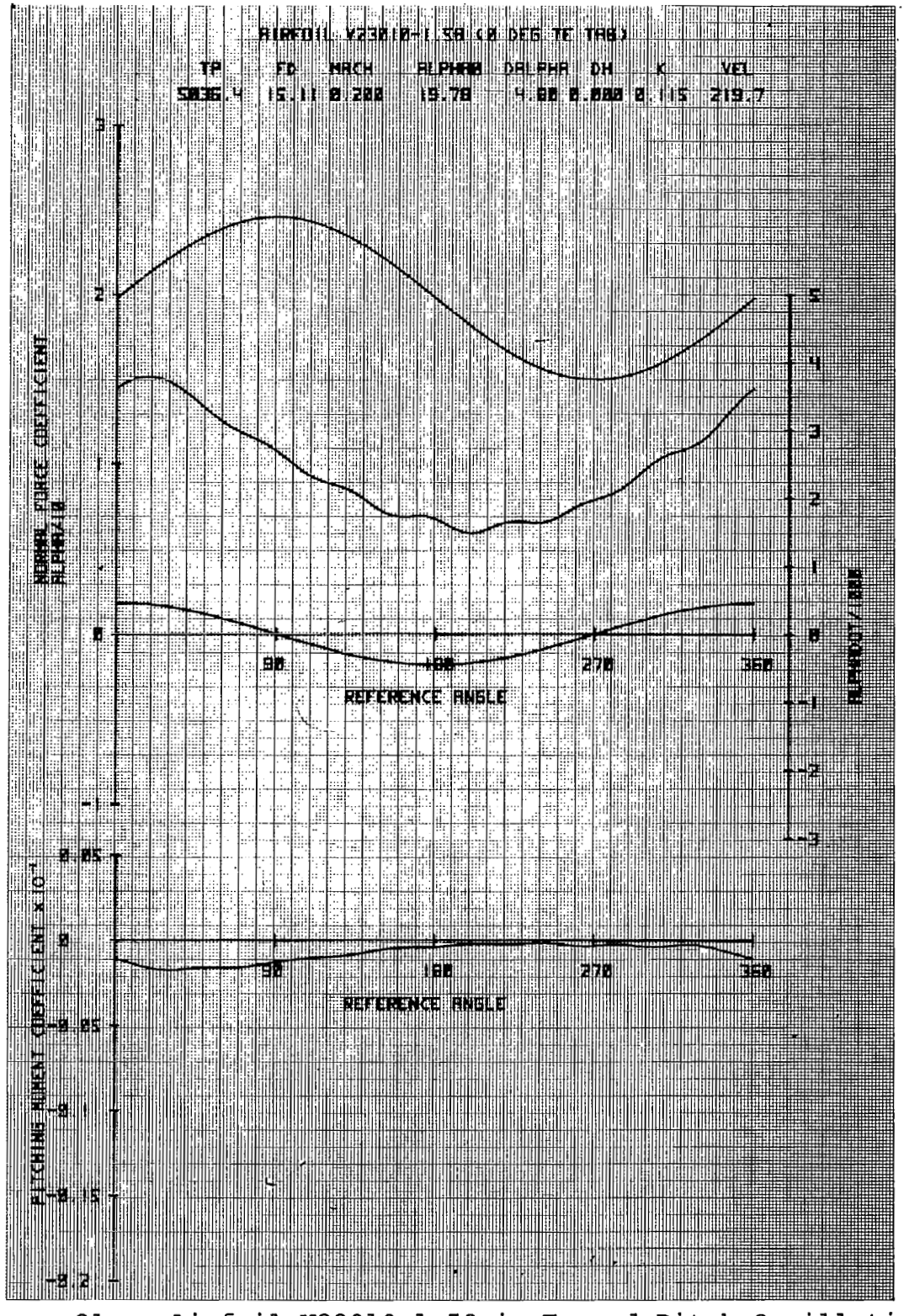

Figure 21a. Airfoil V23010-1.58 in Forced Pitch Oscillation.

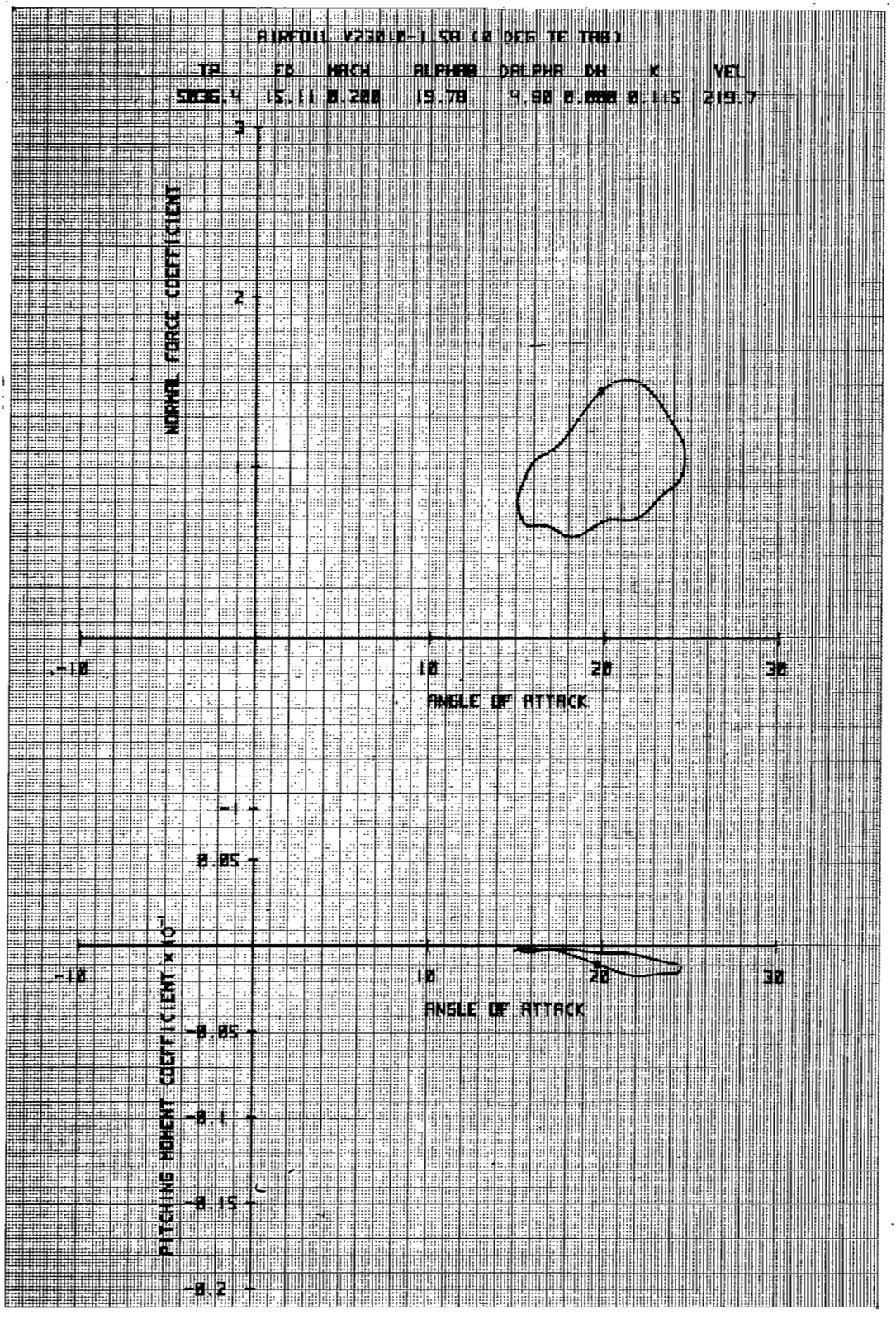

Figure 21b. Airfoil V23010-1.58 in Forced Pitch Oscillation

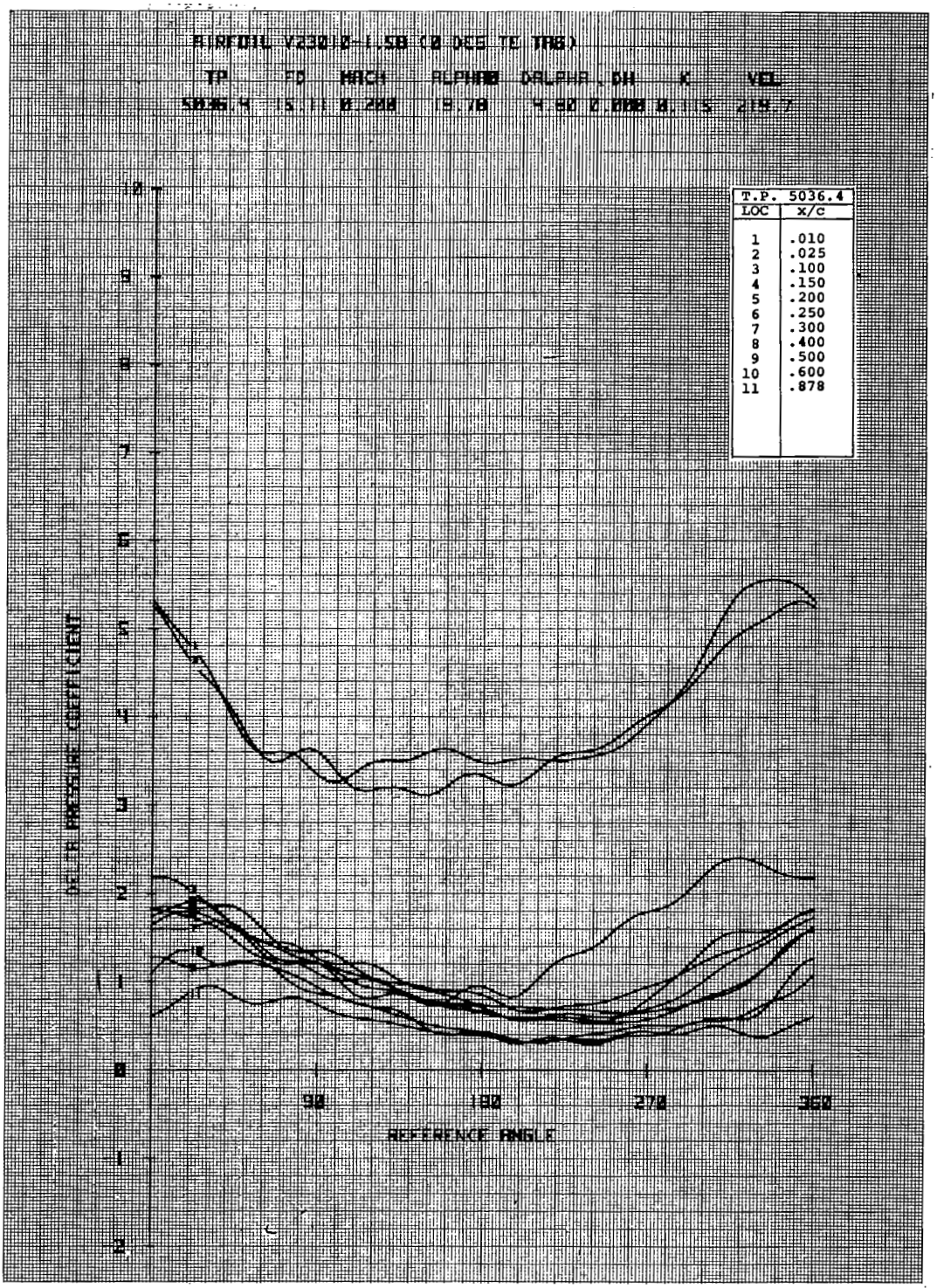

Figure 21c. Airfoil V23010-1.58 in Forced Pitch Oscillation

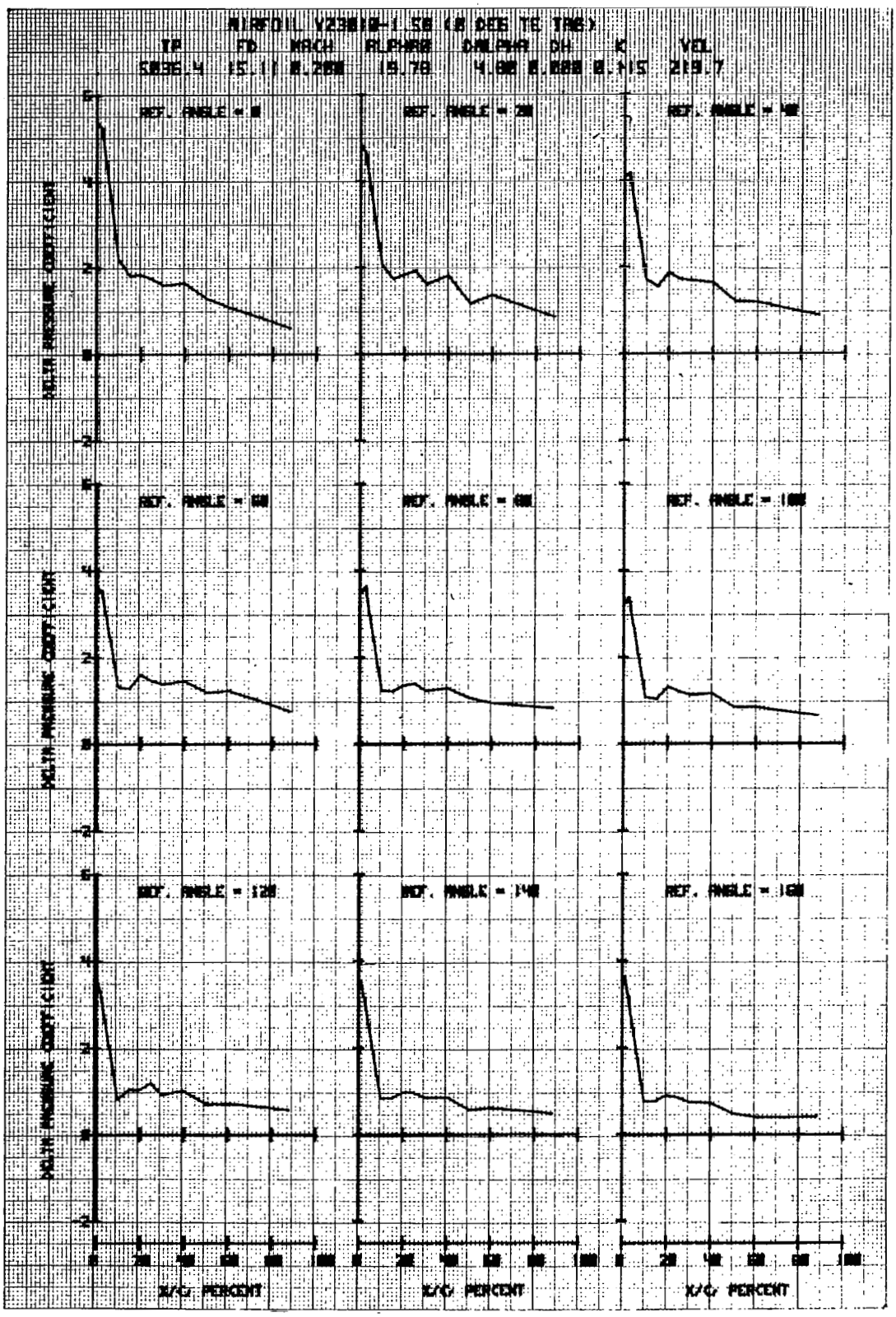

Figure 21d. Airfoil V23010-1.58 in Forced Pitch Oscillation

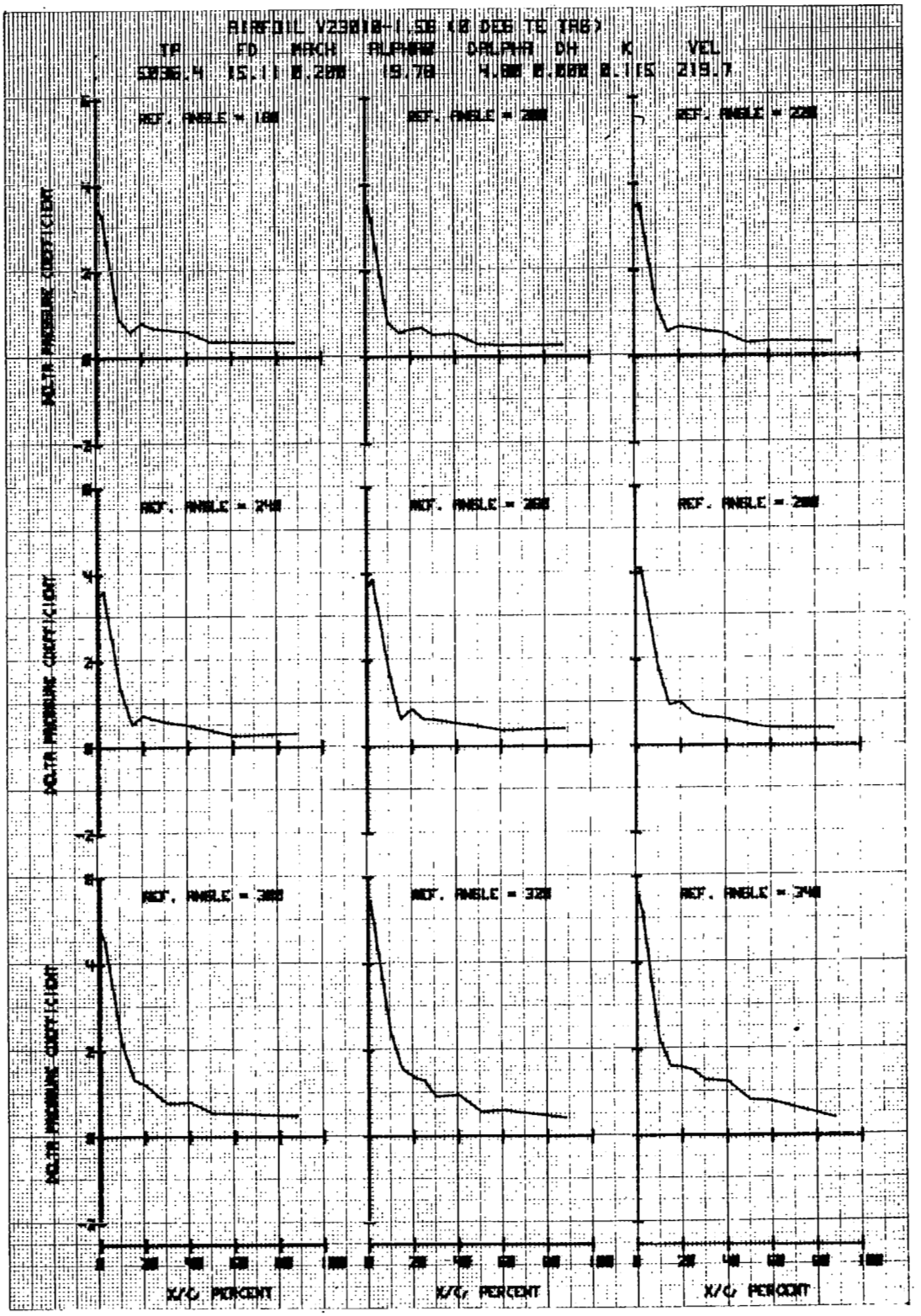

Figure 21e. Airfoil V23010-1.58 in Forced Pitch Oscillation

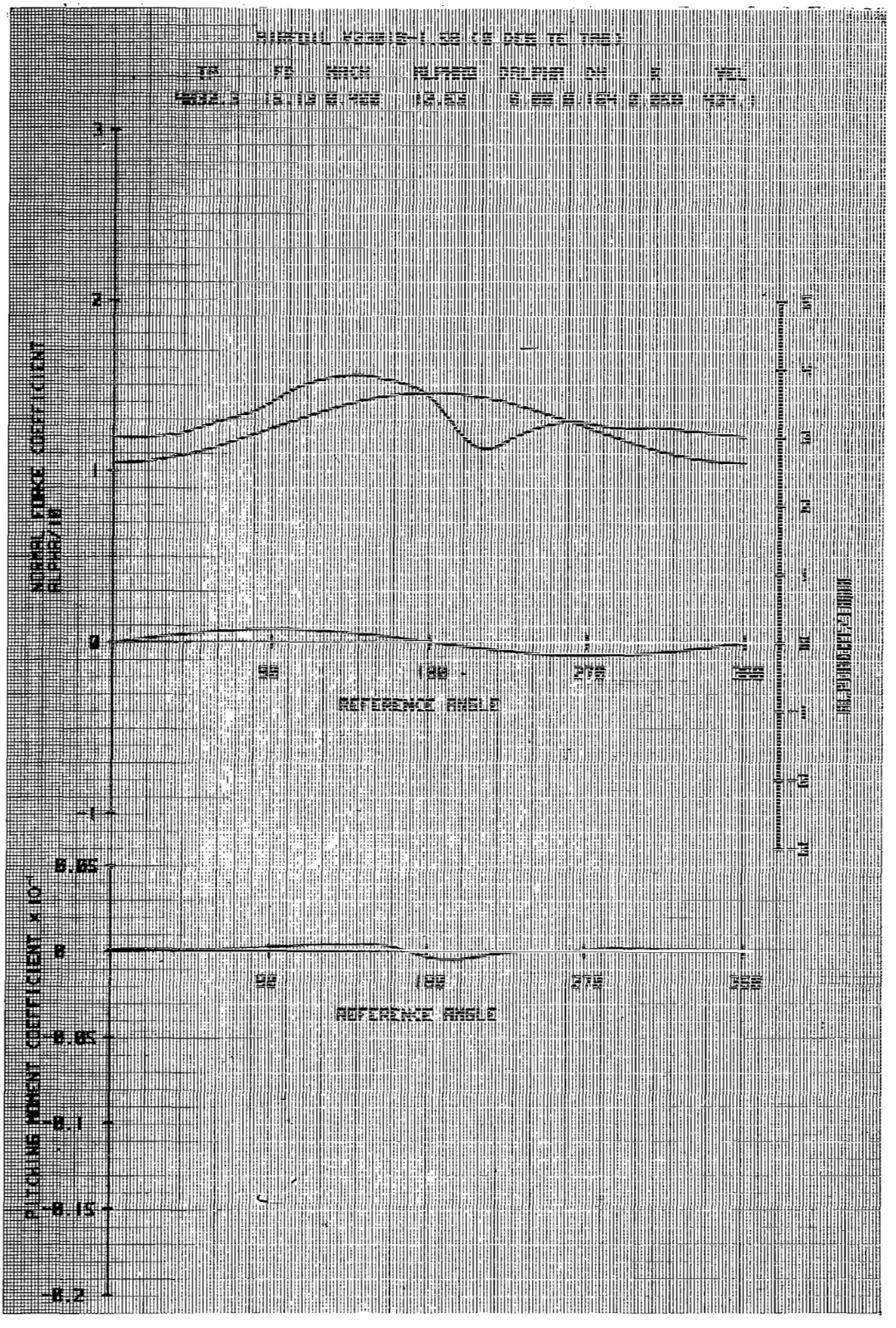

Figure 22a. Airfoil V23010.1-58 in Vertical Translation

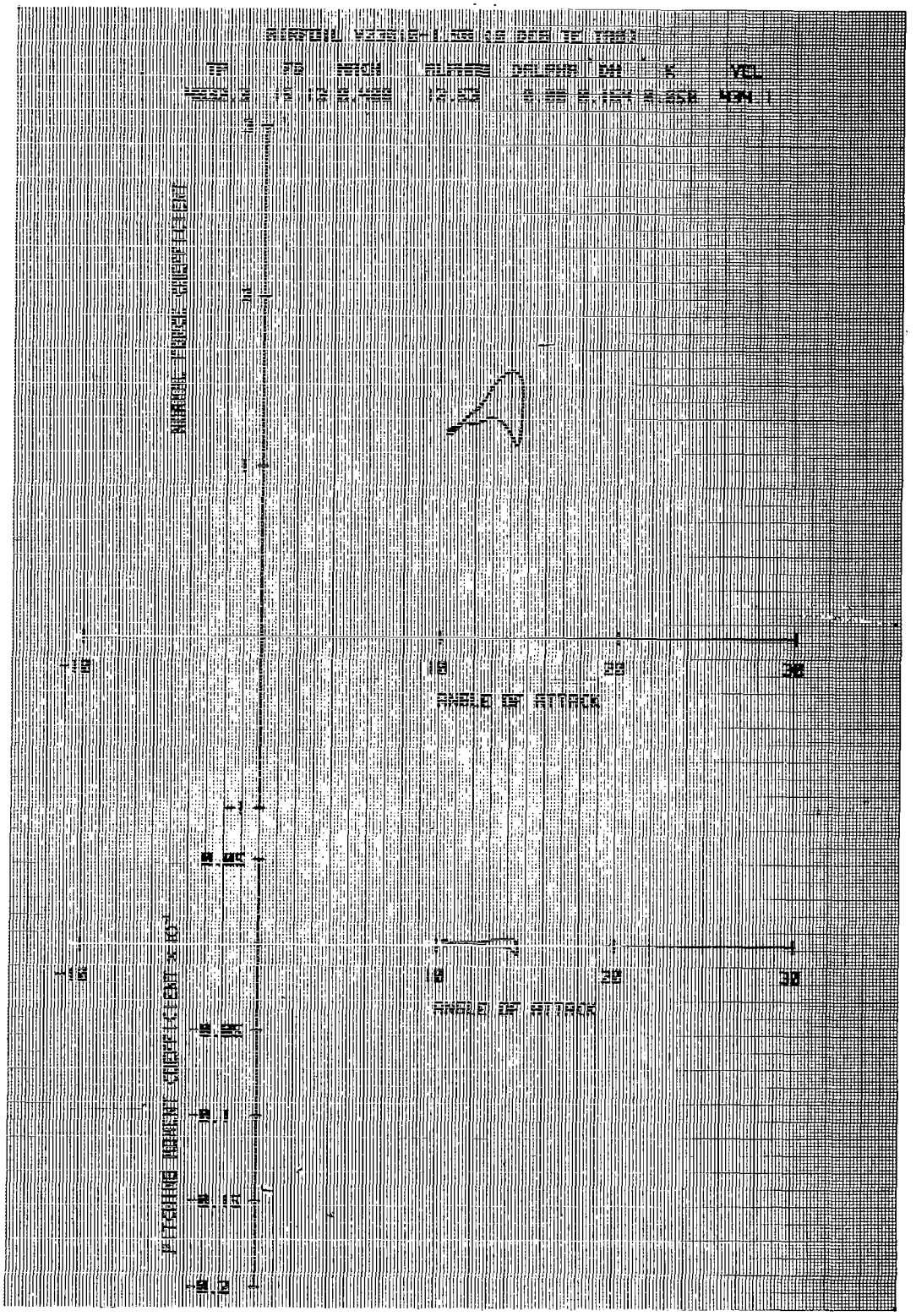

Figure 22b. Airfoil V23010-1.58 in Vertical Translation

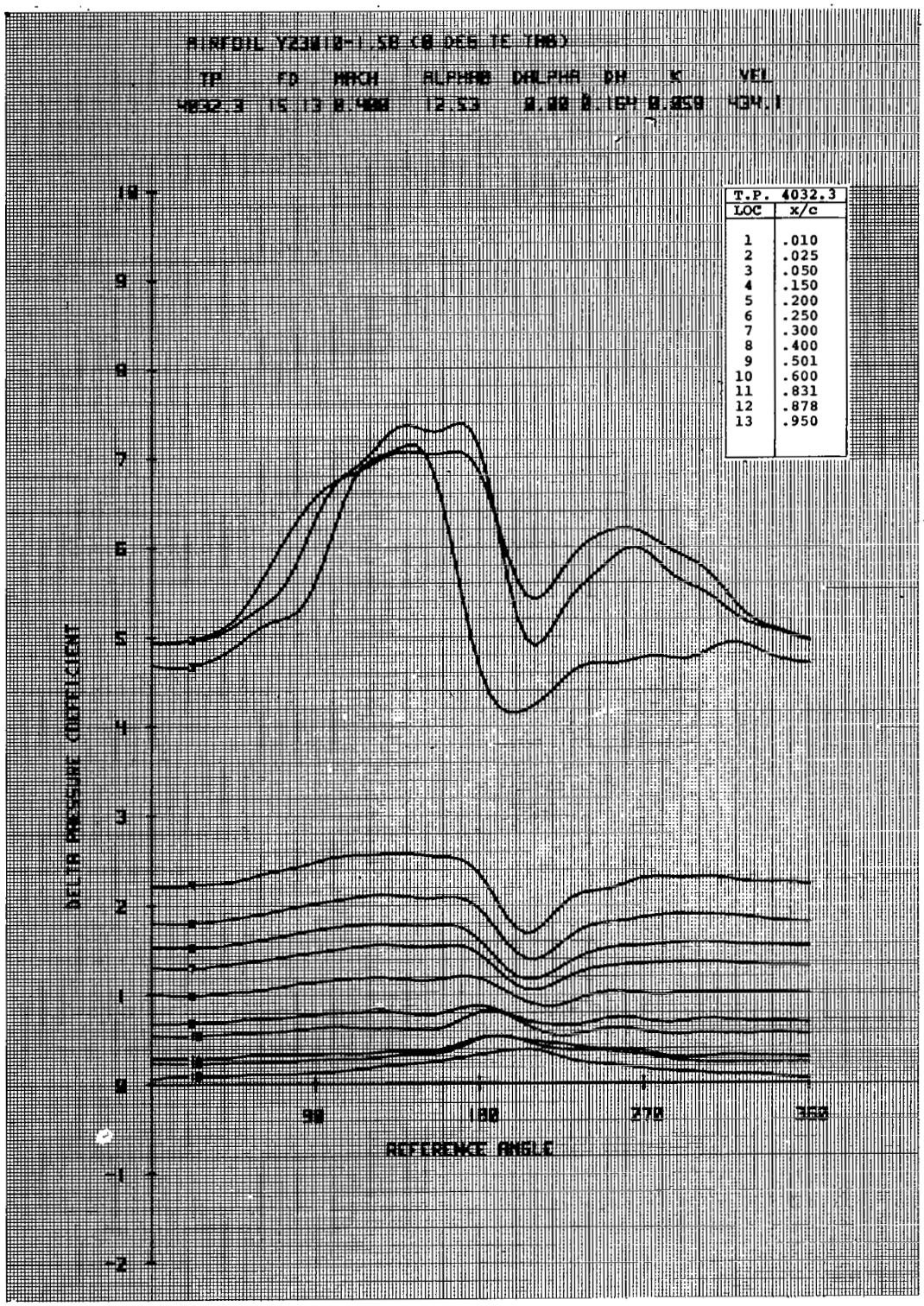

Figure 22c. Airfoil V23010-1.58 in Vertical Translation

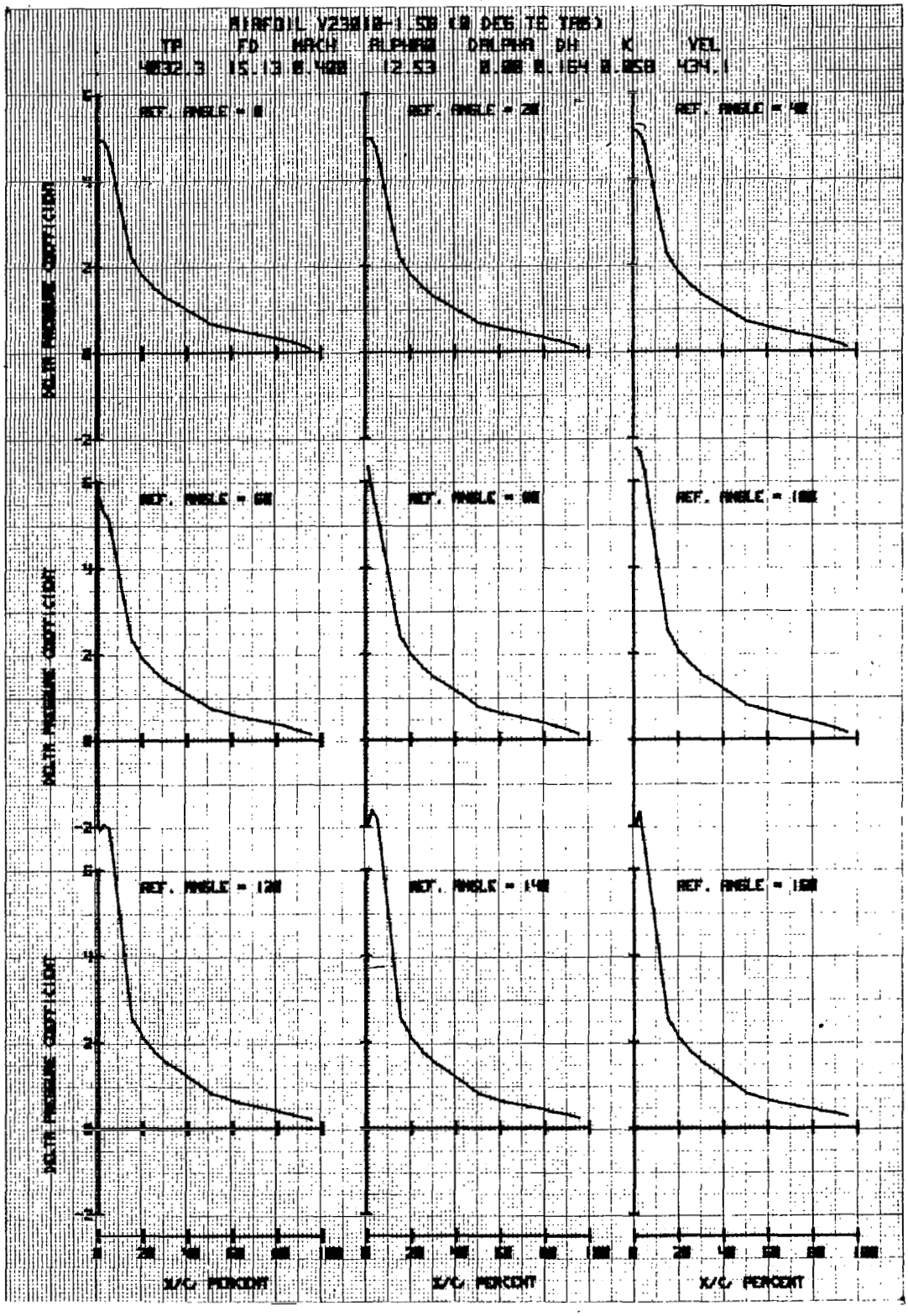

Figure 22d. Airfoil V23010-1.58 in Vertical Translation

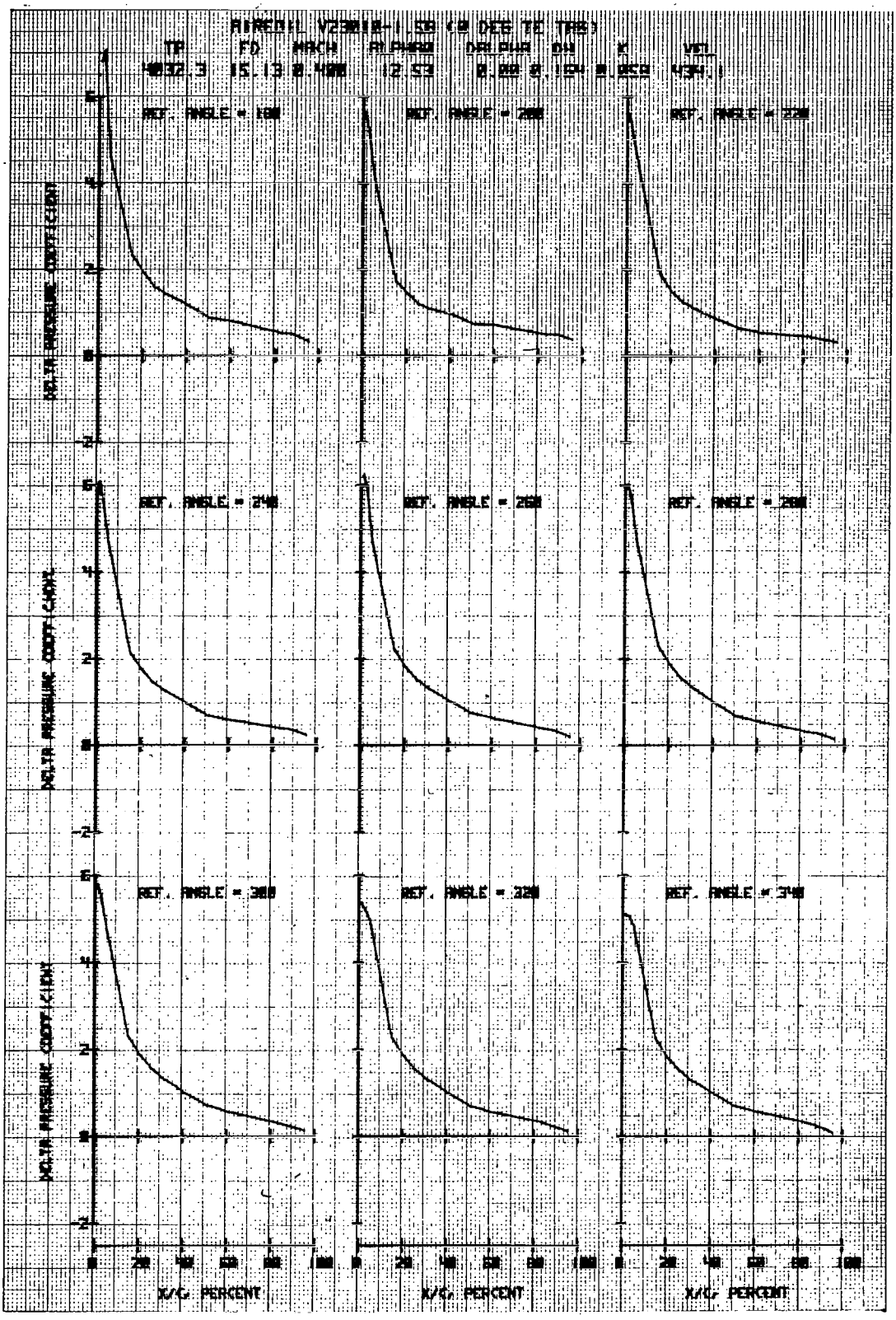

Figure 22e. Airfoil V23010-1.58 in Vertical Translation

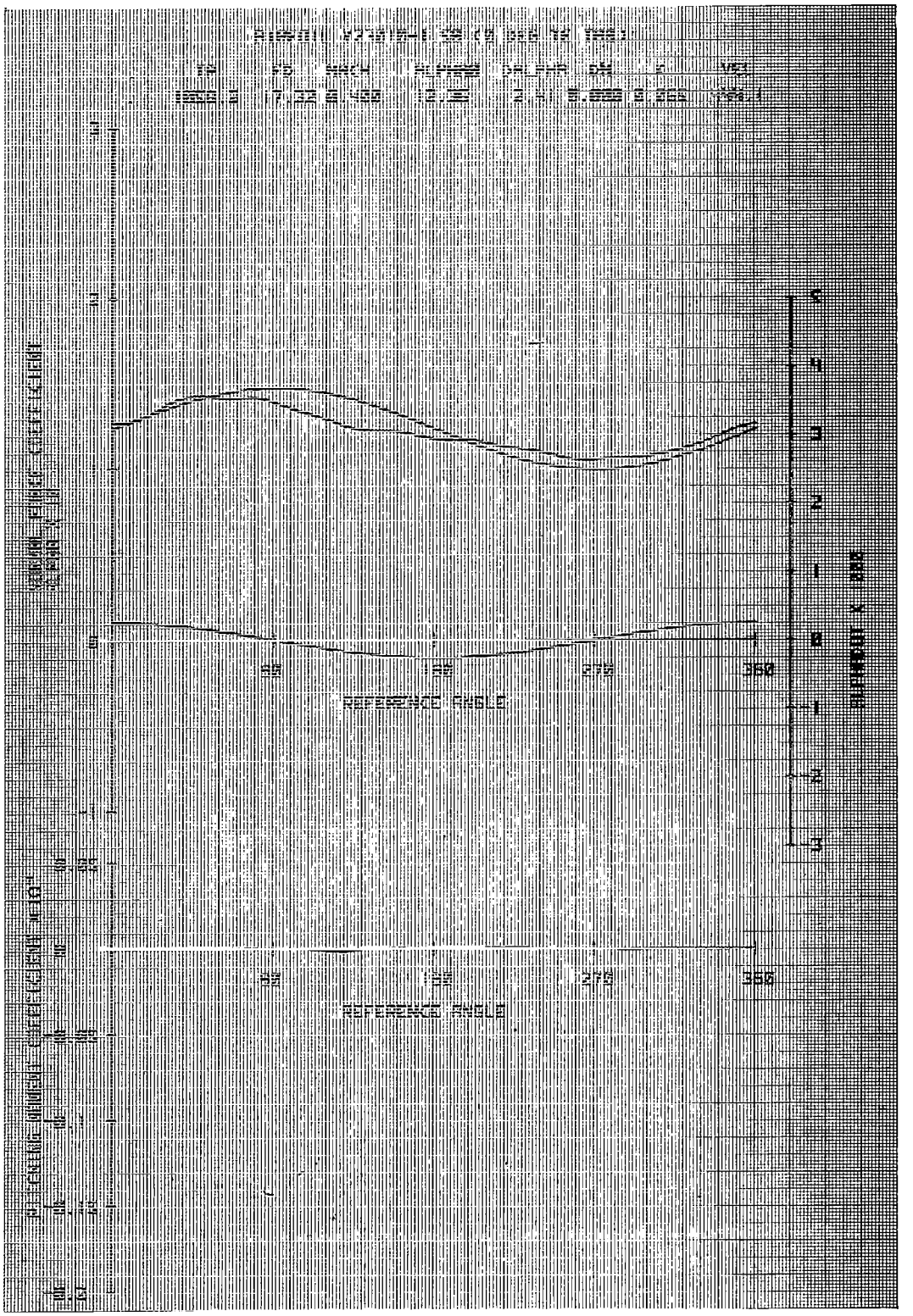

Figure 23a. Airfoil V23010-1.58 in Forced Pitch Oscillation

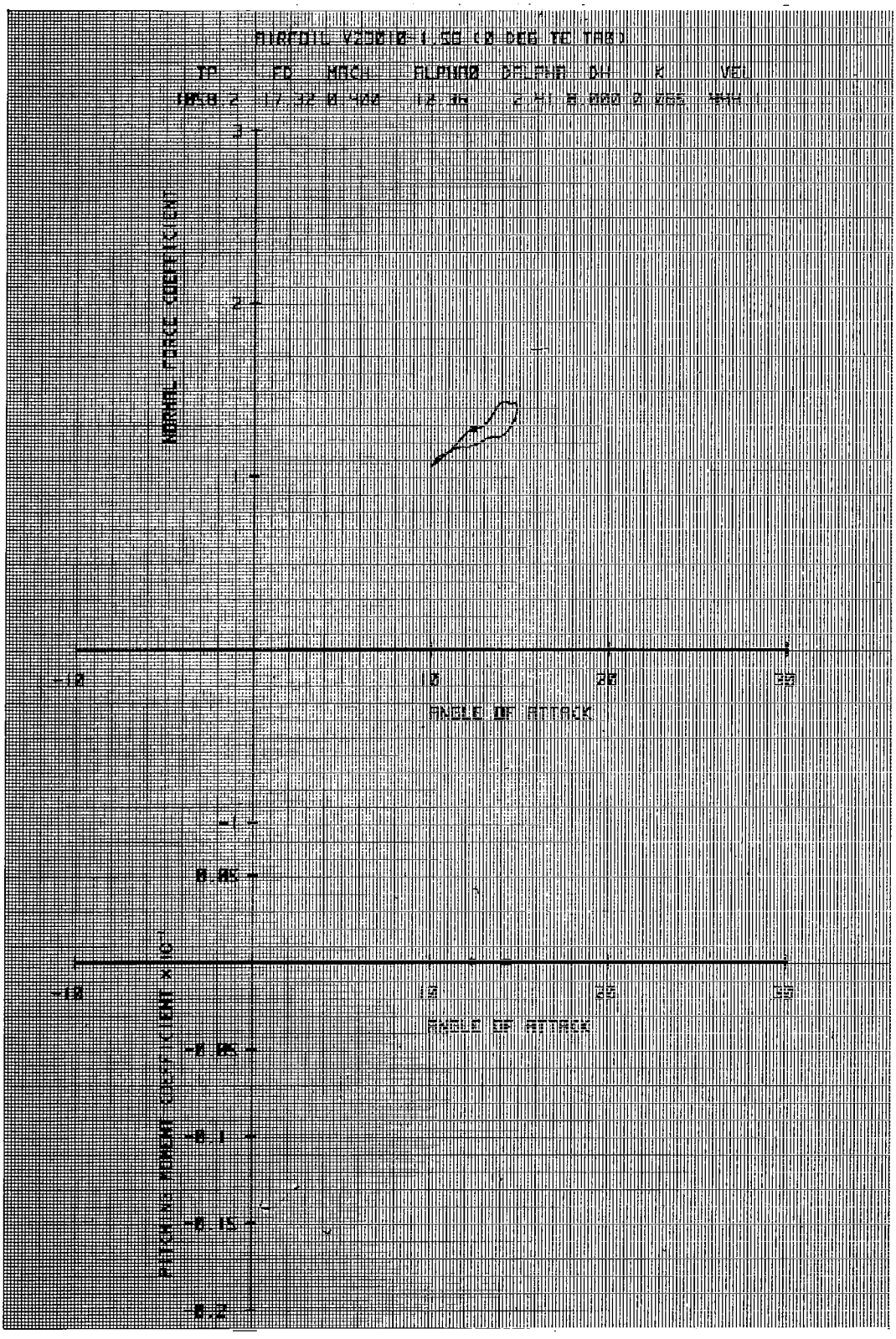

Figure 23b. Airfoil V23010-1.58 in Forced Pitch Oscillation

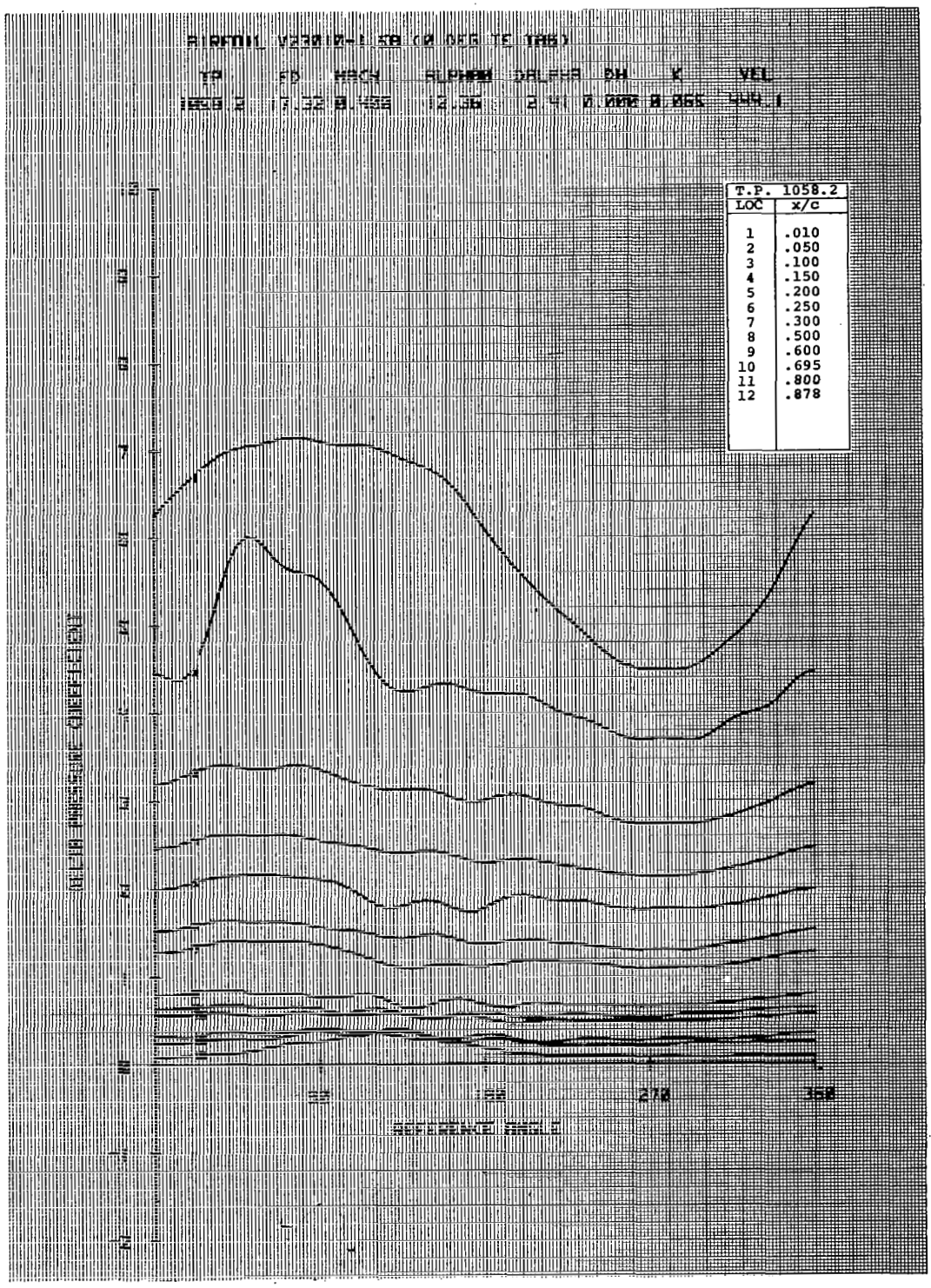

Figure 23c. Airfoil V23010-1.58 in Forced Pitch Oscillation

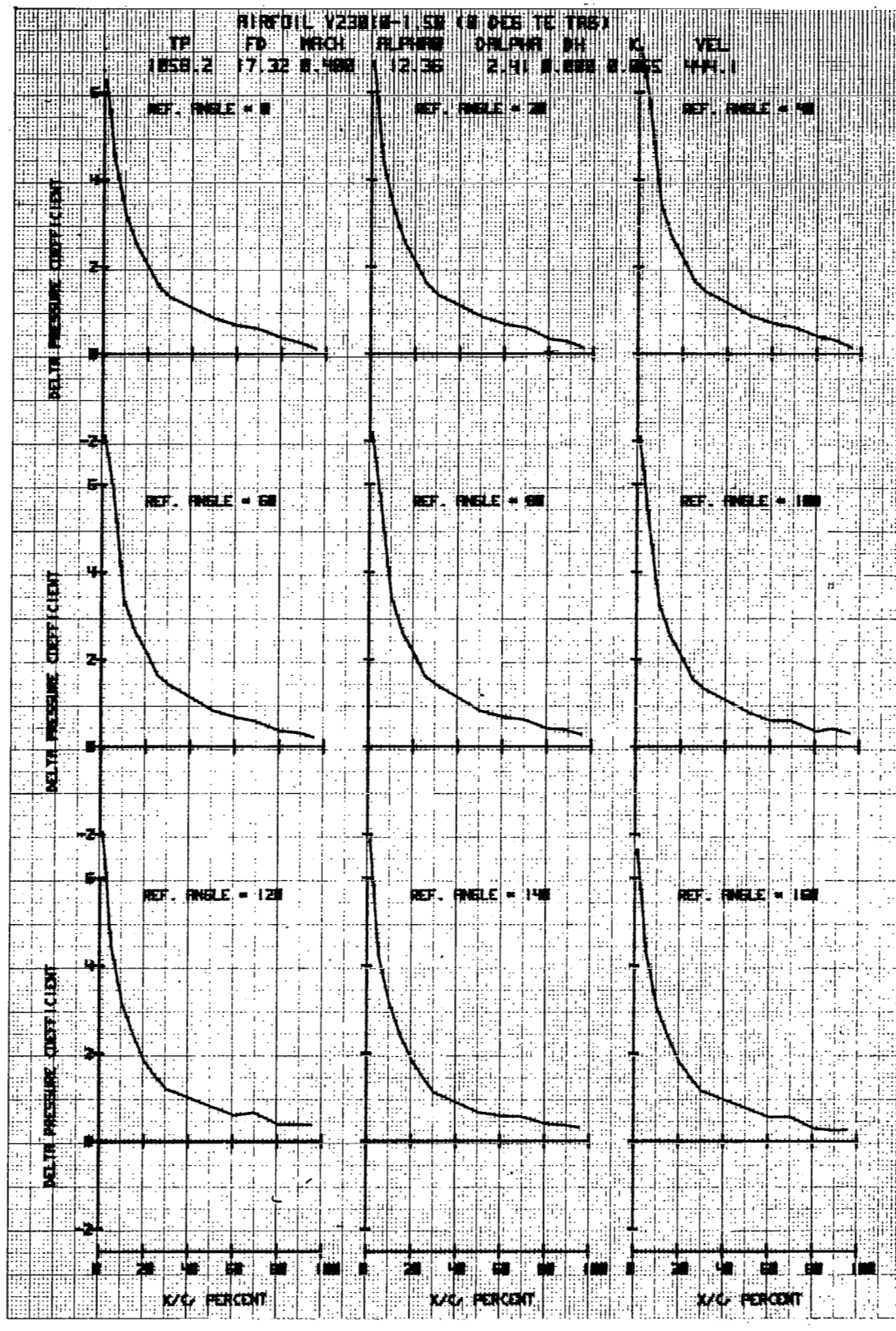

Figure 23d. Airfoil V23010-1.58 in Forced Pitch Oscillation

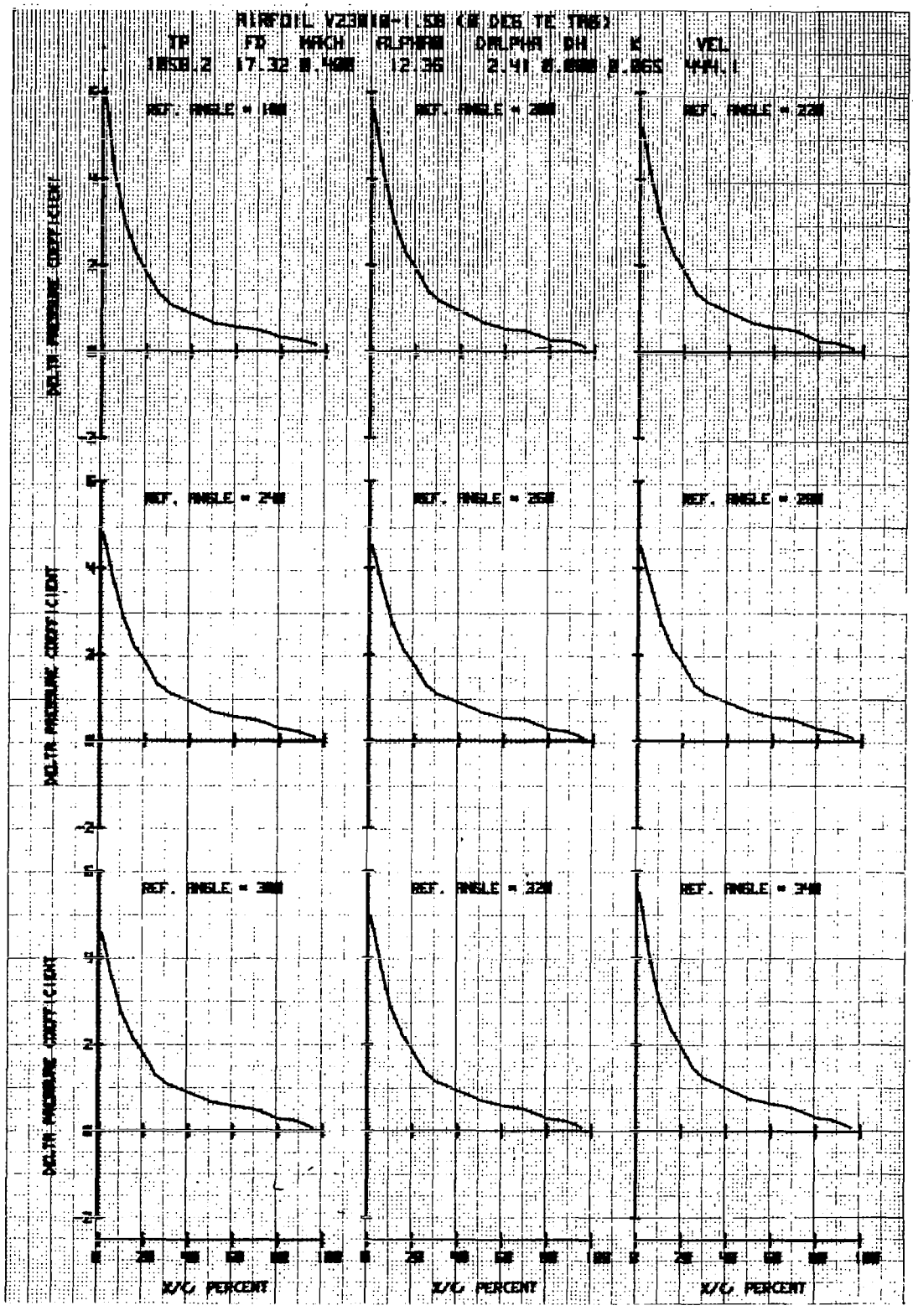

Figure 23e. Airfoil V23010-1.58 in Forced Pitch Oscillation

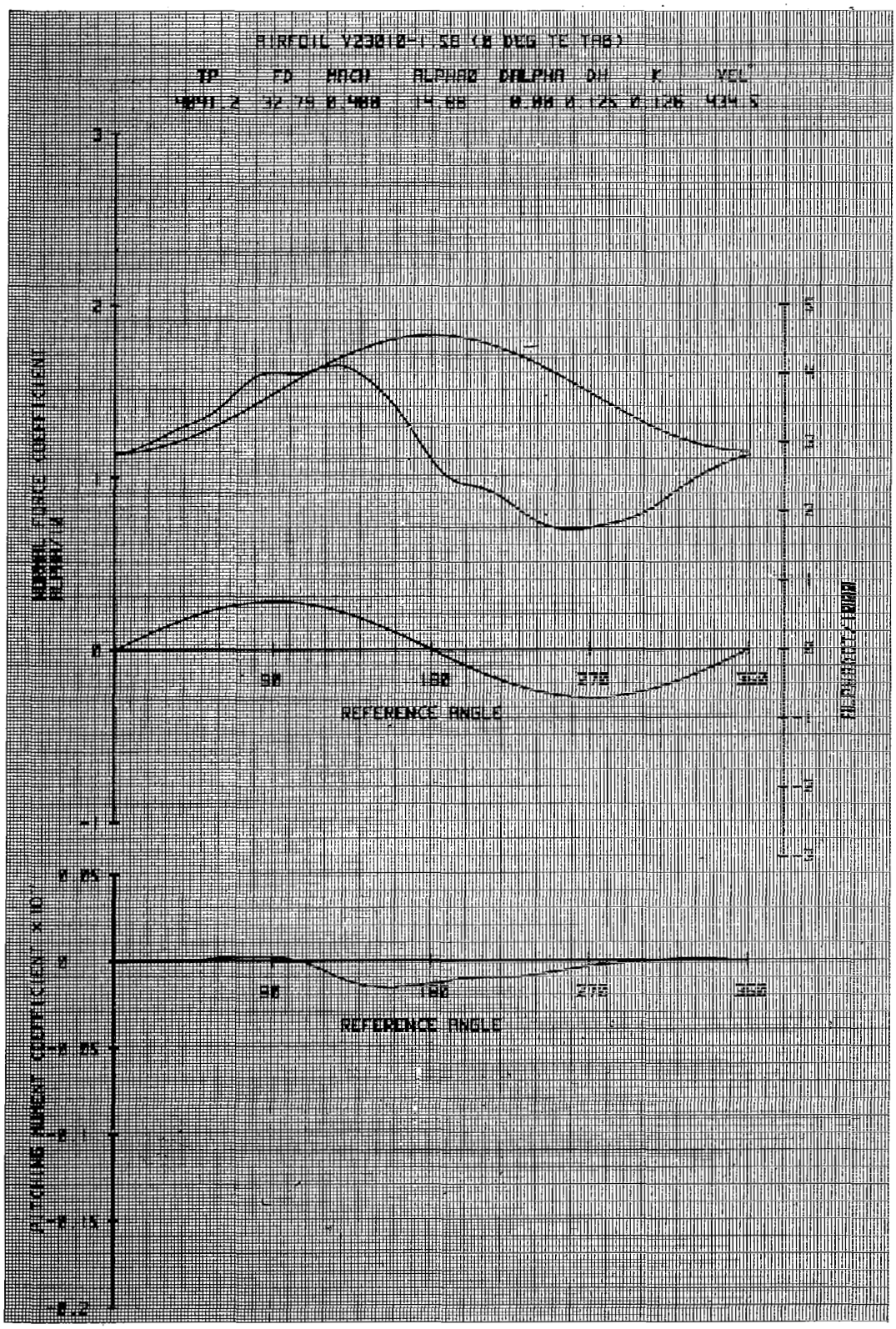

Figure 24a. Airfoil V23010-1.58 in Vertical Translation

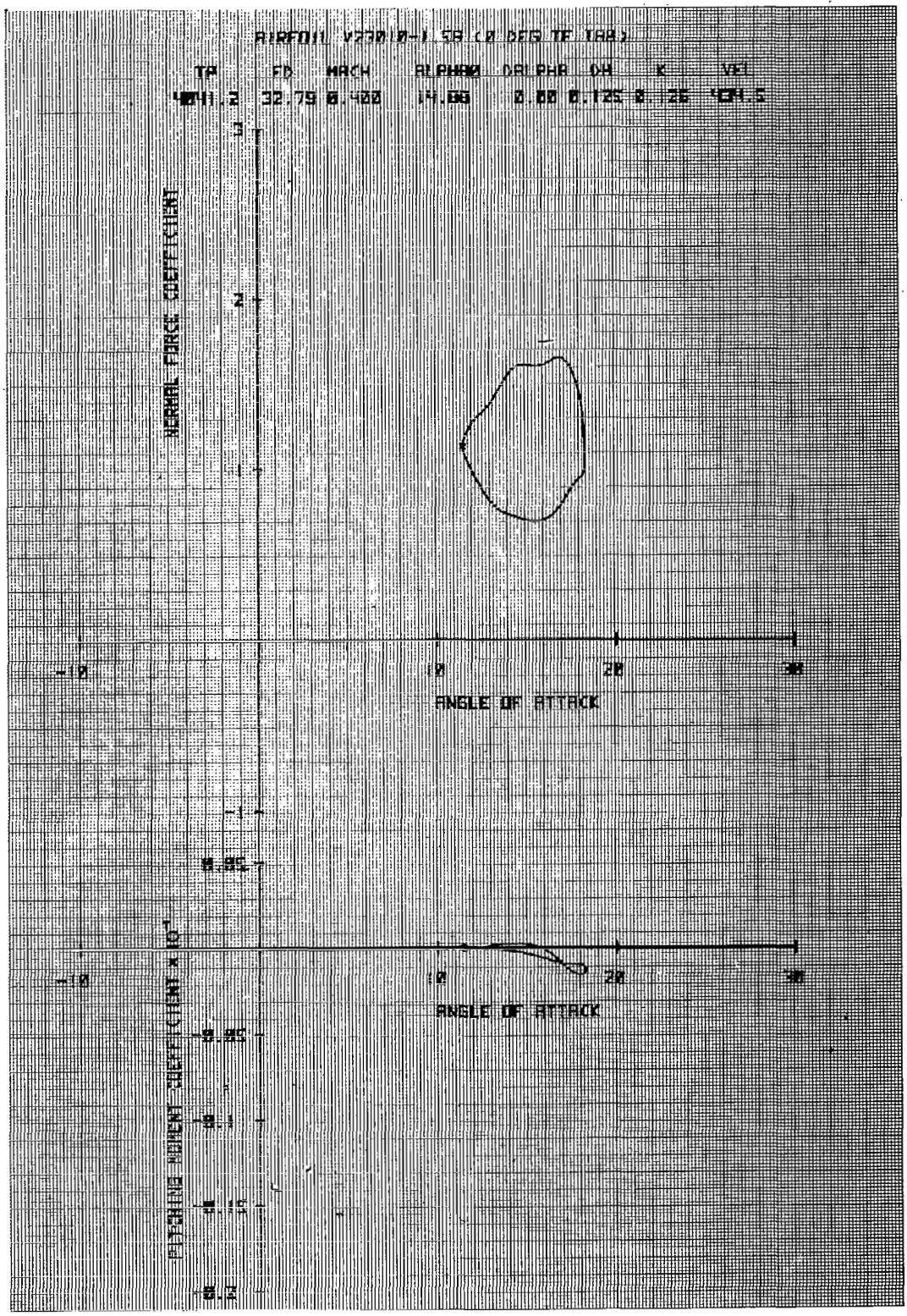

Figure 24b. Airfoil V23010-1.58 in Vertical Translation

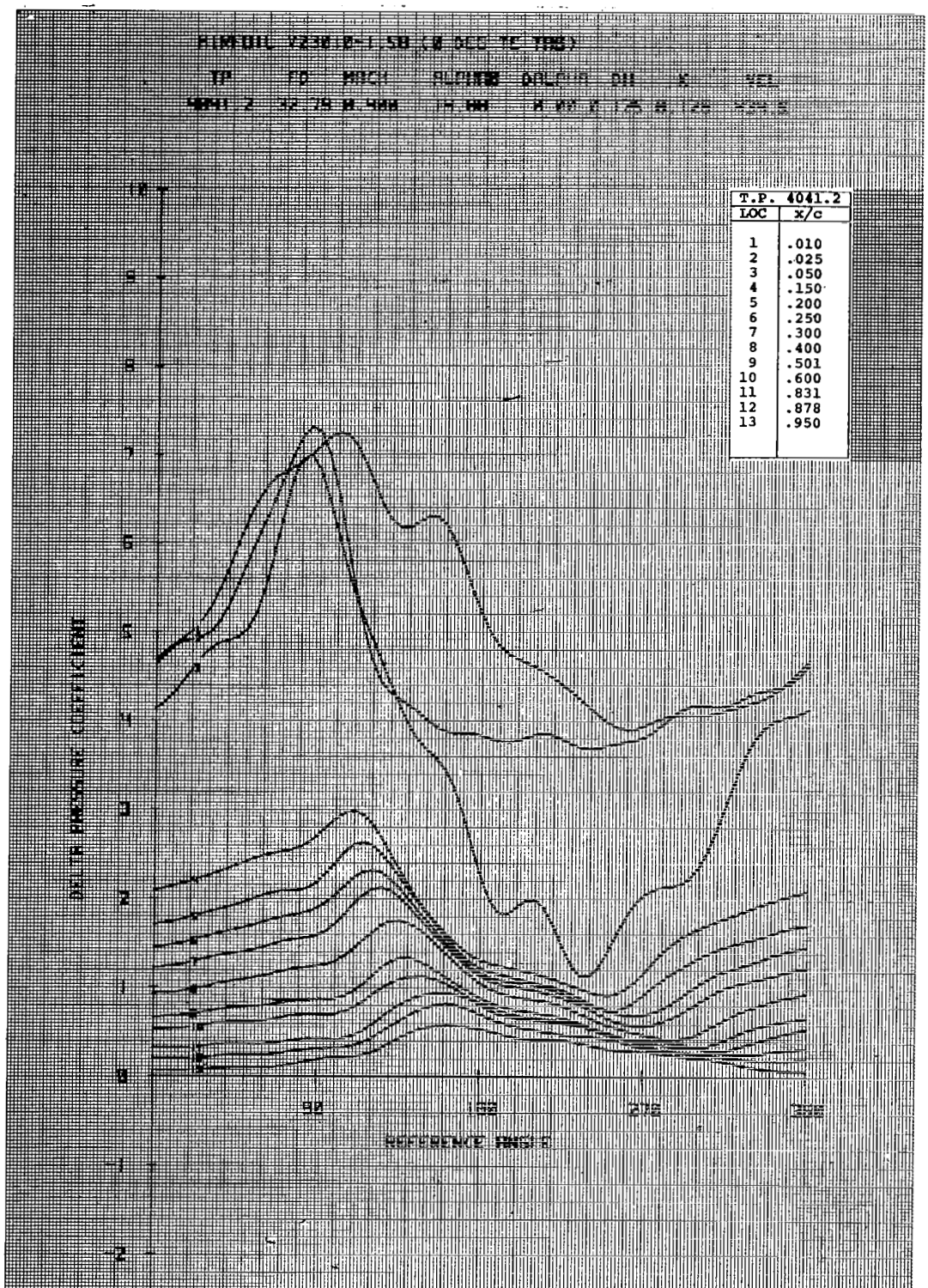

Figure 24c. Airfoil V23010-1.58 in Vertical Translation

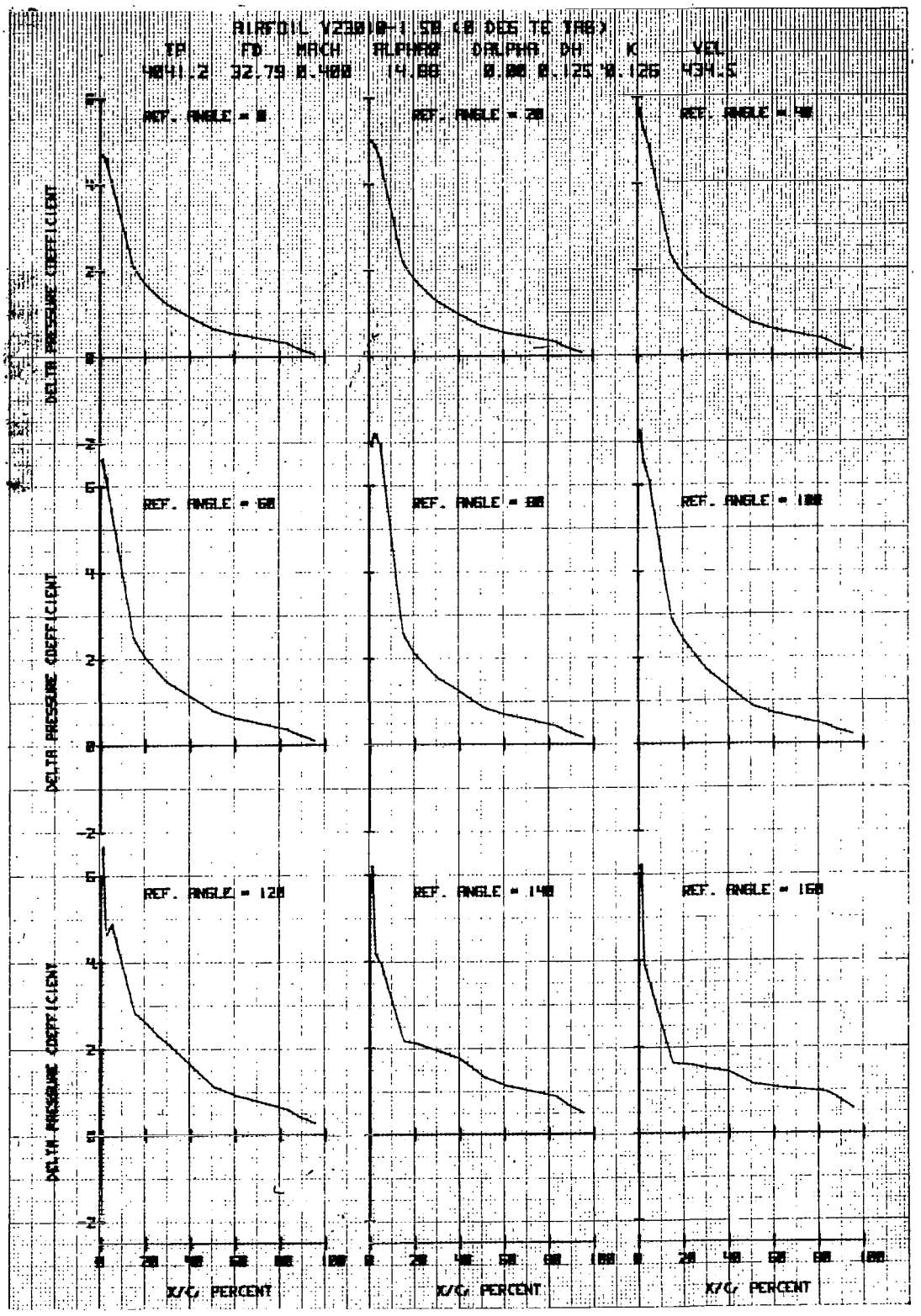

Figure 24d. Airfoil V23010-1.58 in Vertical Translation

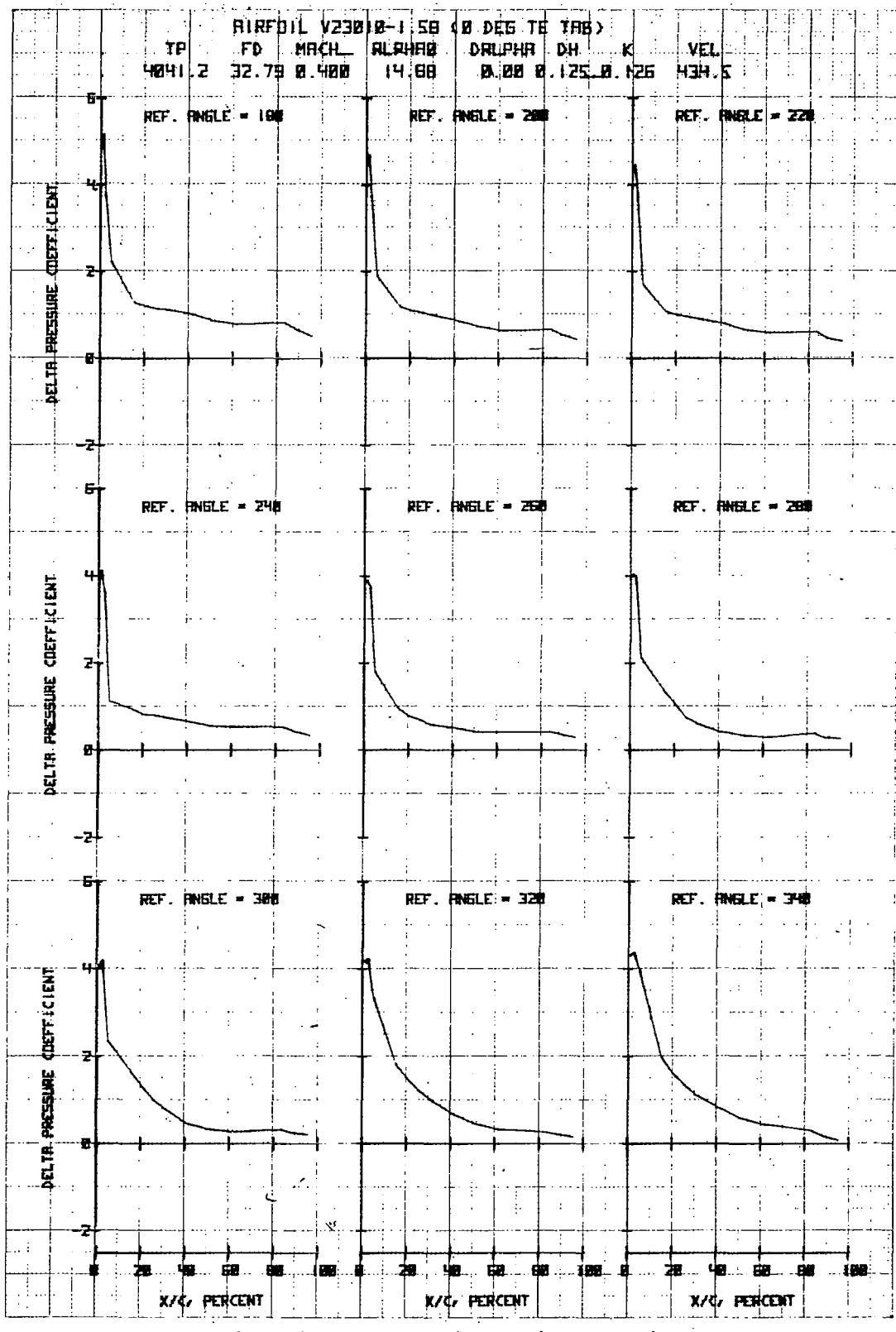

Figure 24e. Airfoil V23010-1.58 in Vertical Translation

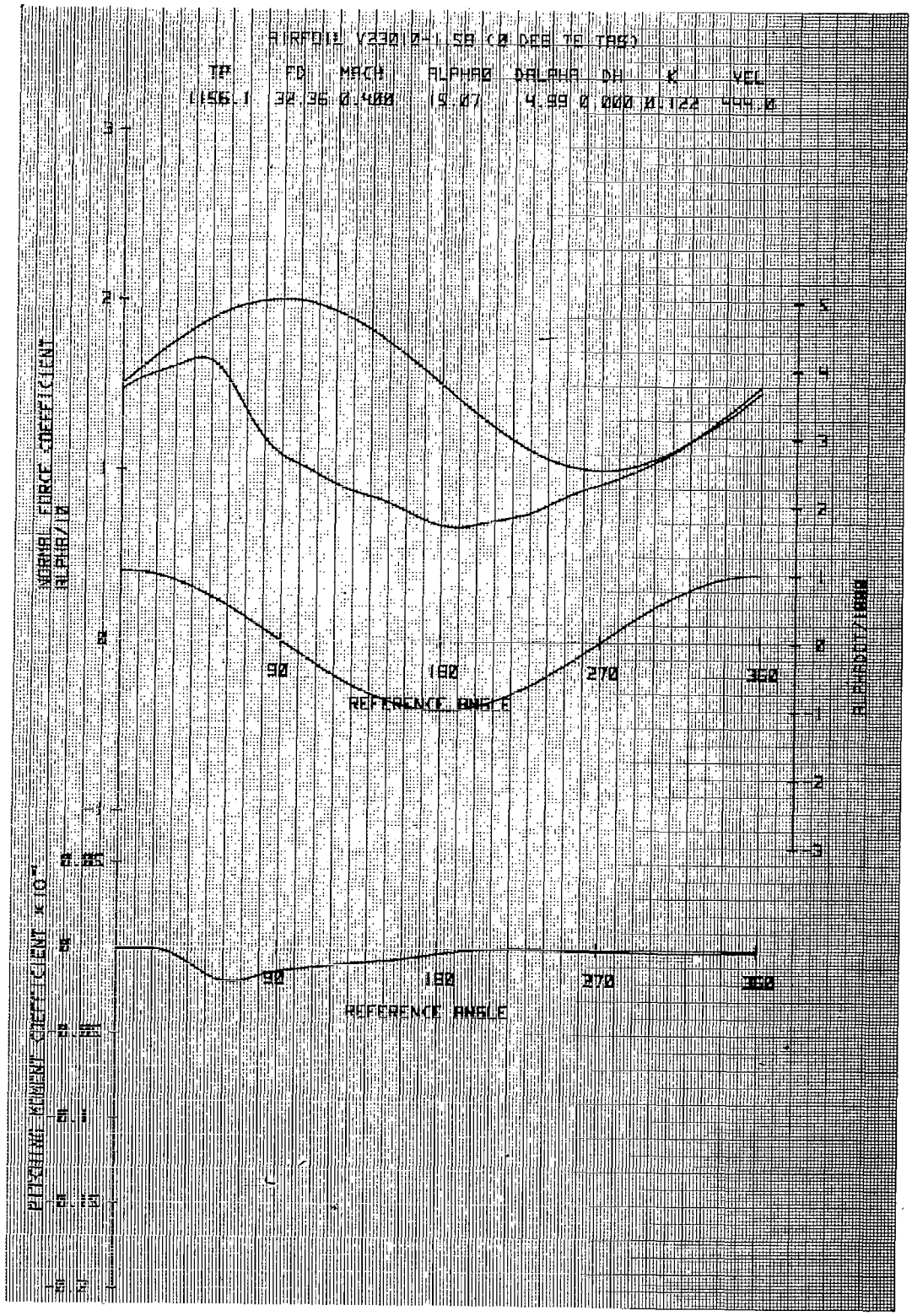

Figure 25a. Airfoil V2301O-1.58 in Forced Pitch Oscillation

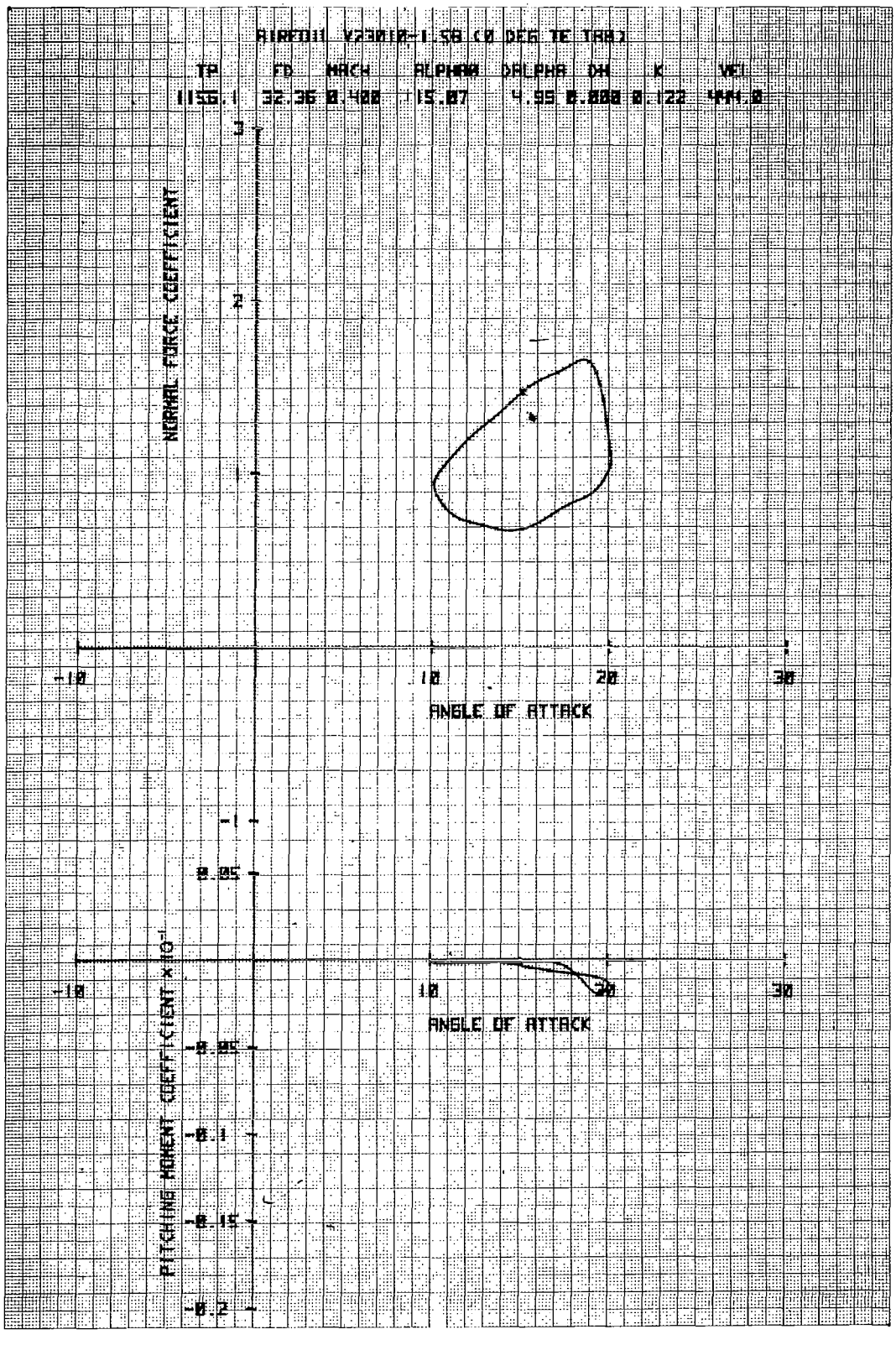

Figure 25b. Airfoil V23010-1.58 in Fowced Pitch Oscillation

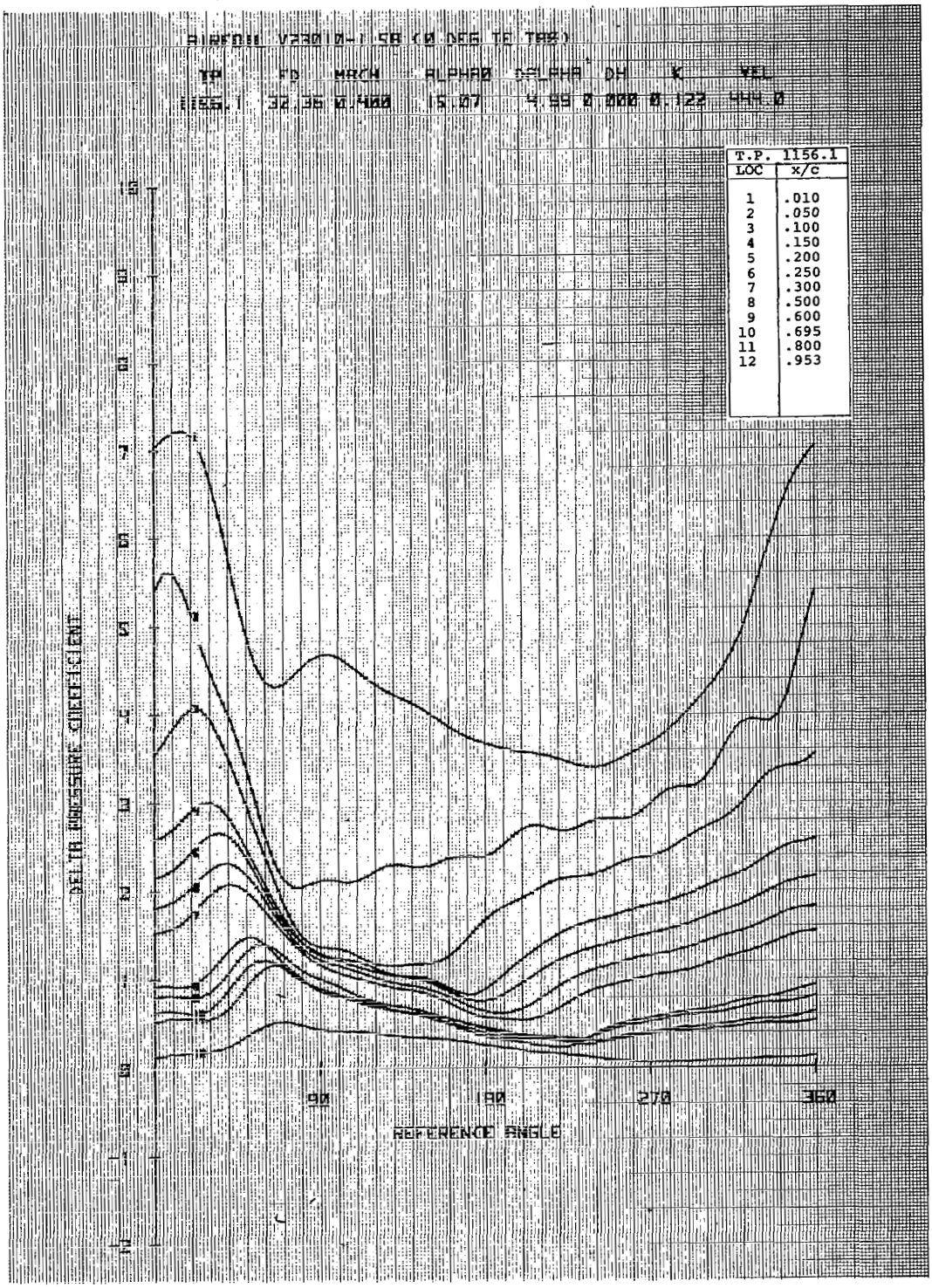

Figure 25c. Airfoil V23010-1.58 in Forced Pitch Oscillation

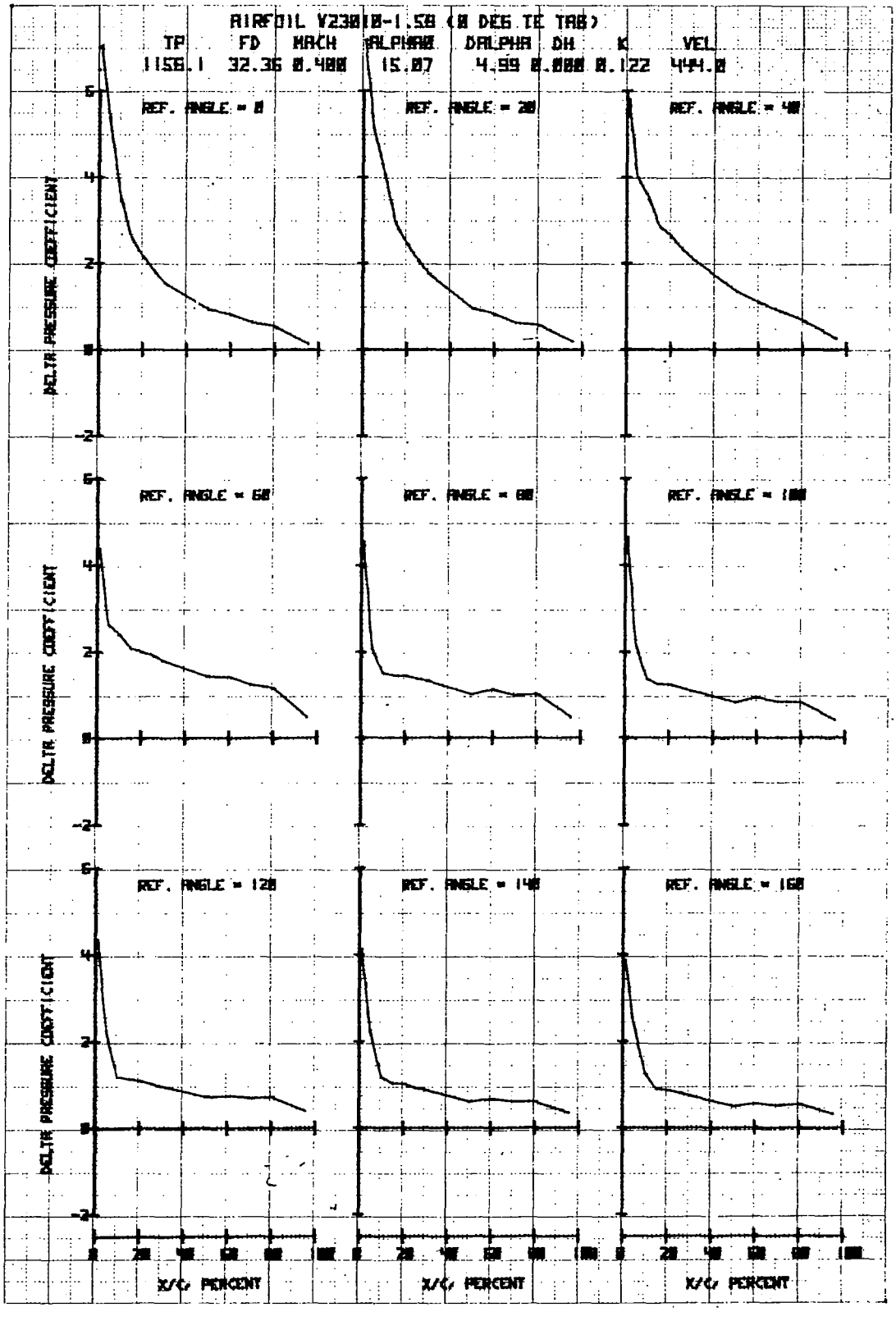

Figure 25d. Airfoil V23010-1.58 in Forced Pitch Oscillation

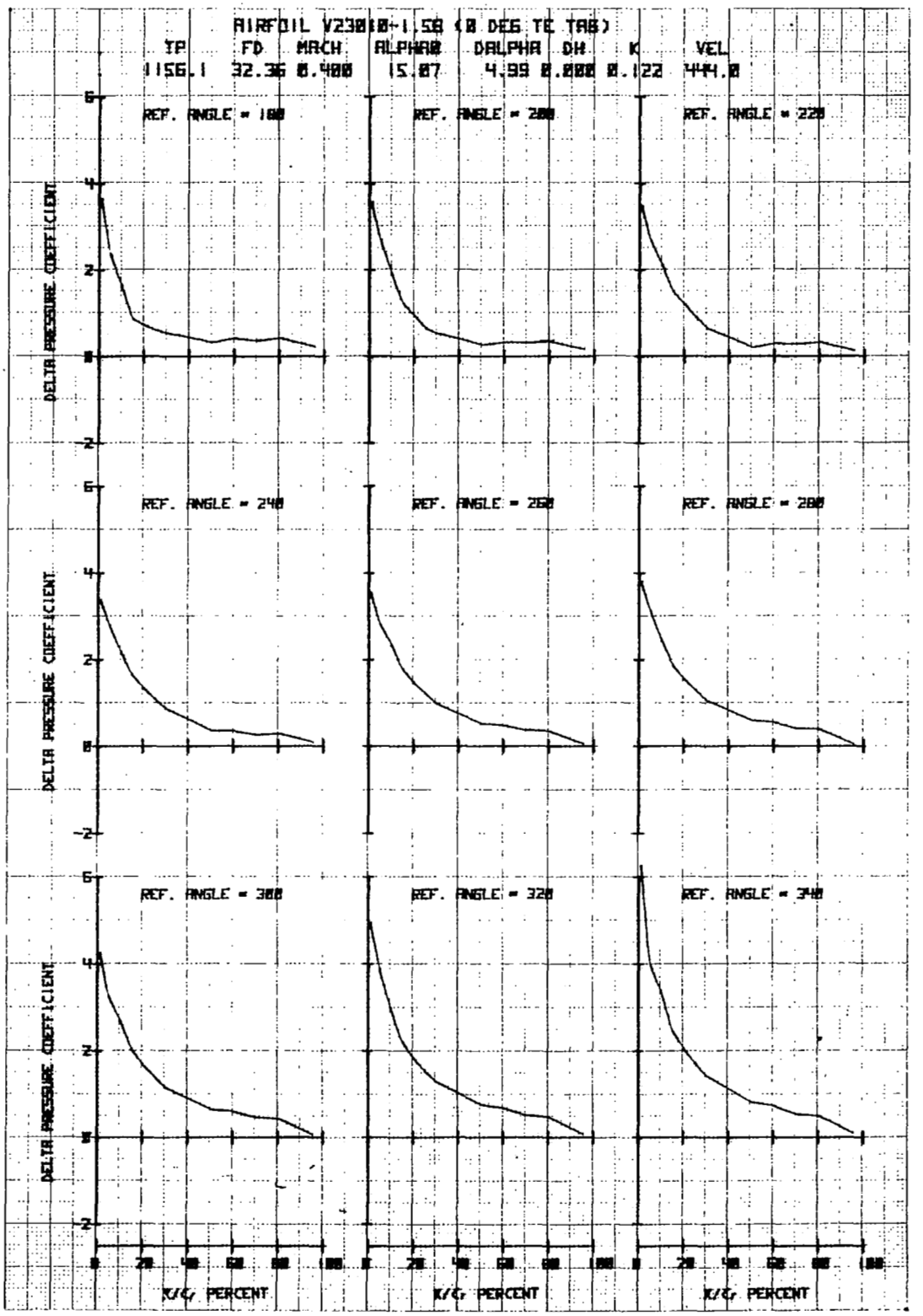

Figure 25e. Airfoil V23010-1.58 in Forced Pitch Oscillation

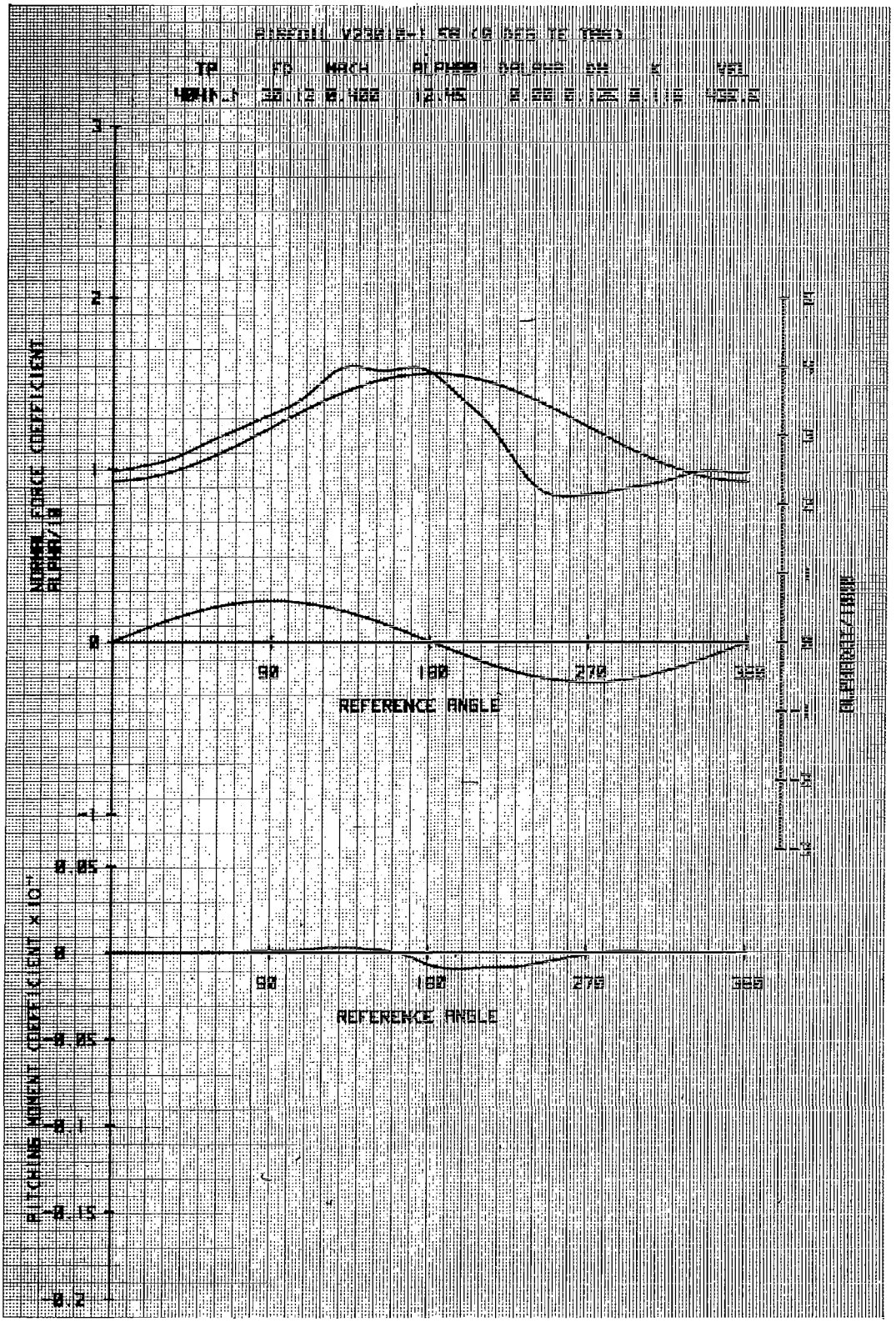

Figure 26a. Airfoil V23010-1.58 in Vertical Translation

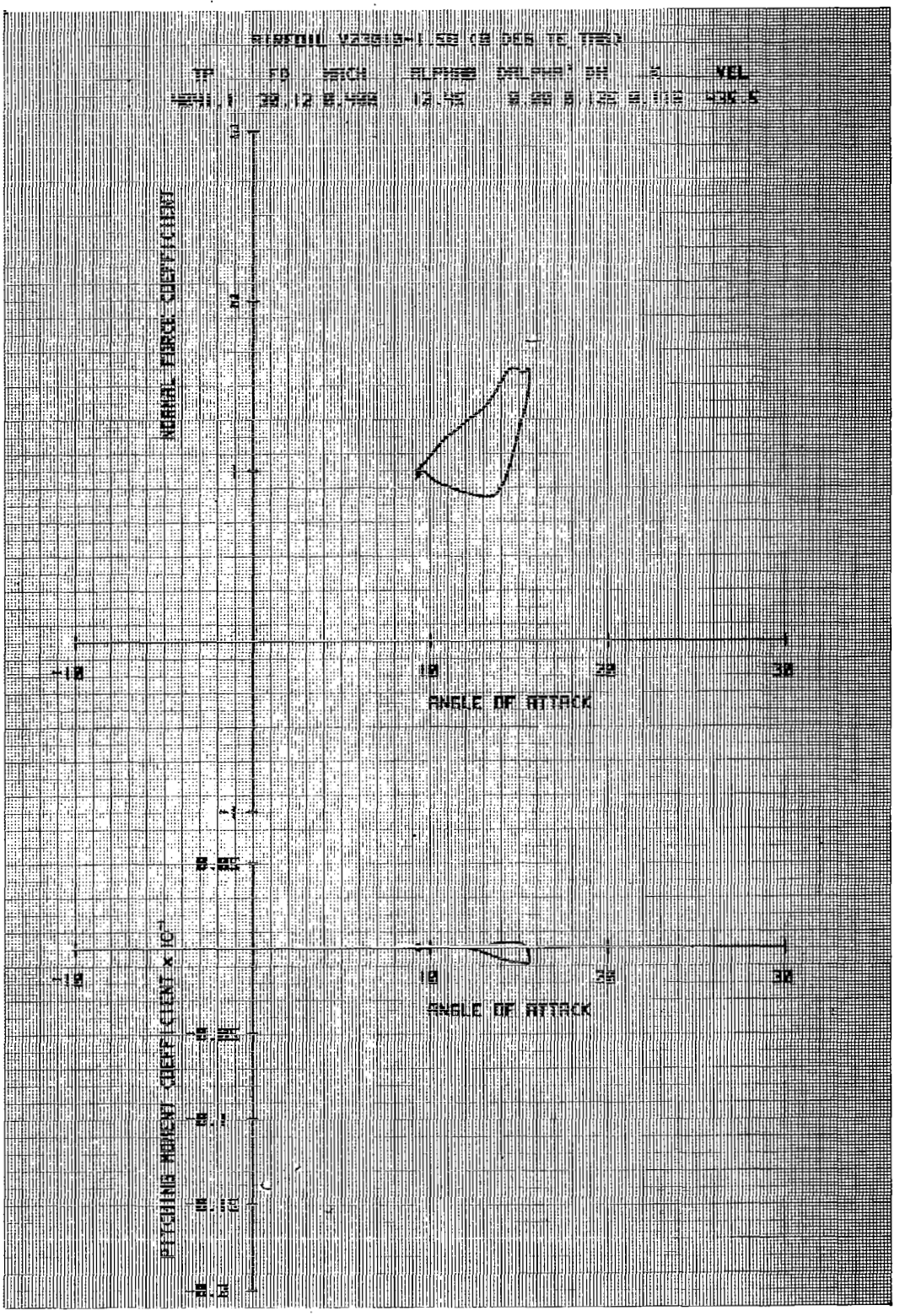

Figure 26b. Airfoil V23010-1.58 in Vertical Translation

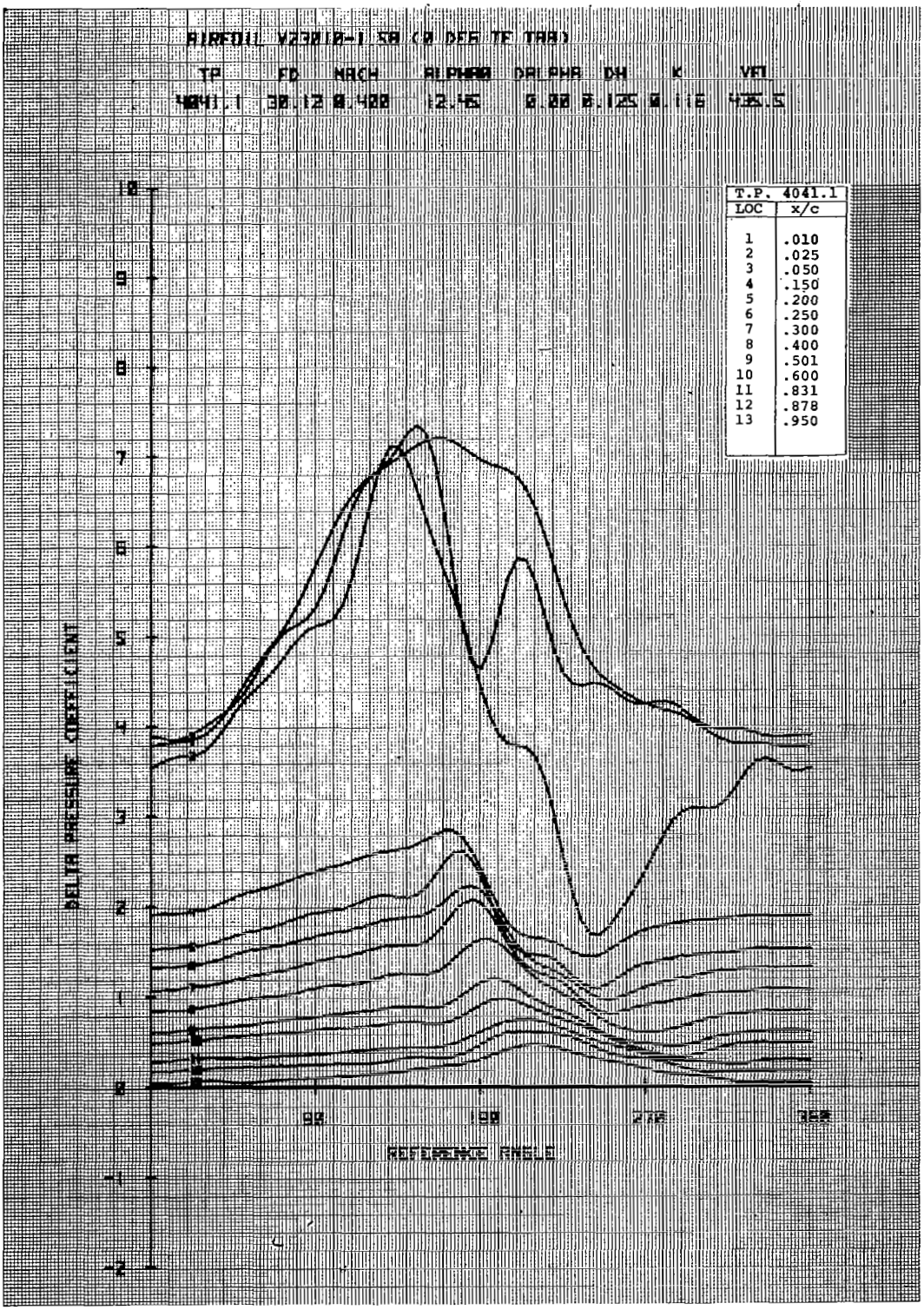

Figure 26c. Airfoil V23010-1.58 in Vertical Translation

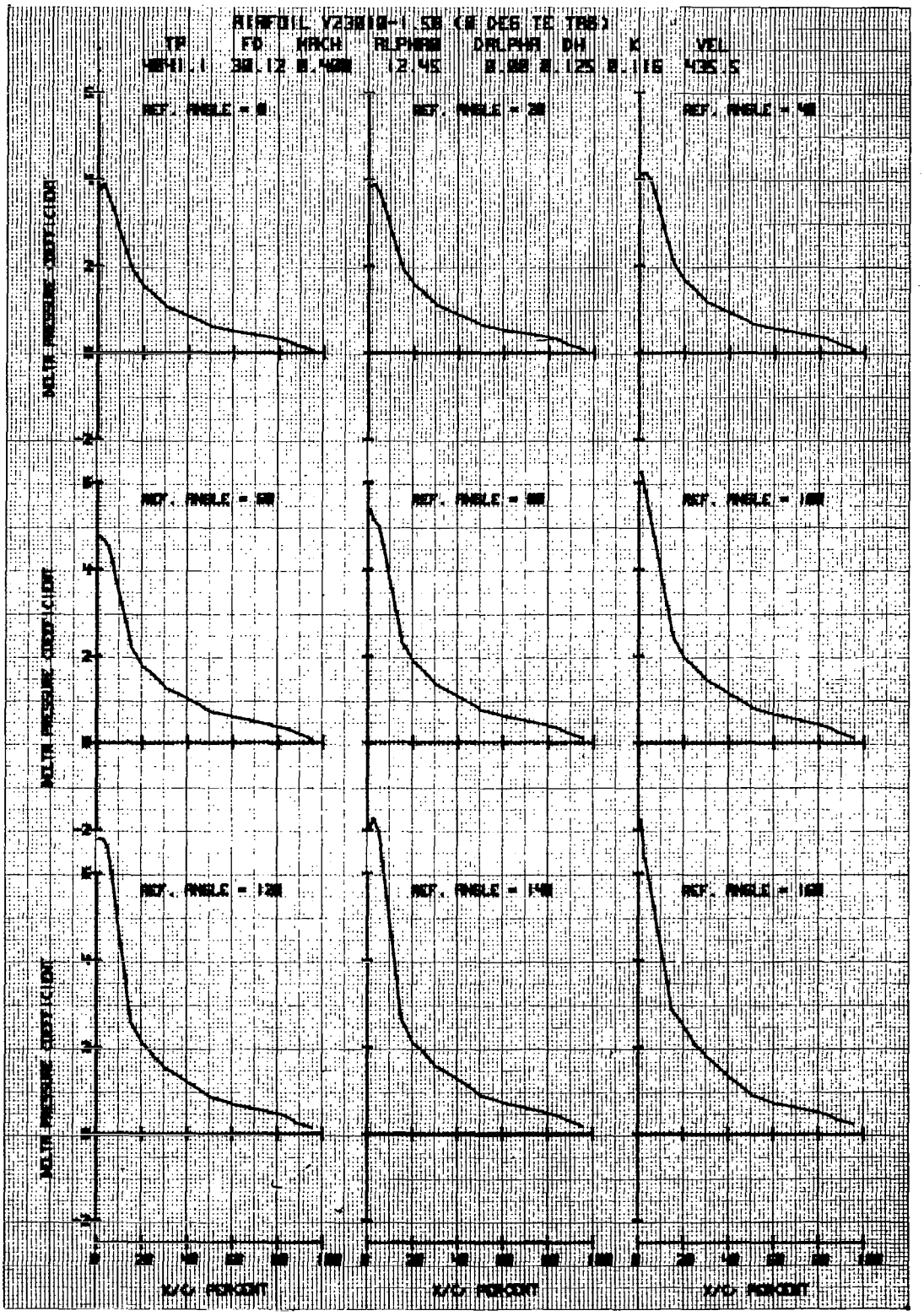

Figure 26d. Airfoil V23010-1.58 in Vertical Translation

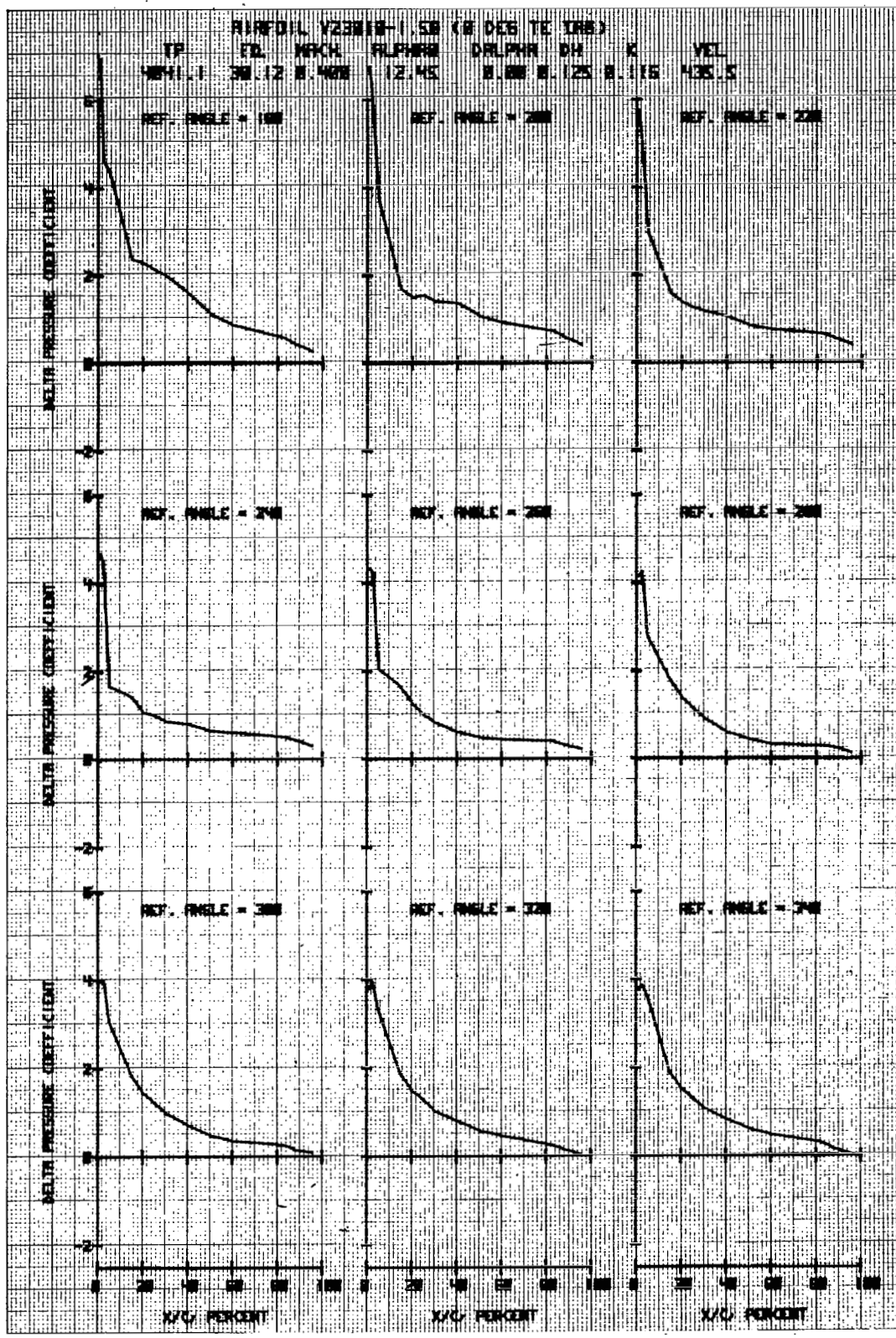

Figure 26e. Airfoil V23010-1.58 in Vertical Translation

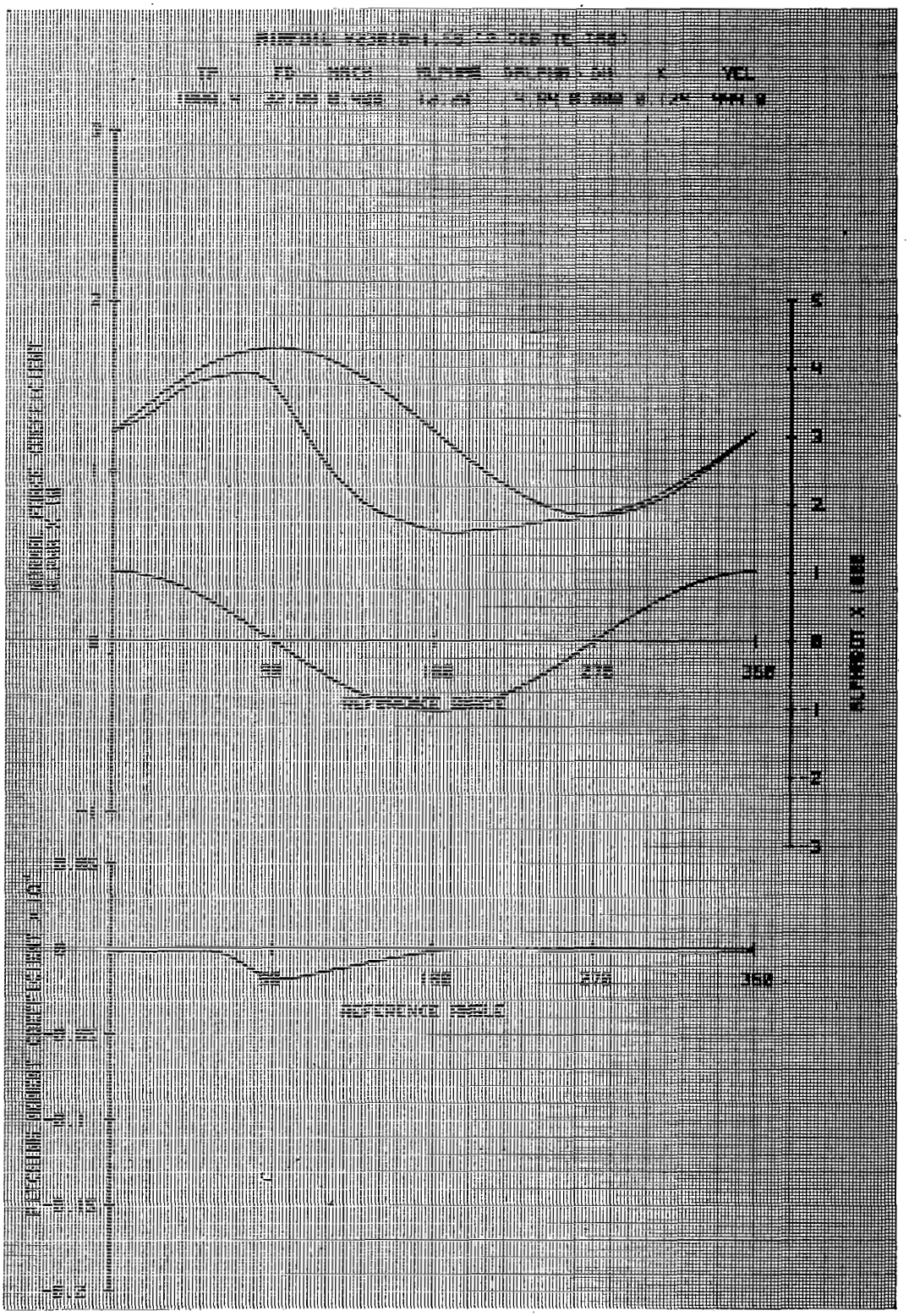

Figure 27a. Airfoil V23010-1.58 in Forced Pitch Oscillation

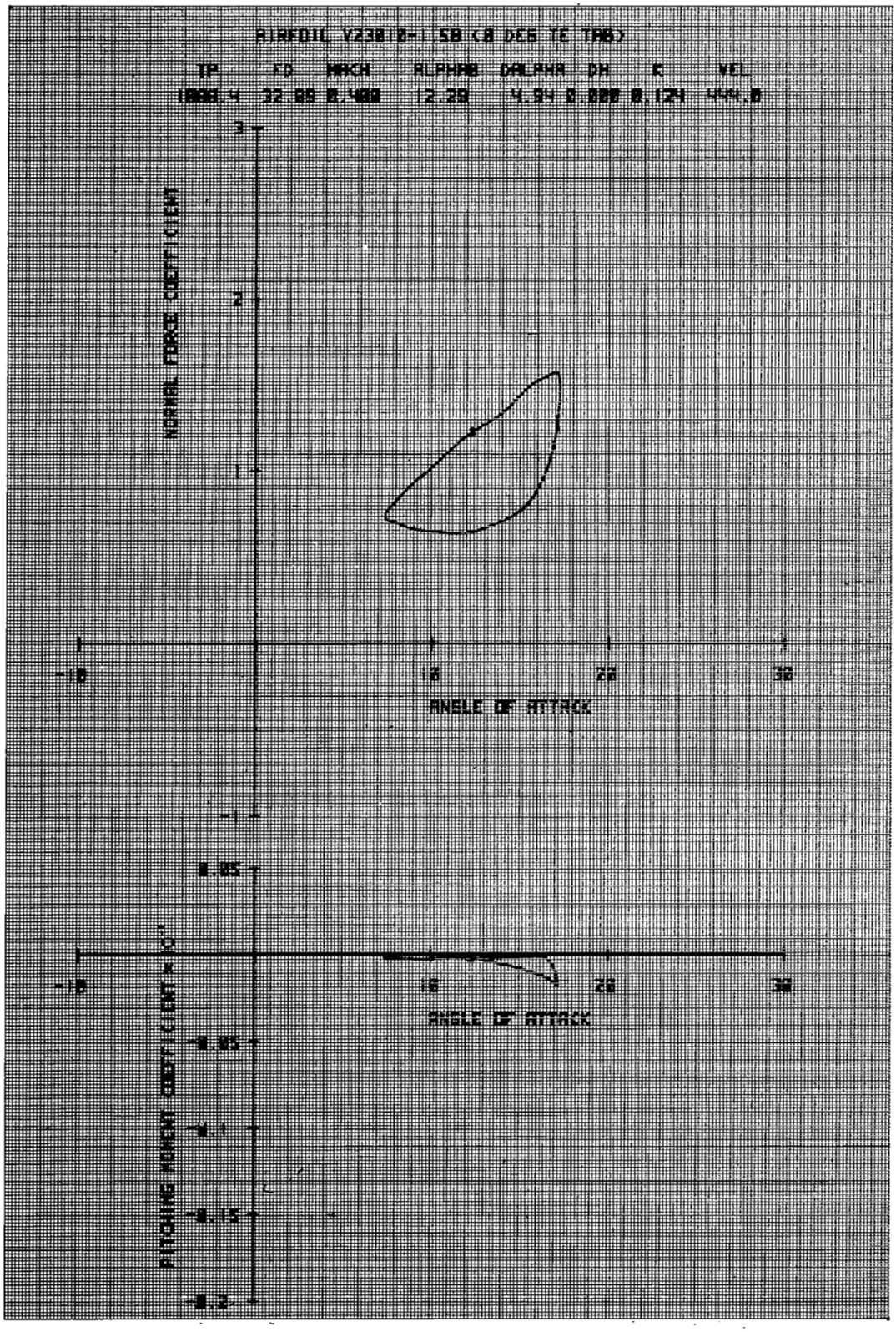

Figure 27b. Airfoil V23010-1.58 in Forced Pitch Oscillation

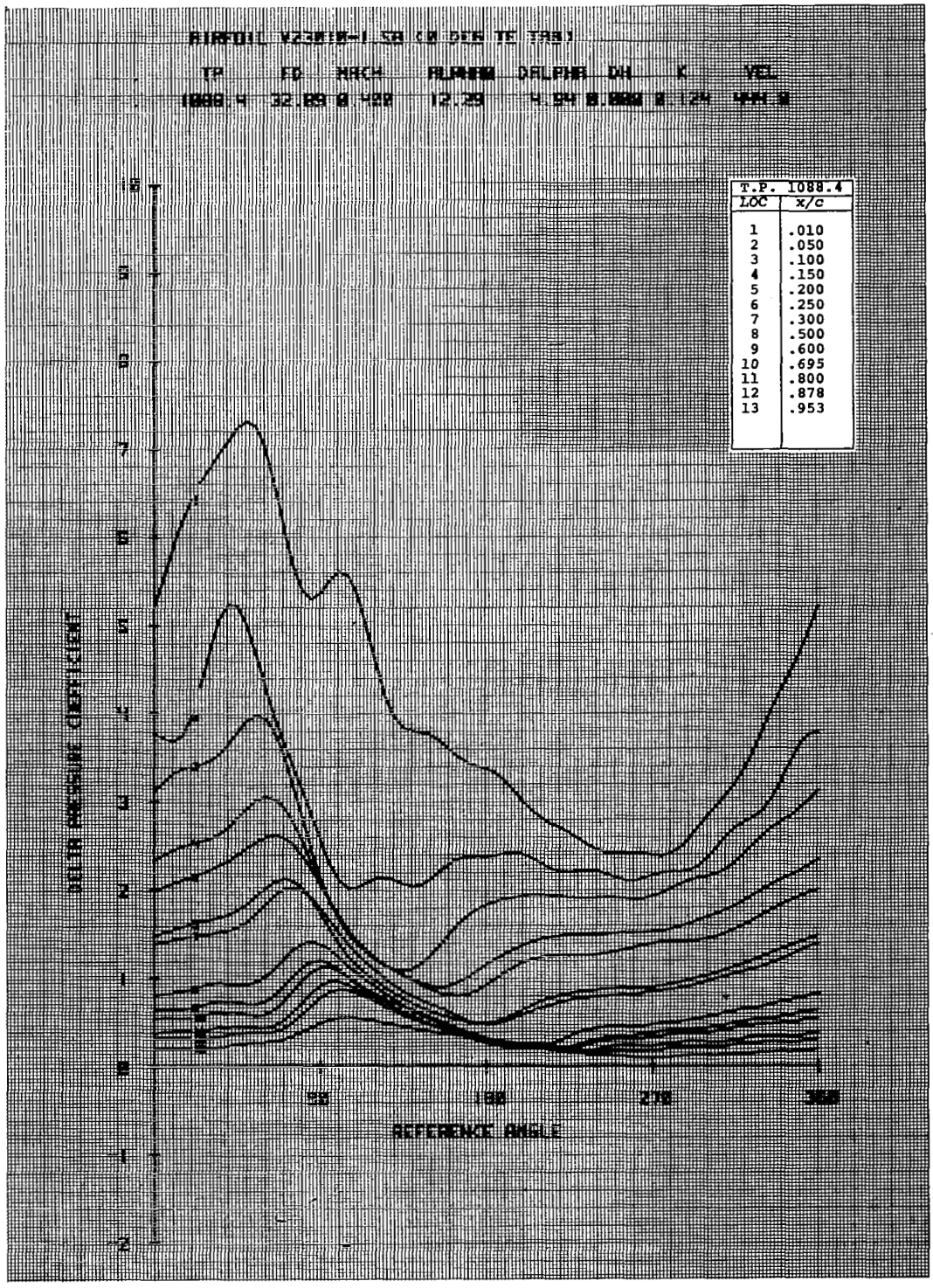

Figure 27c. Airfoil V23010-1.58 in Forced Pitch Oscillation

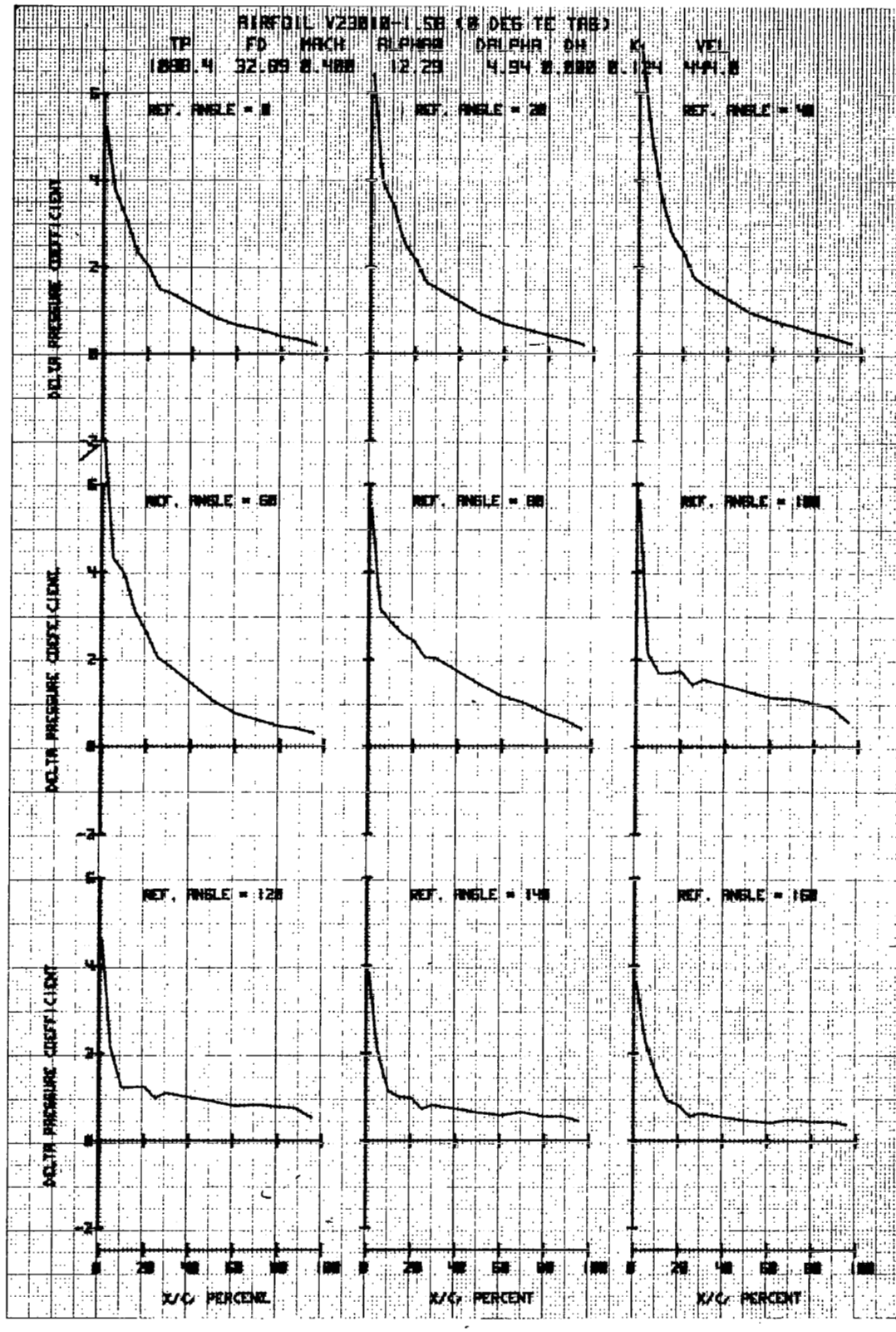

Figure 27d. Airfoil V23010-1.58 in Forced Pitch Oscillation

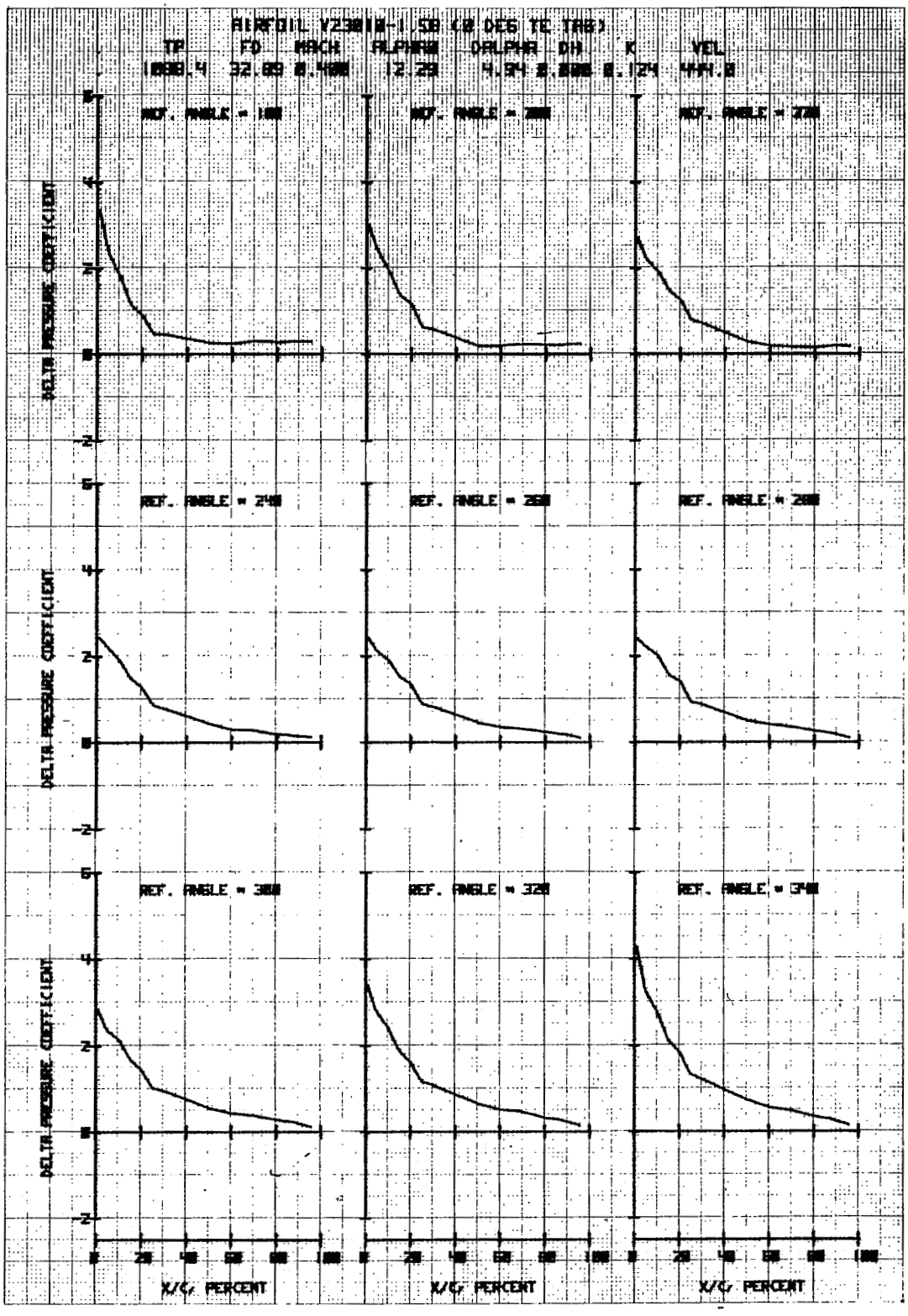

Figure 27e. Airfoil V23010-1.58 in Forced Pitch Oscillation

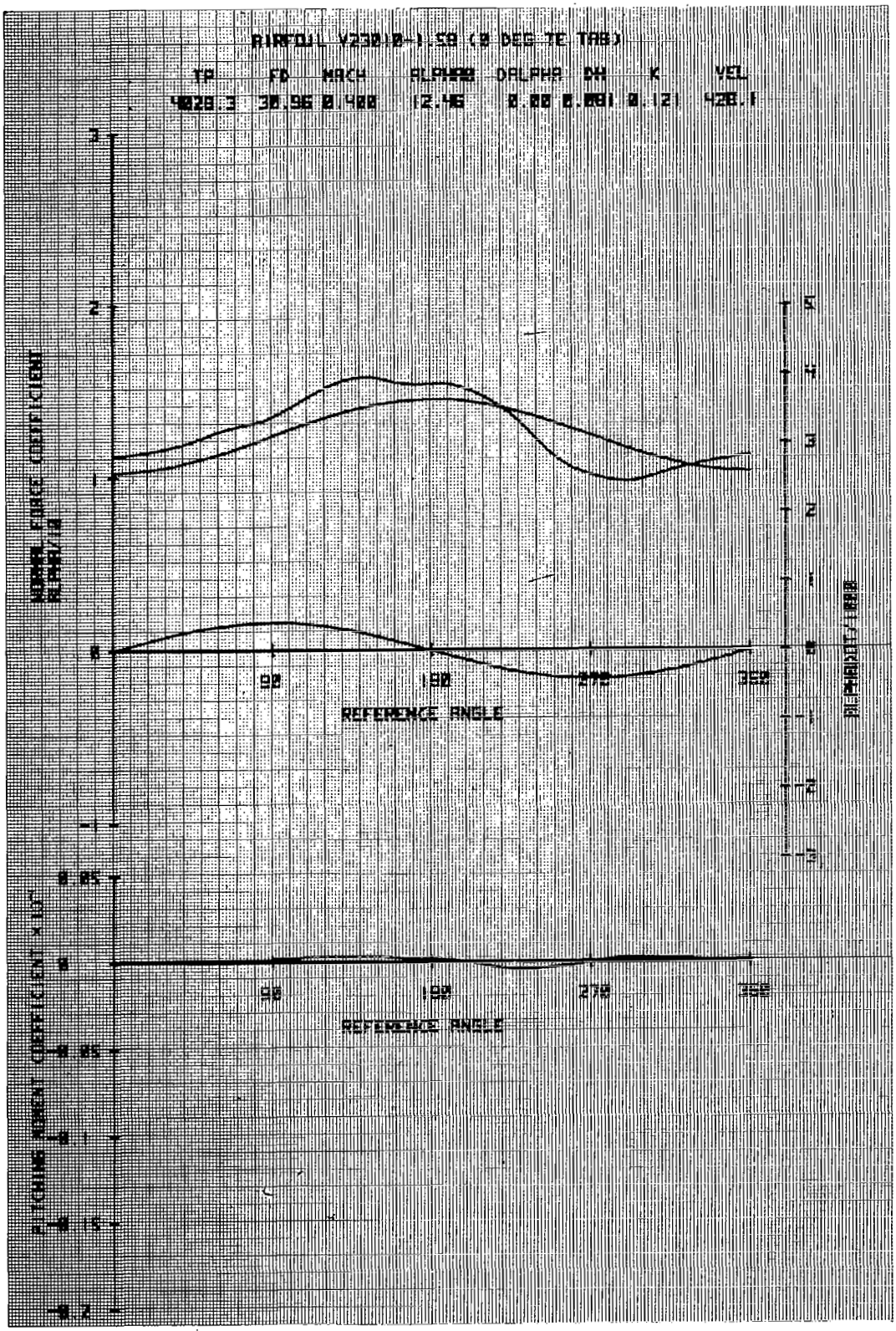

Figure 28a. Airfoil V23010-1.58 in Vertical Translation

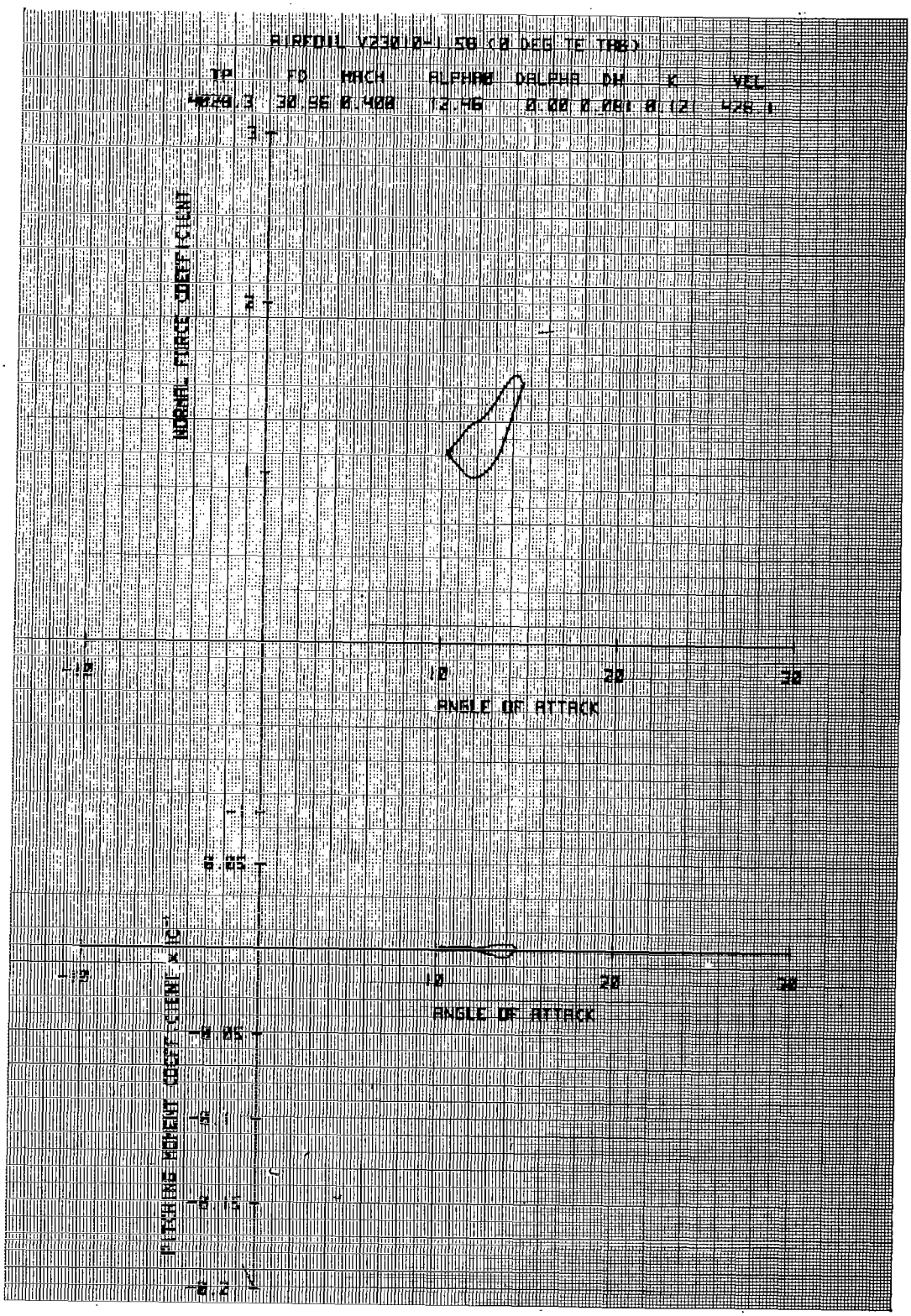

Figure 28b. Airfoil V23010-1.58 in Vertical Translation

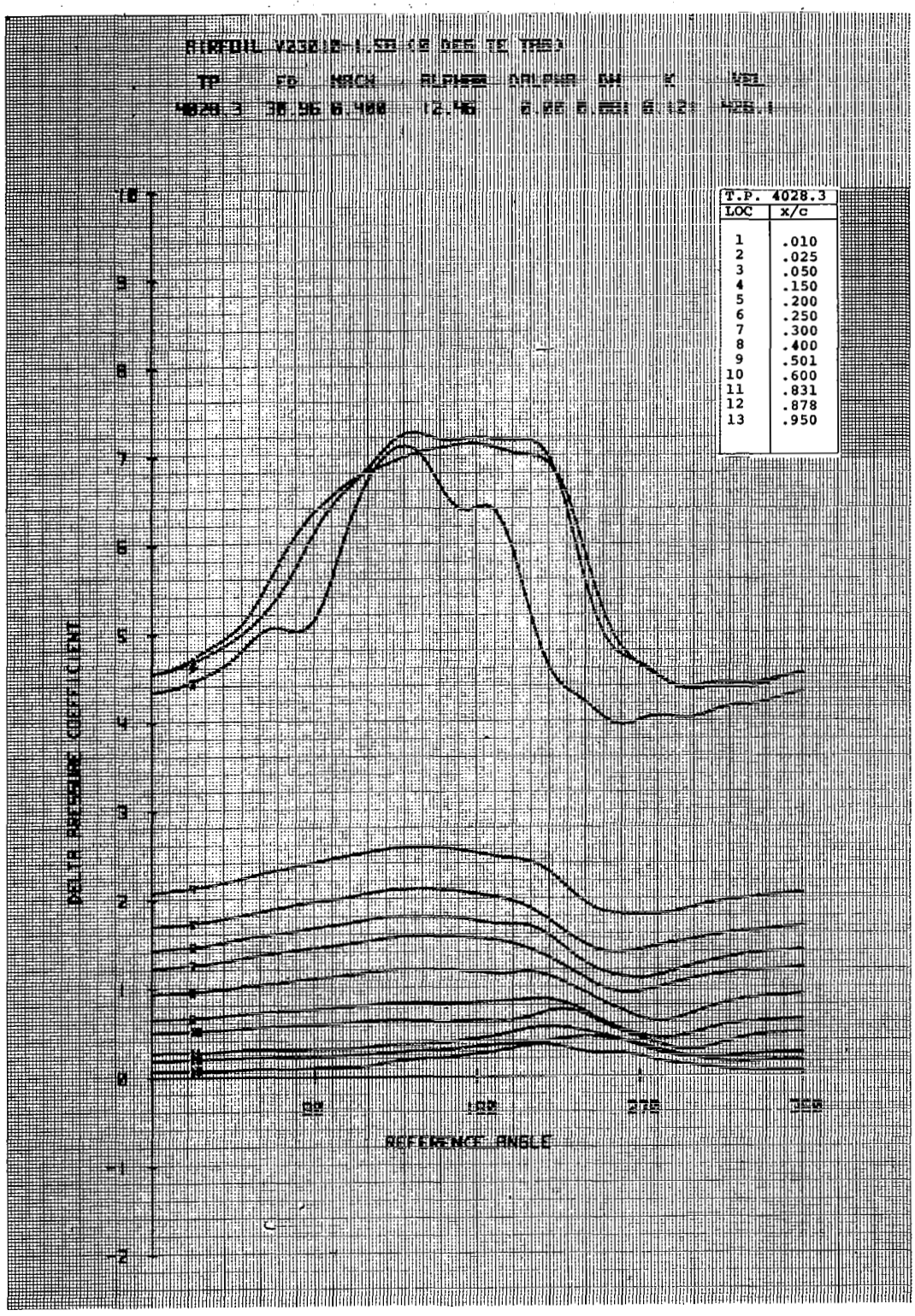

Figure 28c. Airfoil V23010-1.58 in Vertical Translation

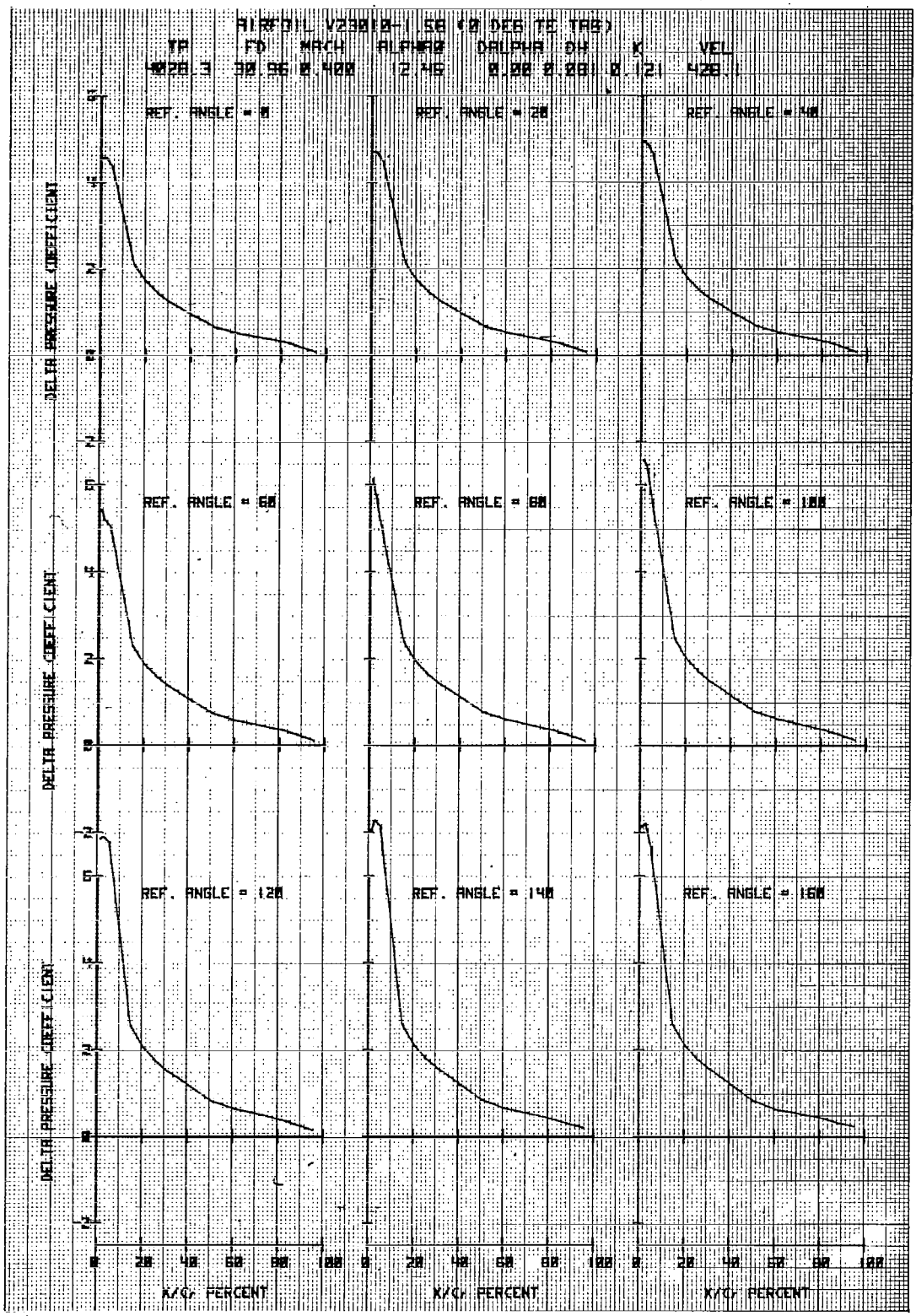

Figure 28d. Airfoil V23010-1.58 in Vertical Translation

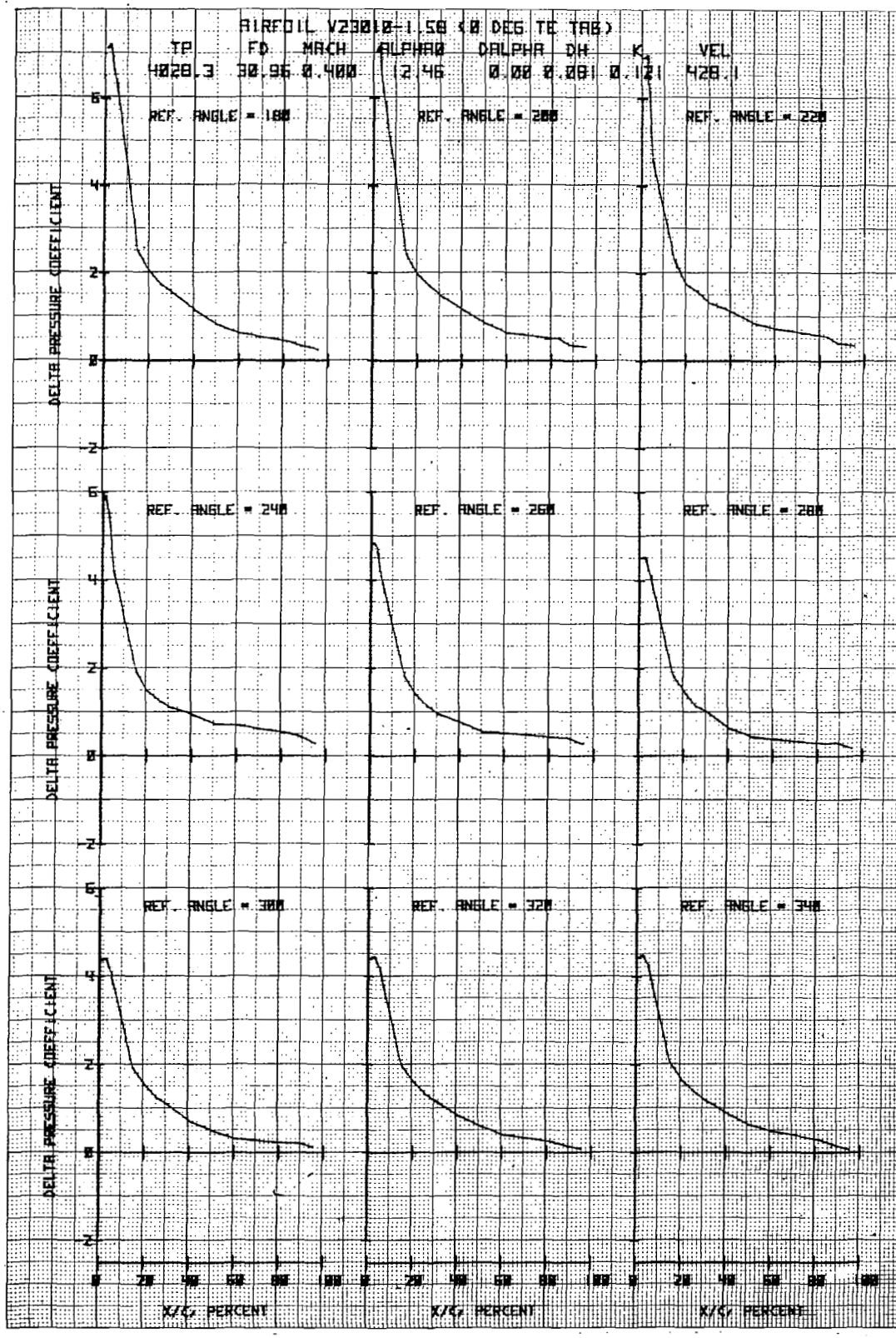

Figure 28e. Airfoil V23010-1.58 in Vertical Translation

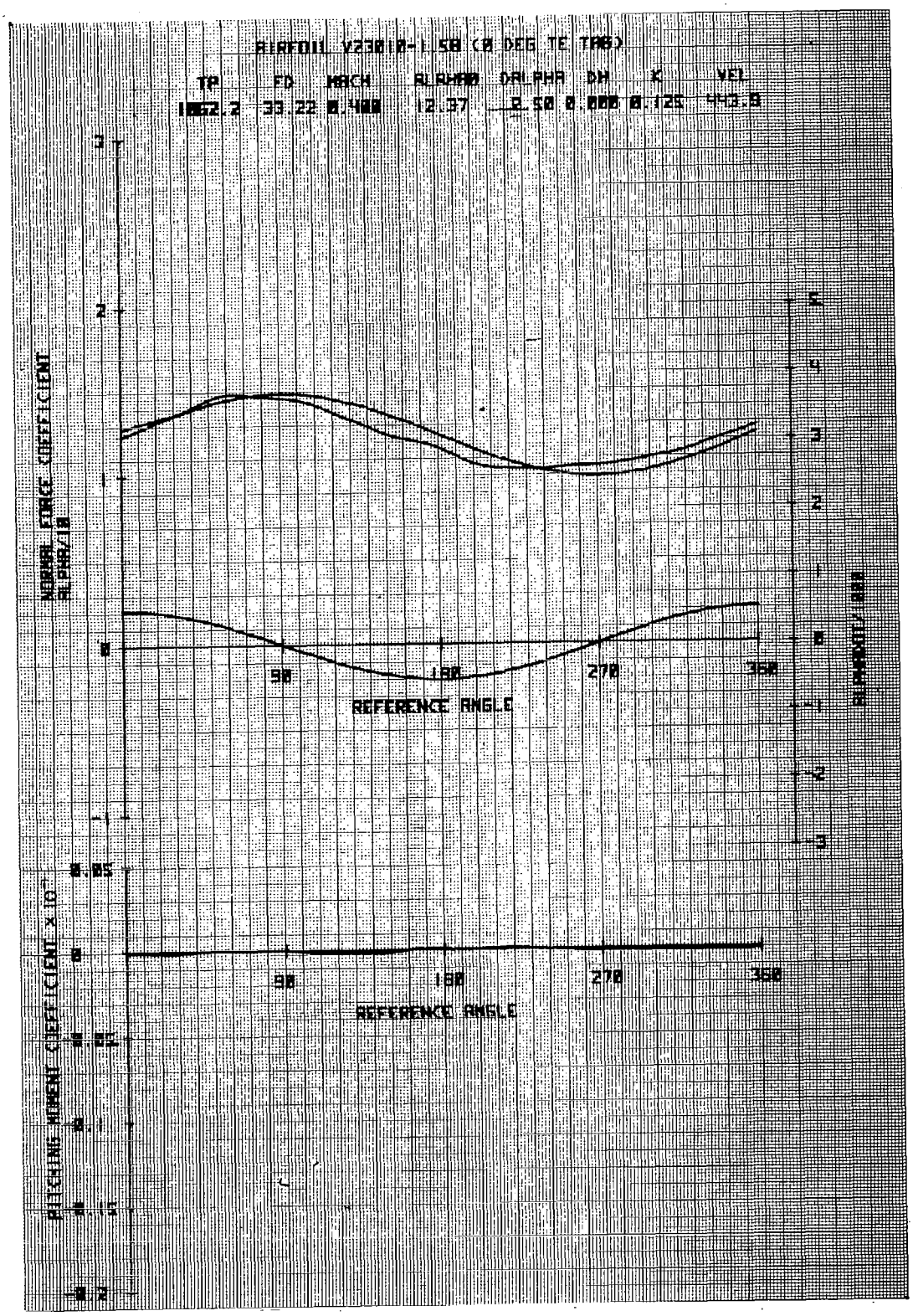

Figure 29a. Airfoil V23010-1.58 in Forced Pitch Oscillation

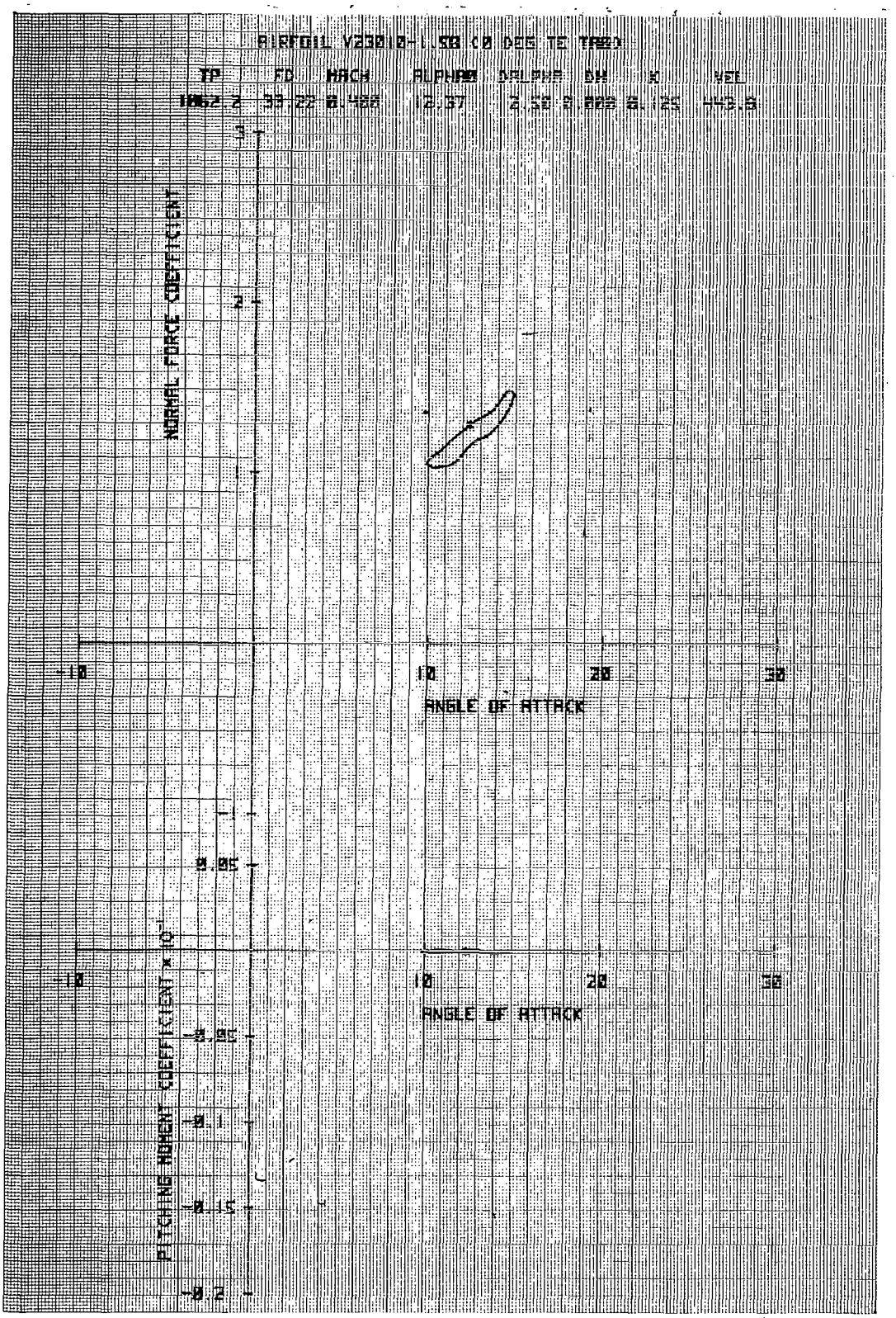

Figure 29b. Airfoil V23010-1.58 in Forced Pitch Oscillation

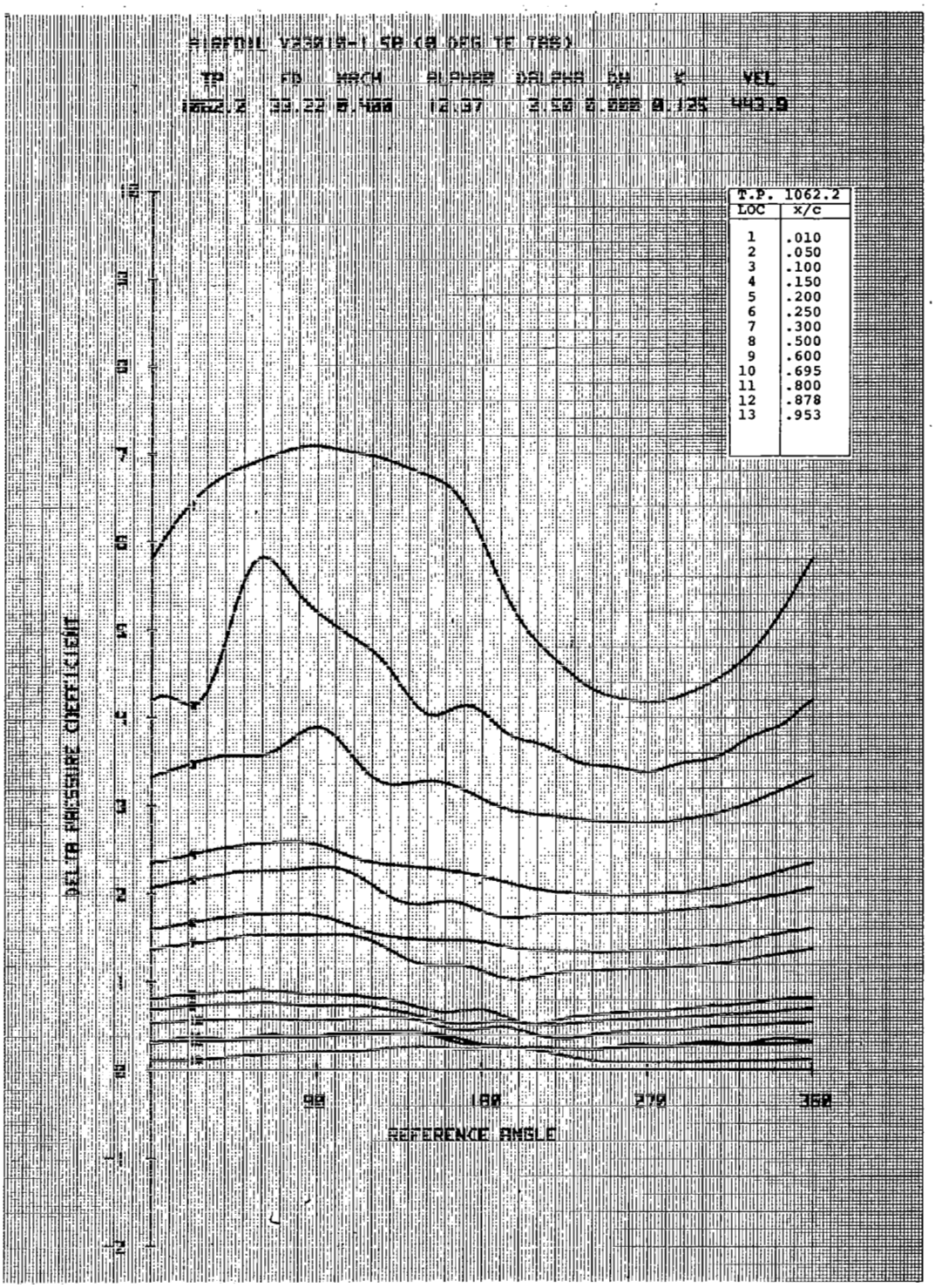

Figure 29c. Airfoil V23010-1.58 in Forced Pitch Oscillation

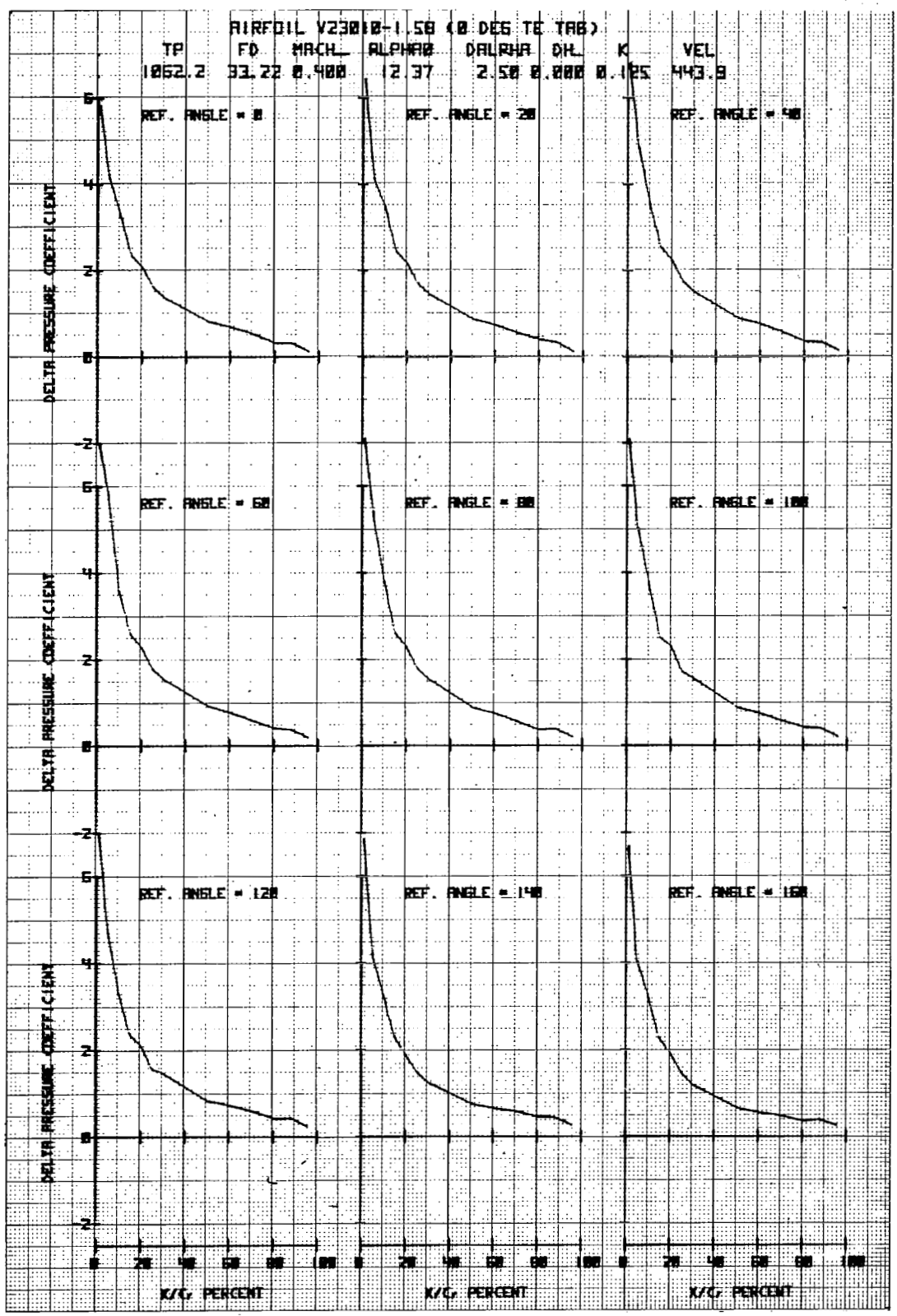

Figure 29d. Airfoil V23010-1.58 in Forced Pitch Oscillation

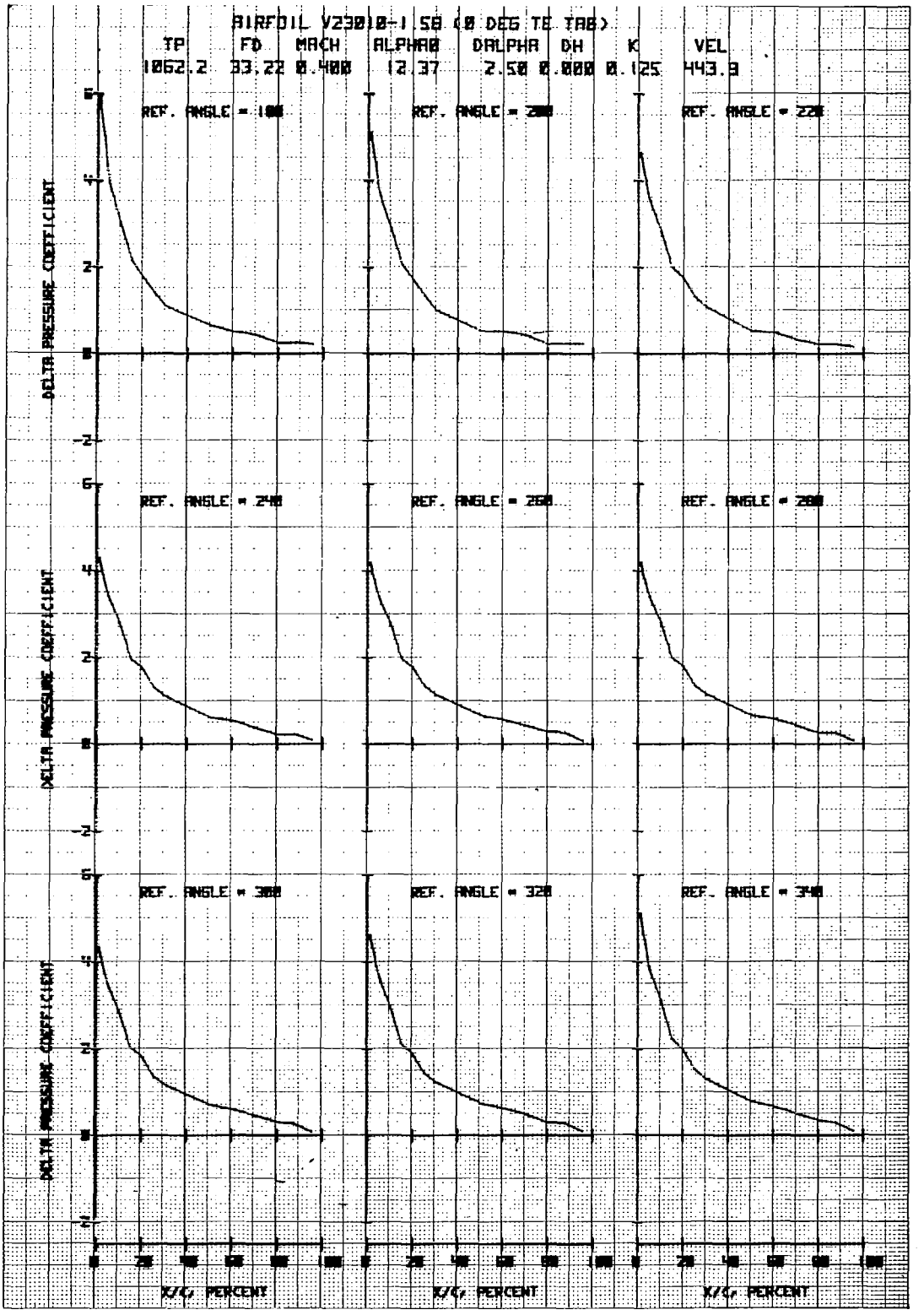

Figure 29e. Airfoil V23010-1.58 in Forced Pitch Oscillation

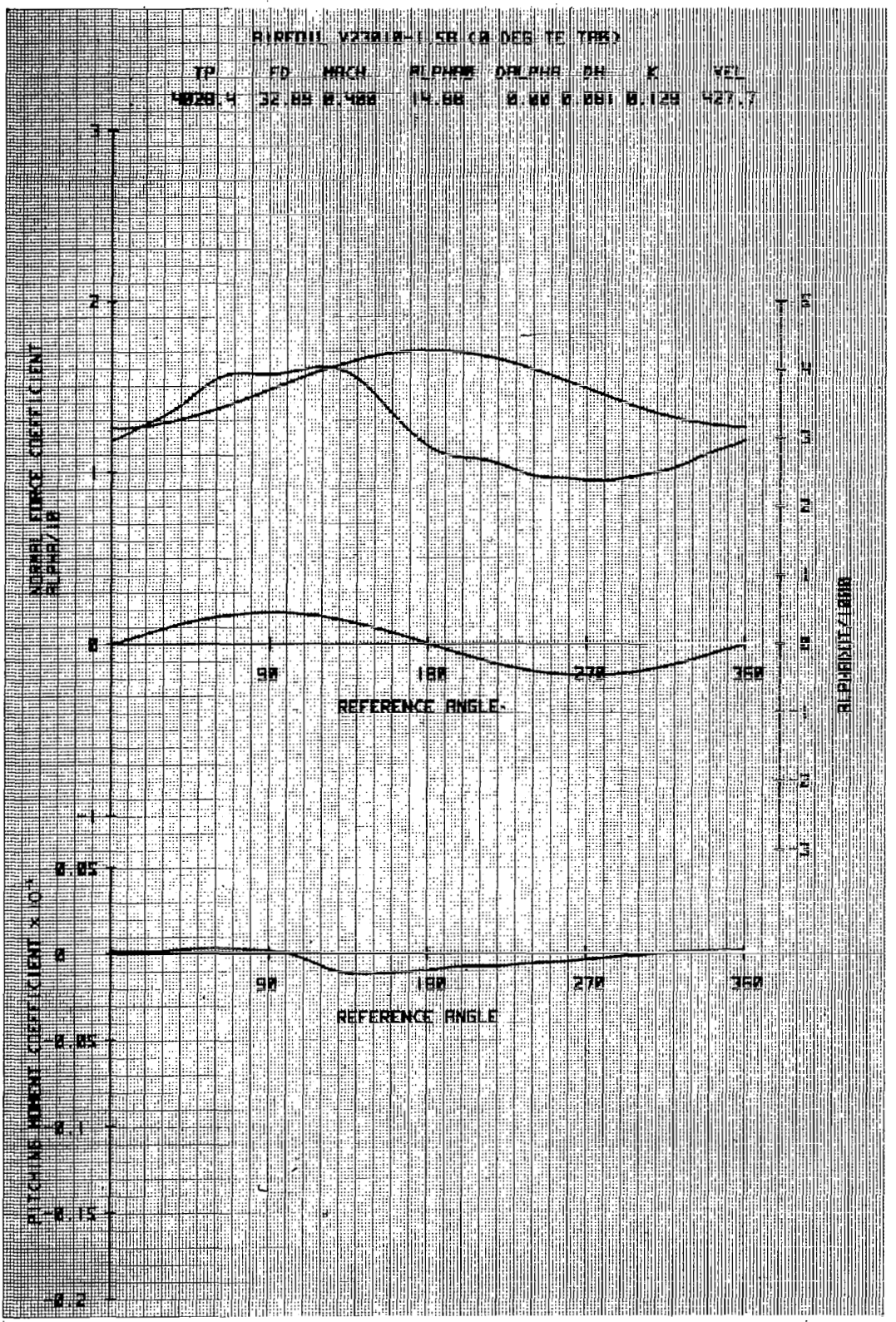

Figure 30a. Airfoil V23010-1.58 in Vertical Translation

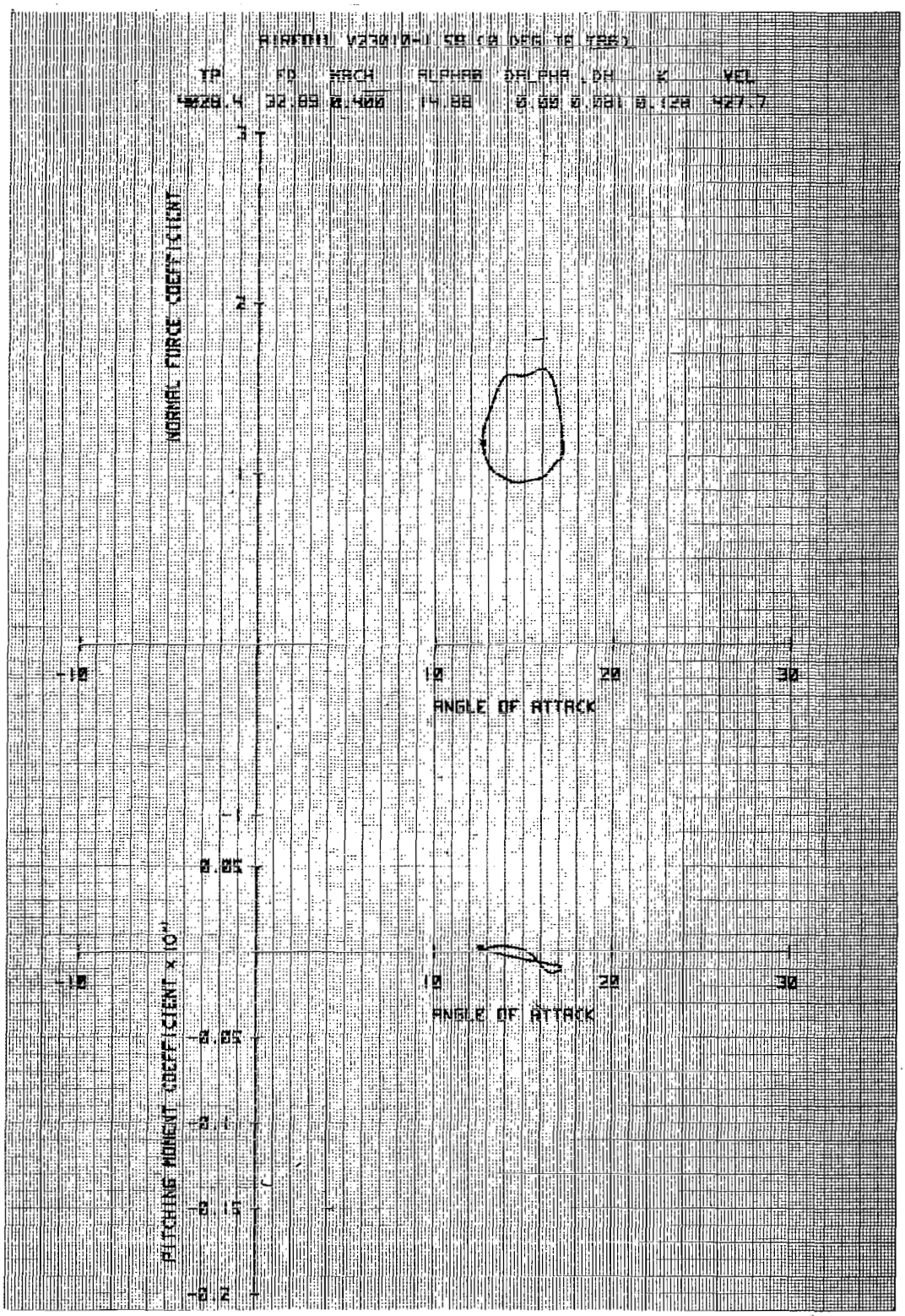

Figure 30b. Airfoil V23010-1.58 in Vertical Translation

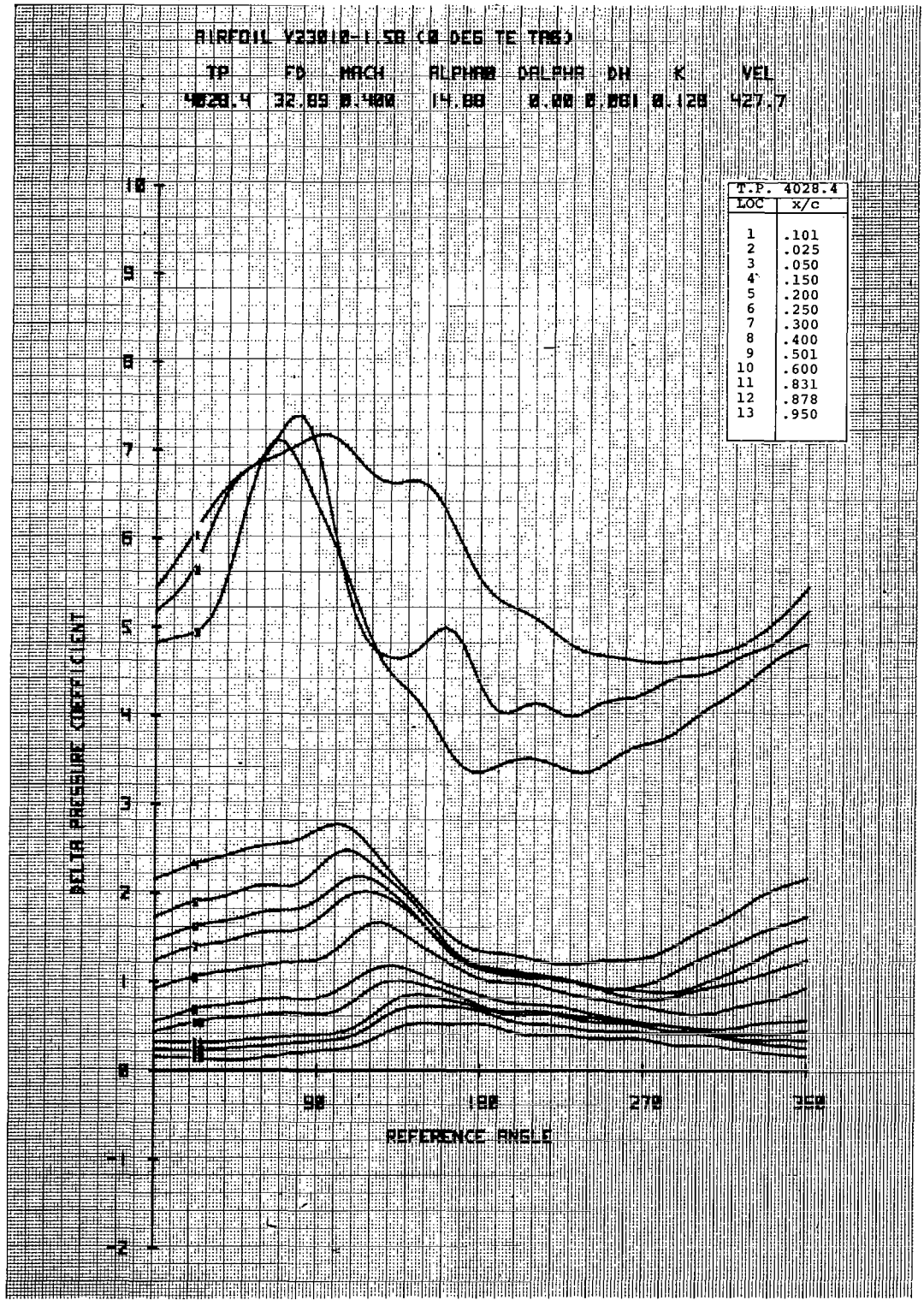

Figure 30c. Airfoil V23010-1.58 in Vertical Translation

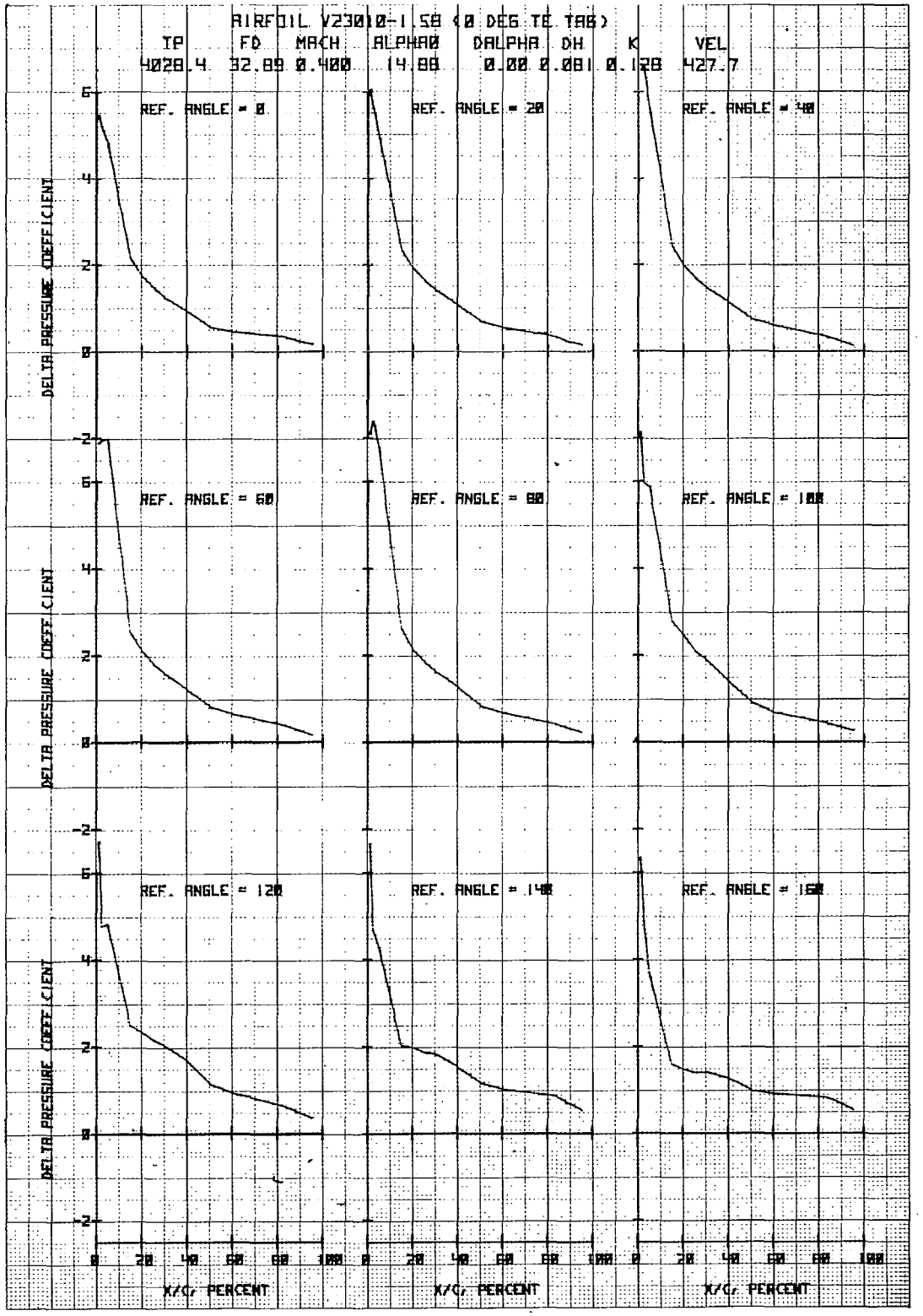

Figure 30d. Airfoil V23010-1.58 in Vertical Translation

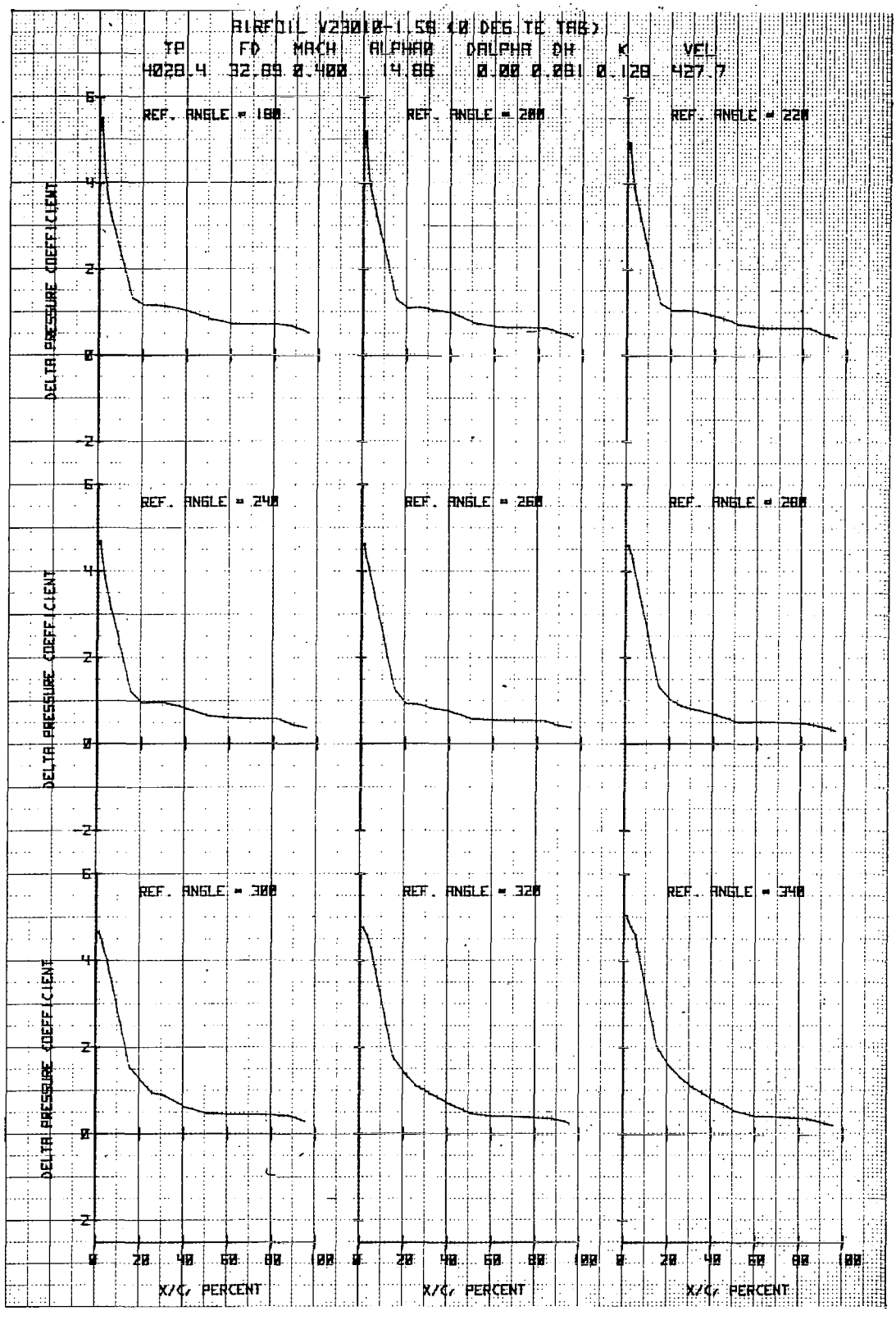

Figure 30e. Airfoil V23010-1.58 in Vertical Translation

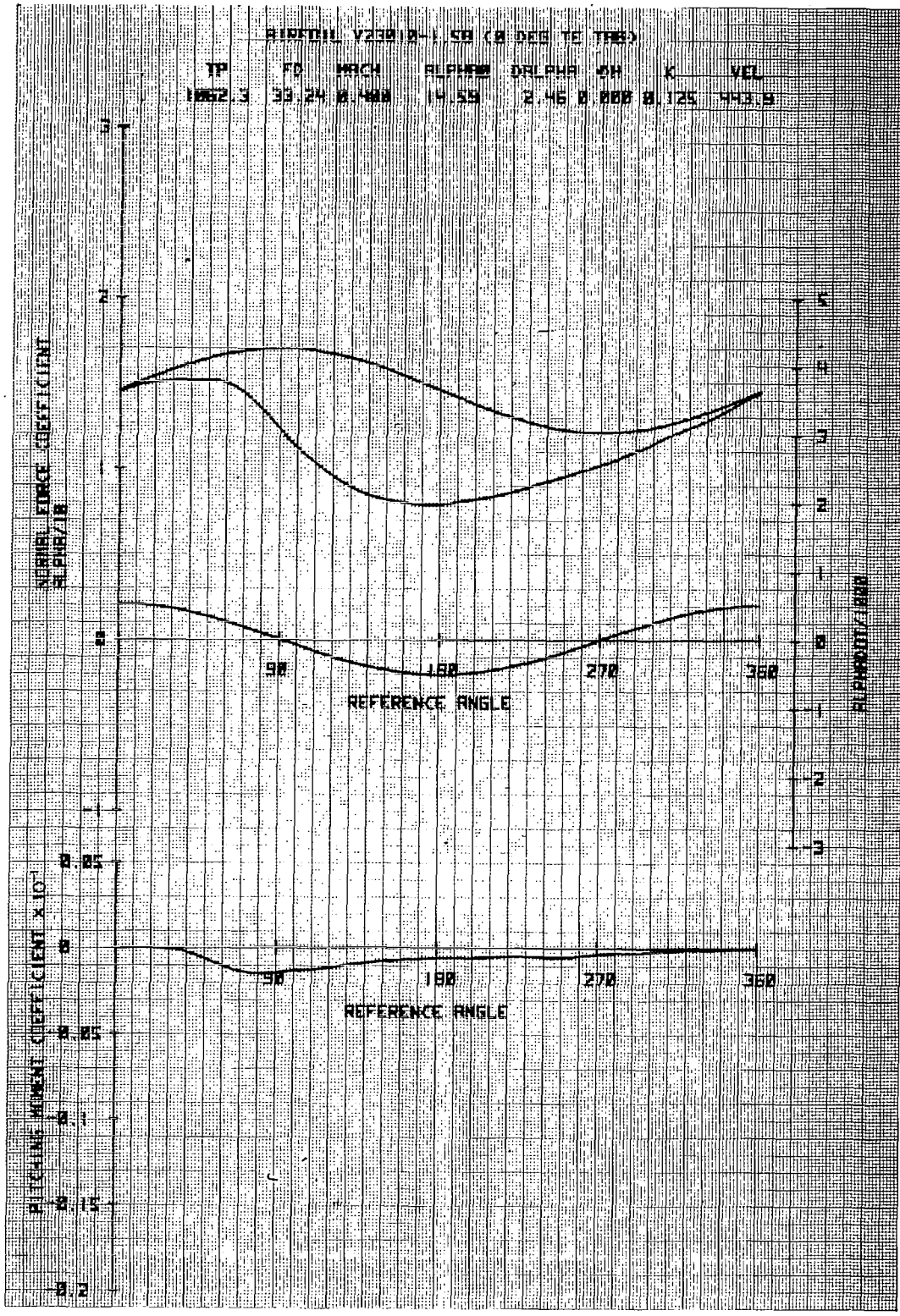

Figure 31a. Airfoil V23010-1.58 in Forced Pitch Oscillation

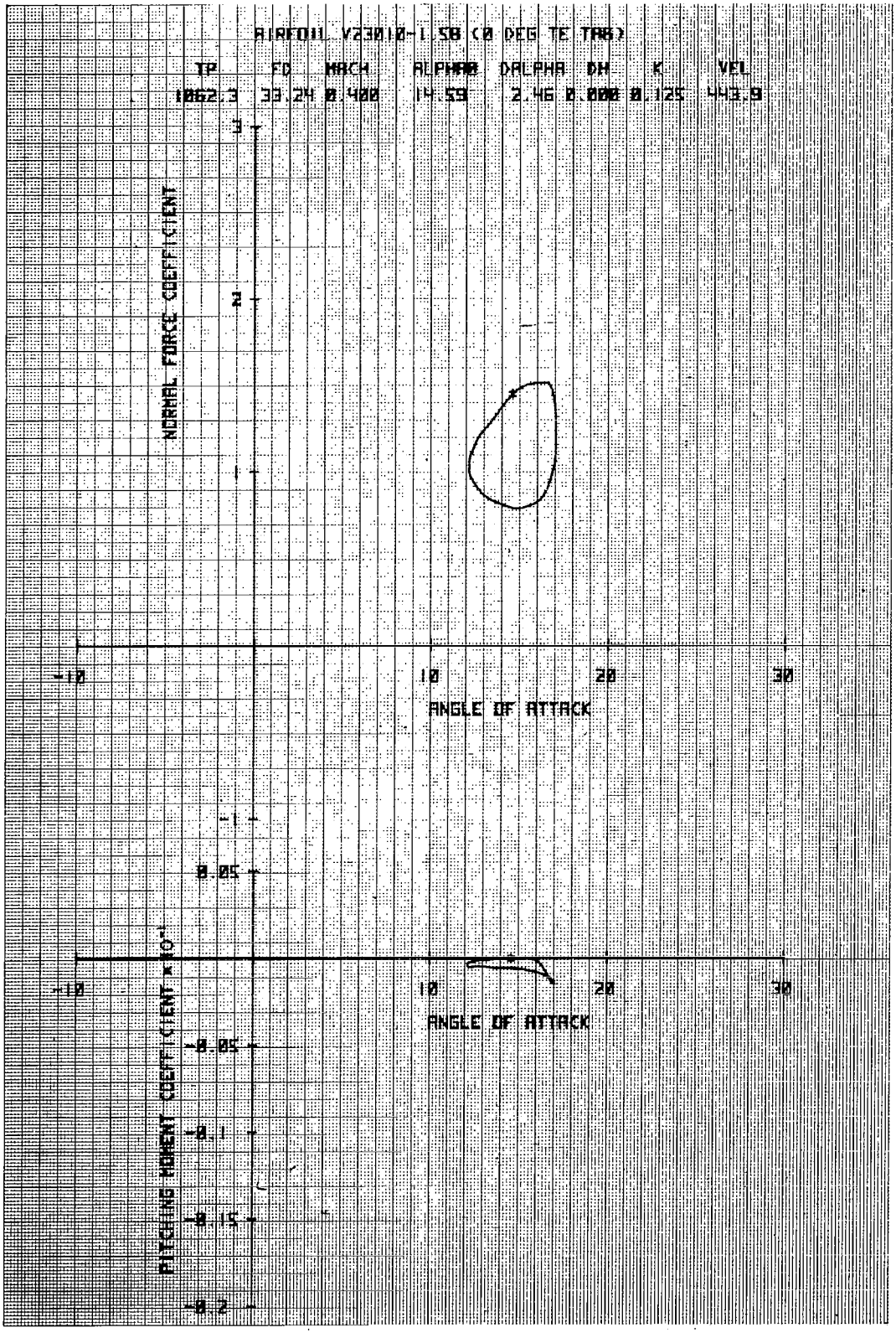

Figure 31b. Airfoil V23010-1.58 in Forced Pitch Oscillation

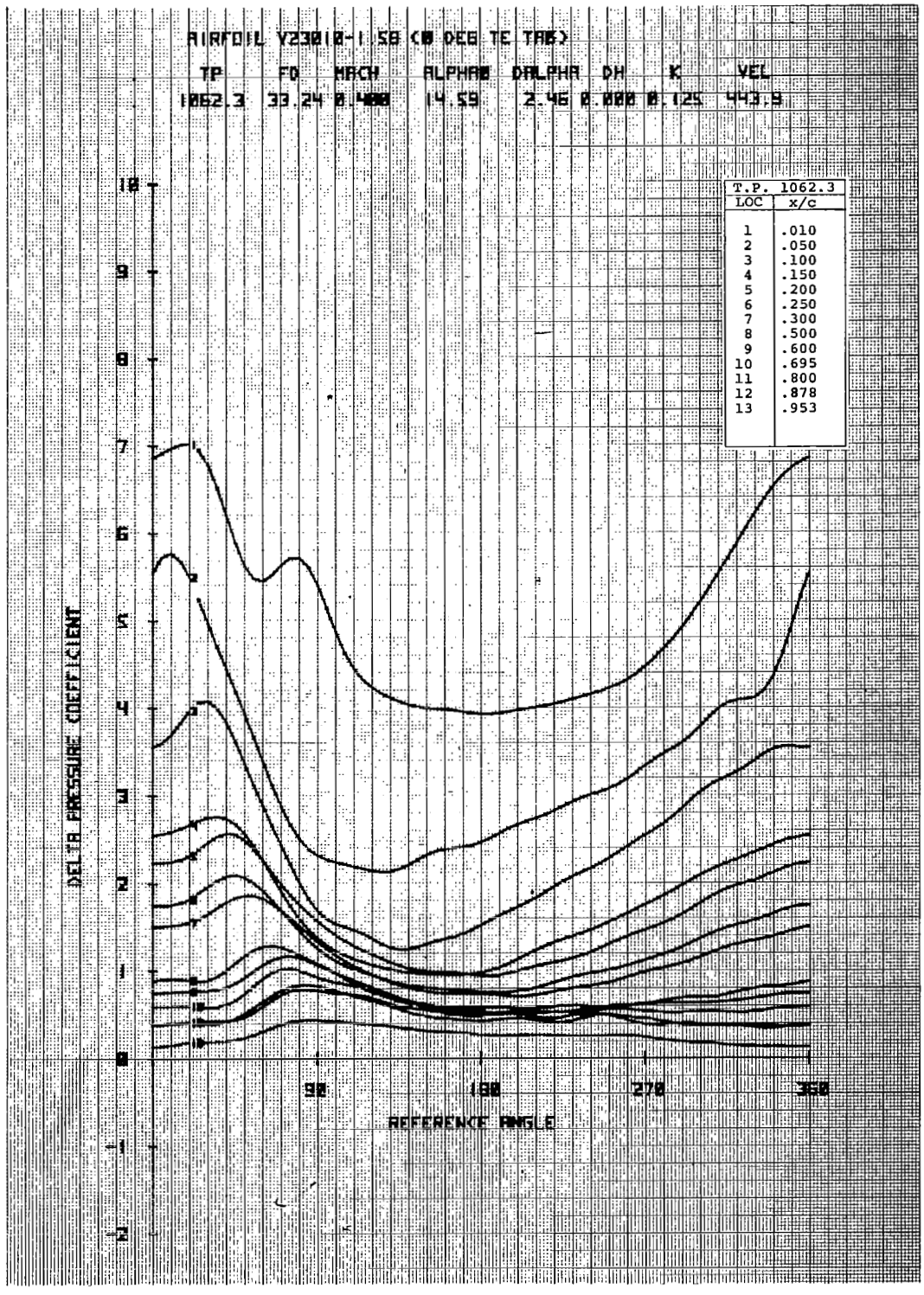

Figure 31c. Airfoil V23010-1.58 in Forced Pitch Oscillation

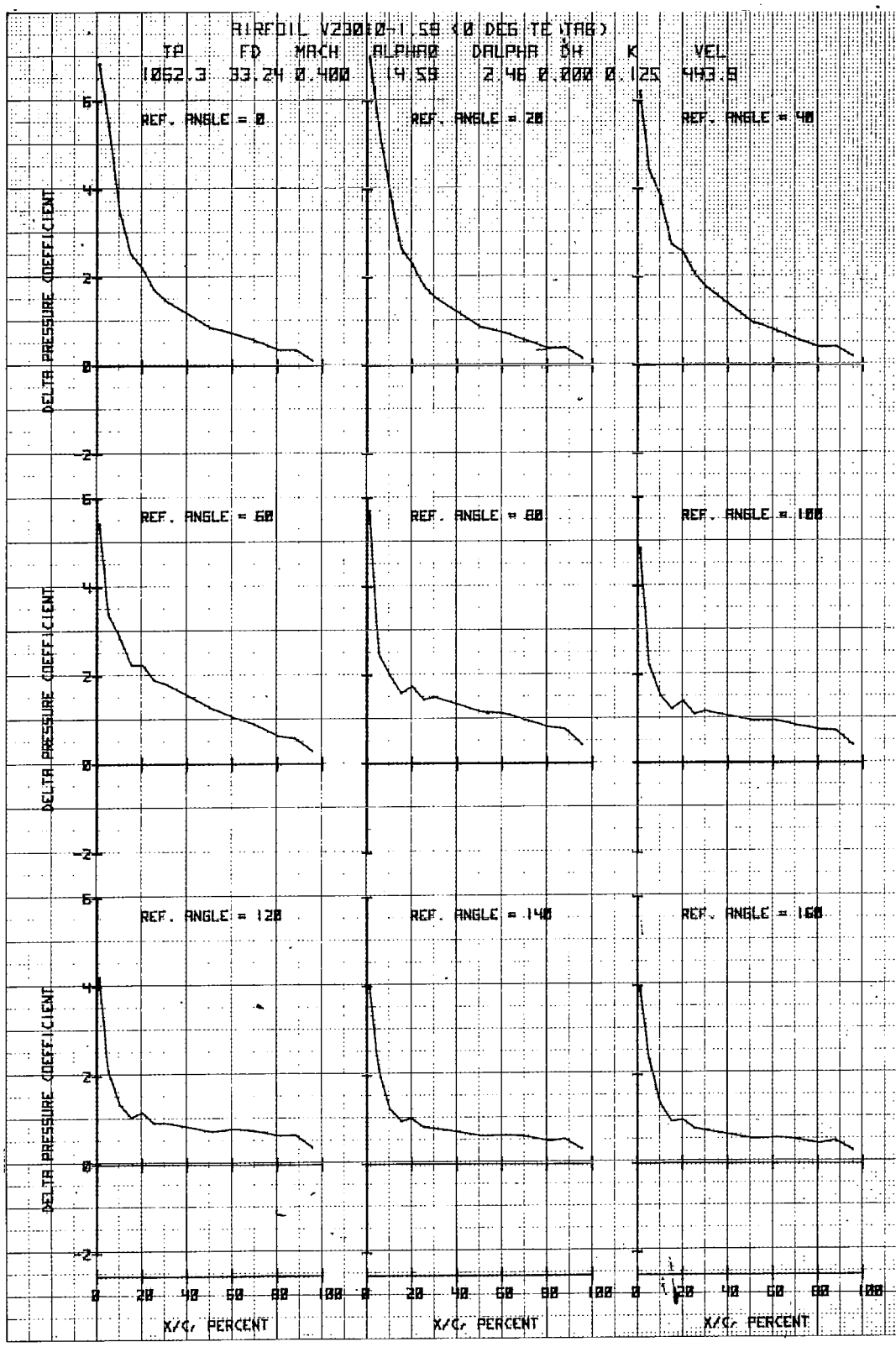

Figure 31d. Airfoil V23010-1.58 in Forced Pitch Oscillation

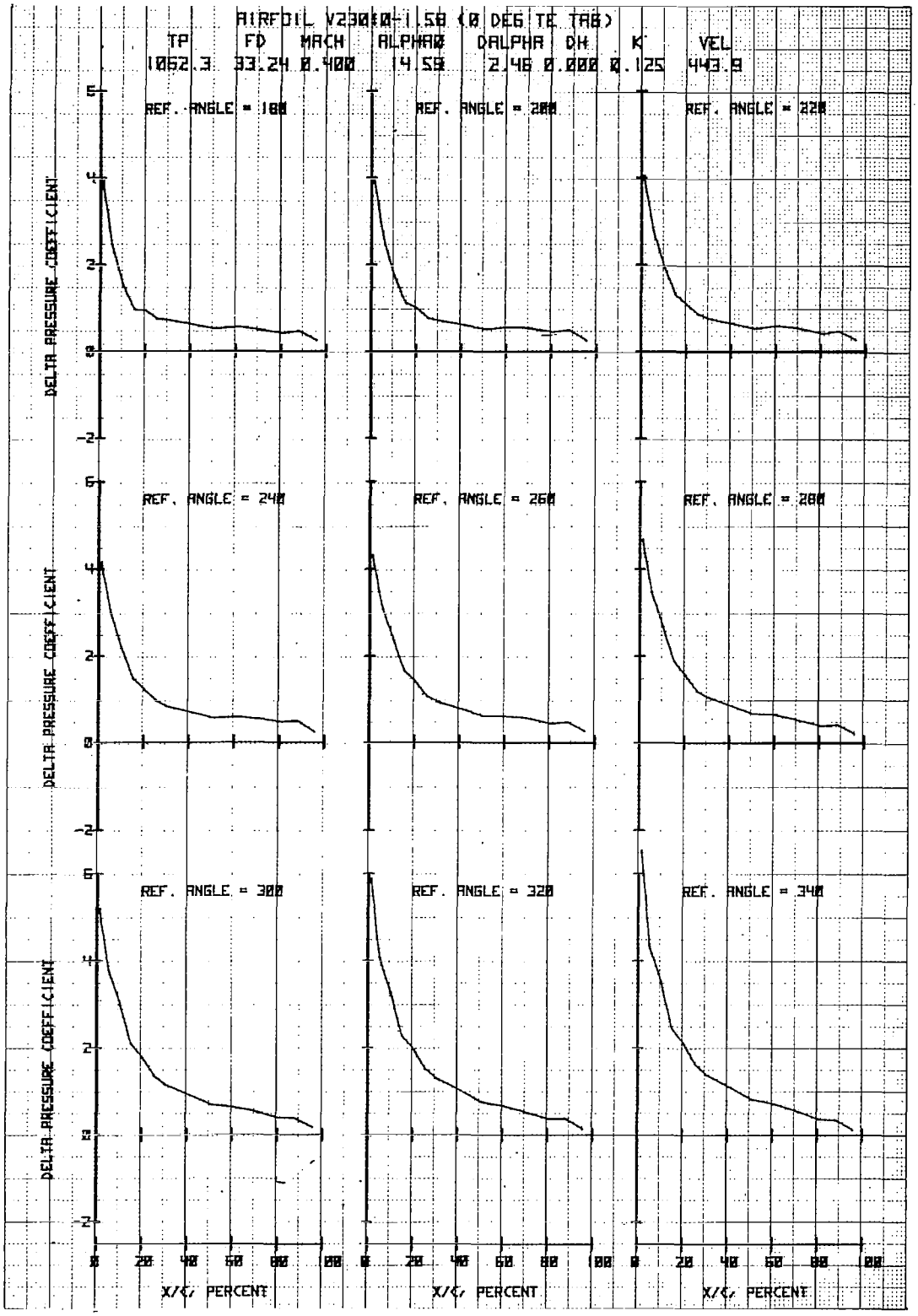

Figure 31e. Airfoil V23010-1.58 in Forced Pitch Oscillation

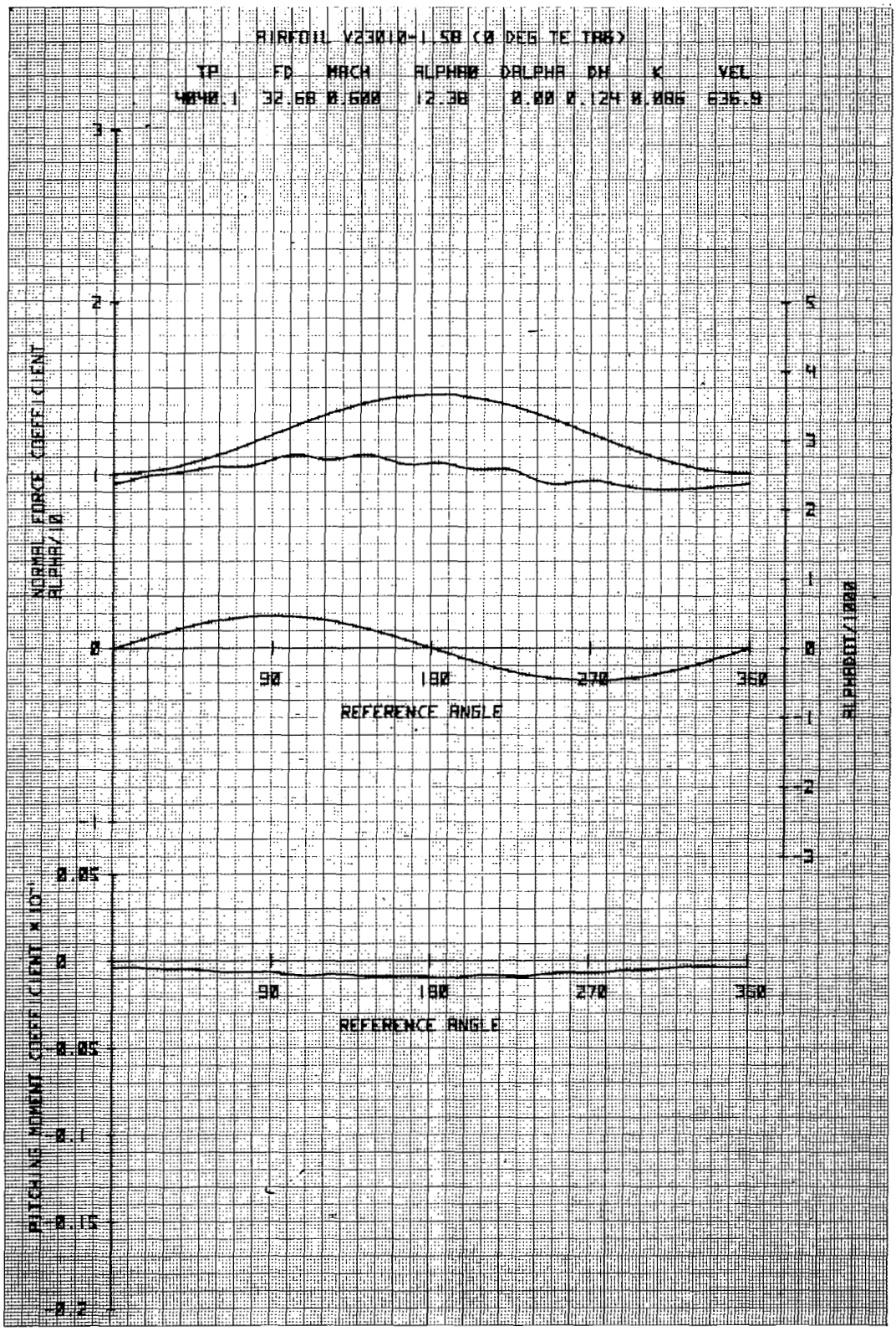

Figure 32a. Airfoil V23010-1.58 in Vertical Translation

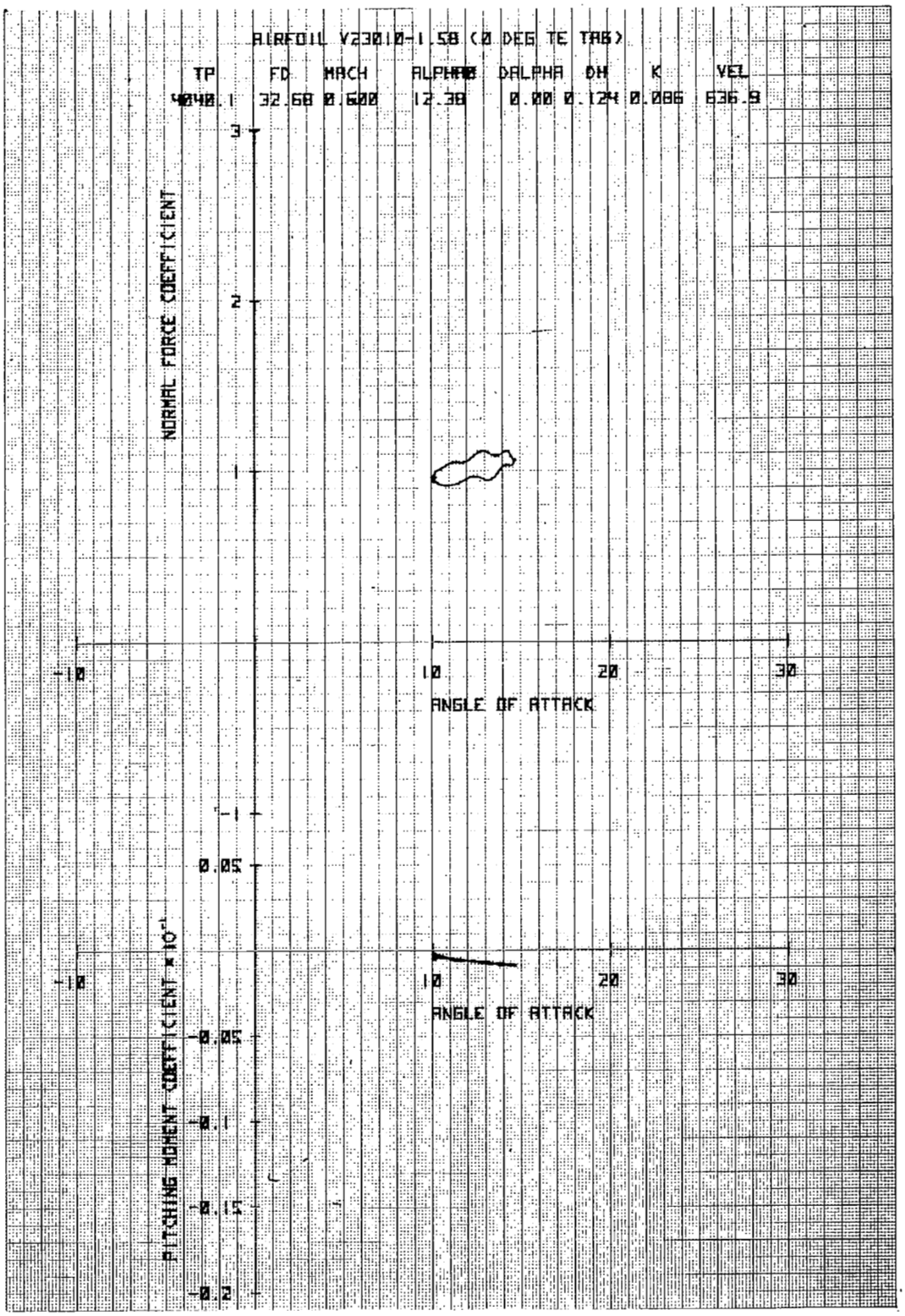

Figure 32b. Airfoil V23010-1.58 in Vertical Translation

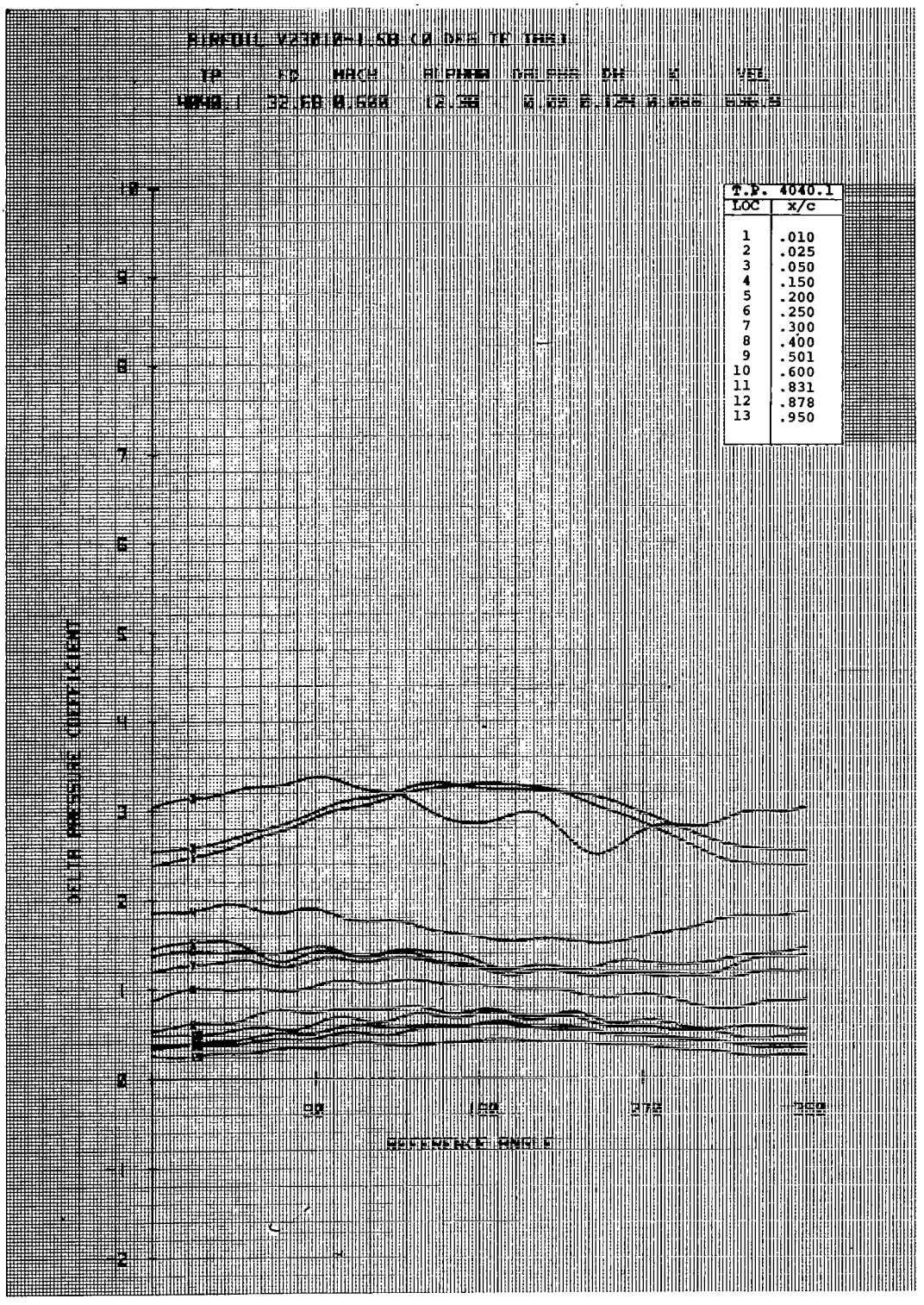

Figure 32c. Airfoil V23010-1.58 in Vertical Translation

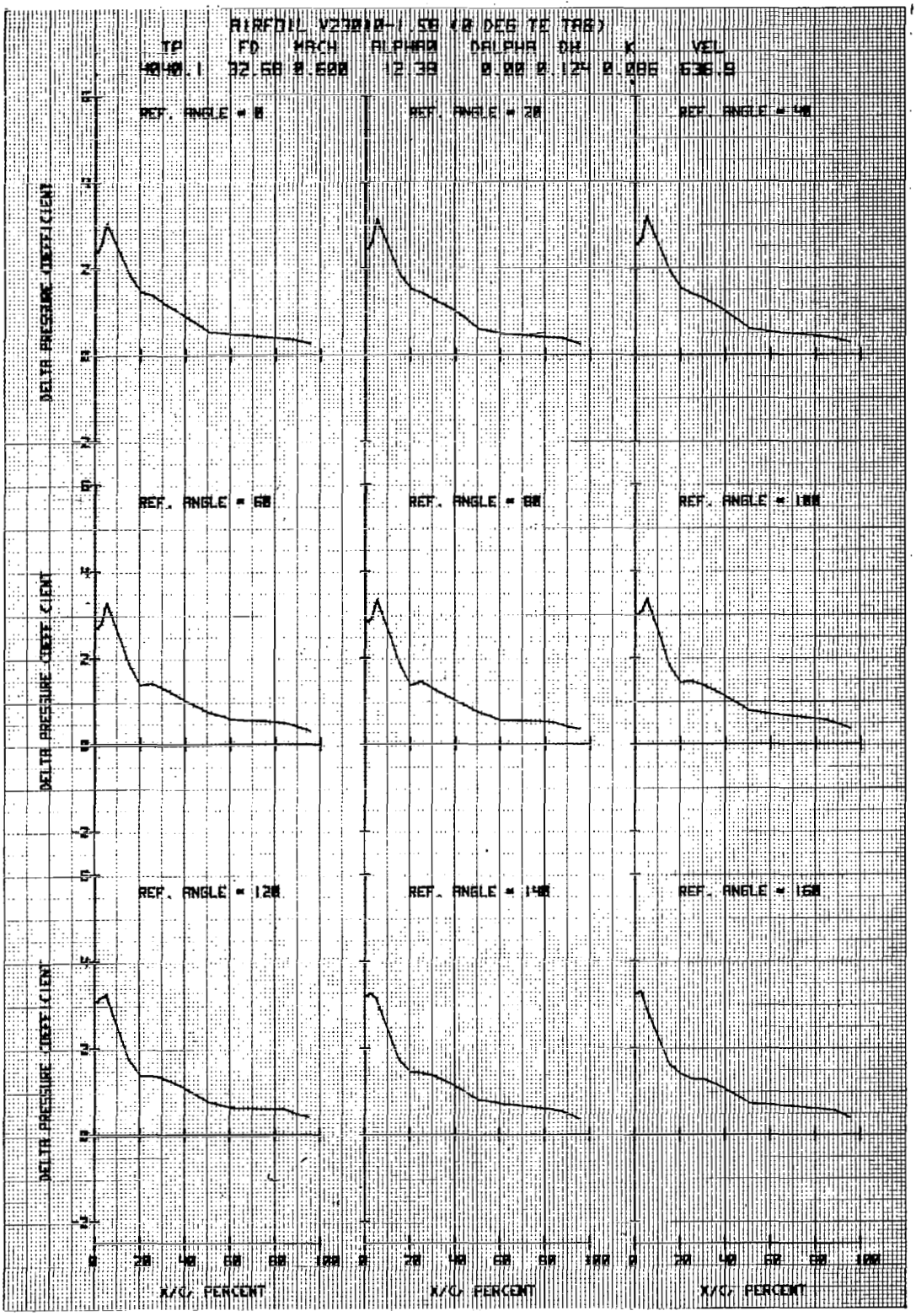

Figure 32d. Airfoil V23010-1.58 in Vertical Translation

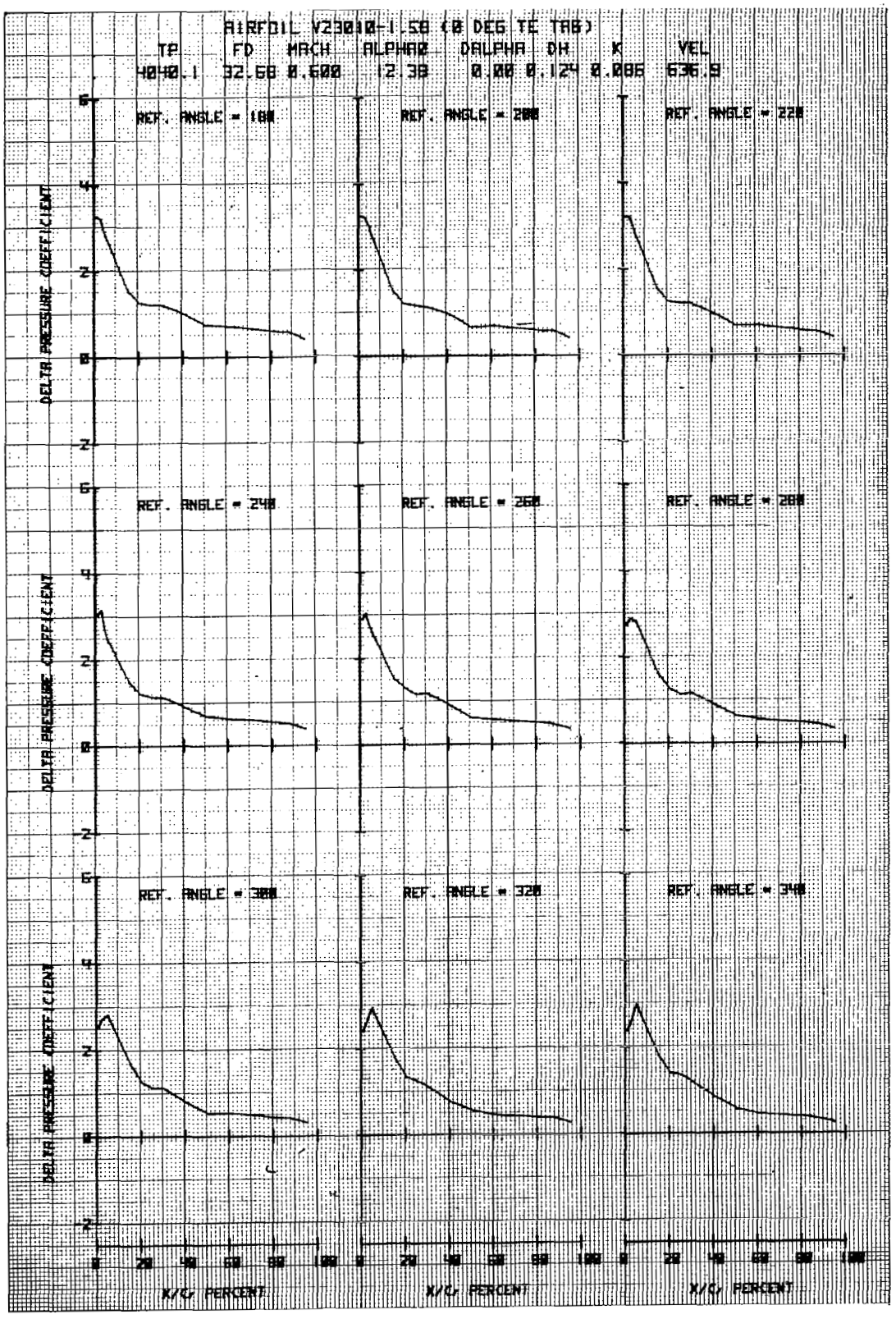

Figure 32e. Airfoil V23010-1.58 in Vertical Translation

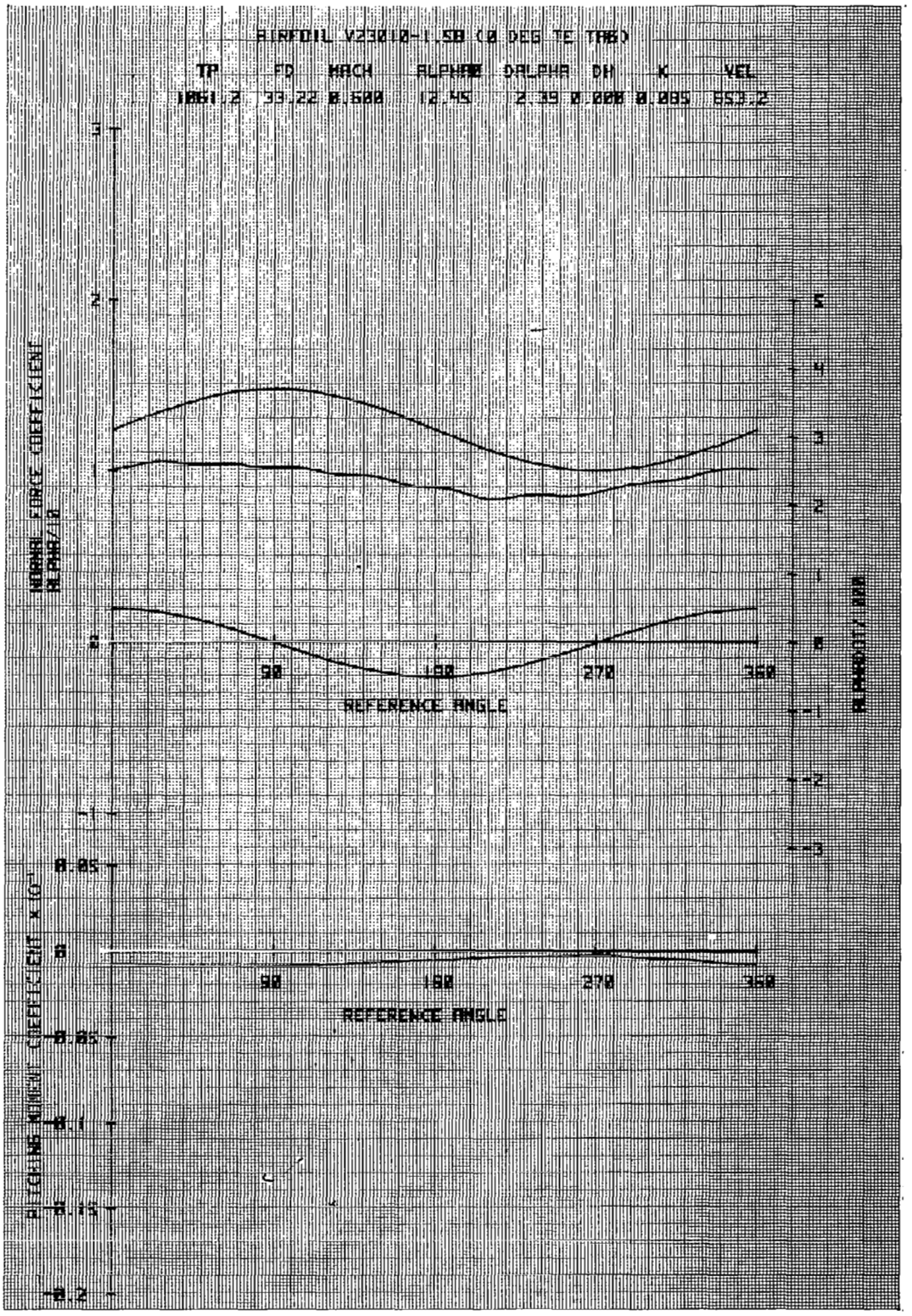

Figure 33a. Airfoil V23010-1.58 in Forced Pitch Oscillation

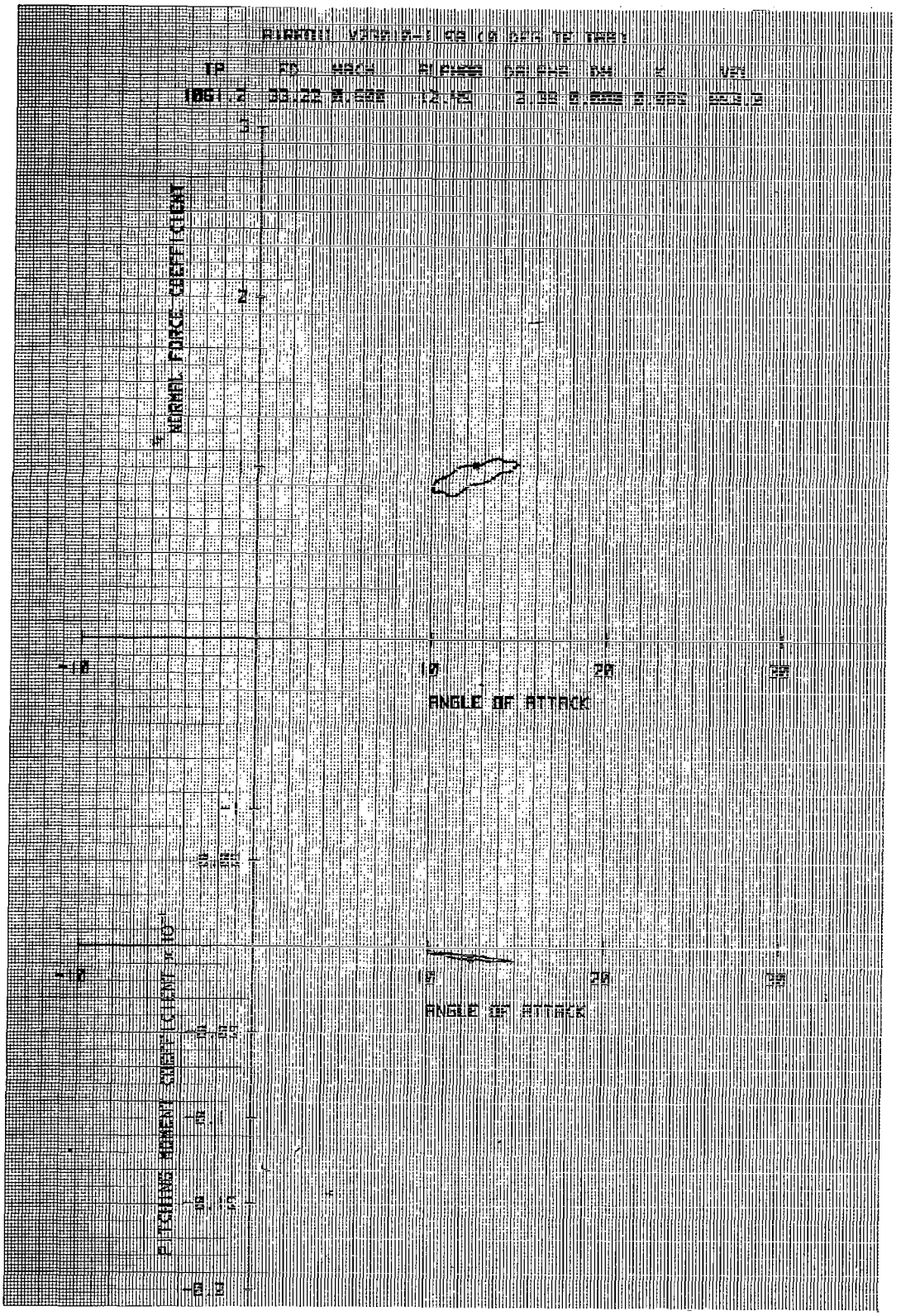

Figure 33b. Airfoil V23010-1.58 in Forced Pitch Oscillation

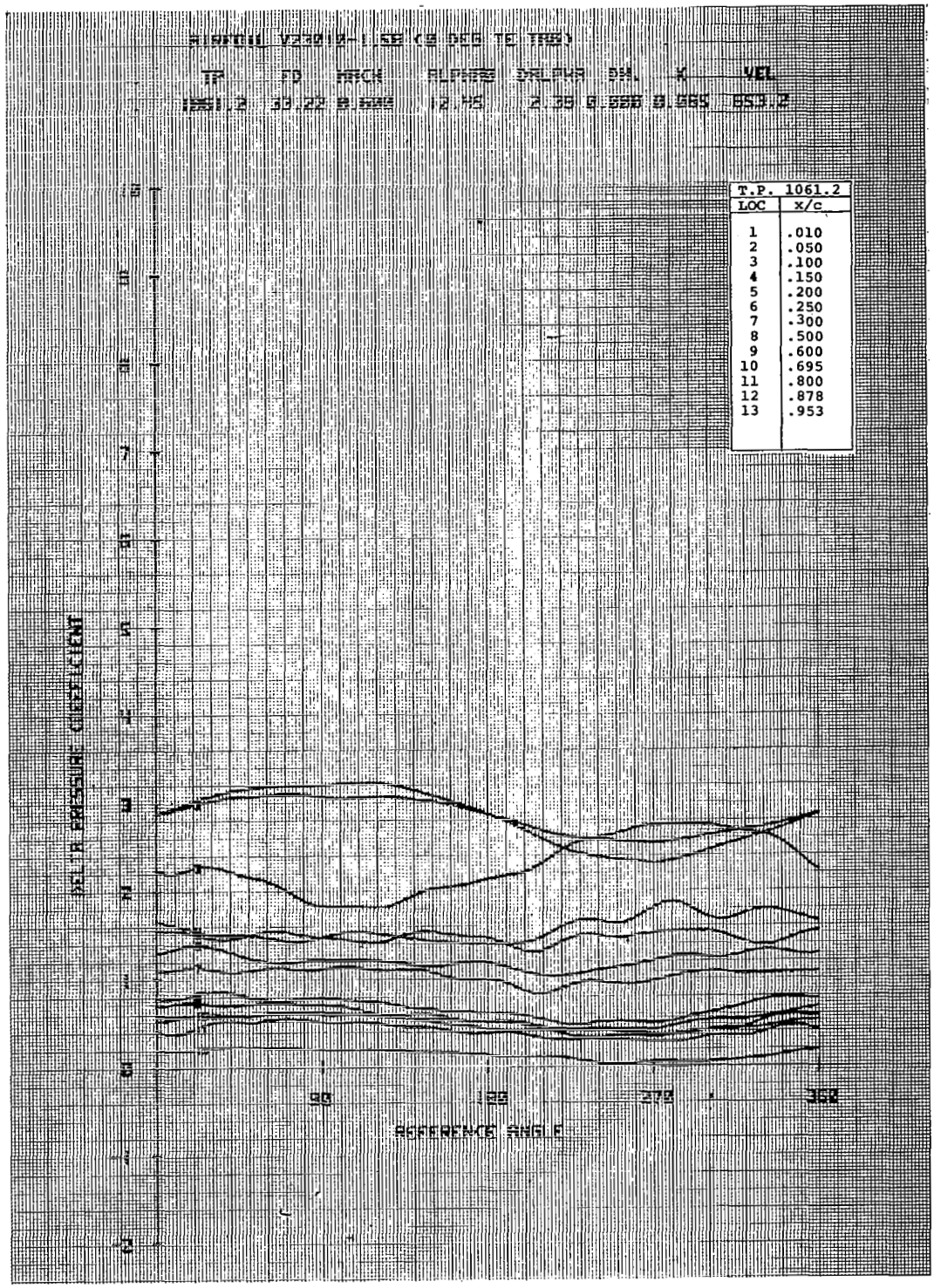

Figure 33c. Airfoil V23010-1.58 in Forced Pitch Oscillation

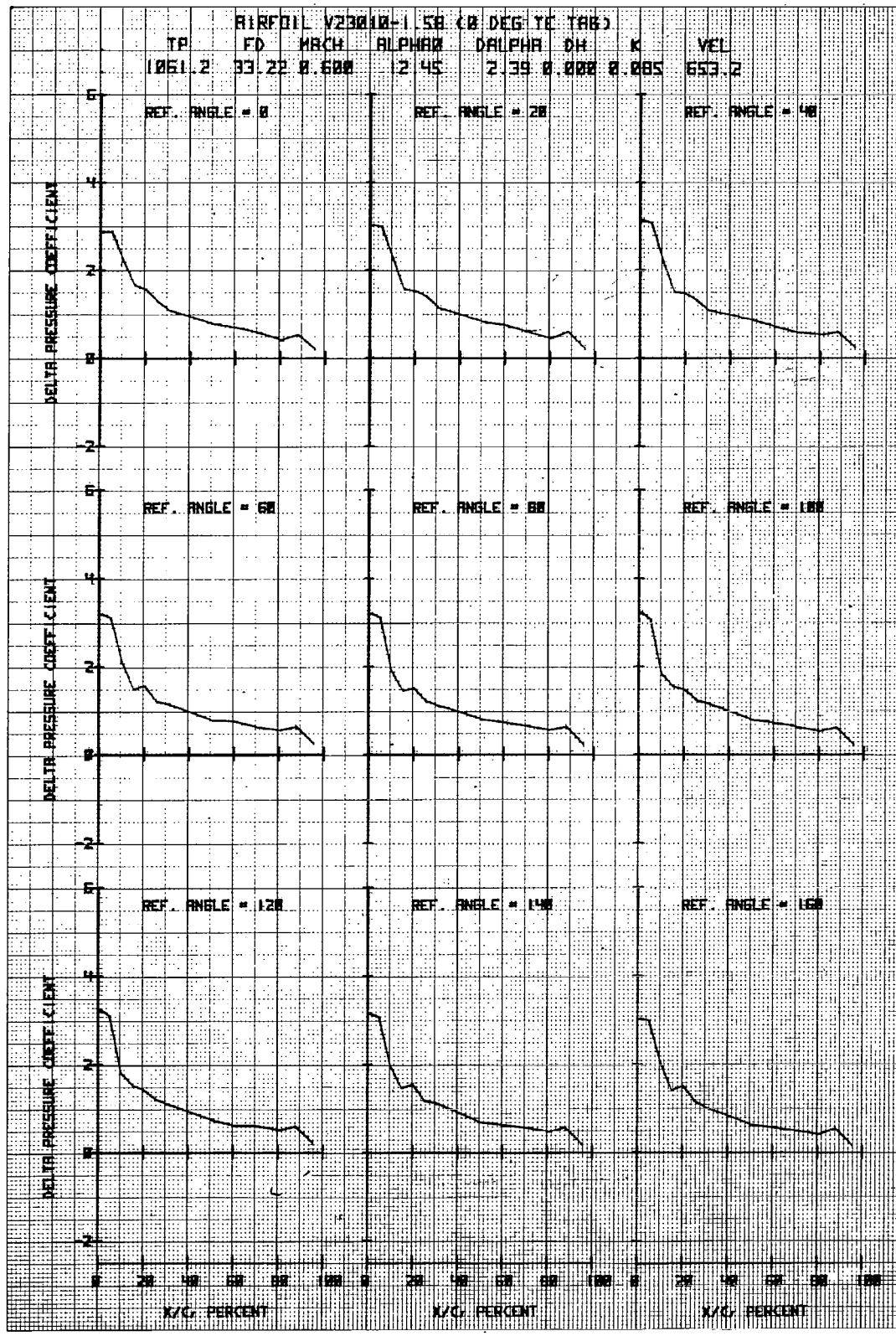

Figure 33d. Airfoil V23010-1.58 in Forced Pitch Oscillation

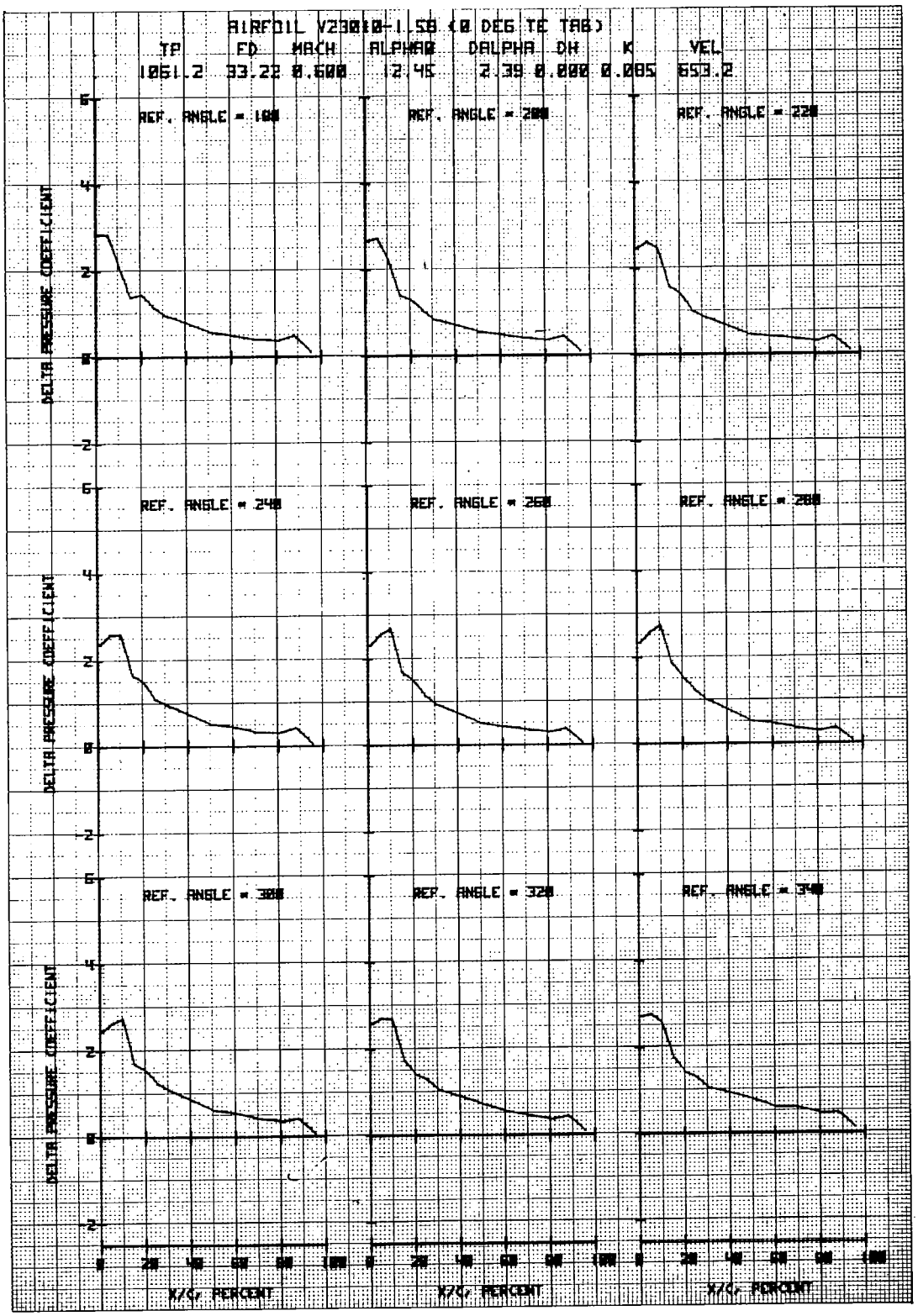

Figure 33e. Airfoil V23010-1.58 in Forced Pitch Oscillation

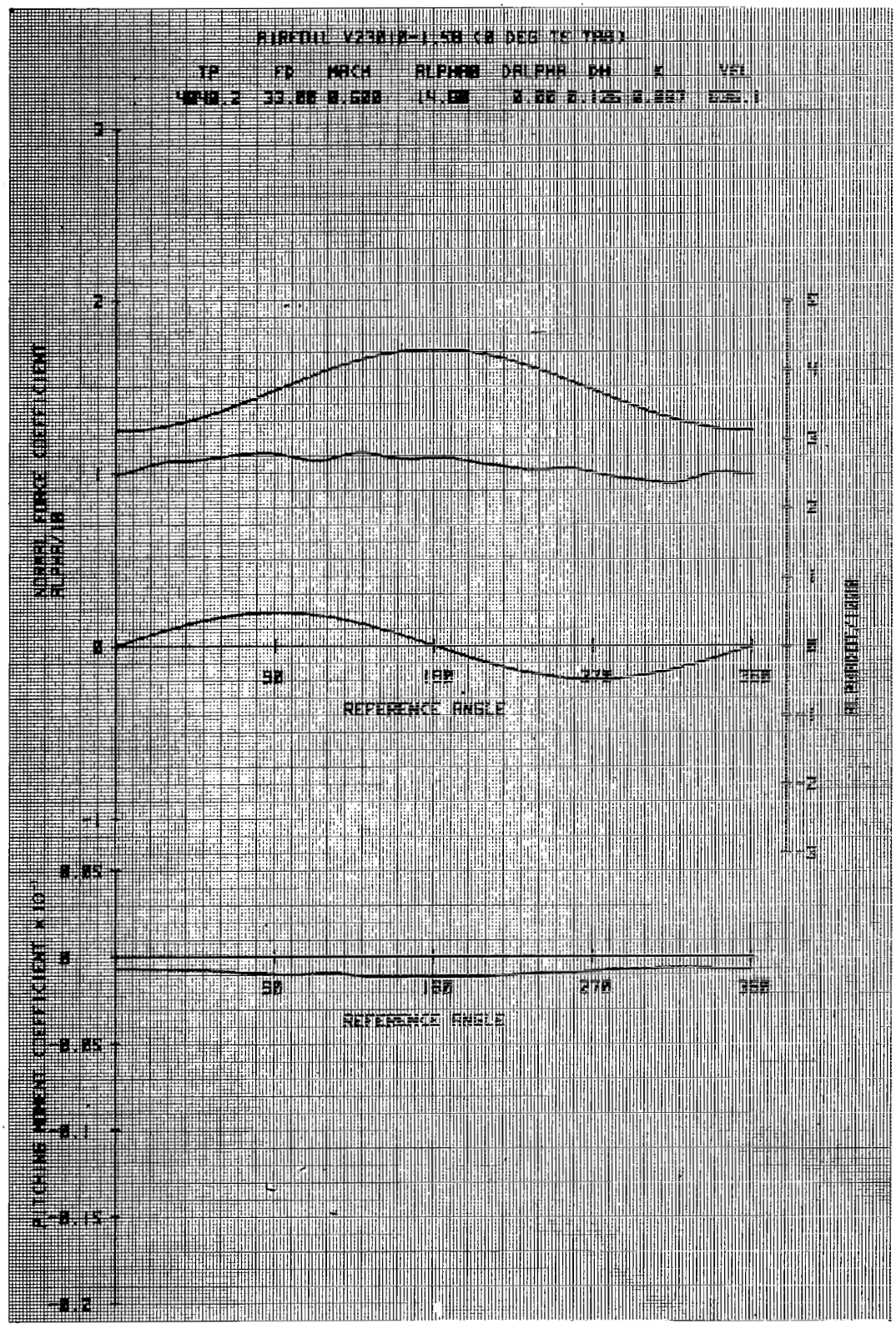

Figure 34a. Airfoil V23010-1.58 in Vertical Translation

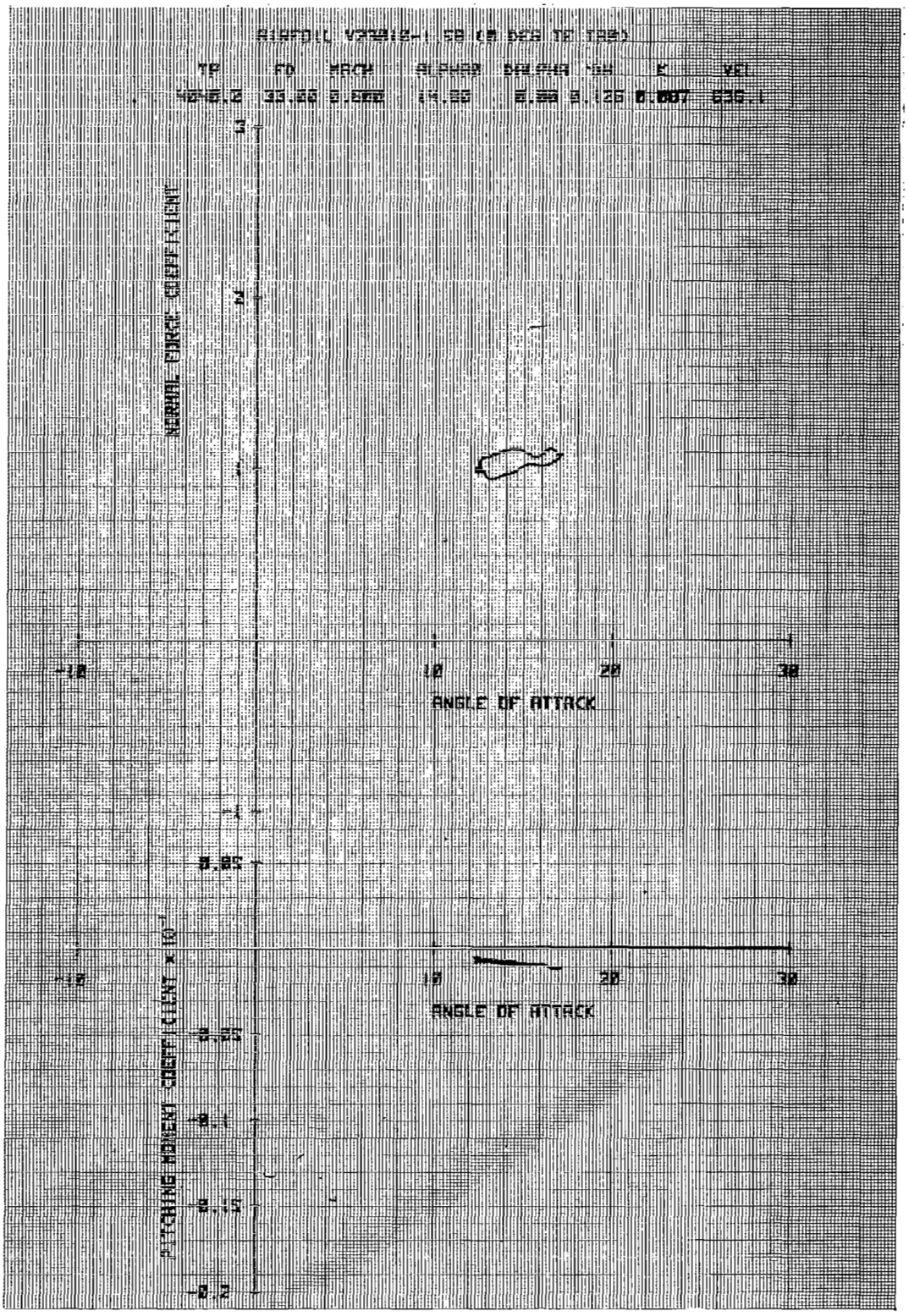

Figure 34b. Airfoil V23010-1.58 in Vertical Translation

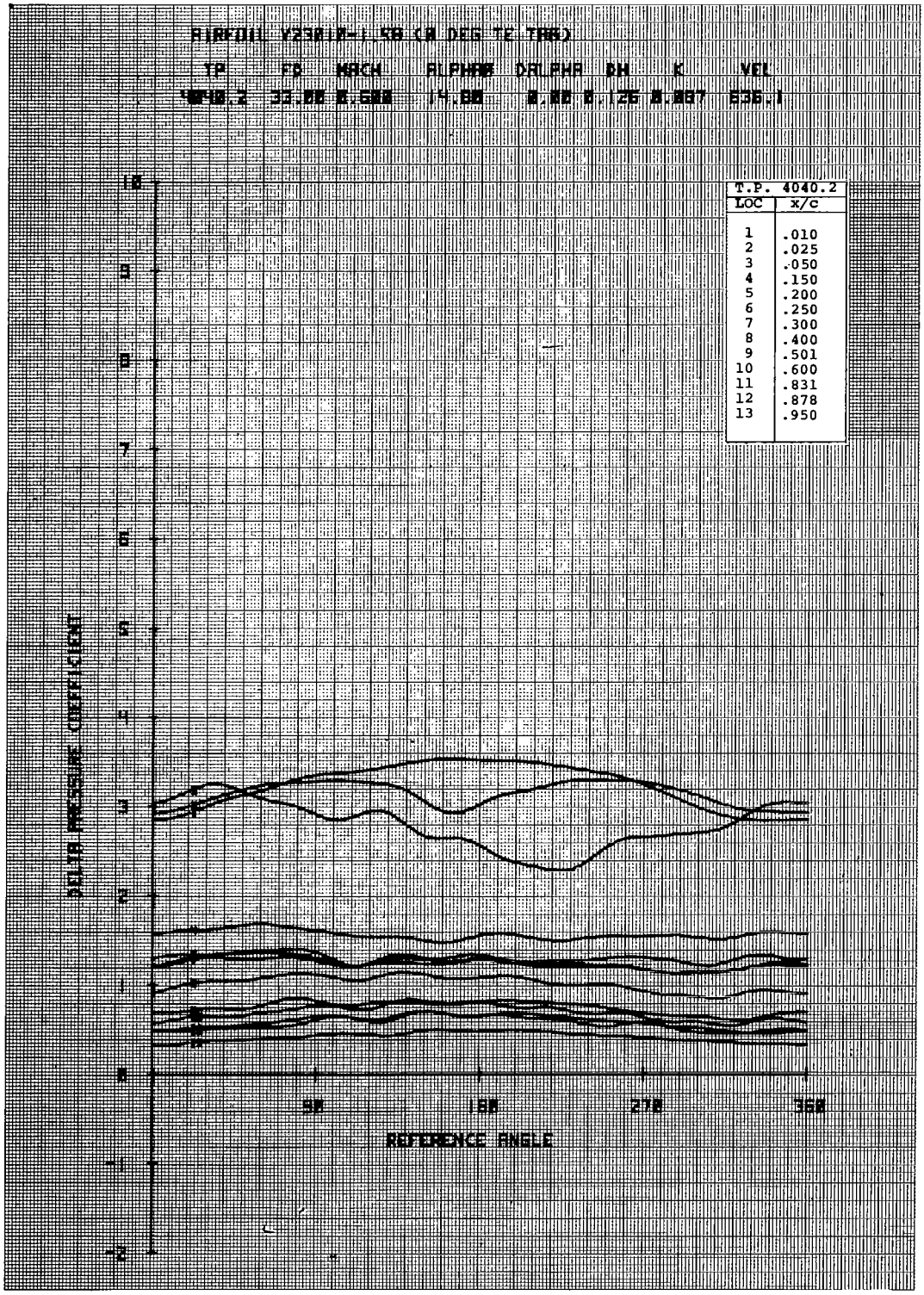

Figure 34c. Airfoil V23010-1.58 in Vertical Translation

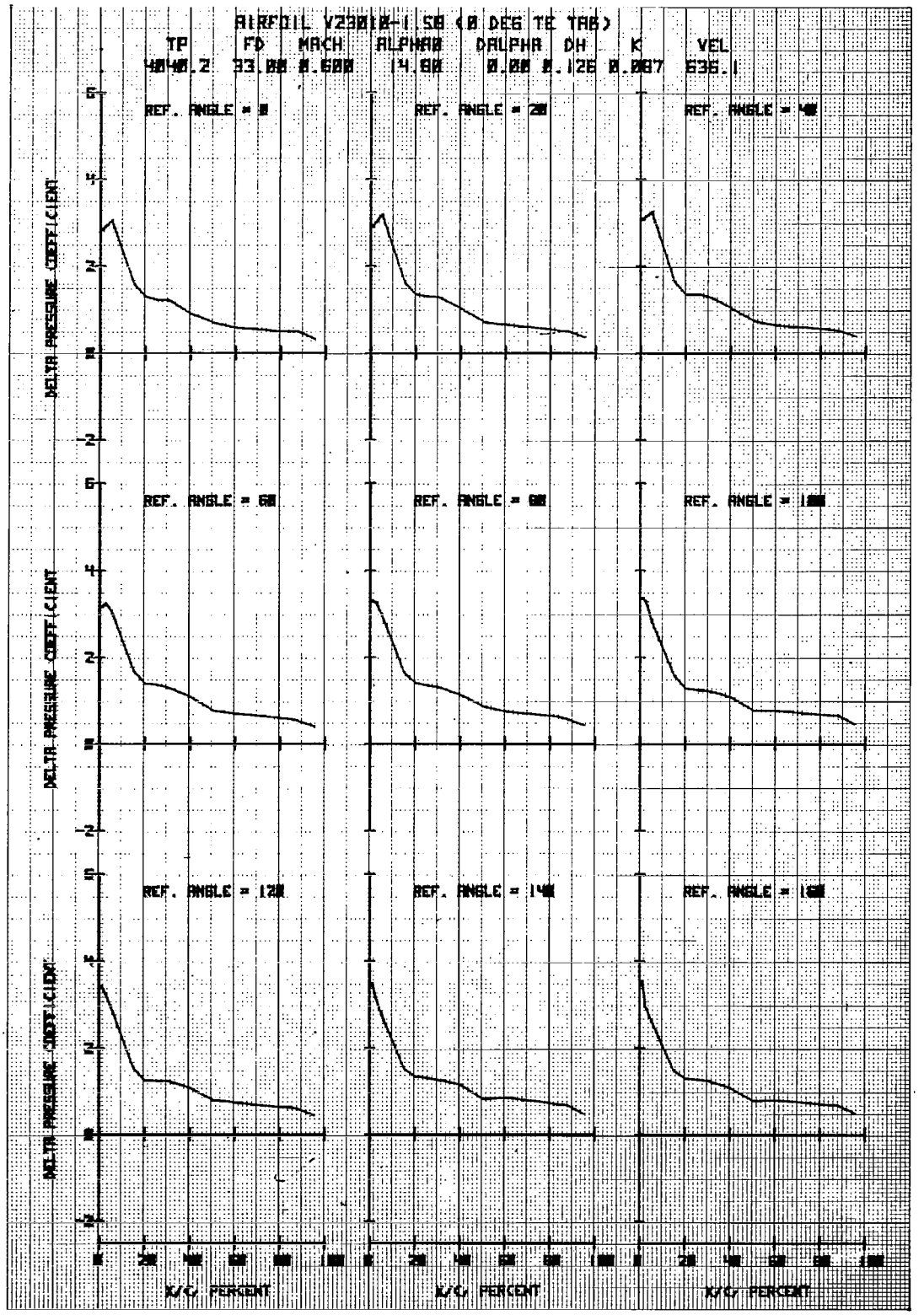

Figure 34d. Airfoil V23010-1.58 in Vertical Translation

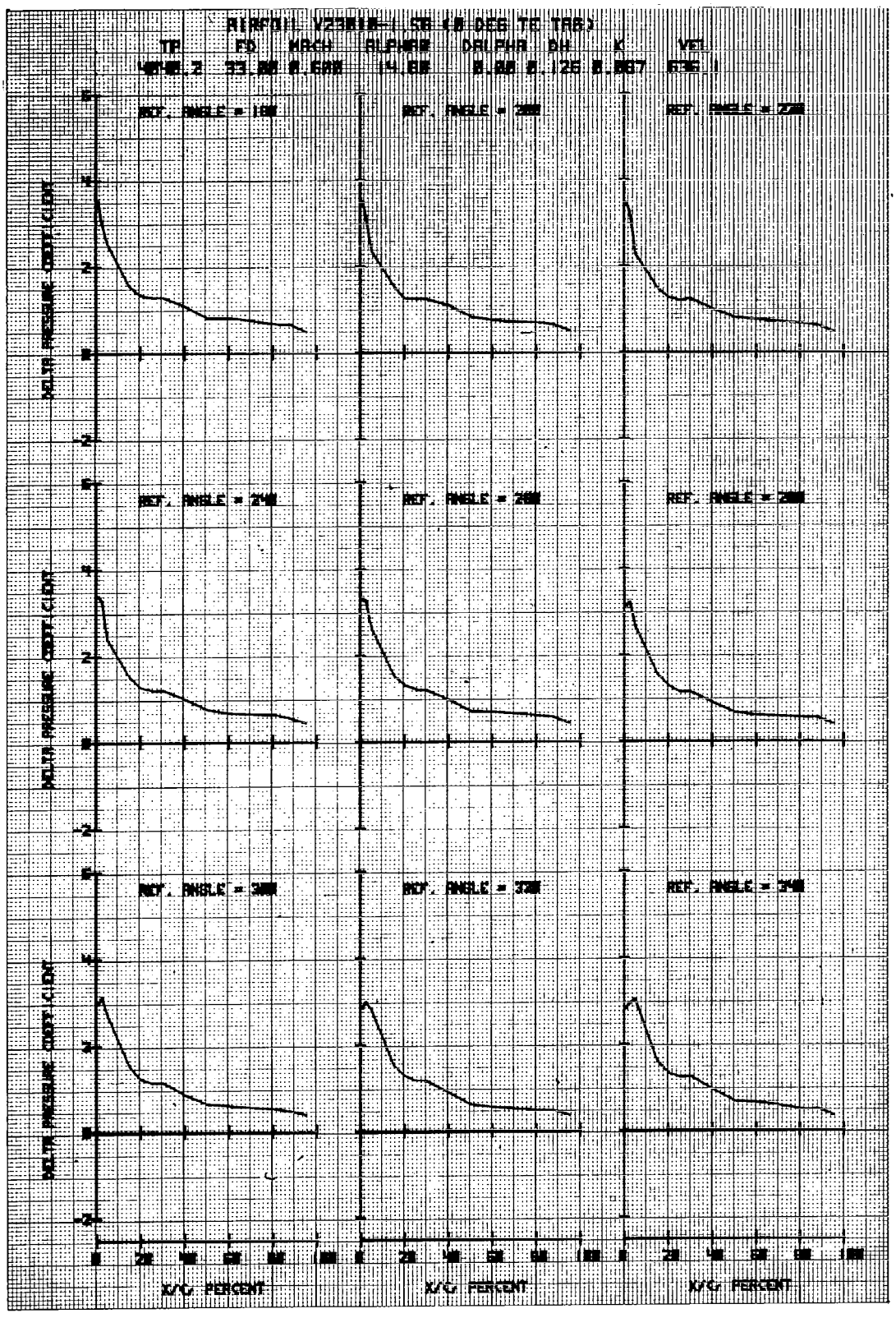

Figure 34e. Airfoil V23010-1.58 in Vertical Translation

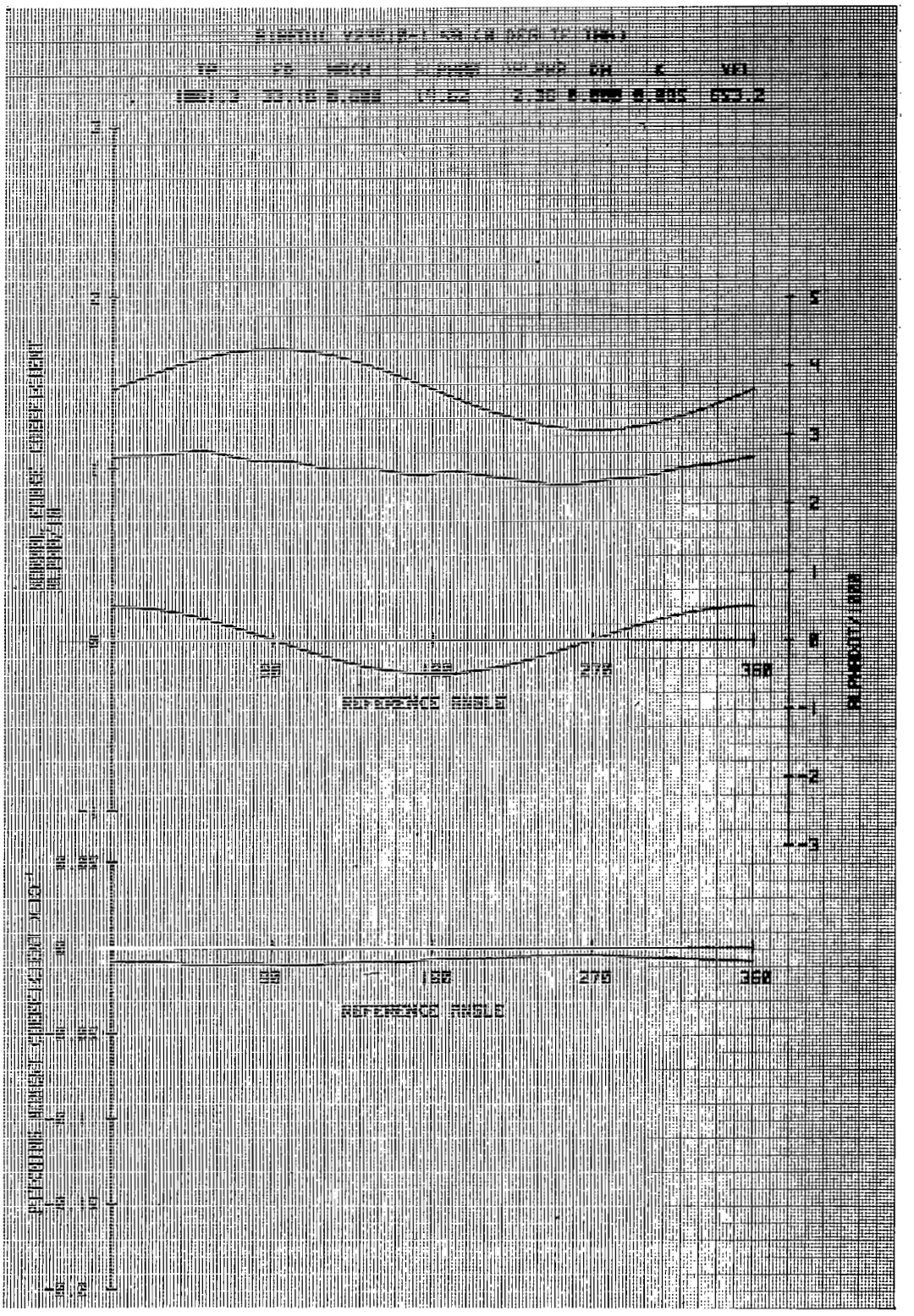

Figure 35a. Airfoil V23010-1.58 in Forced Pitch Oscillation

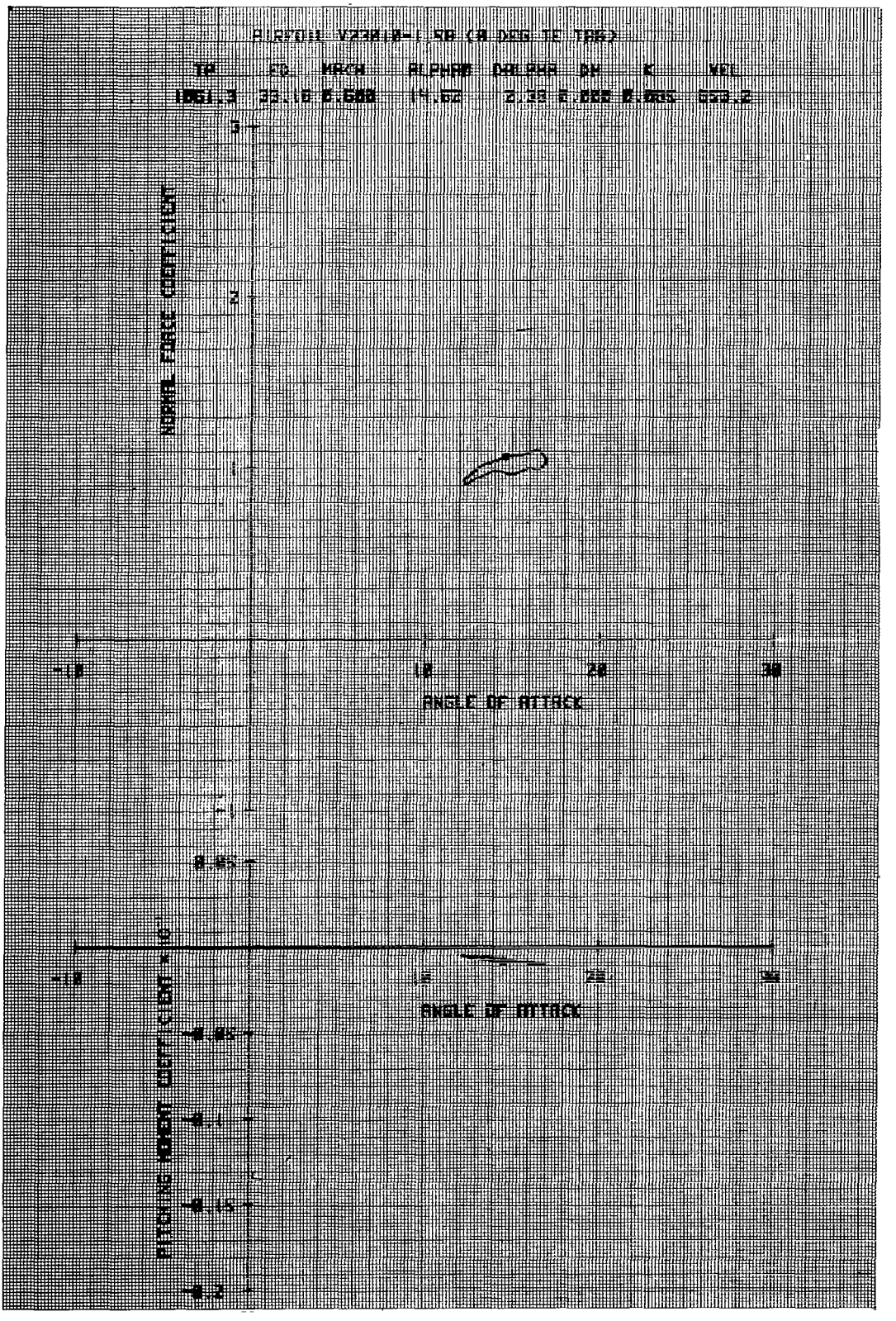

Figure 35b. Airfoil V23010-1.58 in Forced Pitch Oscillation

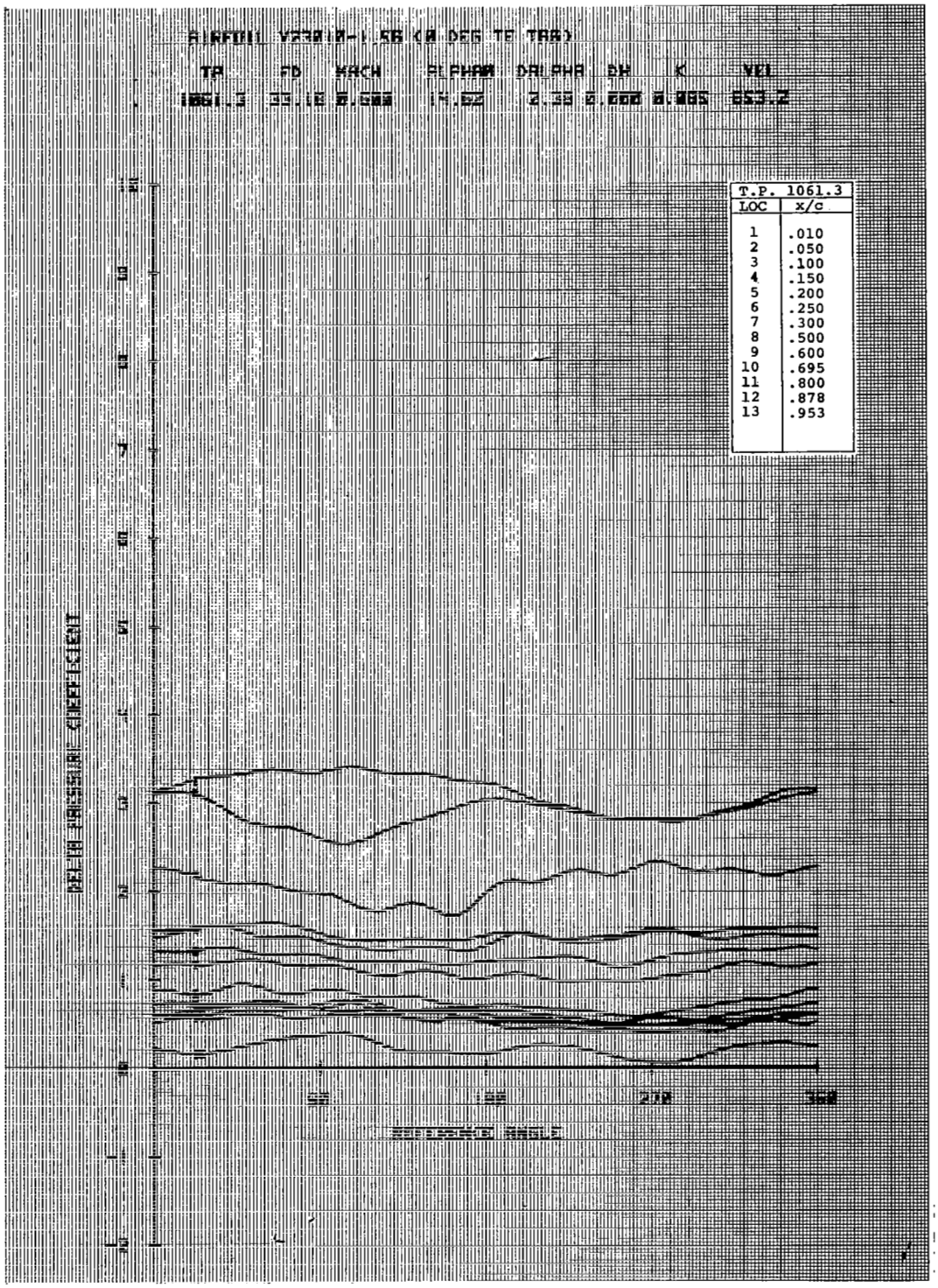

Figure 35c. Airfoil V23010-1.58 in Forced Pitch Oscillation

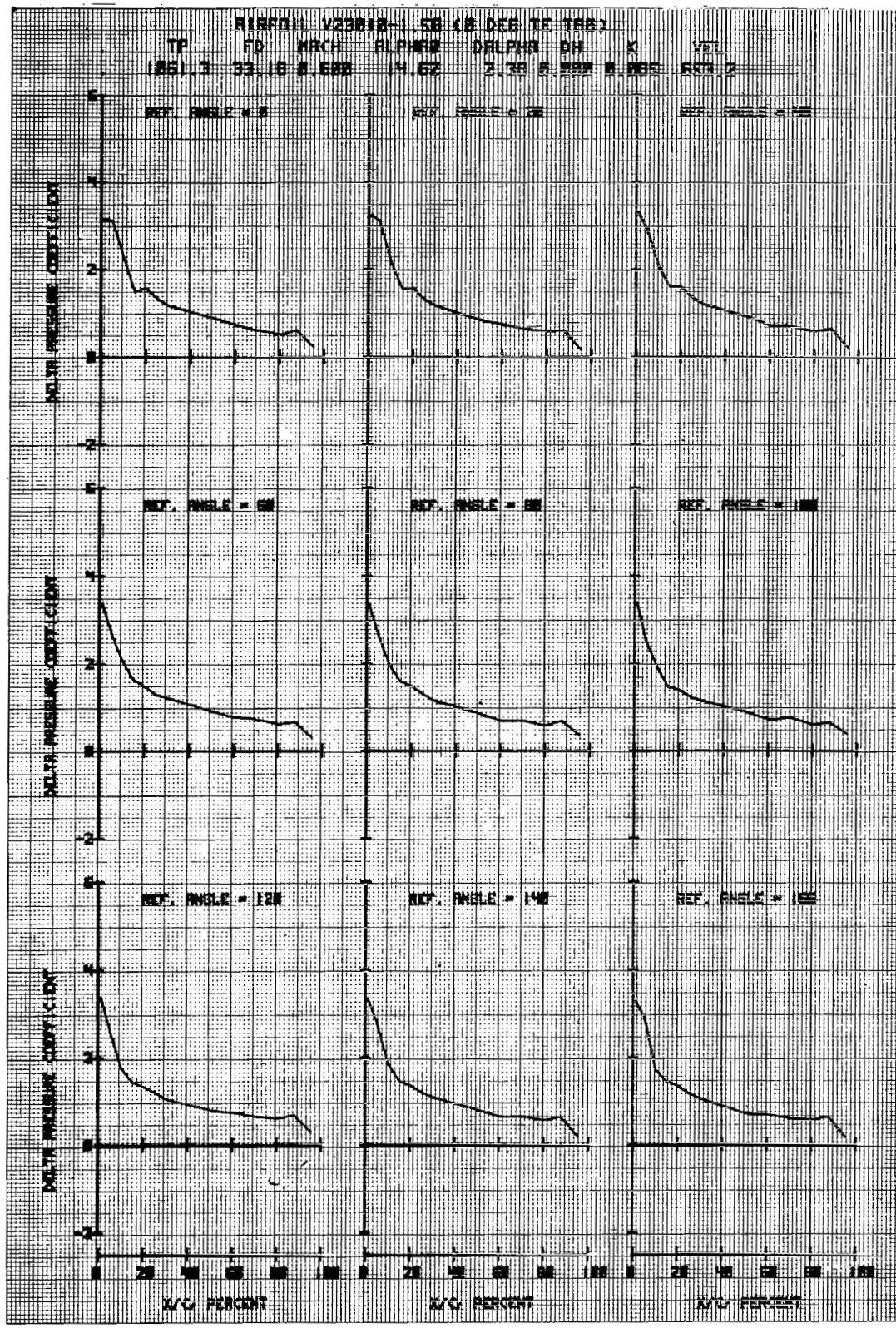

Figure 35d. Airfoil V23010-1.58 in Forced Pitch Oscillation

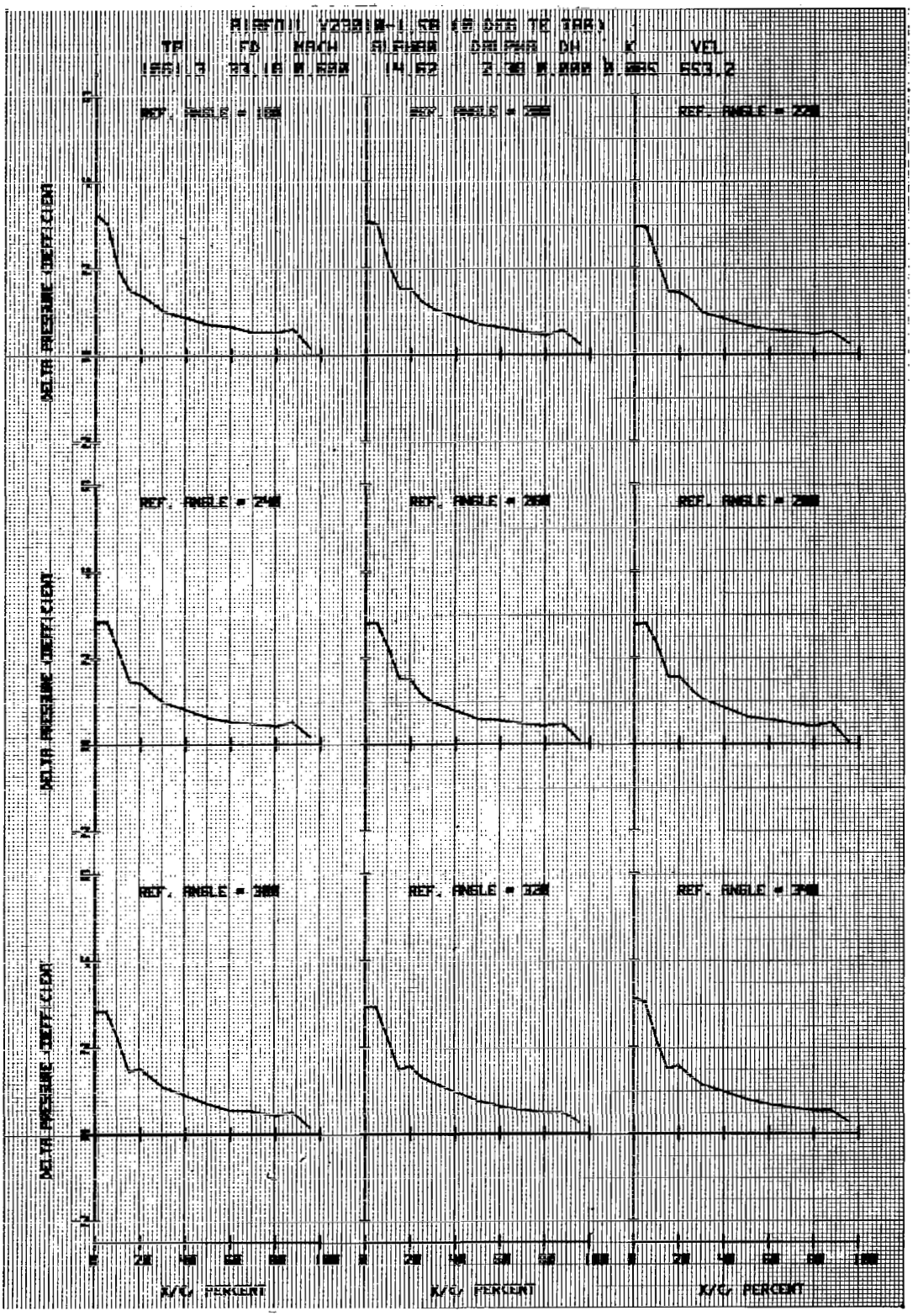

Figure 35e. Airfoil V23010-1.58 in Forced Pitch Oscillation

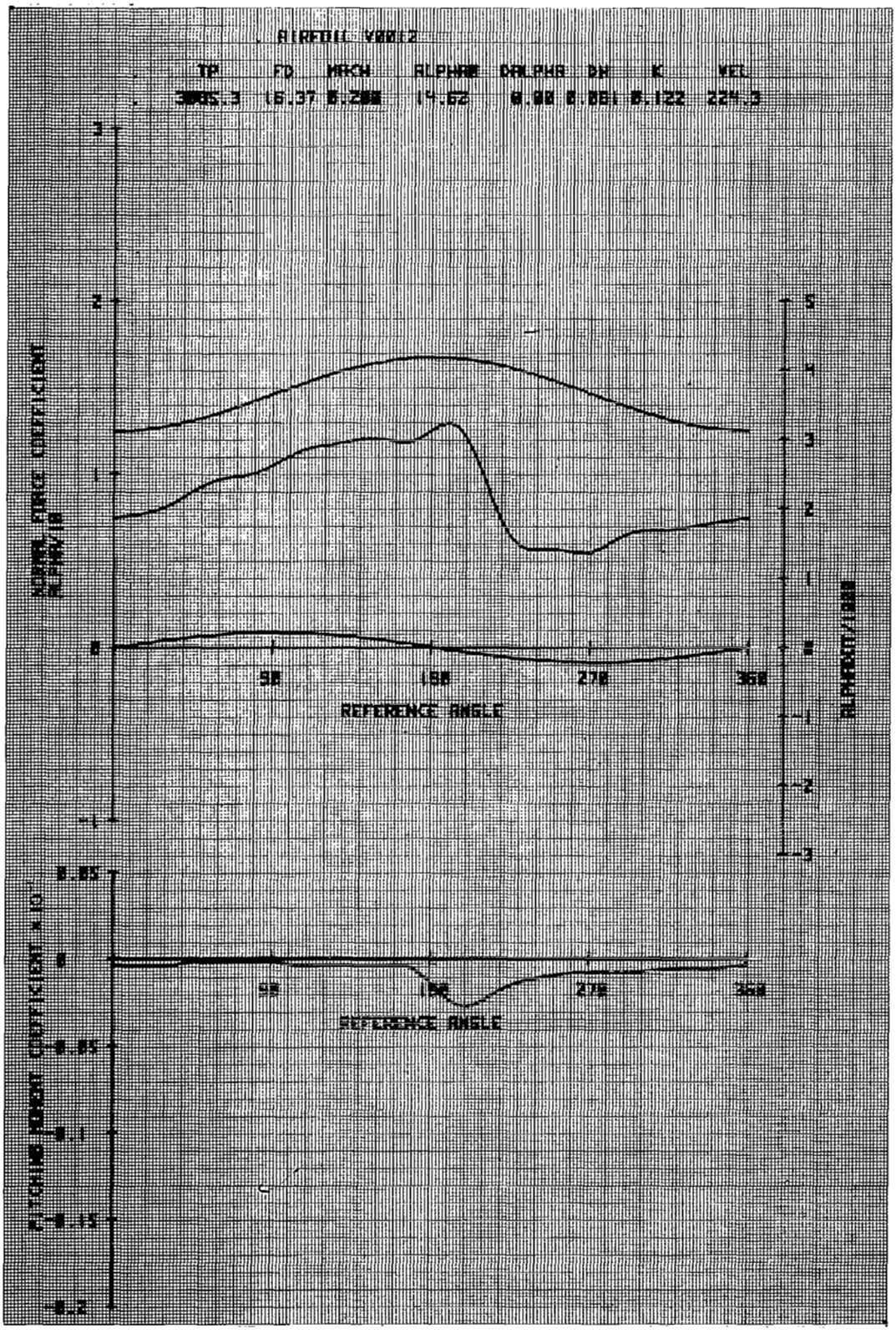

Figure 36a. Airfoil V0012 in Vertical Translation

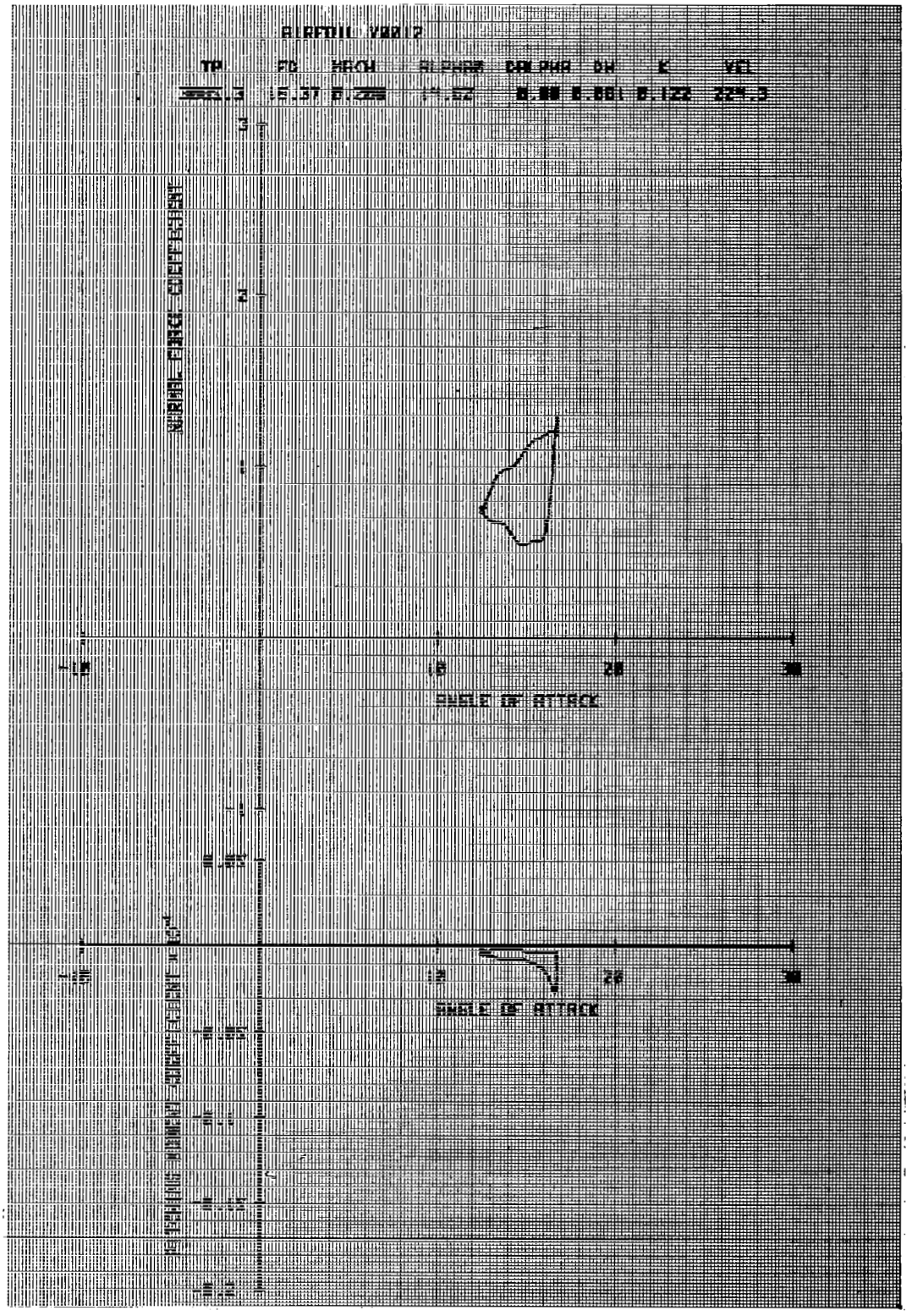

Figure 36b. Airfoil V0012 in Vertical Translation

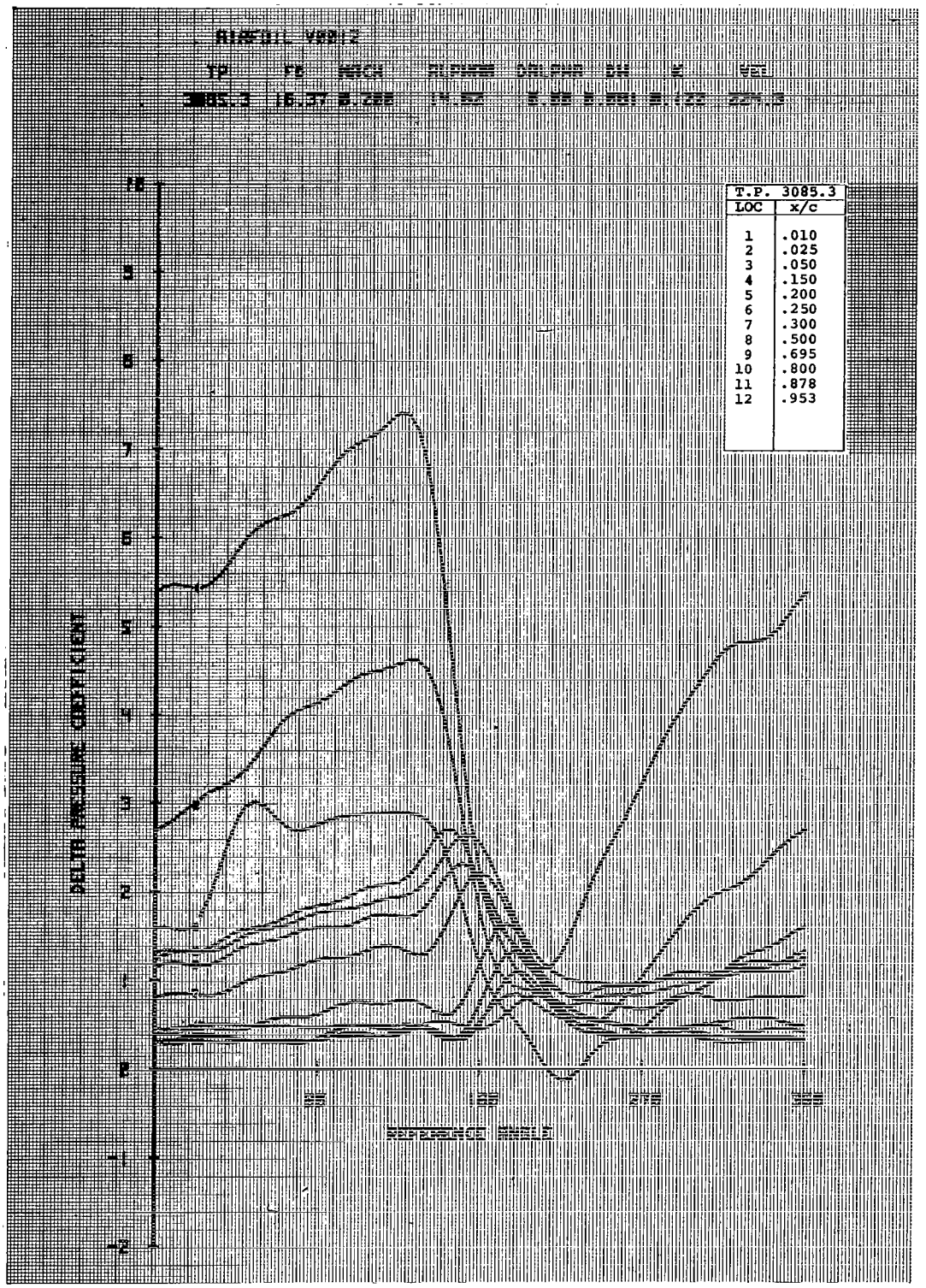

Figure 36c. Airfoil V0012 in Vertical Translation

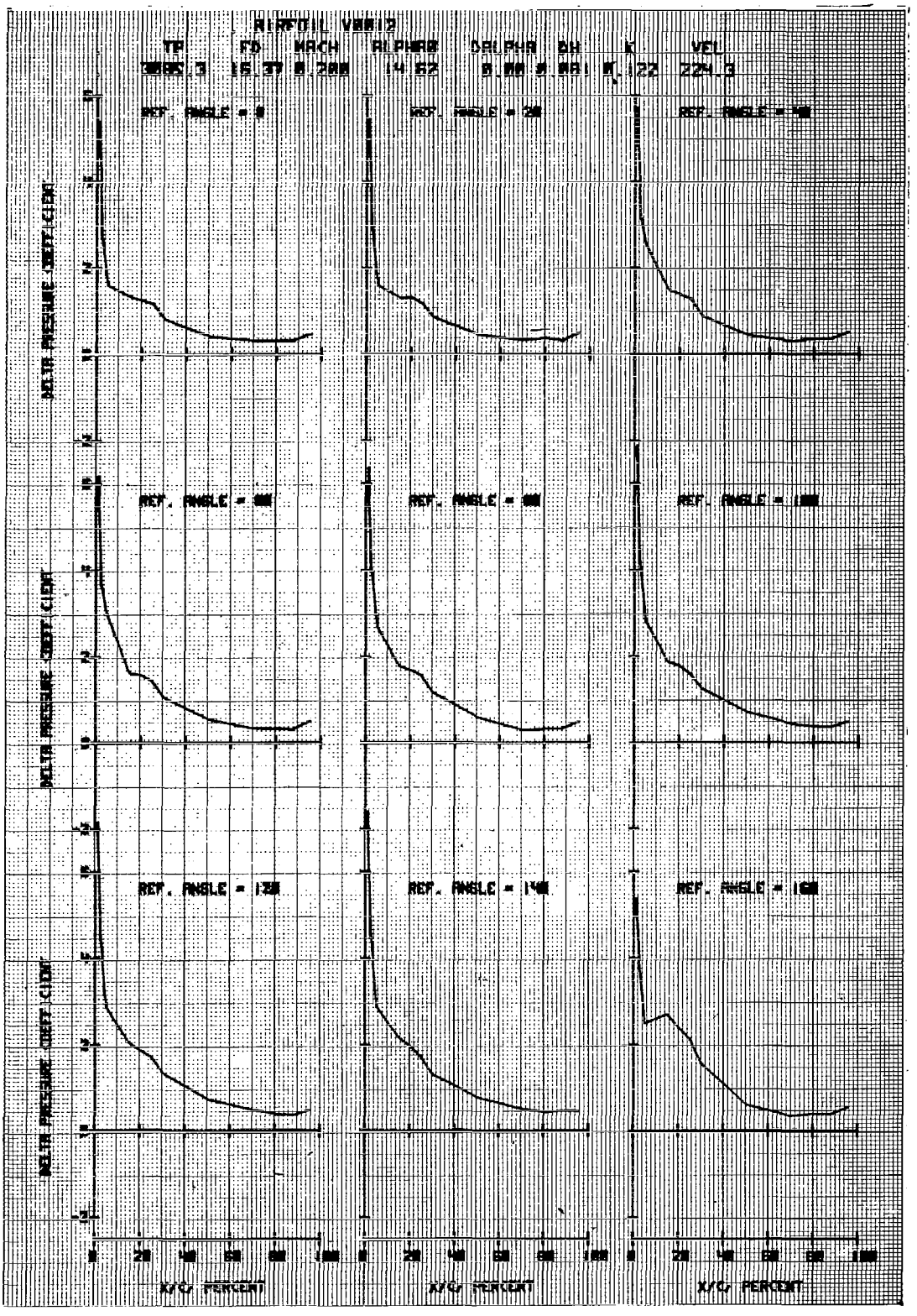

Figure 36d. Airfoil V0012 in Vertical Translation

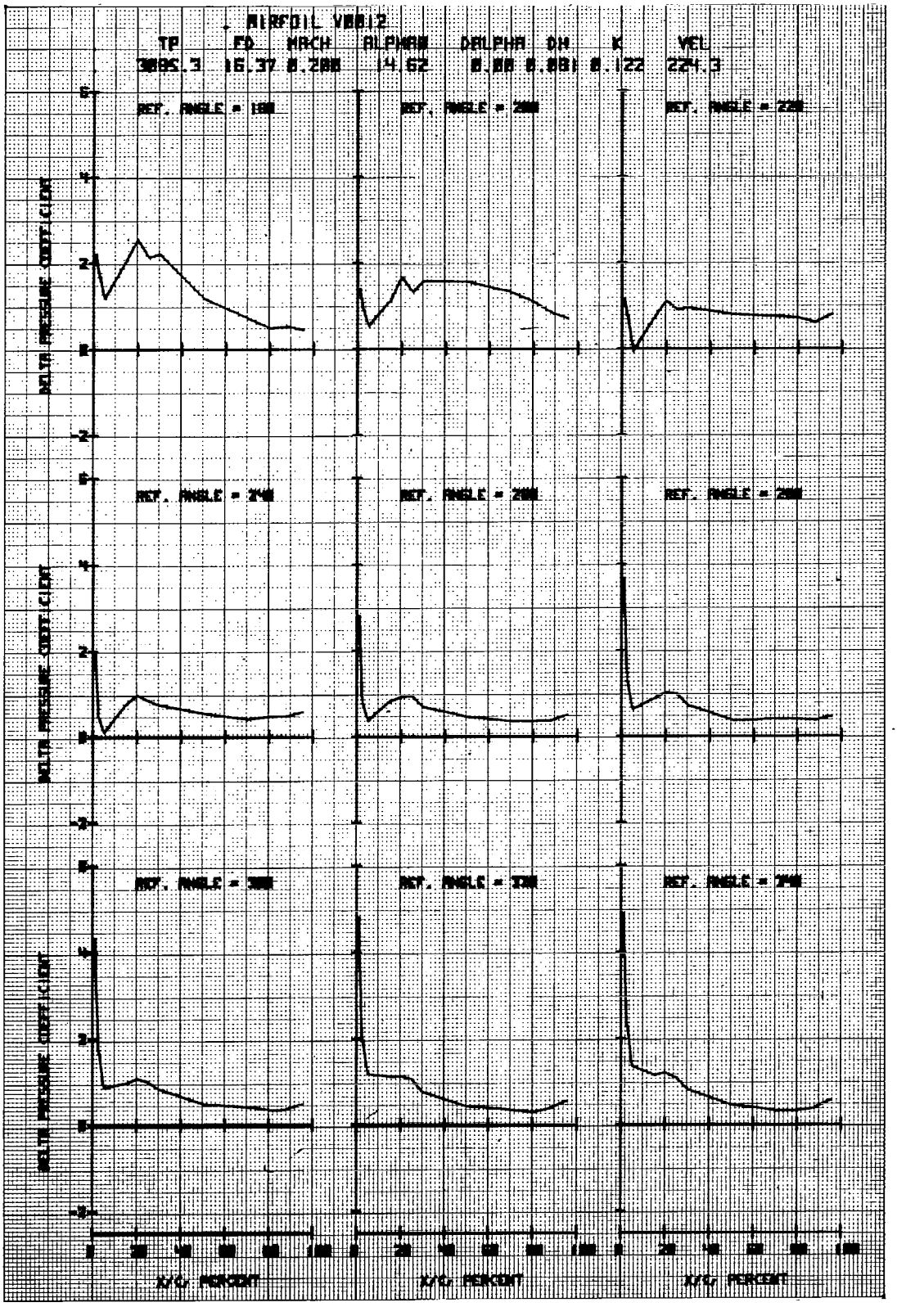

Figure 36e. Airfoil V0012 in Vertical Translation

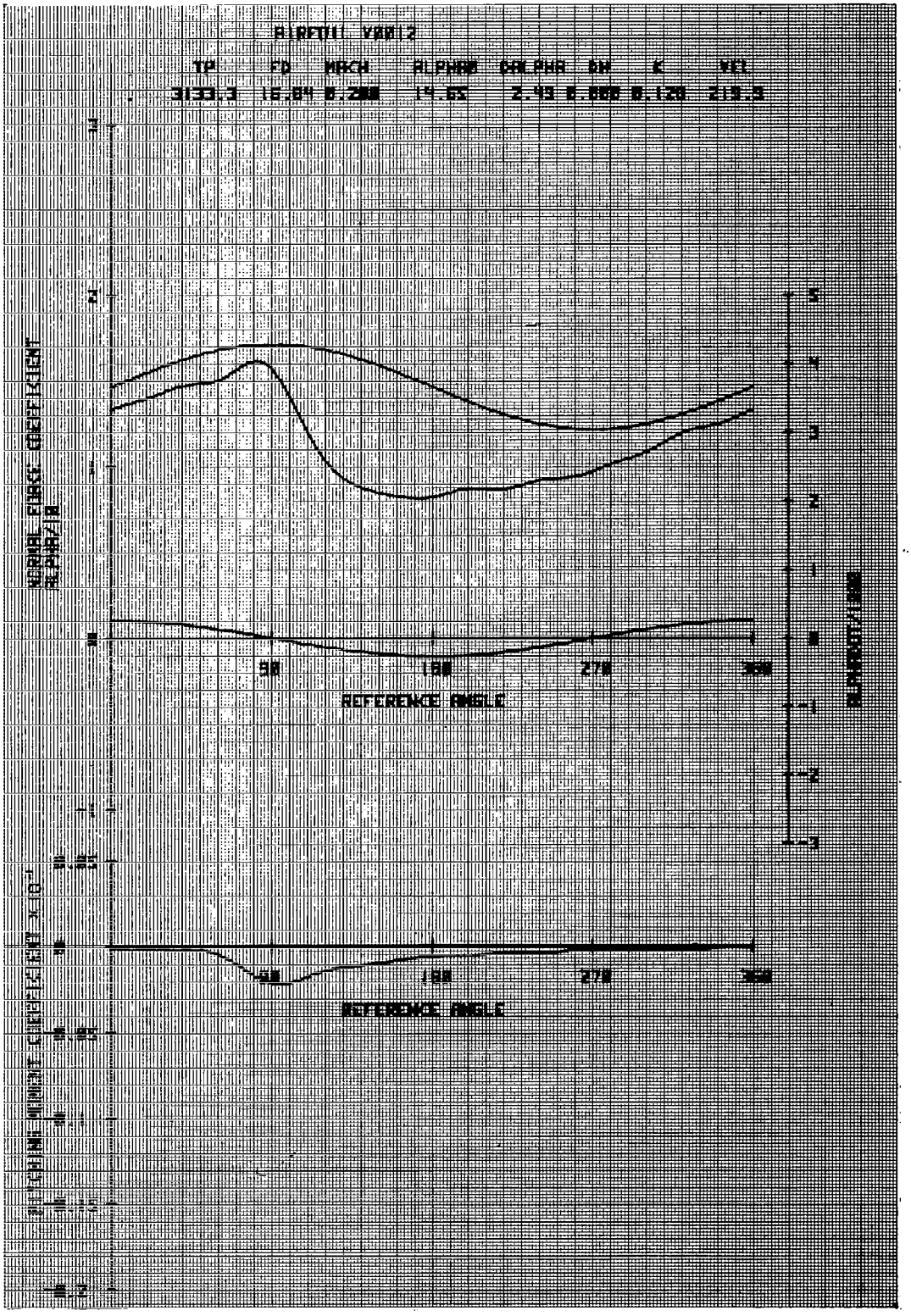

Figure 37a. Airfoil V0012 in Forced Pitch Oscillation

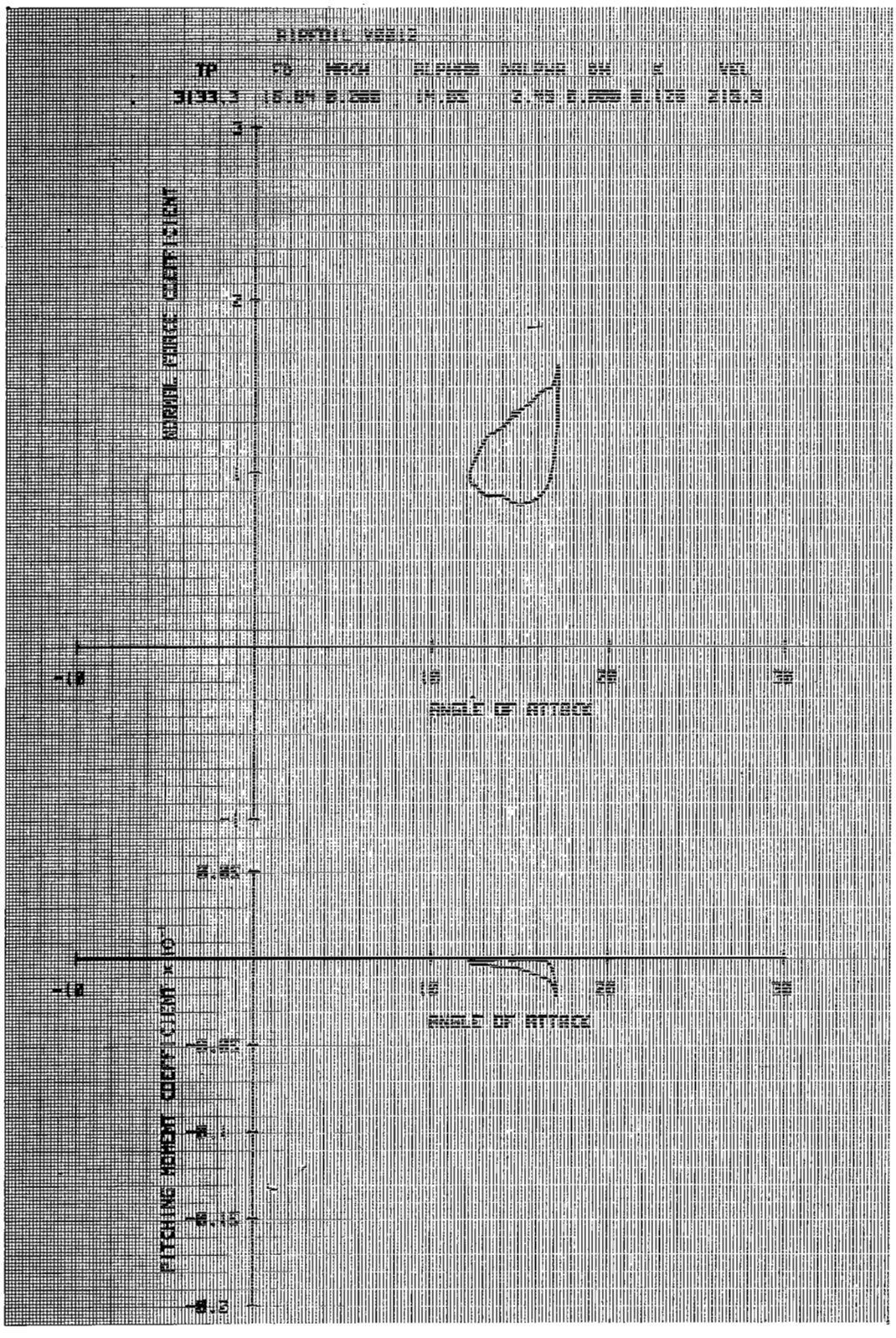

Figure 37b. Airfoil V0012 in Forced Pitch Oscillation

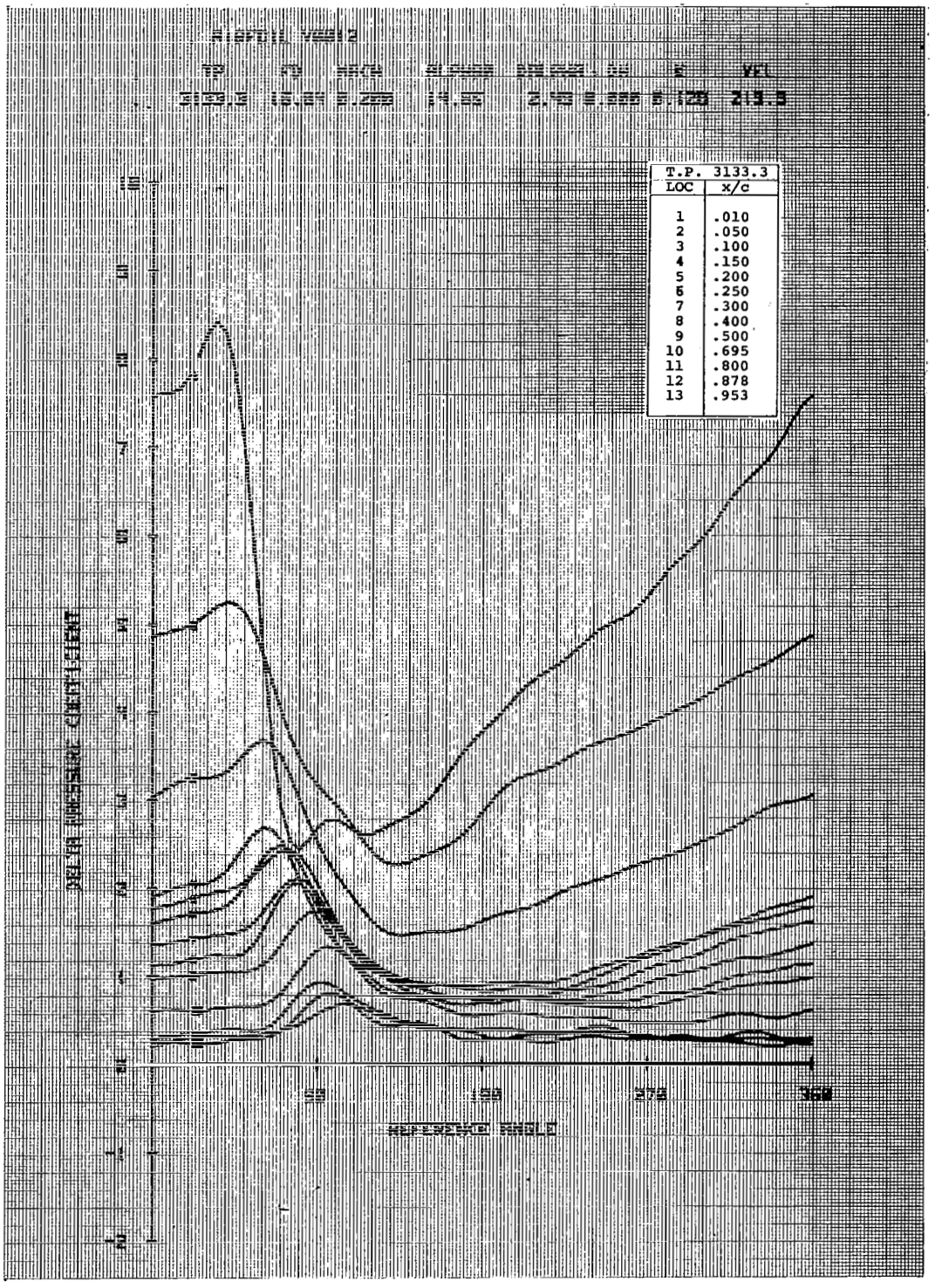

Figure 37c. Airfoil V0012 in Forced Pitch Oscillation

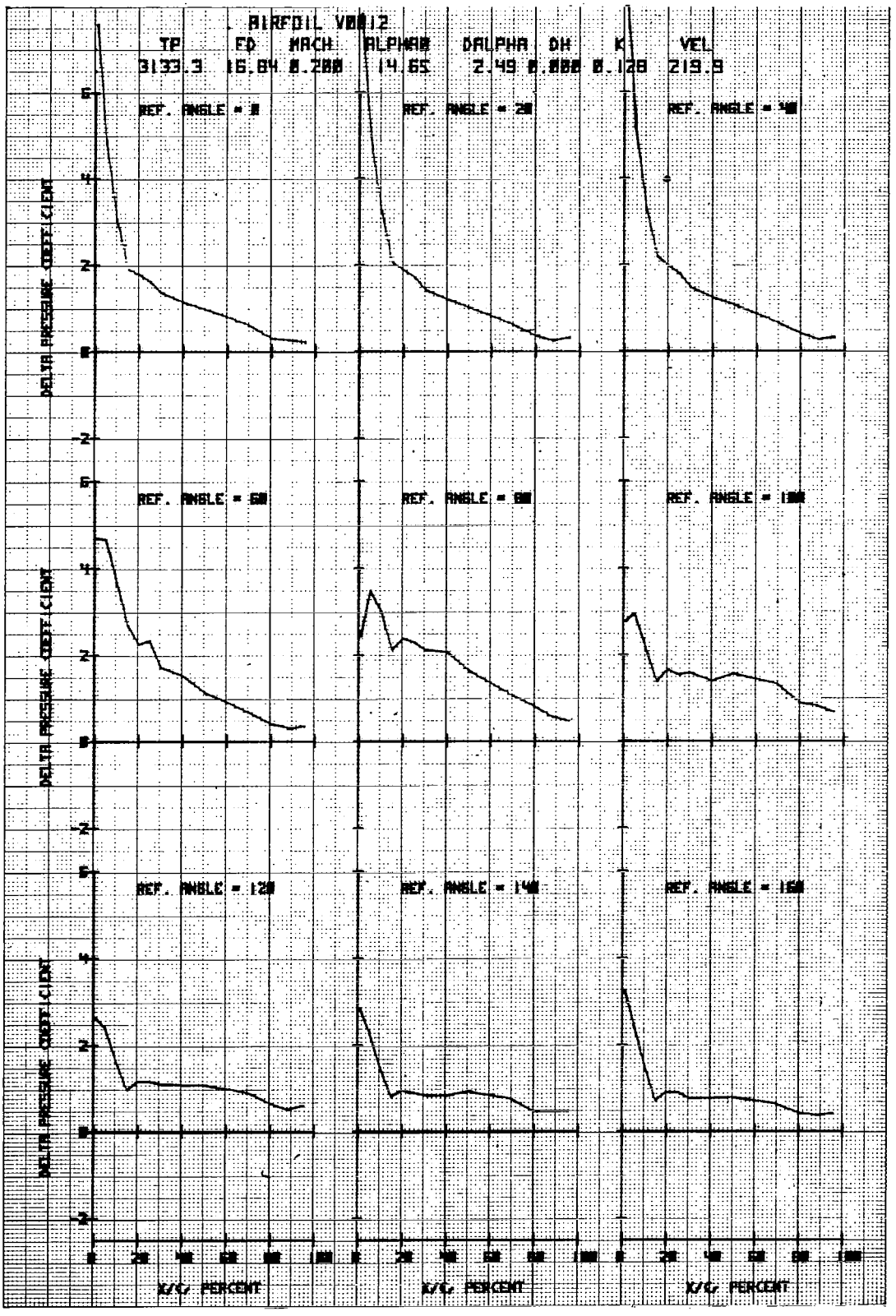

Figure 37d. Airfoil V0012 in Forced Pitch Oscillation

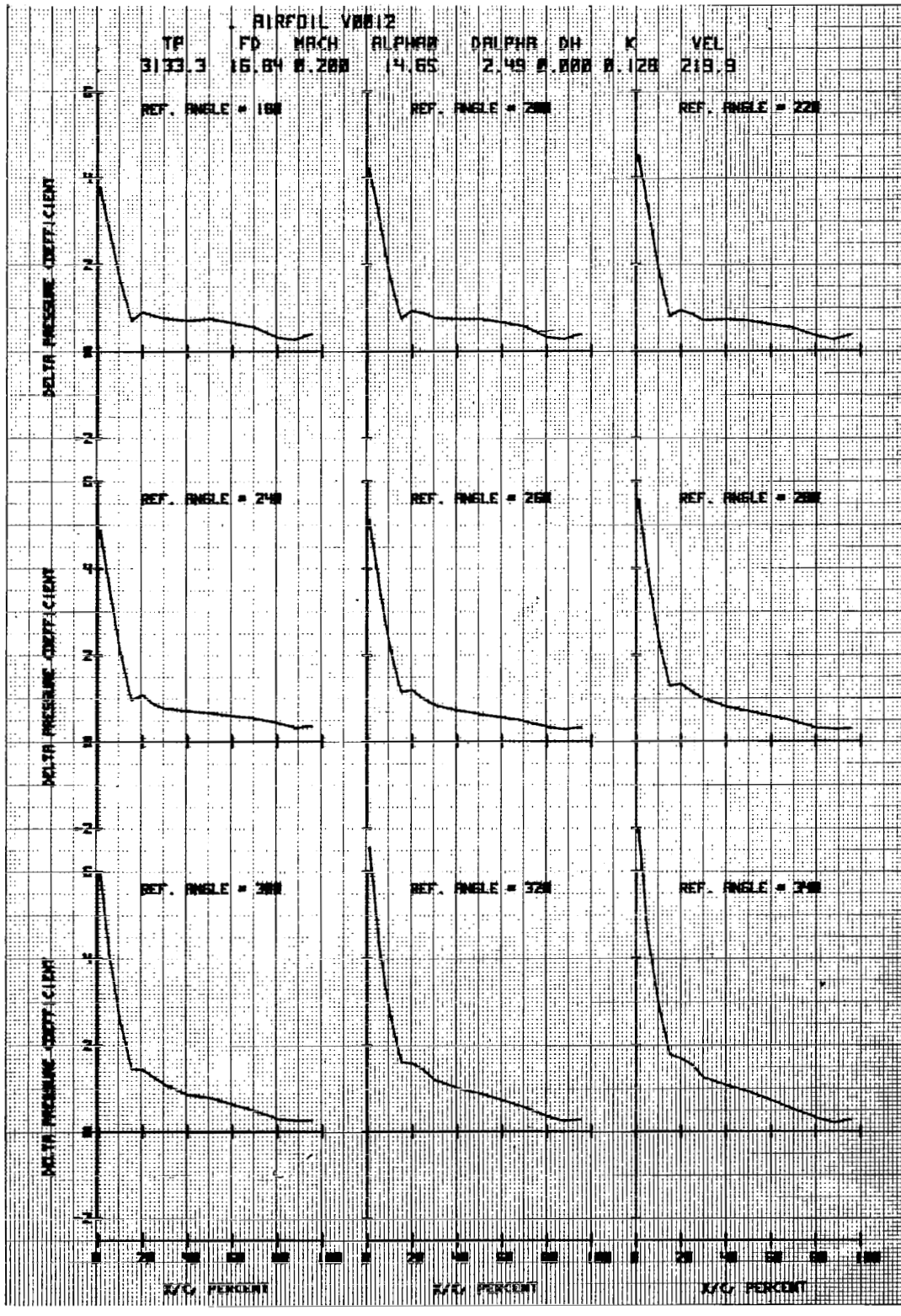

Figure 37e. Airfoil V0012 in Forced Pitch Oscillation

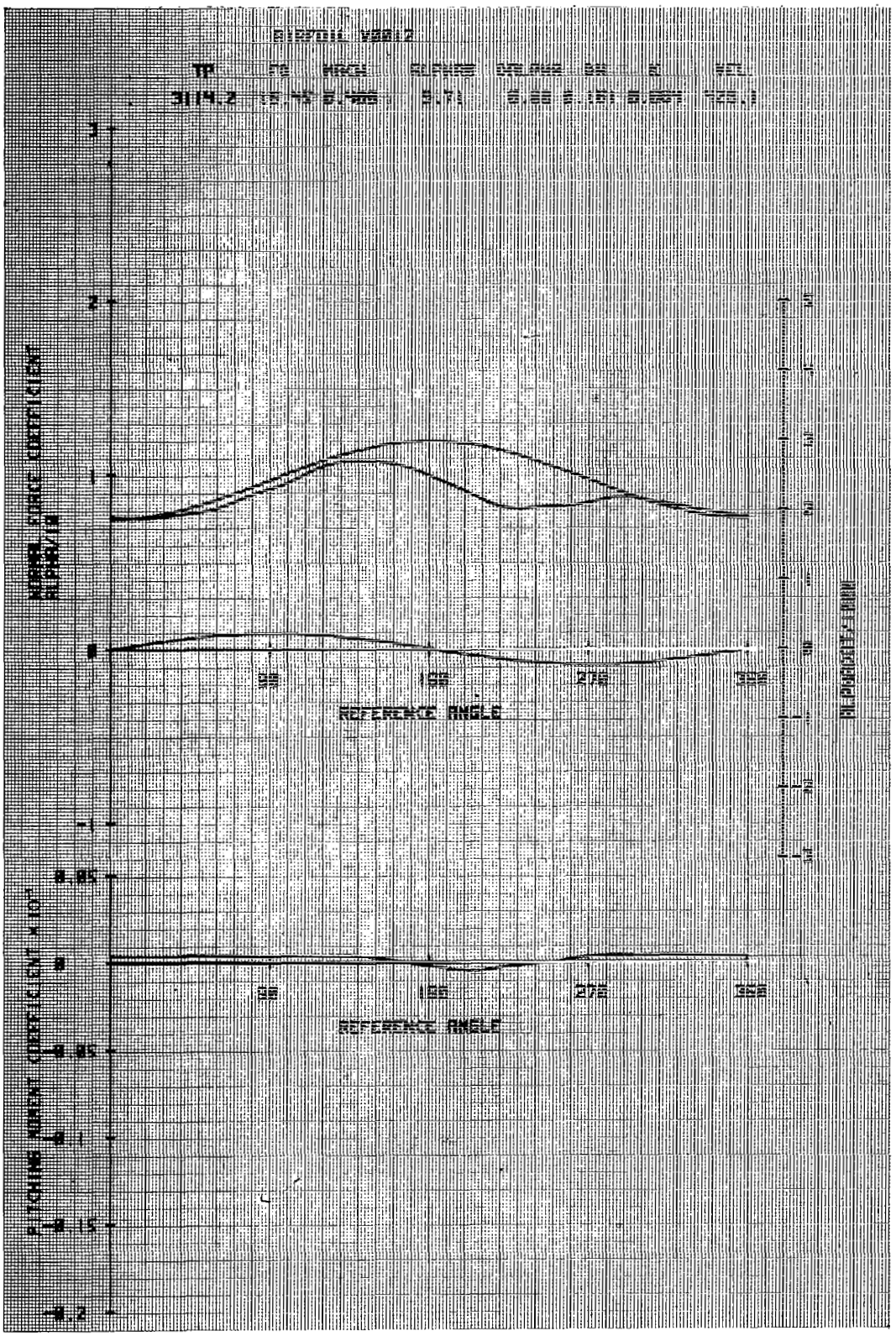

Figure 38a. Airfoil V0012 in Vertical Translation

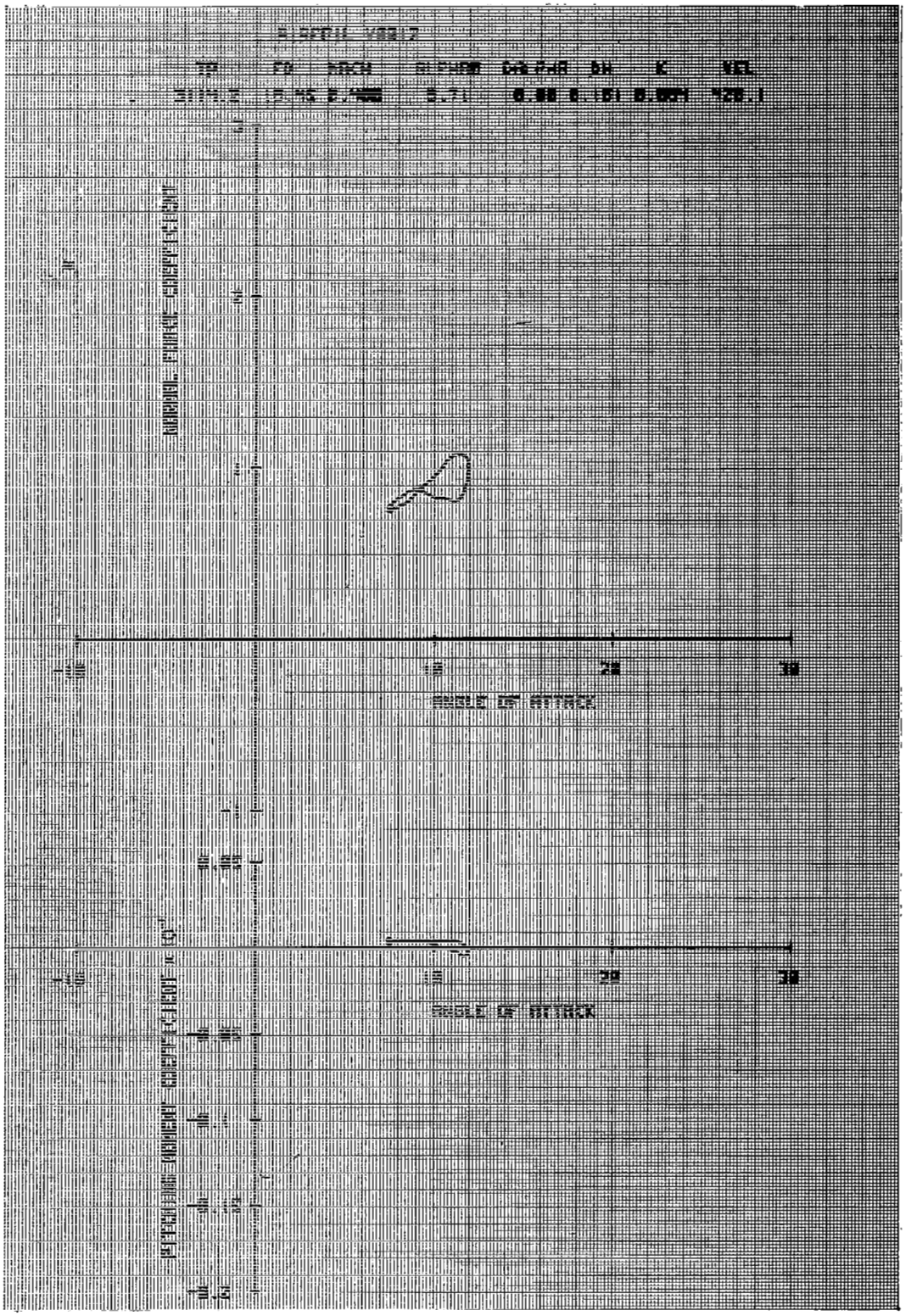

Figure 38b. Airfoil V0012 in Vertical Translation

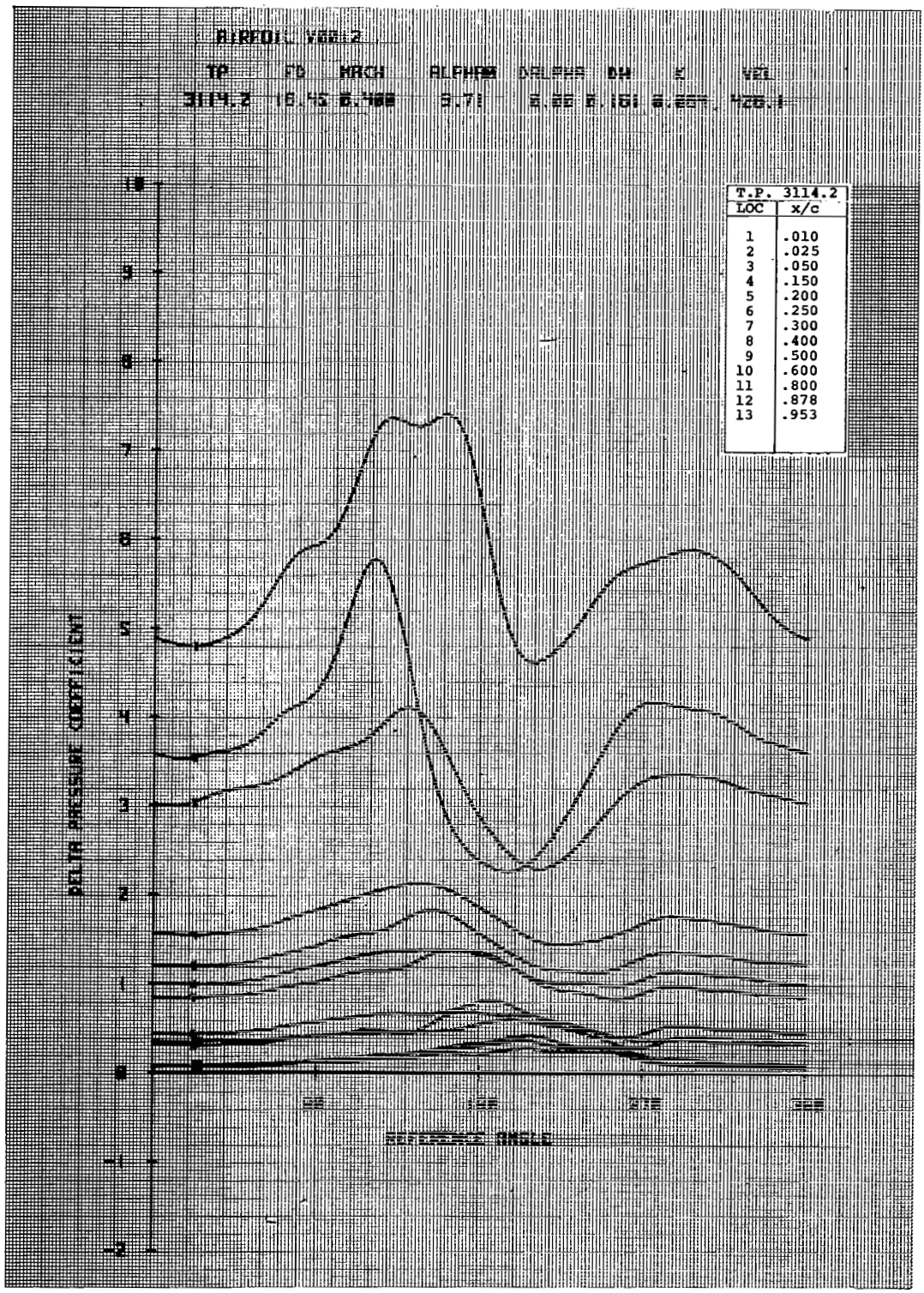

Figure 38c. Airfoil V0012 in Vertical Translation

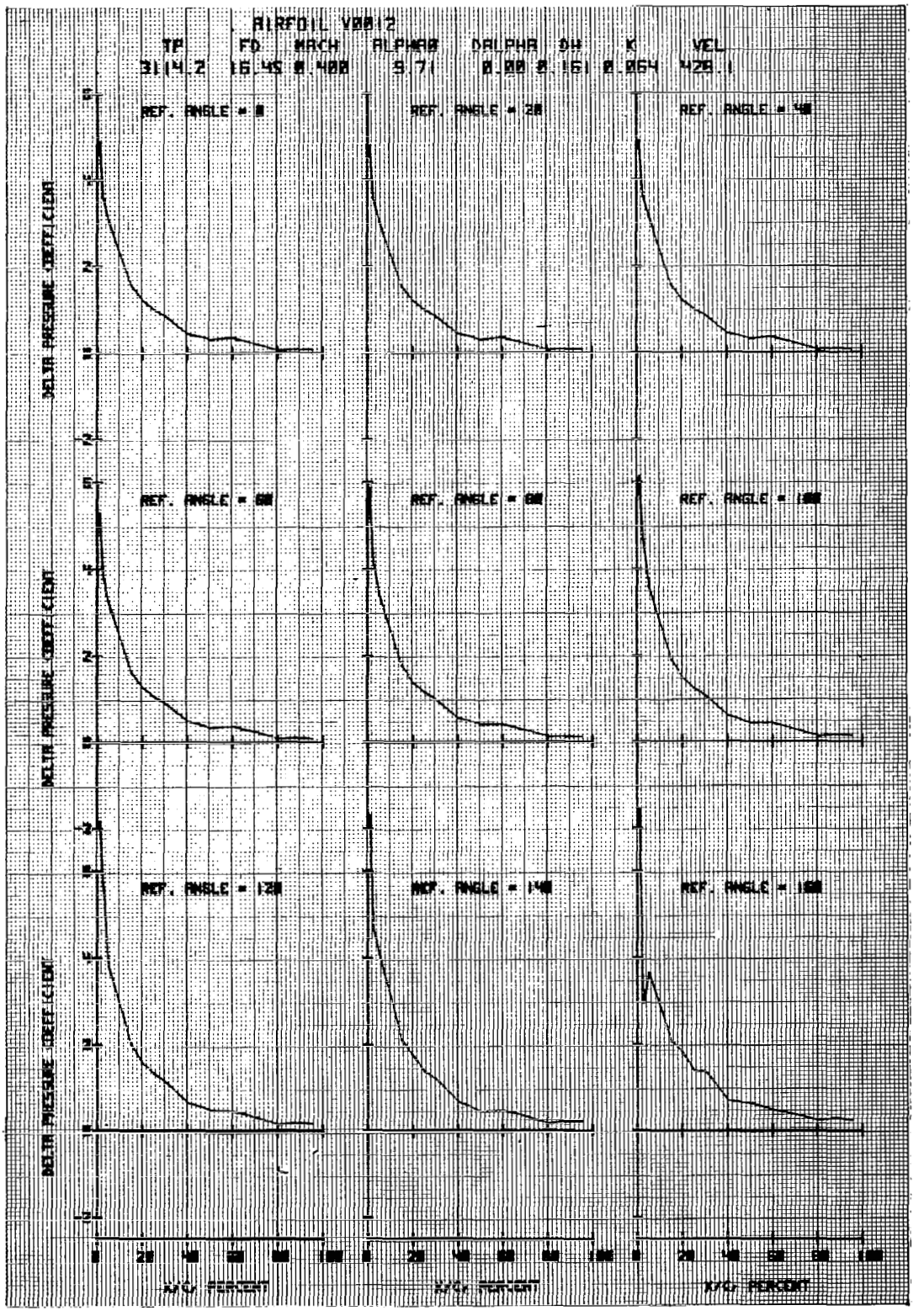

Figure 38d. Airfoil V0012 in Vertical Translation

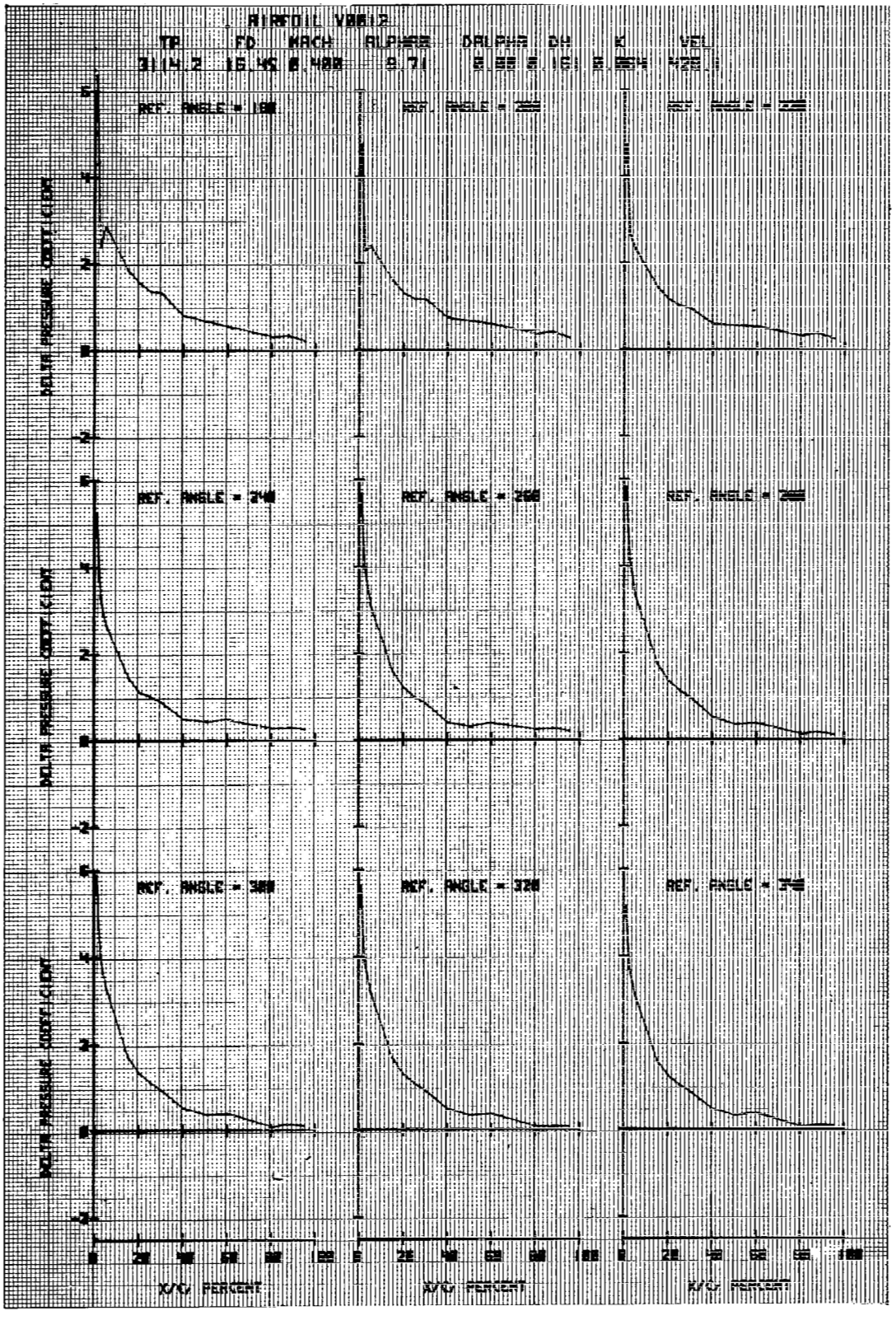

Figure 38e. Airfoil V0012 in Vertical Translation

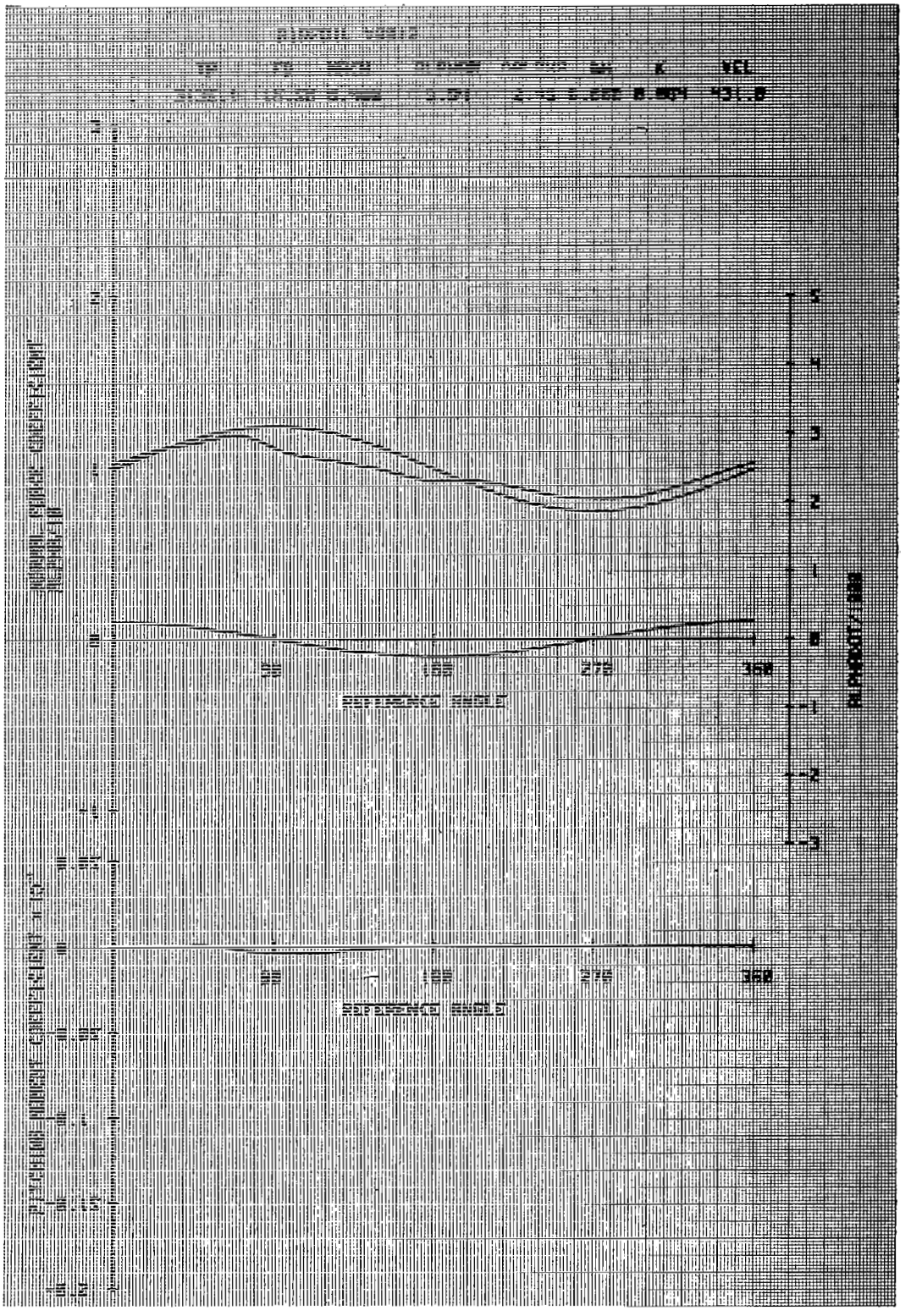

Figure 39a. Airfoil V0012 in Forced Pitch Oscillation

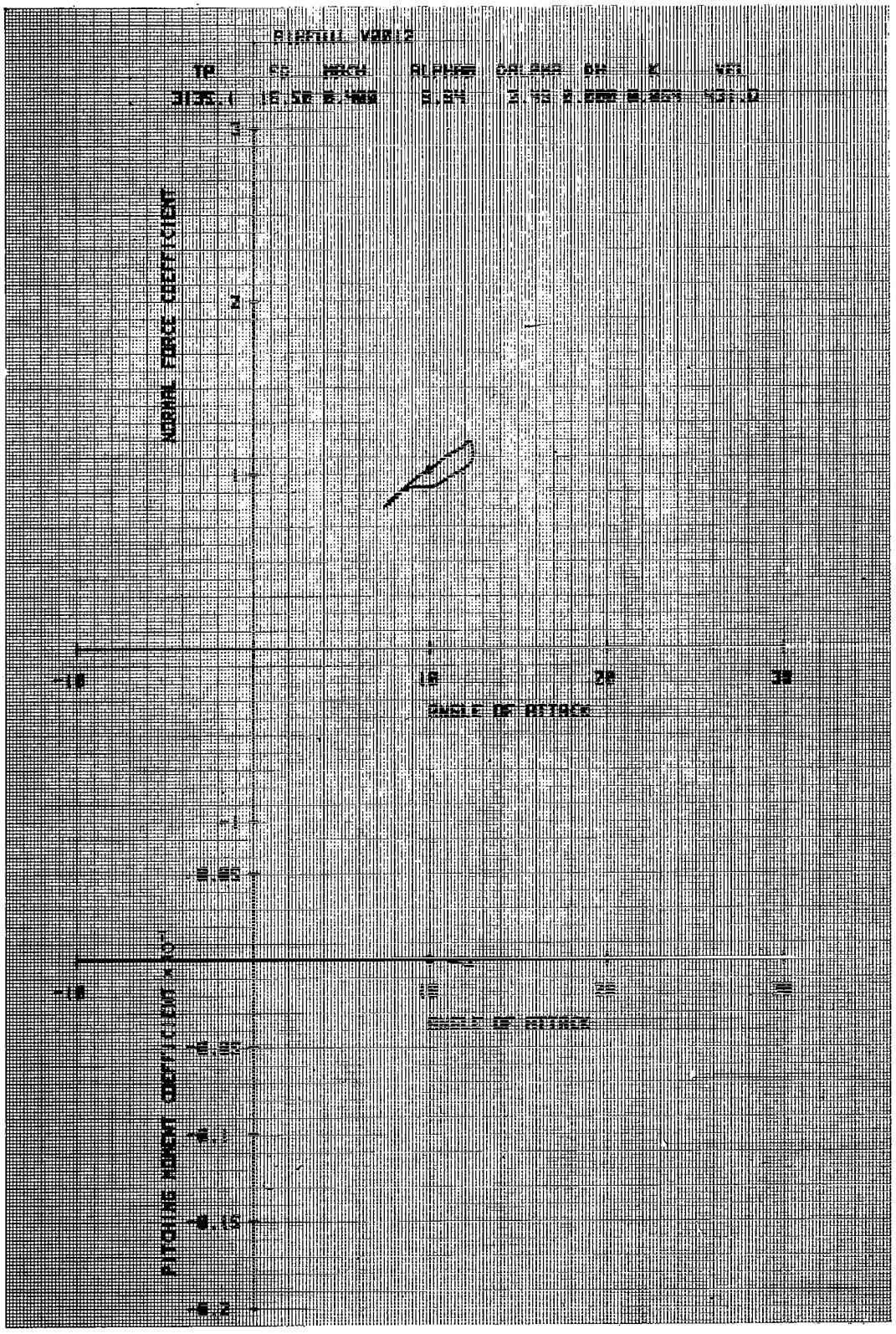

Figure 39b. Airfoil V0012 in Forced Pitch Oscillation

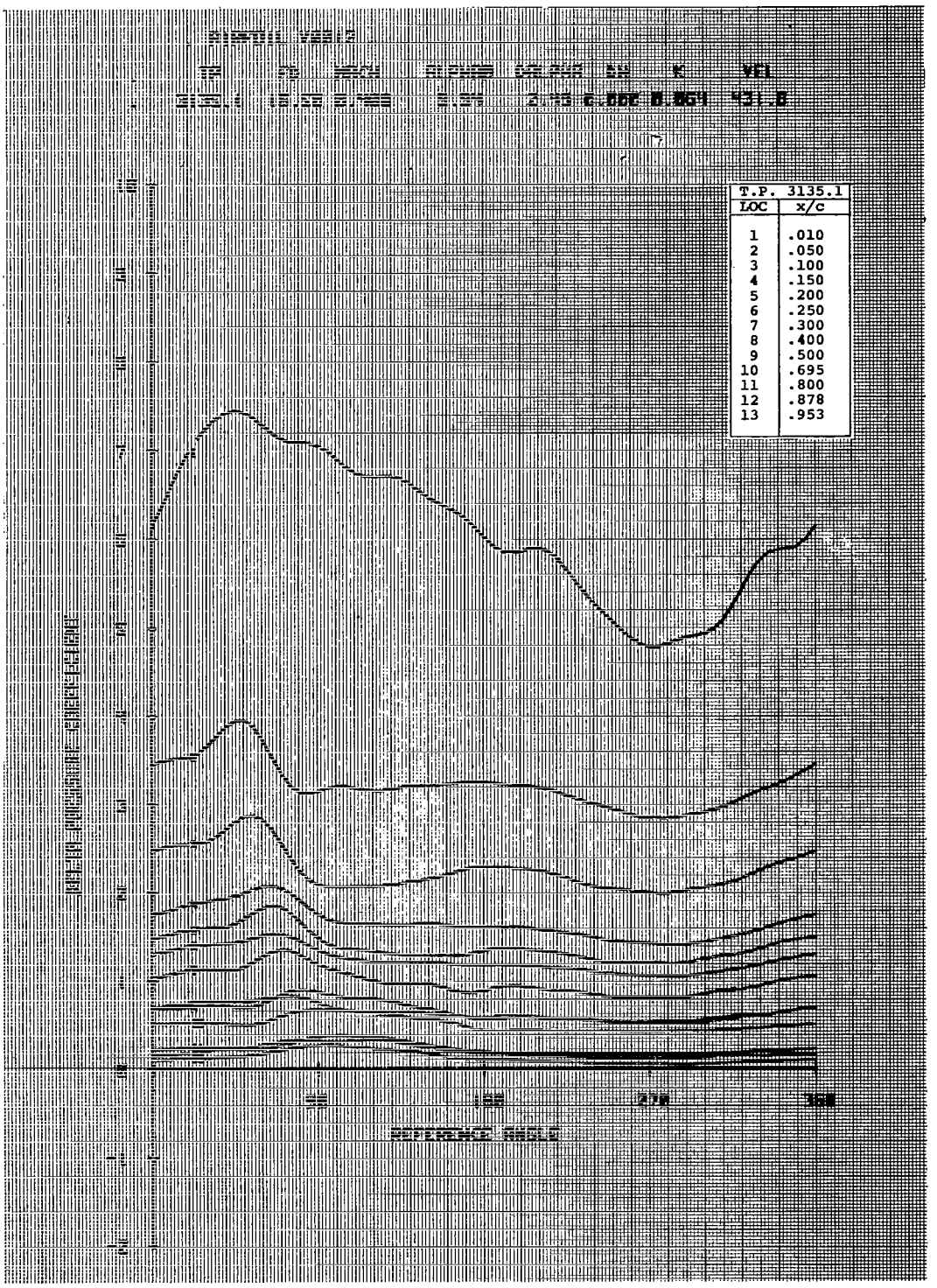

Figure 39c. Airfoil V0012 in Forced Pitch Oscillation

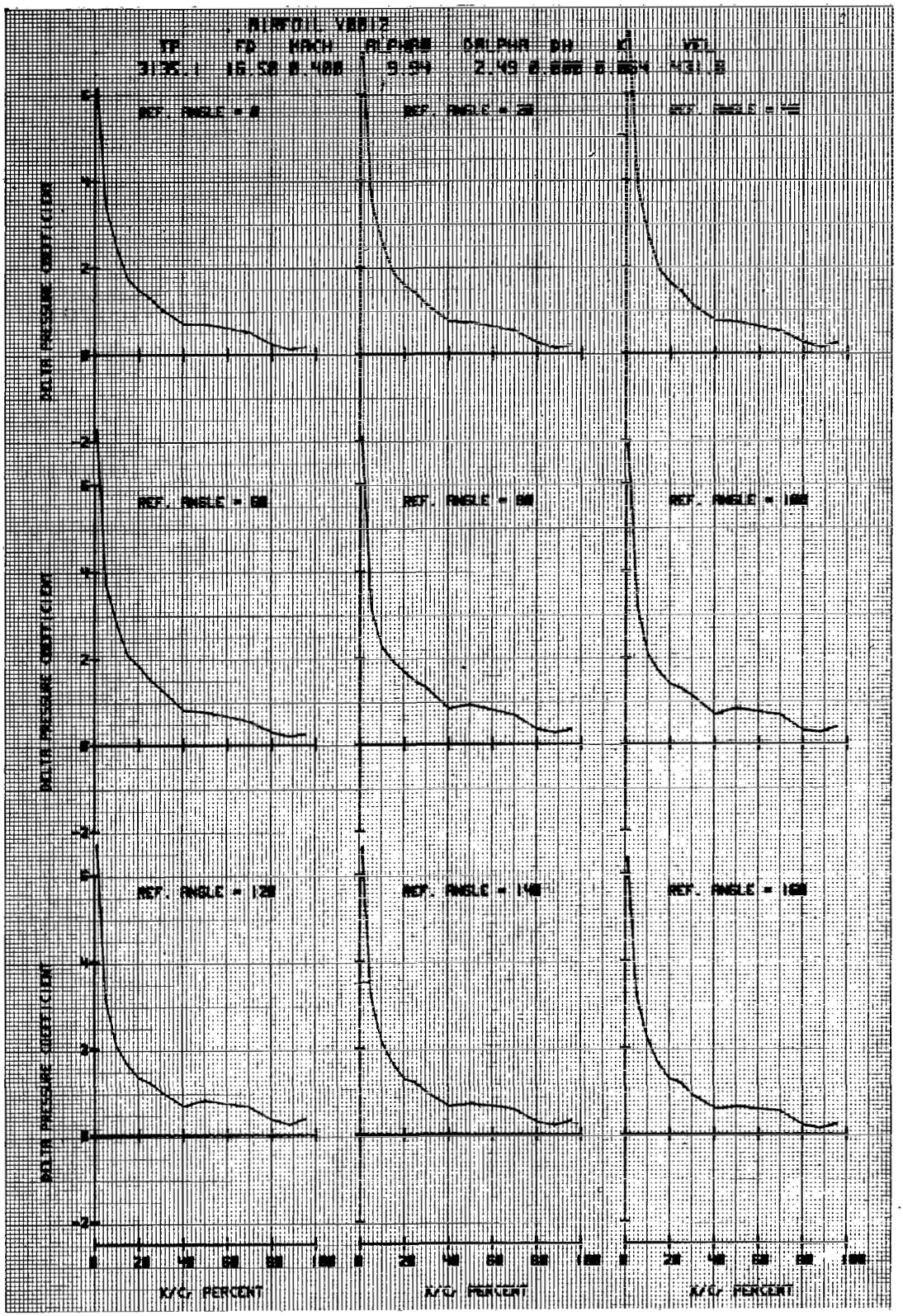

Figure 39d. Airfoil V0012 in Forced Pitch Oscillation

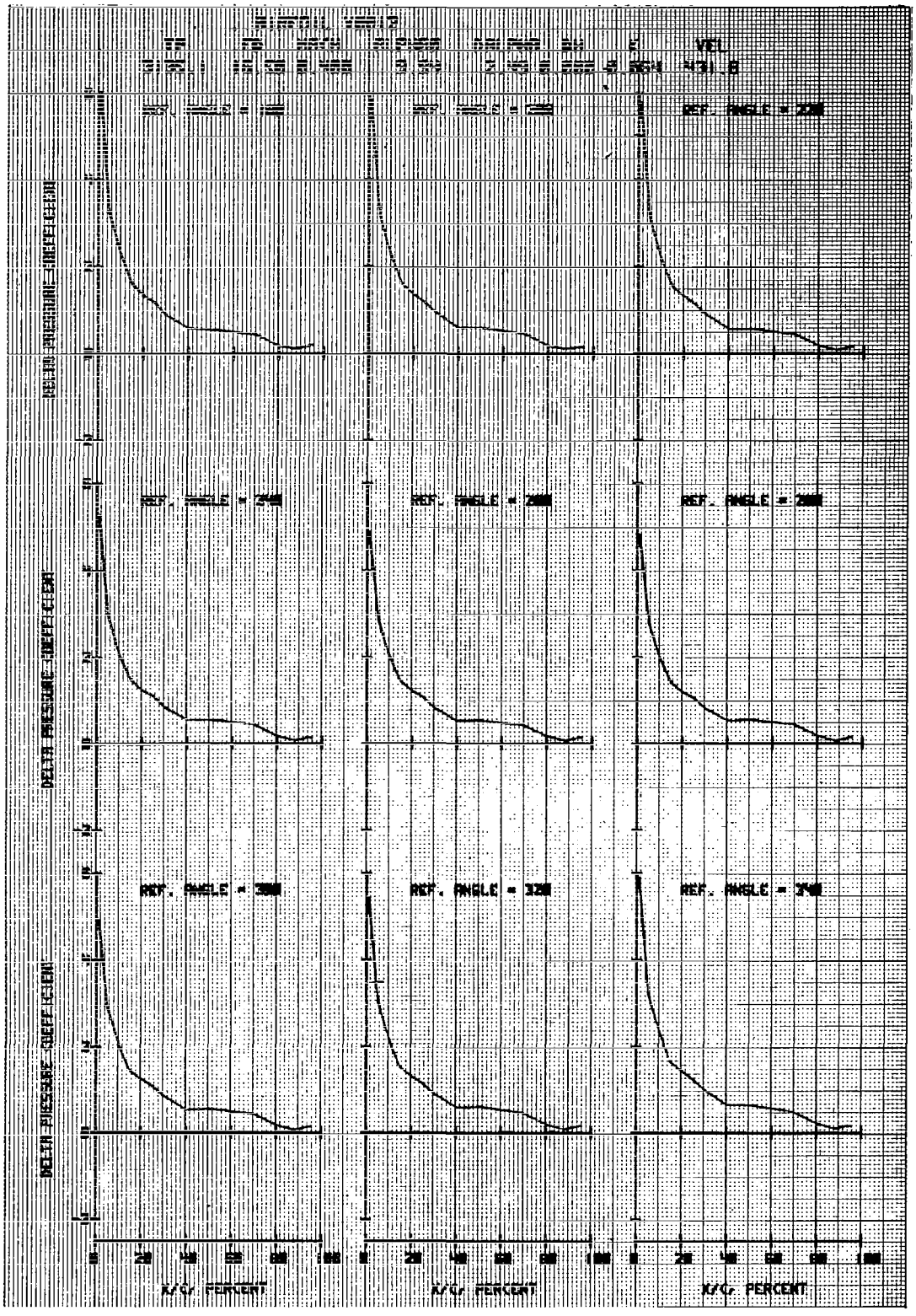

Figure 39e. Airfoil V0012 in Forced Pitch Oscillation

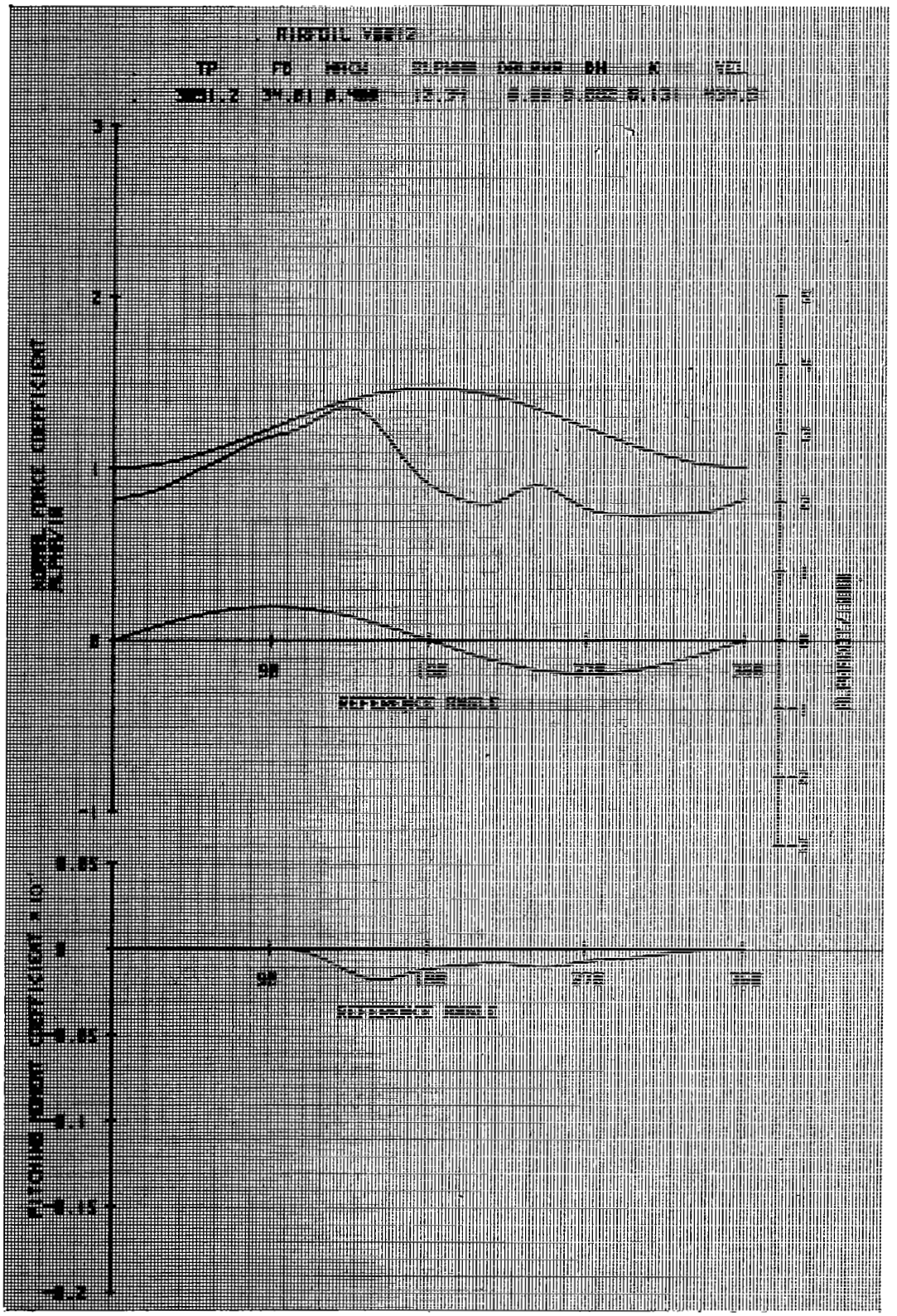

Figure 40a. Airfoil V0012 in Vertical Translation

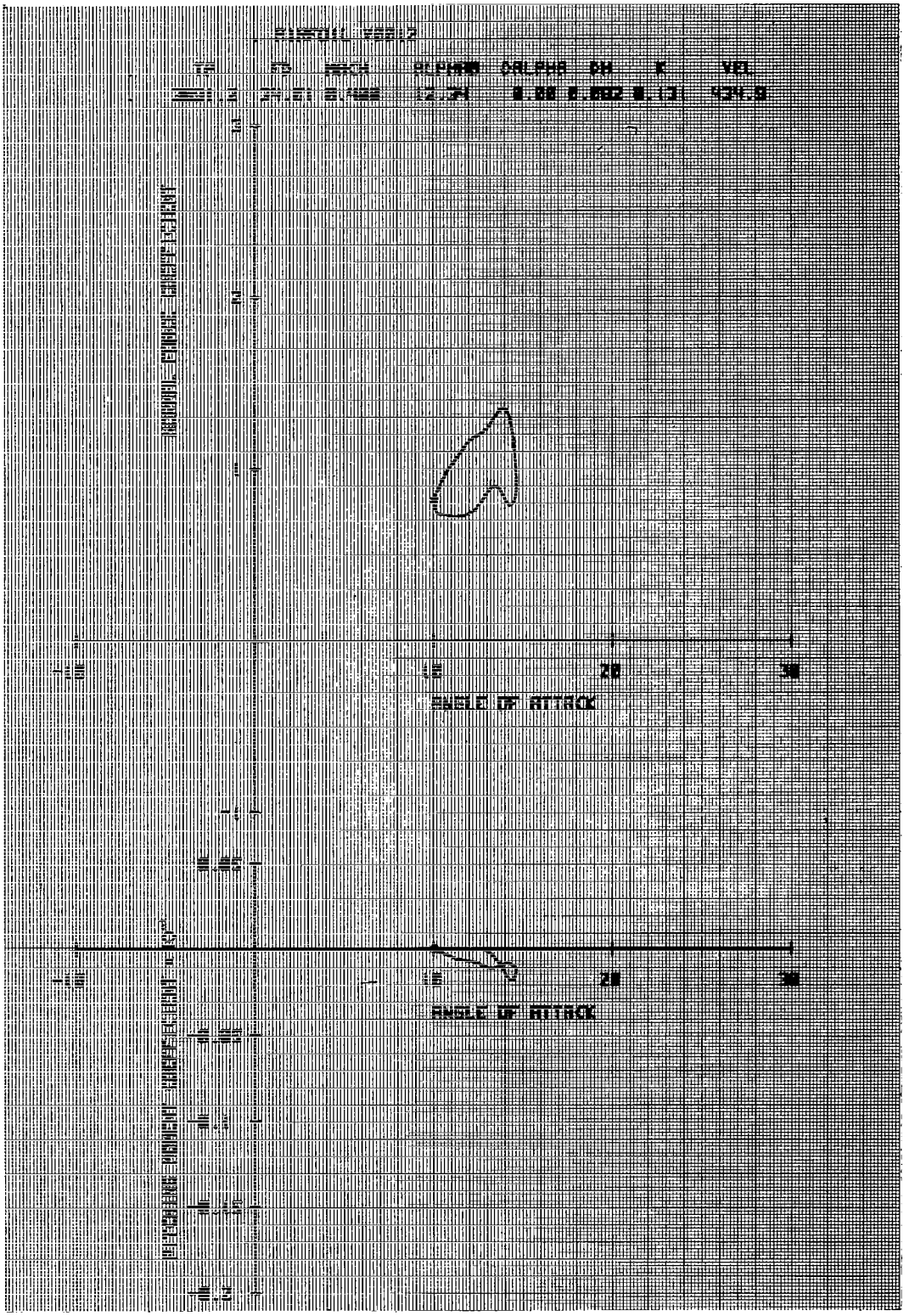

Figure 40b. Airfoil V0012 in Vertical Translation

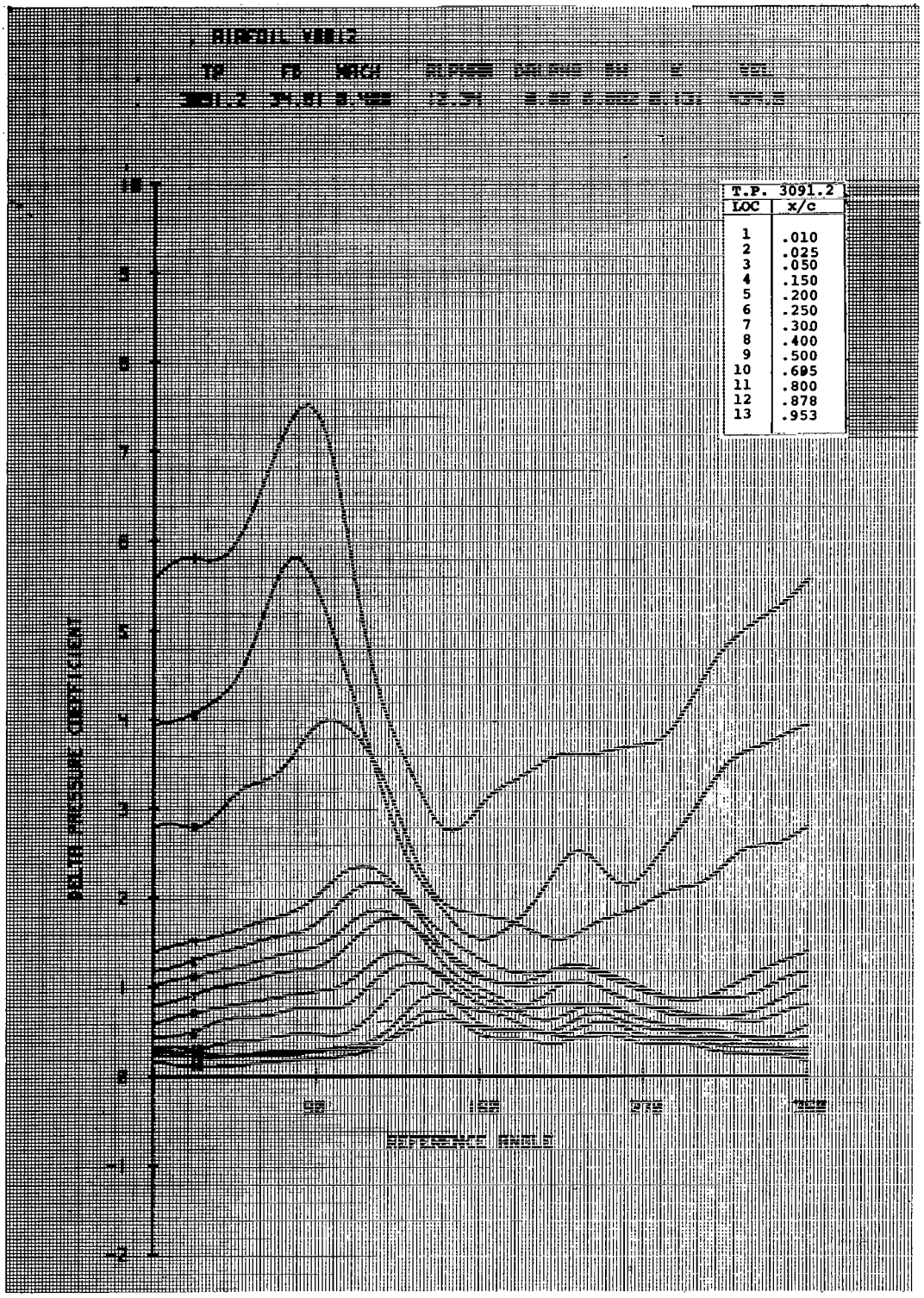

Figure 40c. Airfoil V0012 in Vertical Translation

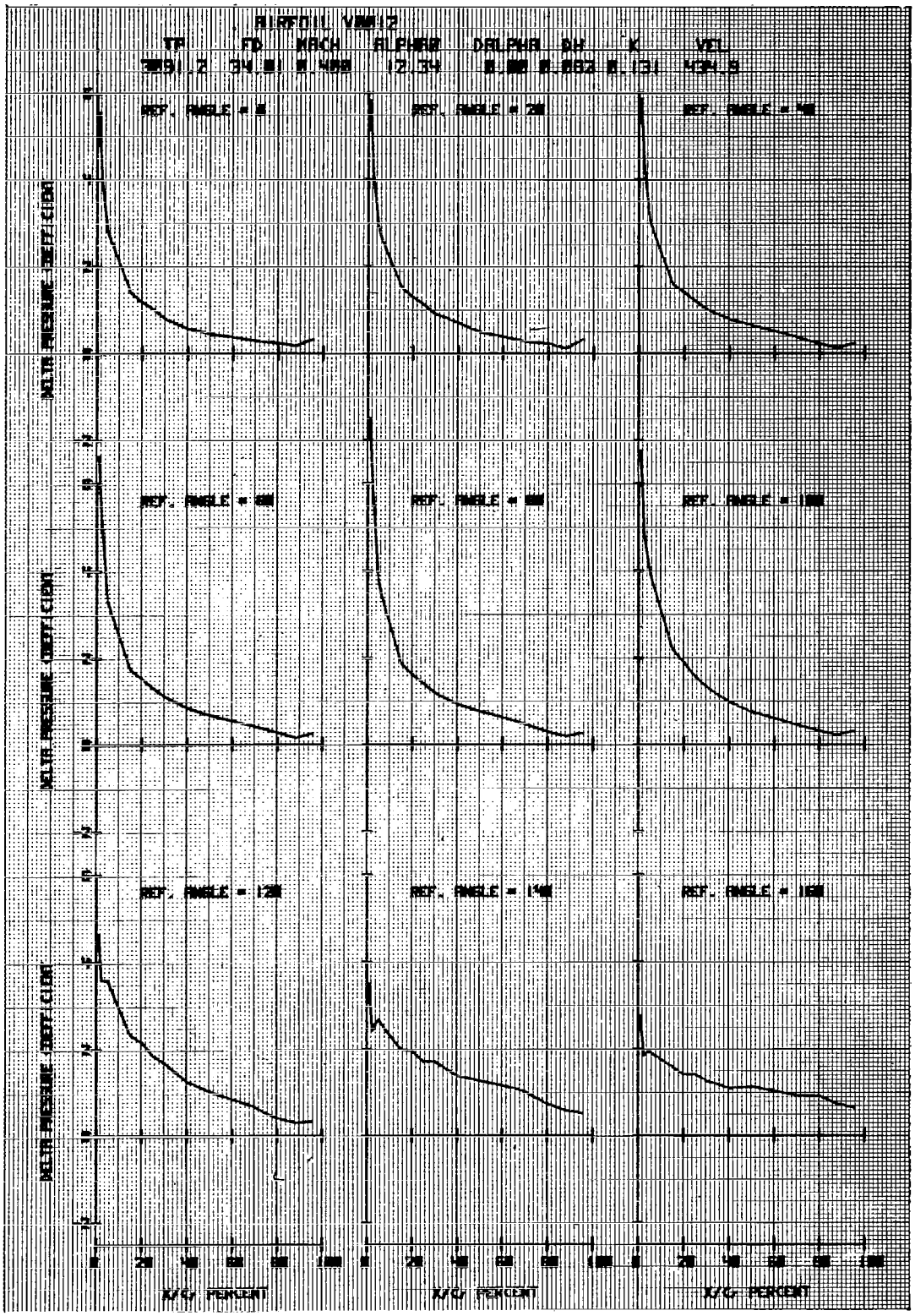

Figure 40d. Airfoil V0012 in Vertical Translation

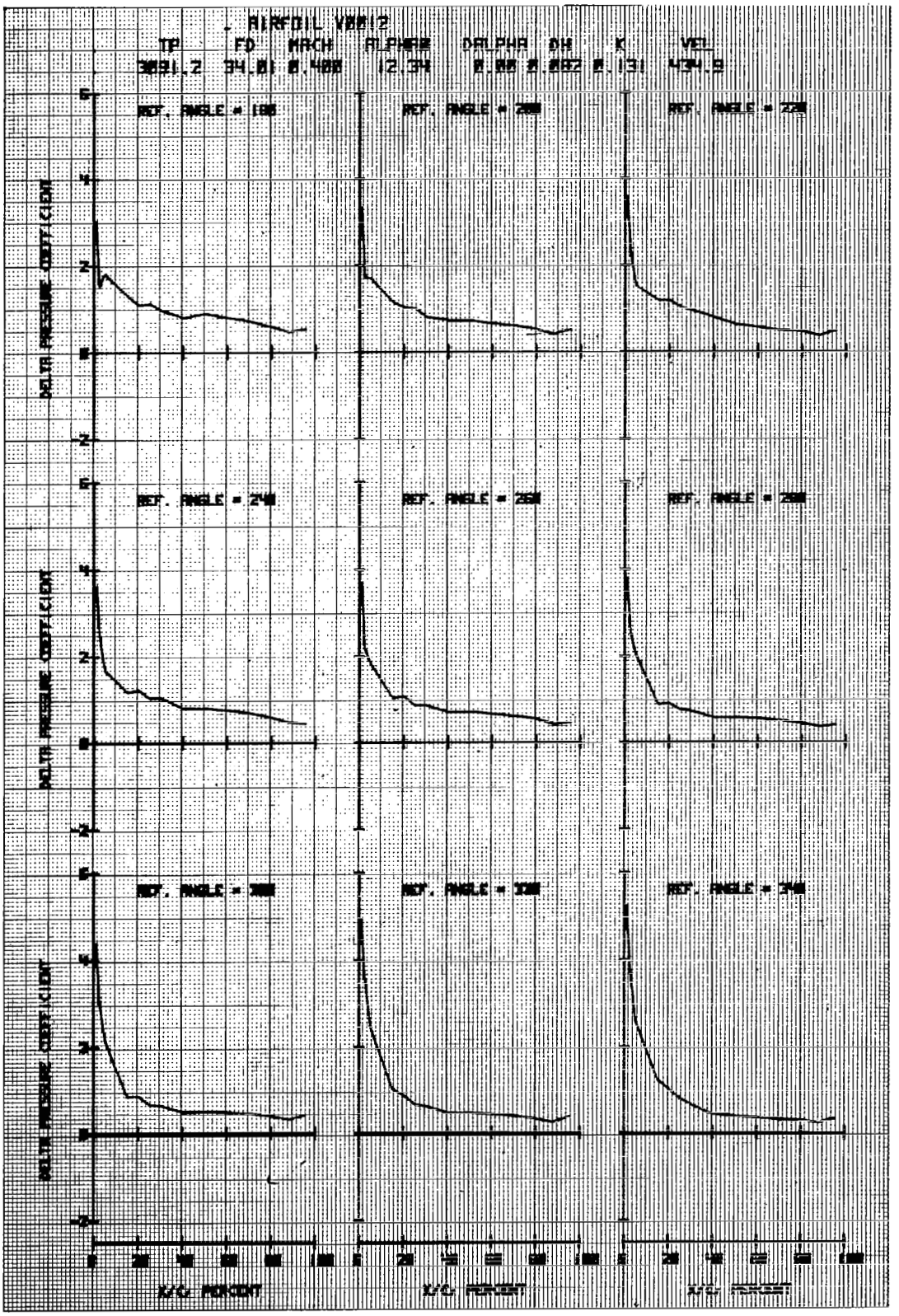

Figure 40e. Airfoil V0012 in Vertical Translation

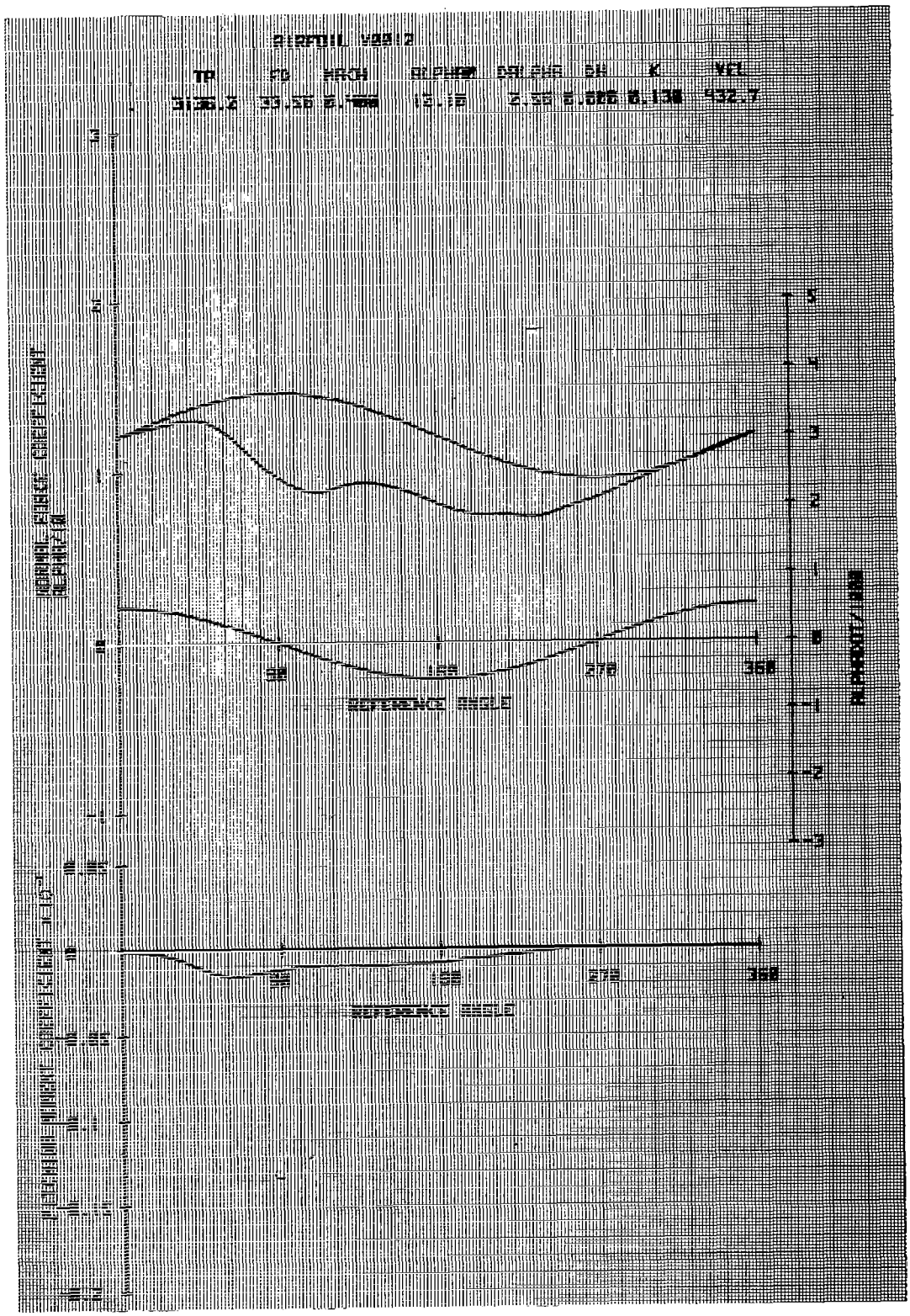

Figure 41a. Airfoil V0012 in Forced Pitch Oscillation

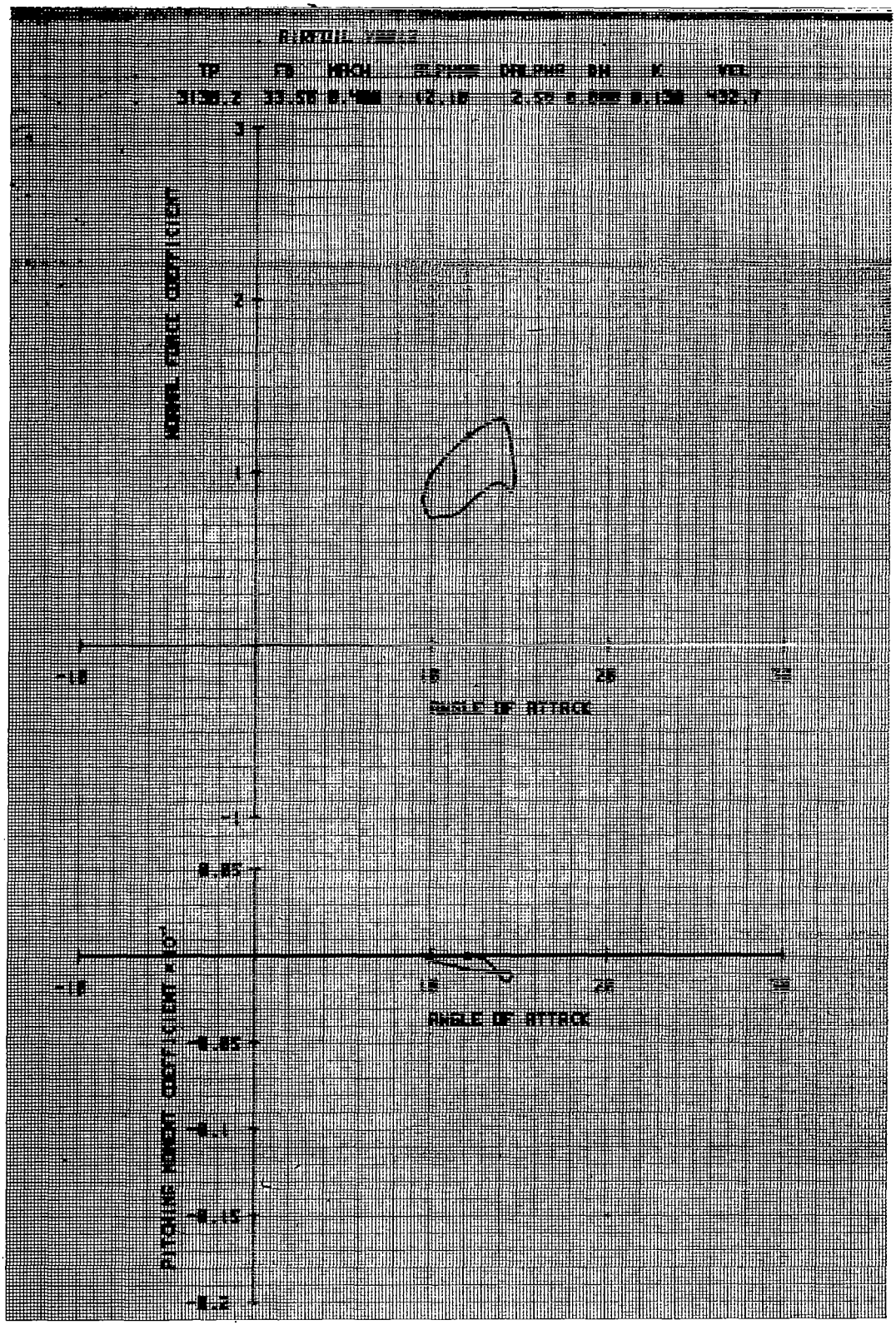

Figure 41b. Airfoil V0012 in Forced Pitch Oscillation

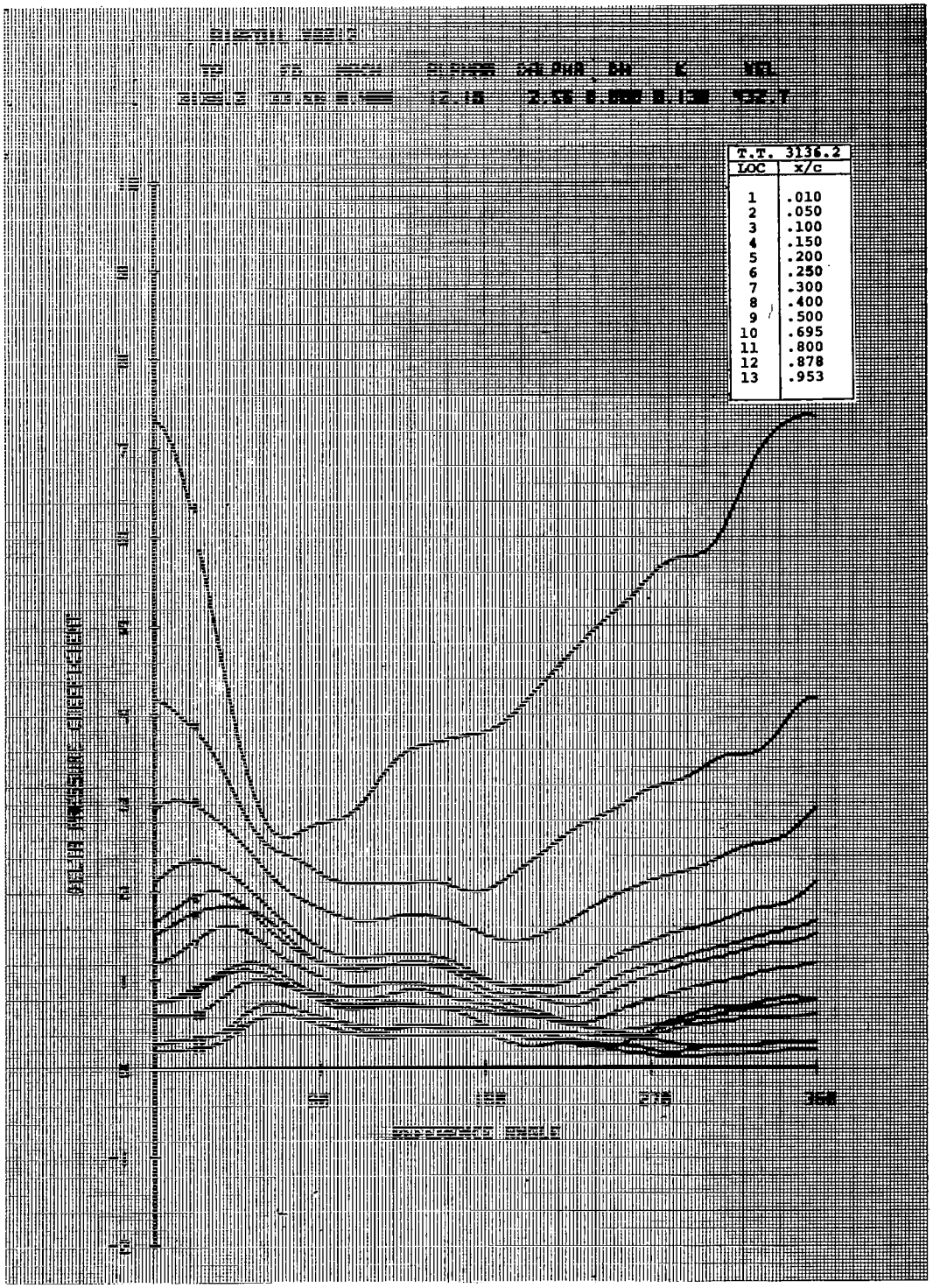

Figure 41c. Airfoil V0012 in Forced Pitch Oscillation

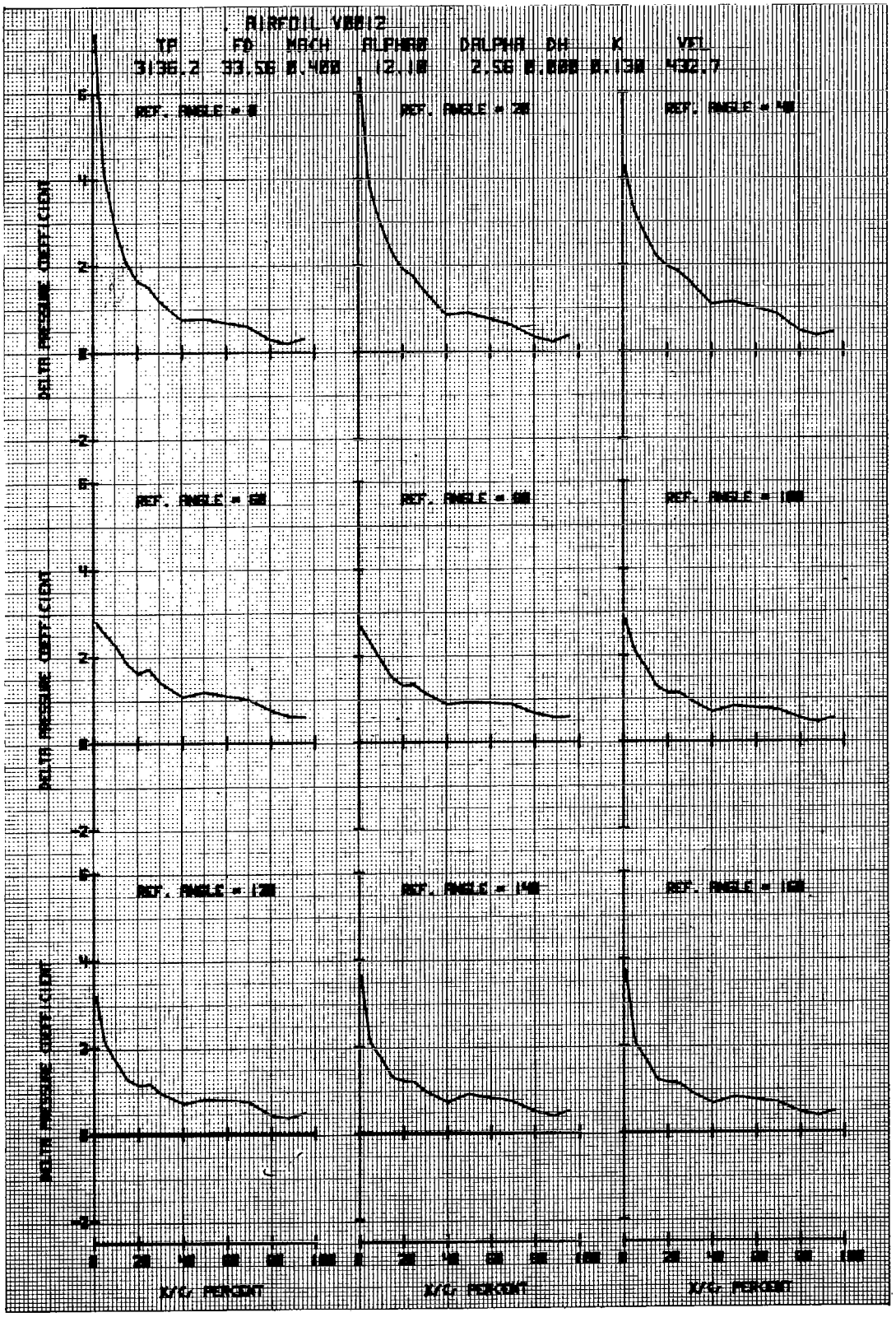

Figure 41d. Airfoil V0012 in Forced Pitch Oscillation

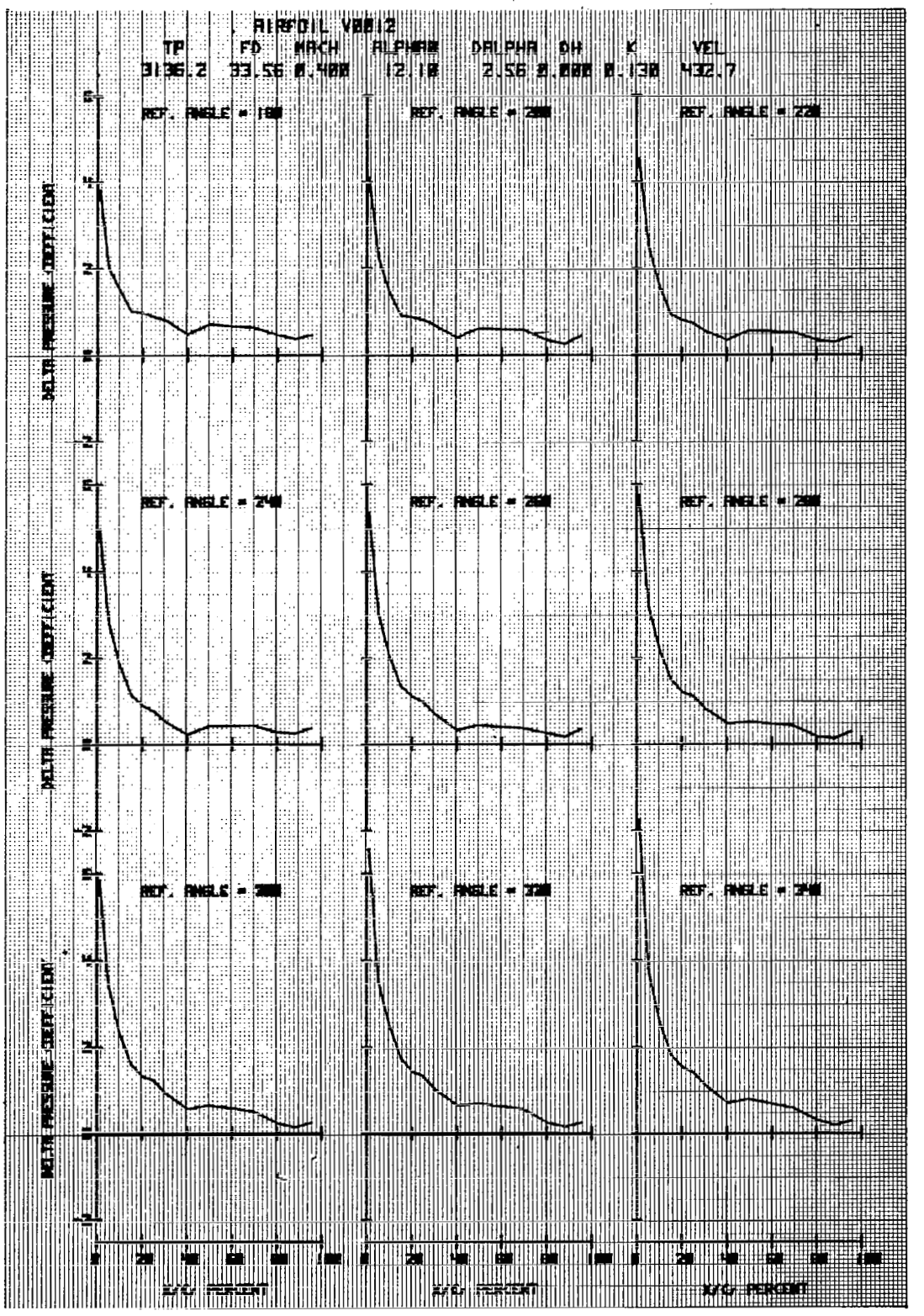

Figure 4le. Airfoil V0012 in Forced Pitch Oscillation

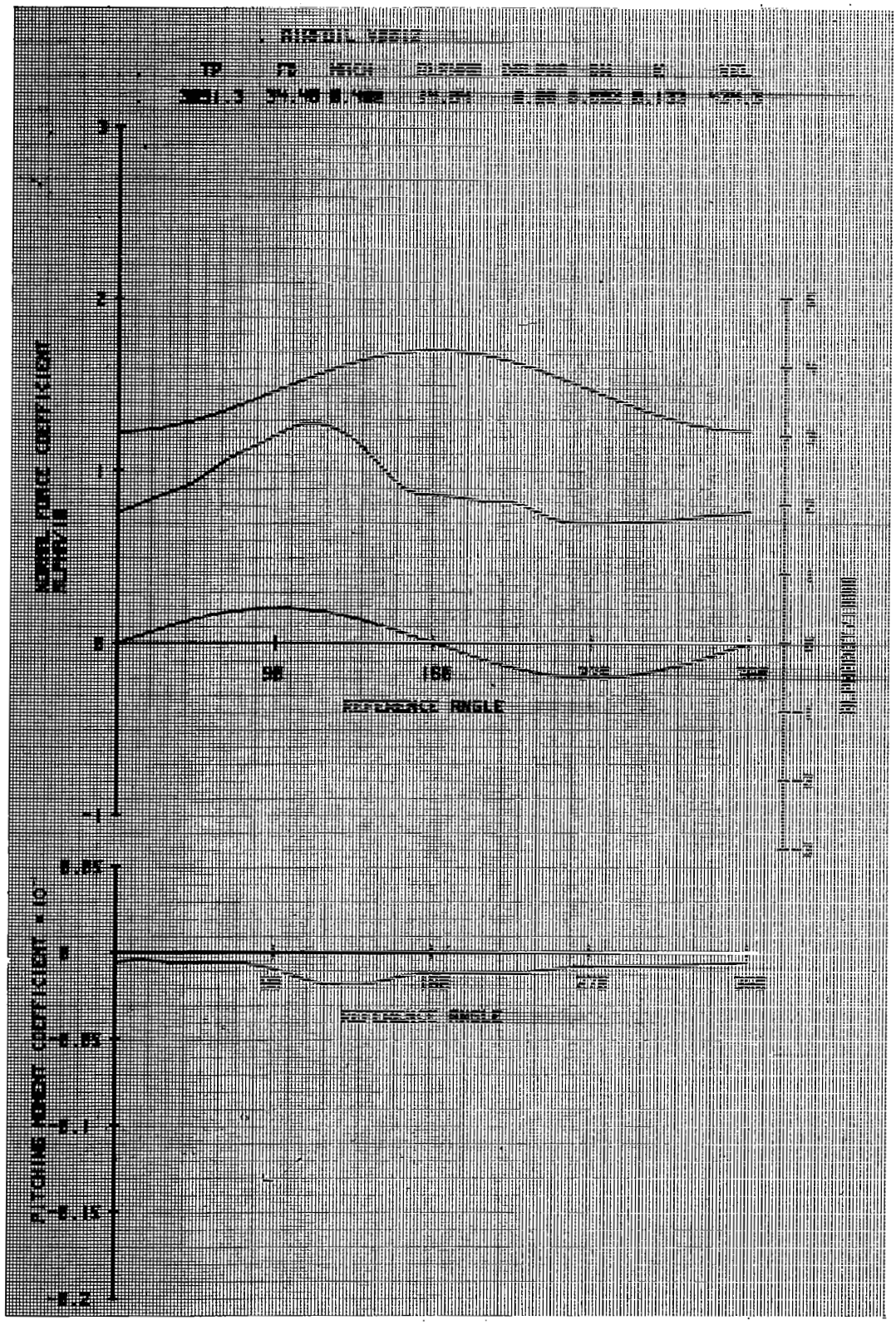

Figure 42a. Airfoil V0012 in Vertical Translation

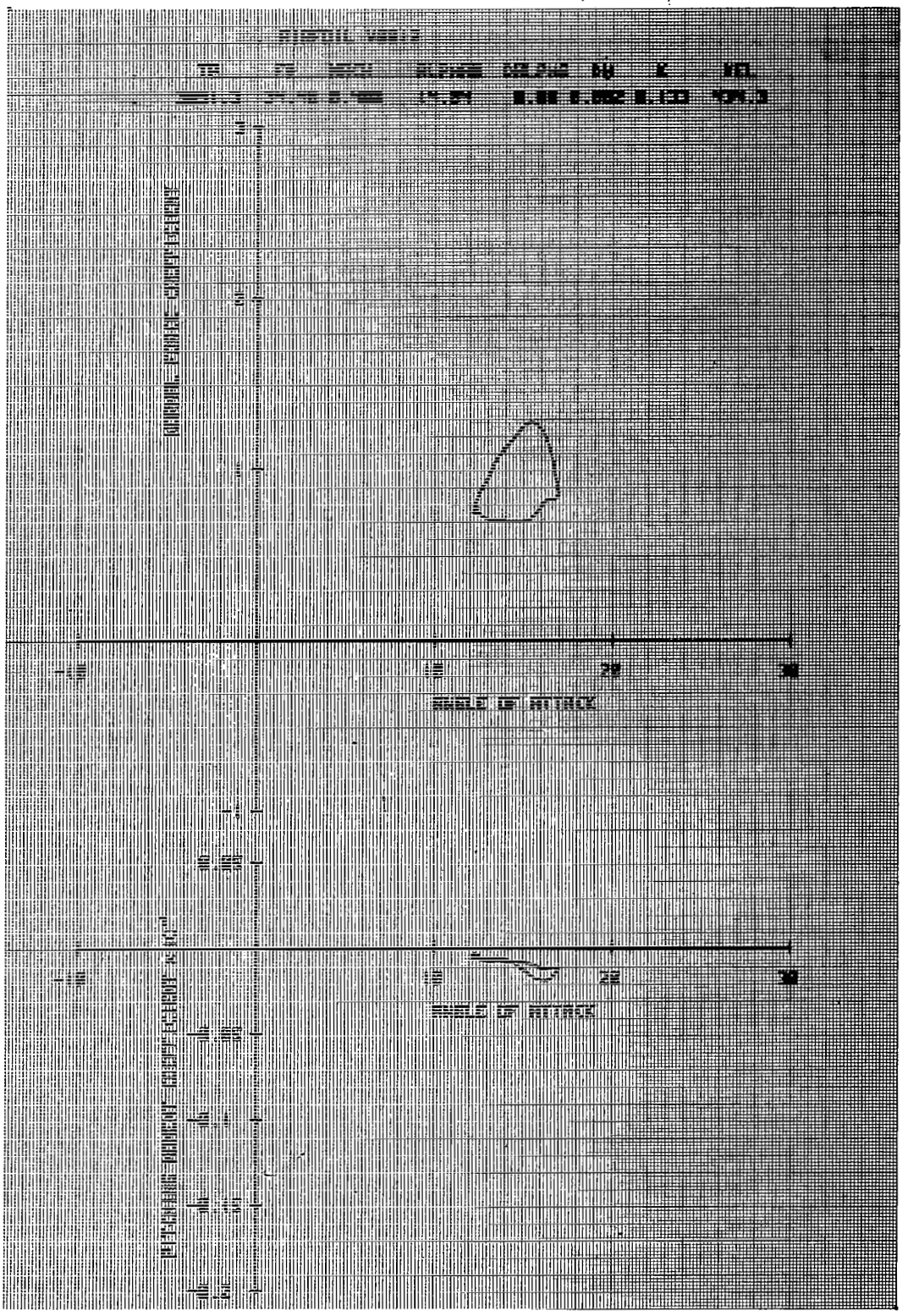

Figure 42b. Airfoil V0012 in Vertical Translation

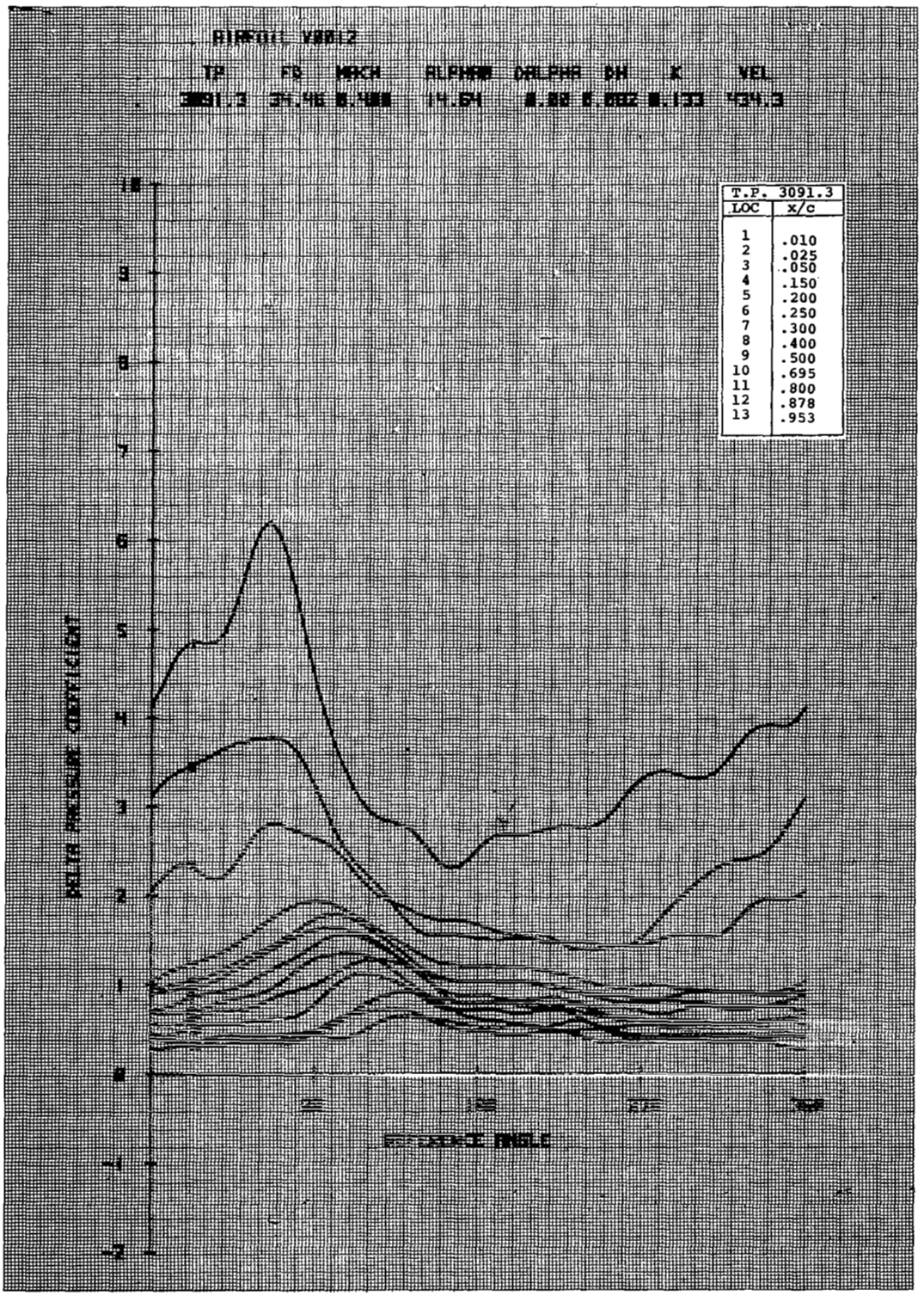

Figure 42c. Airfoil V0012 in Vertical Translation

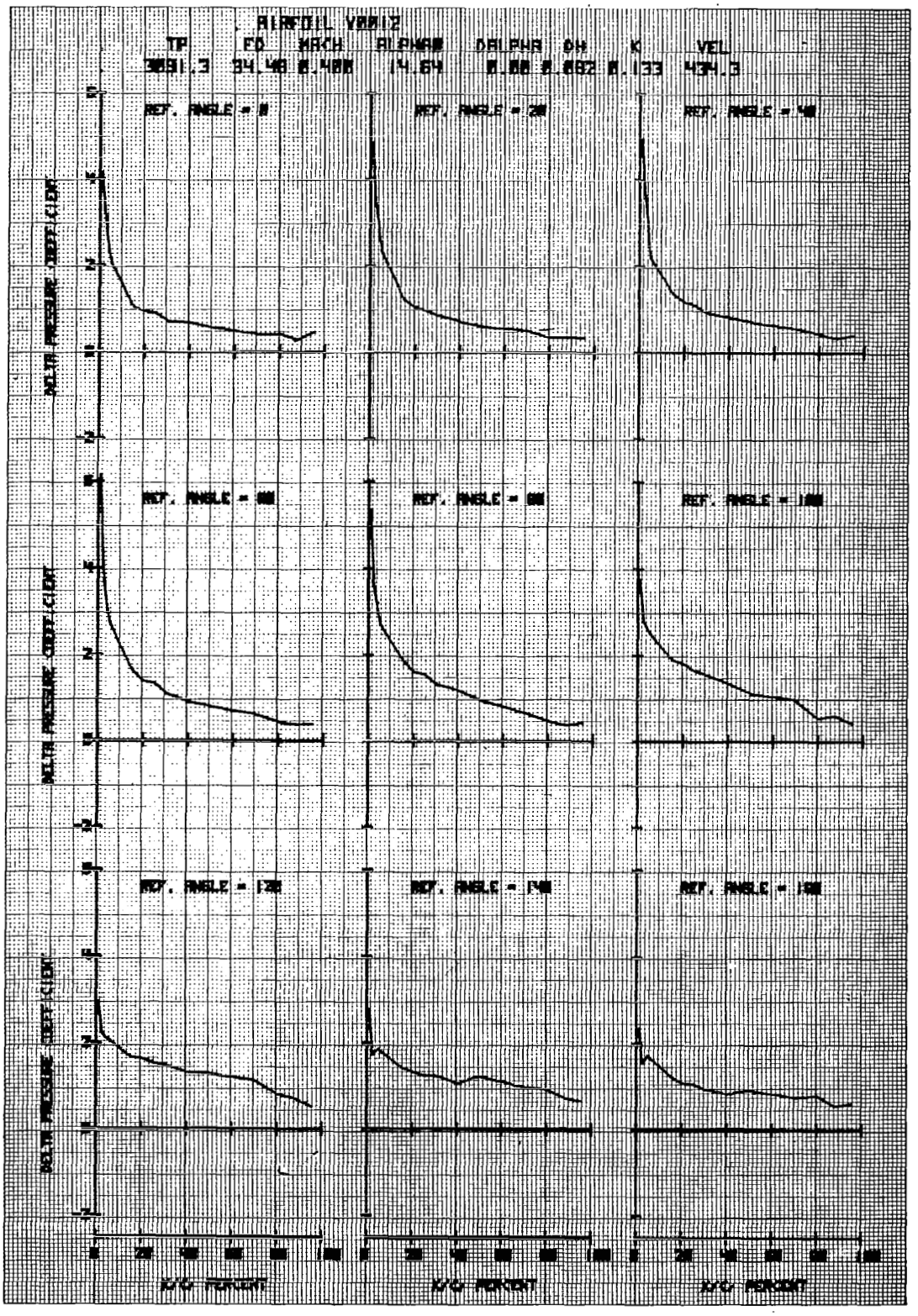

Figure 42d. Airfoil V0012 in Vertical Translation

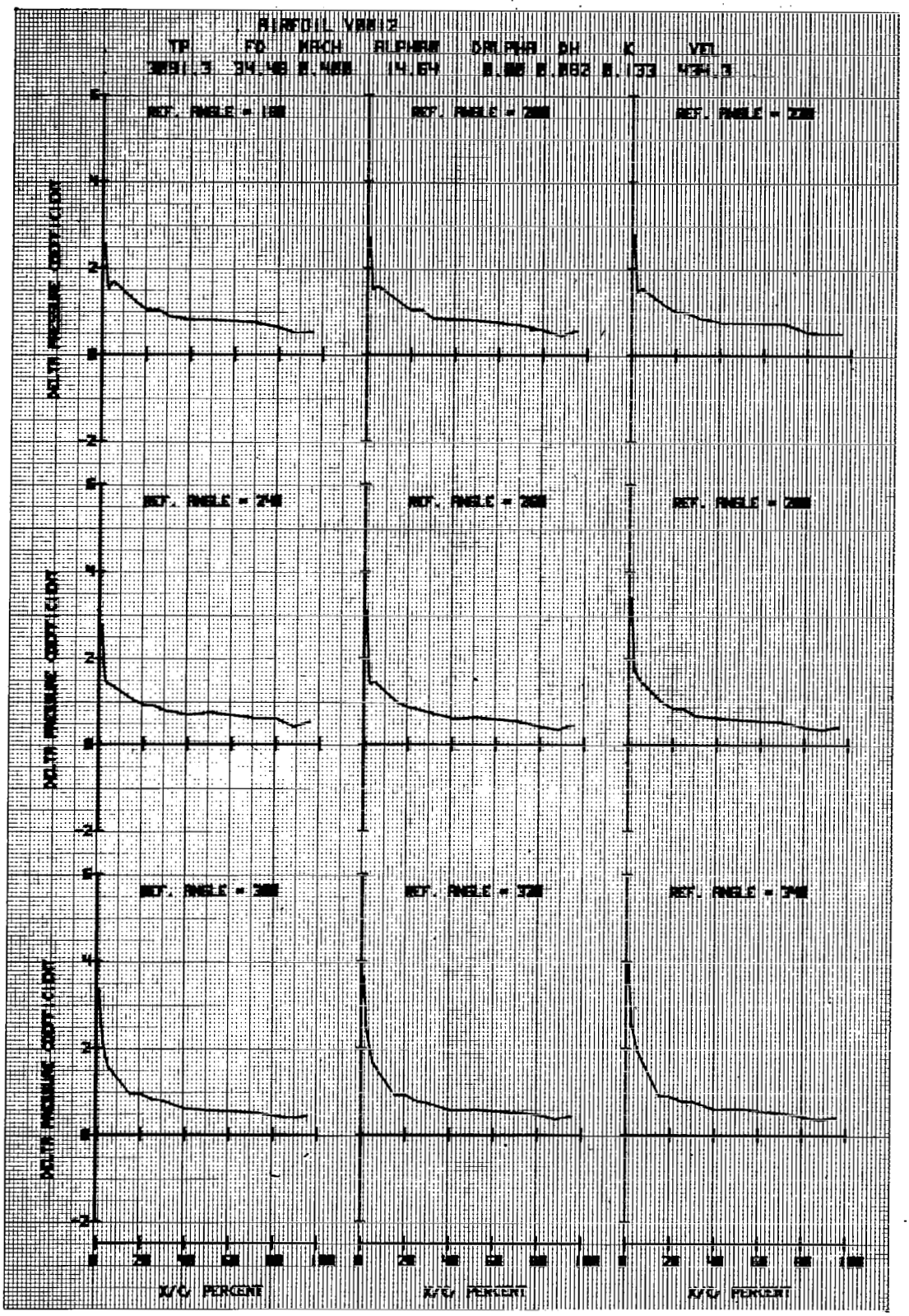

Figure 42e. Airfoil V0012 in Vertical Translation

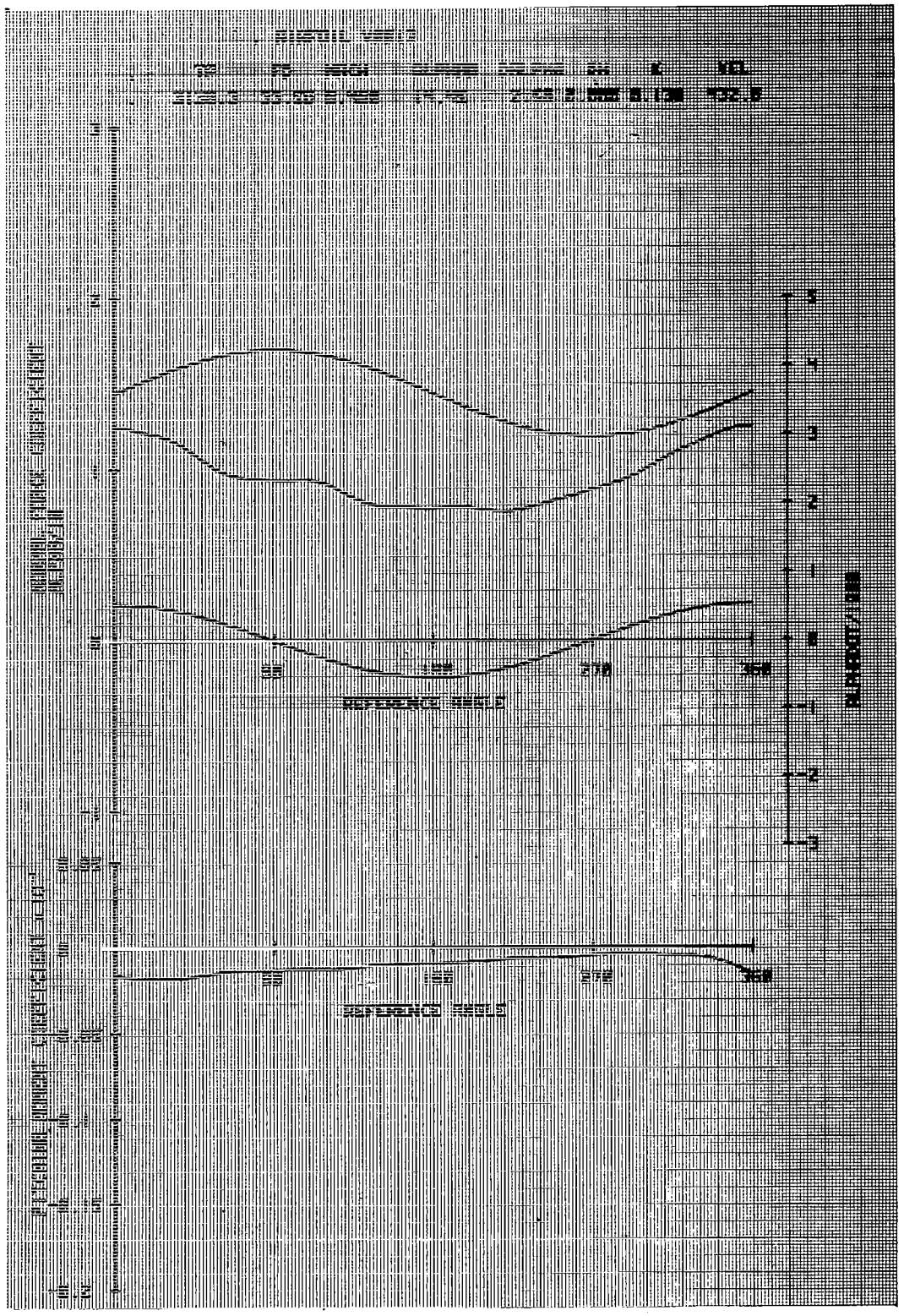

Figure 43a. Airfoil V0012 in Forced Pitch Oscillation

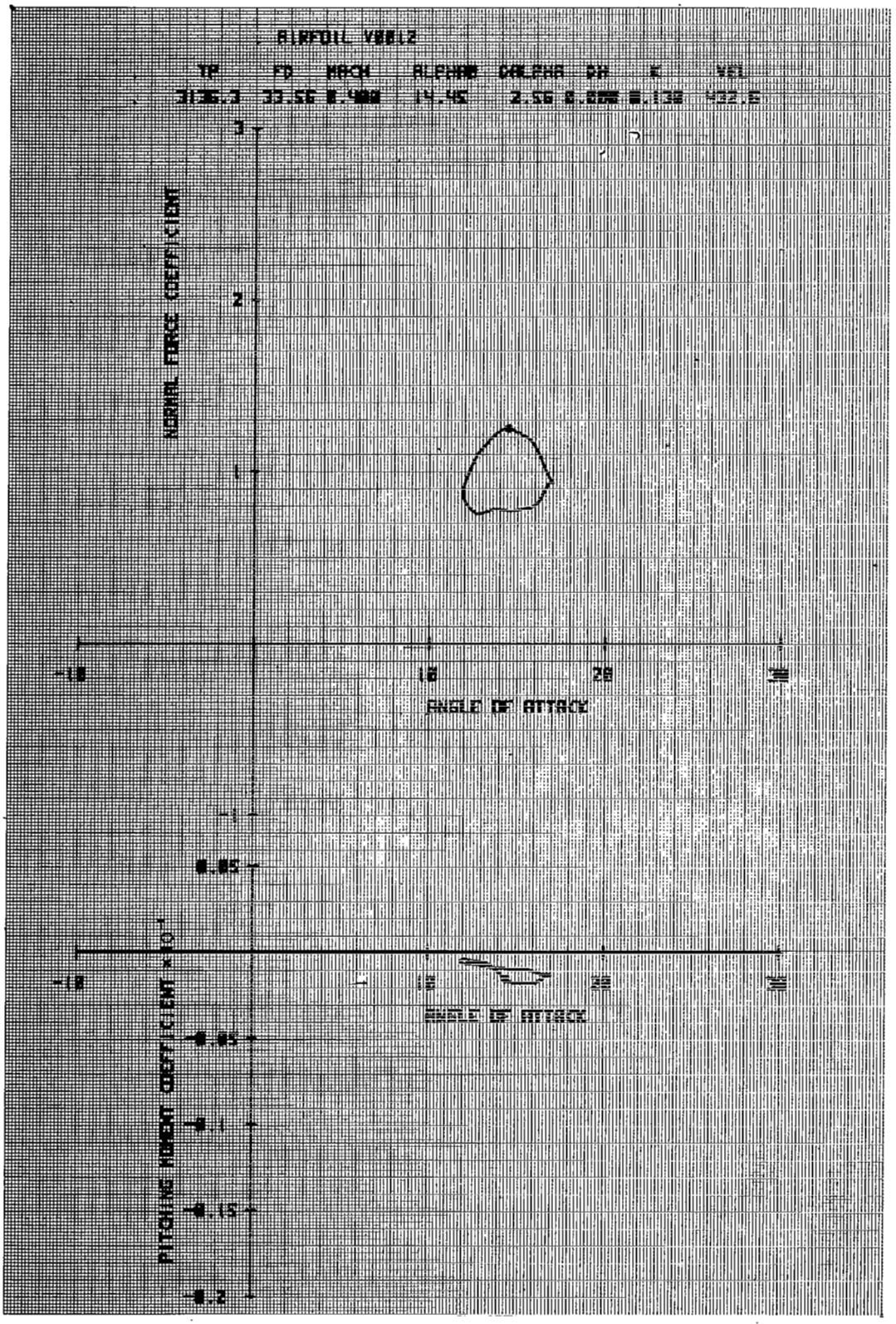

Figure 43b. Airfoil V0012 in Forced Pitch Oscillation

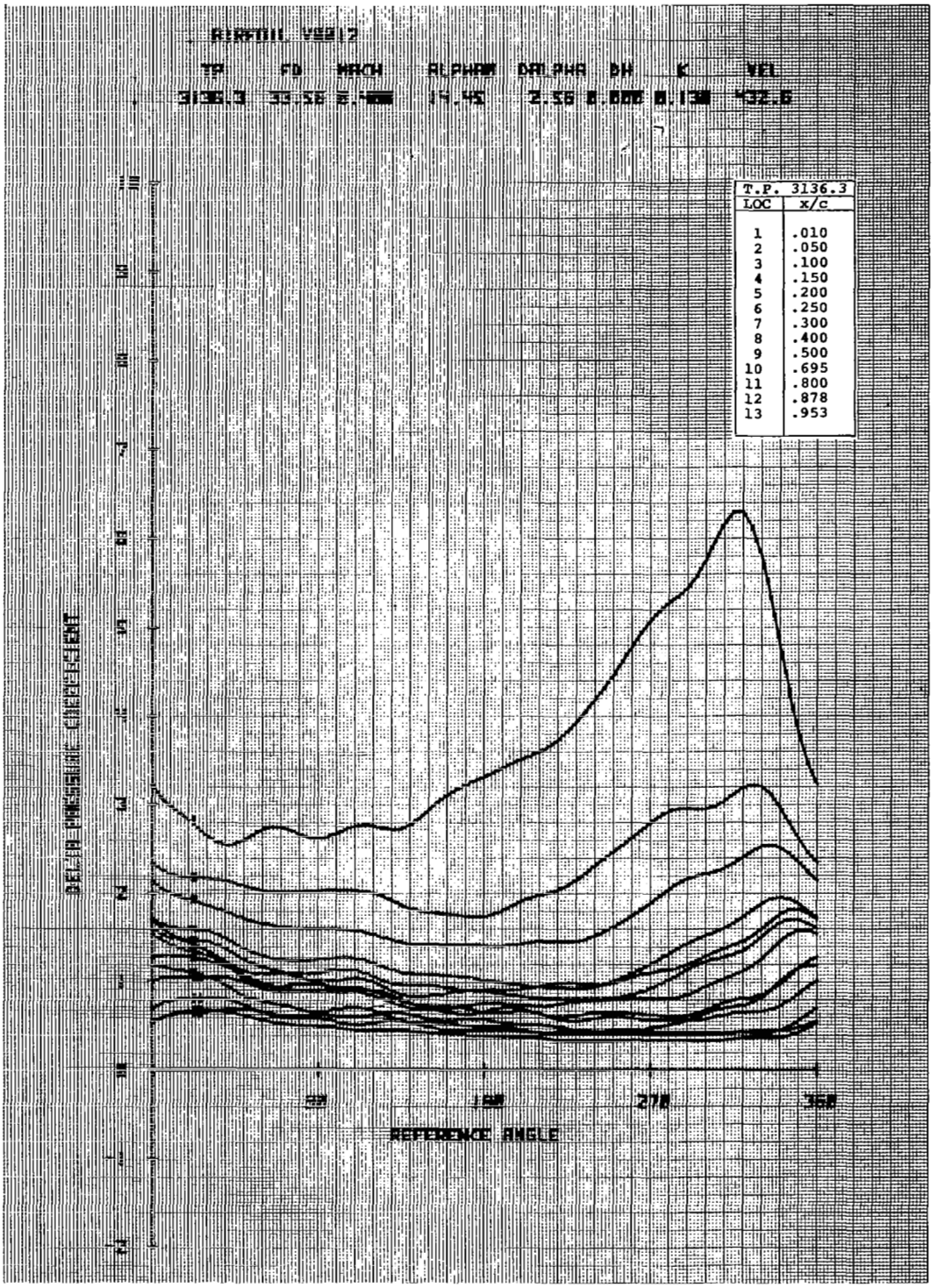

Figure 43c. Airfoil V0012 in Forced Pitch Oscillation

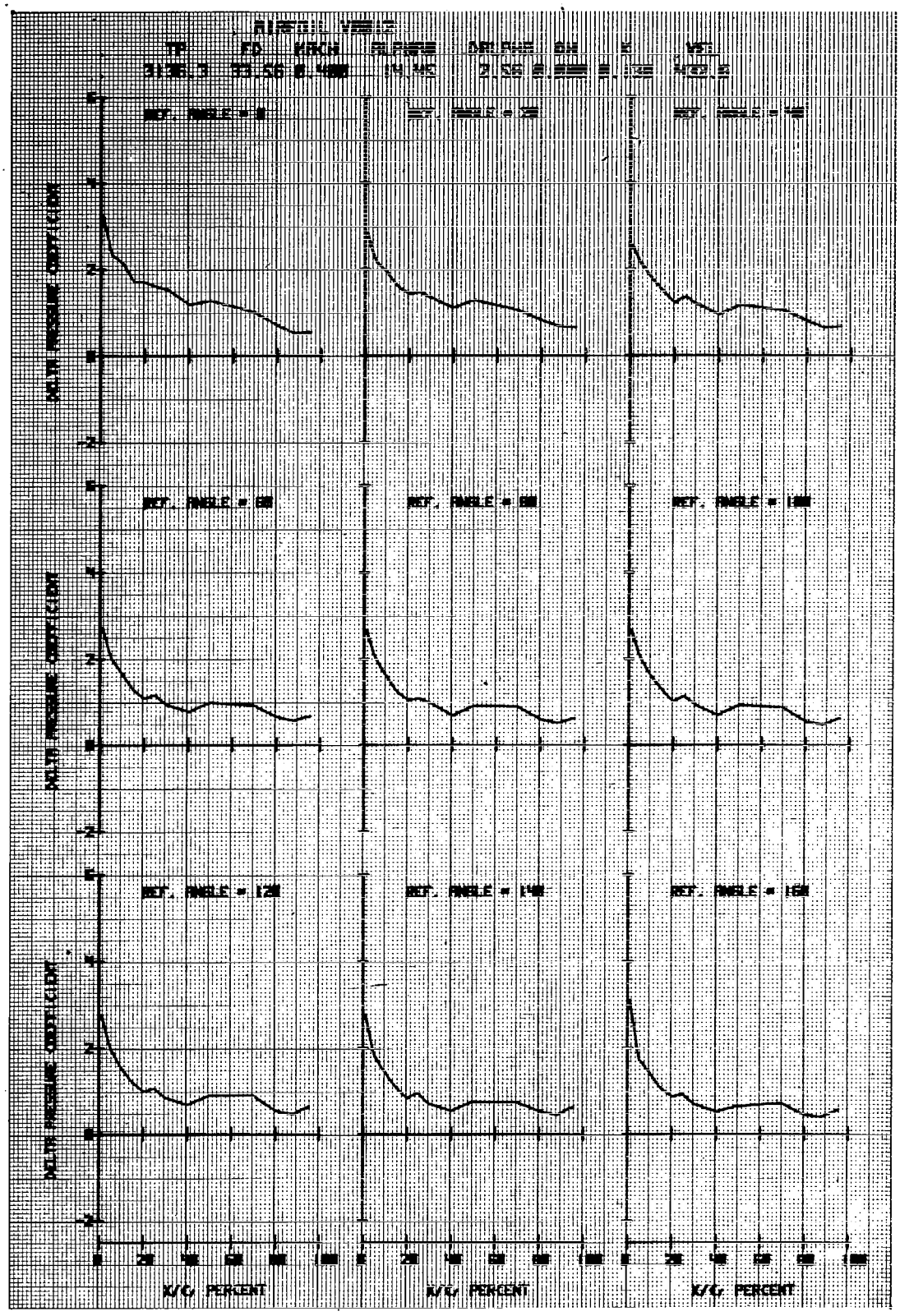

Figure 43d. Airfoil V0012 in Forced Pitch Oscillation

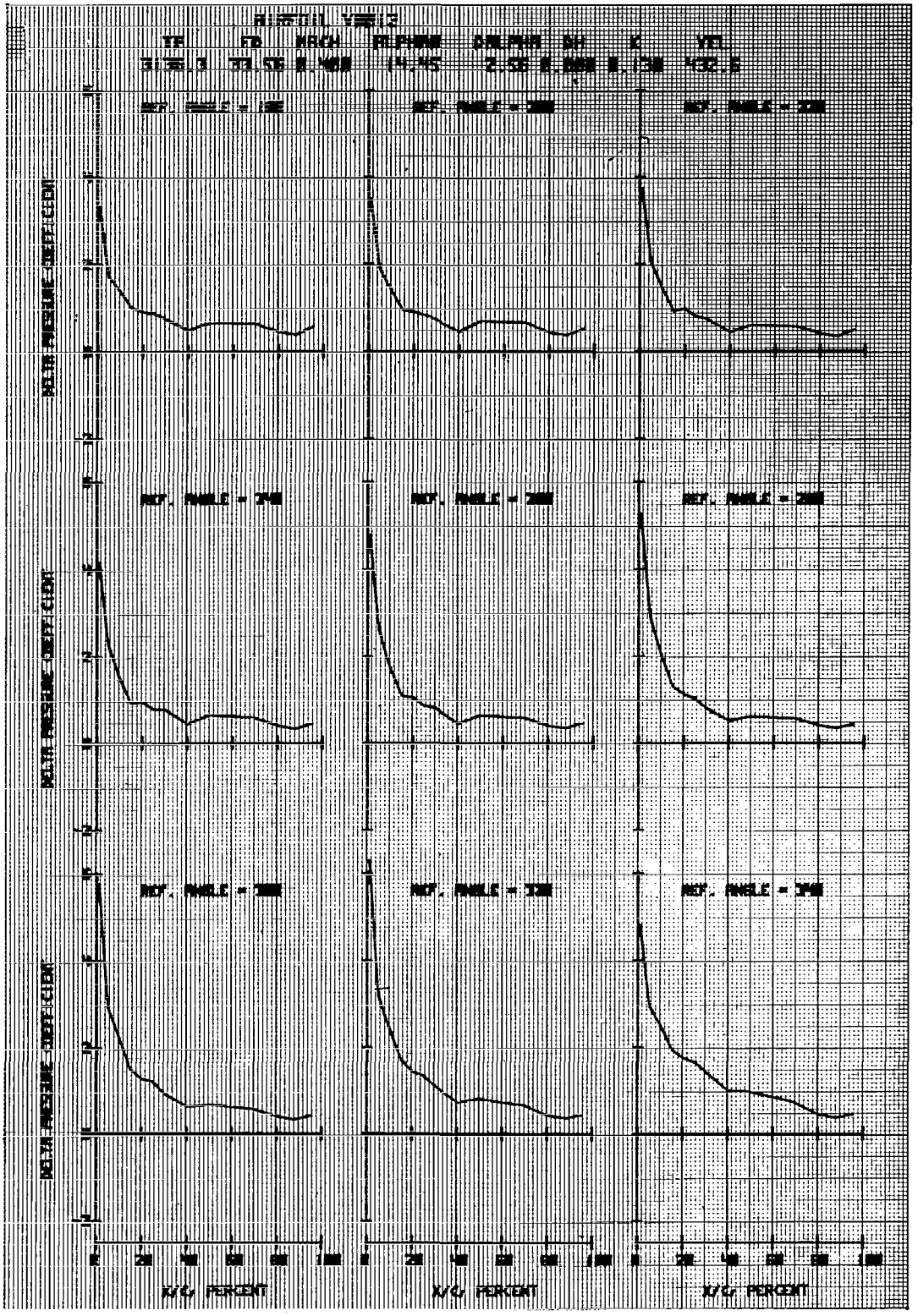

Figure 43e. Airfoil V0012 in Forced Pitch Oscillation

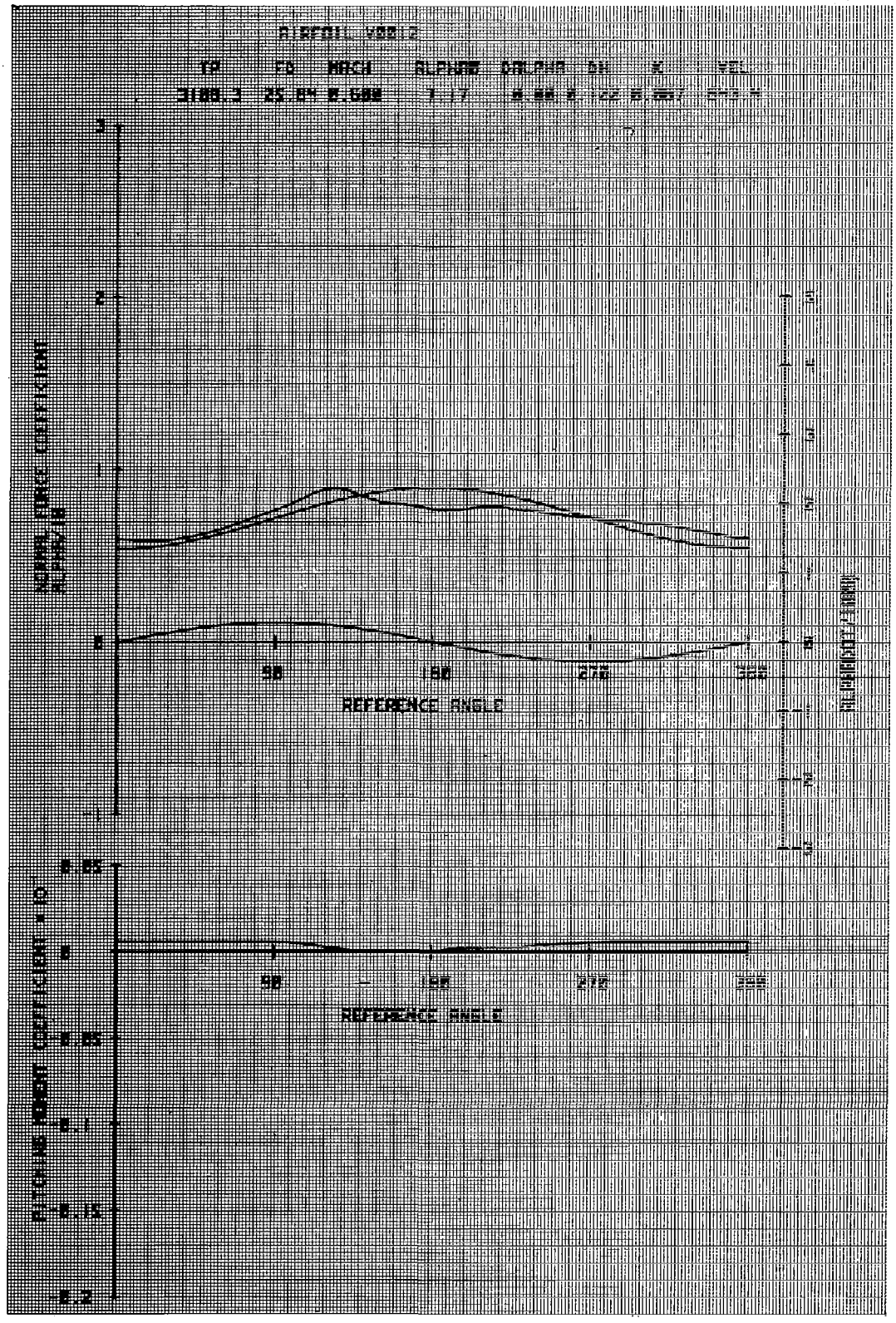

Figure 44a. Airfoil V0012 in Vertical Translation

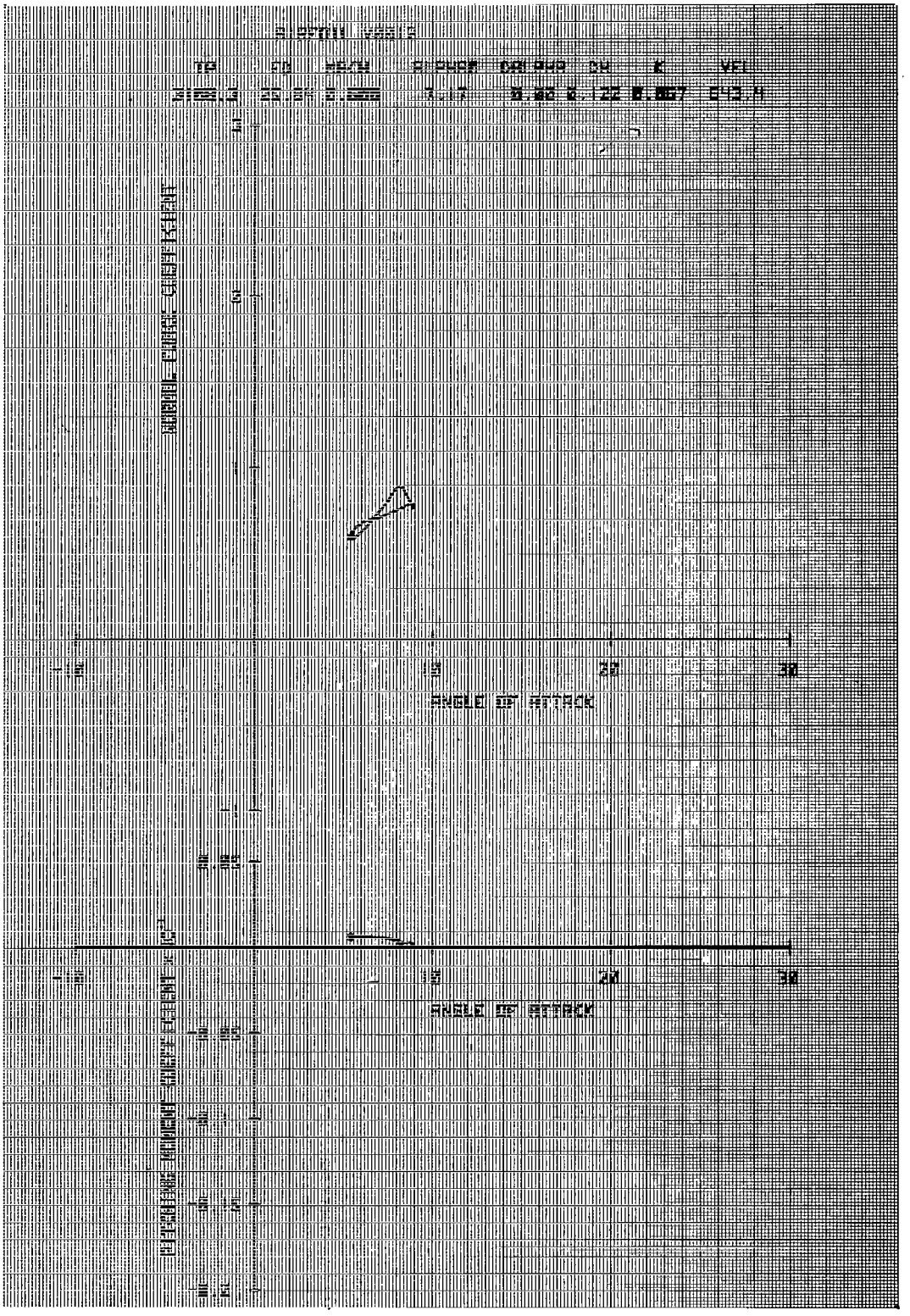

Figure 44b. Airfoil V0012 in Vertical Translation

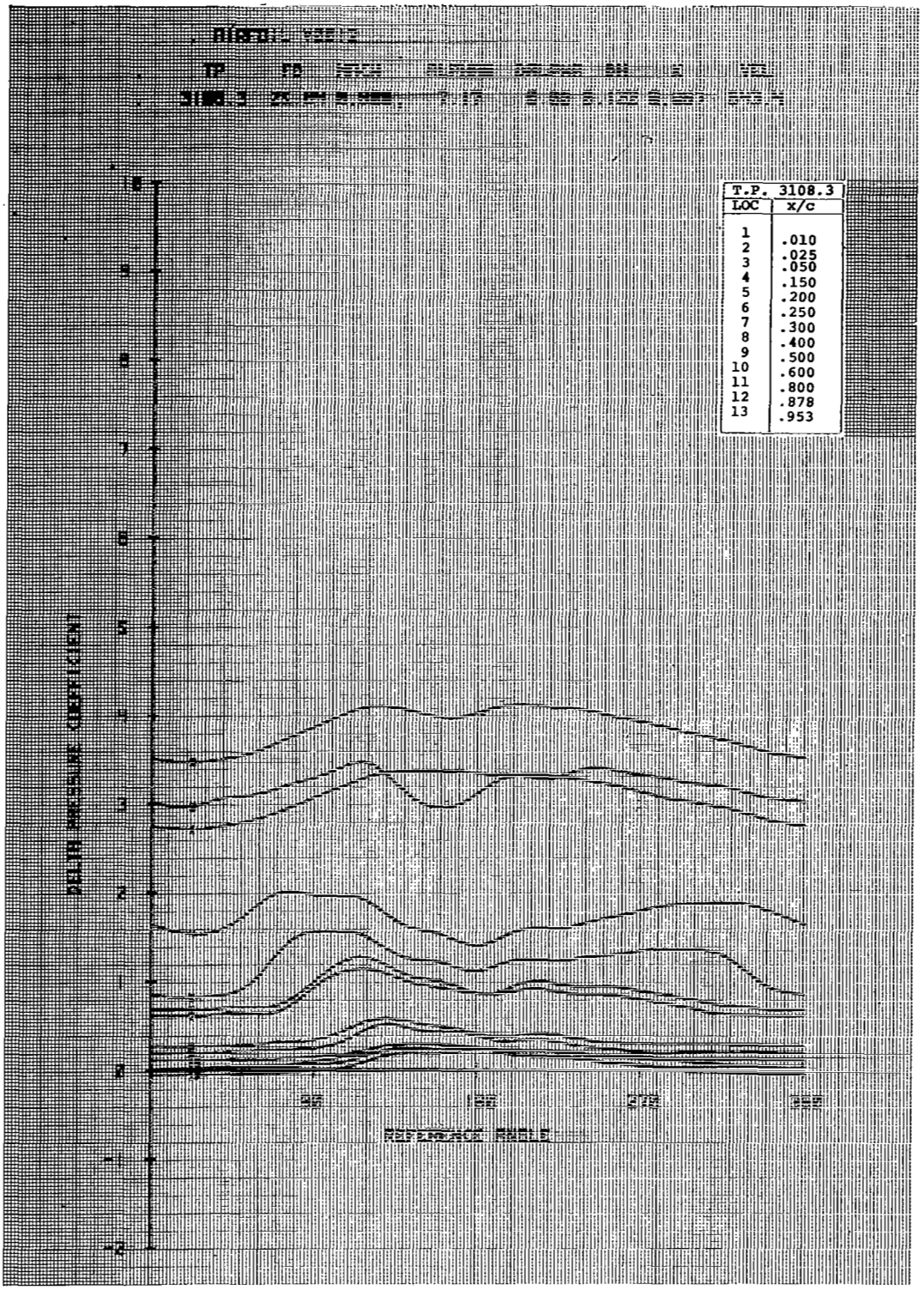

Figure 44c. Airfoil V0012 in Vertical Translation

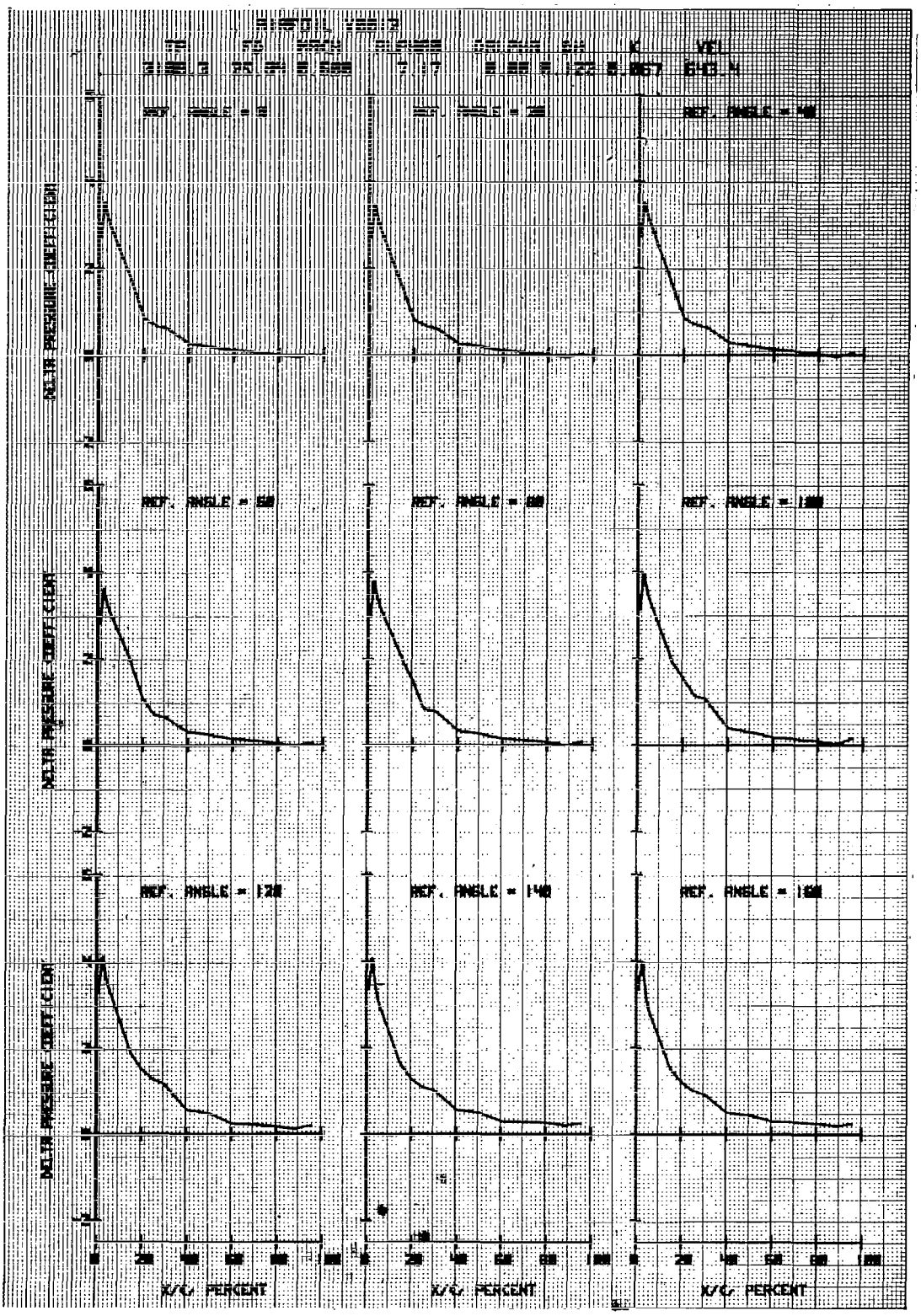

Figure 44d. Airfoil V0012 in Vertical Translation

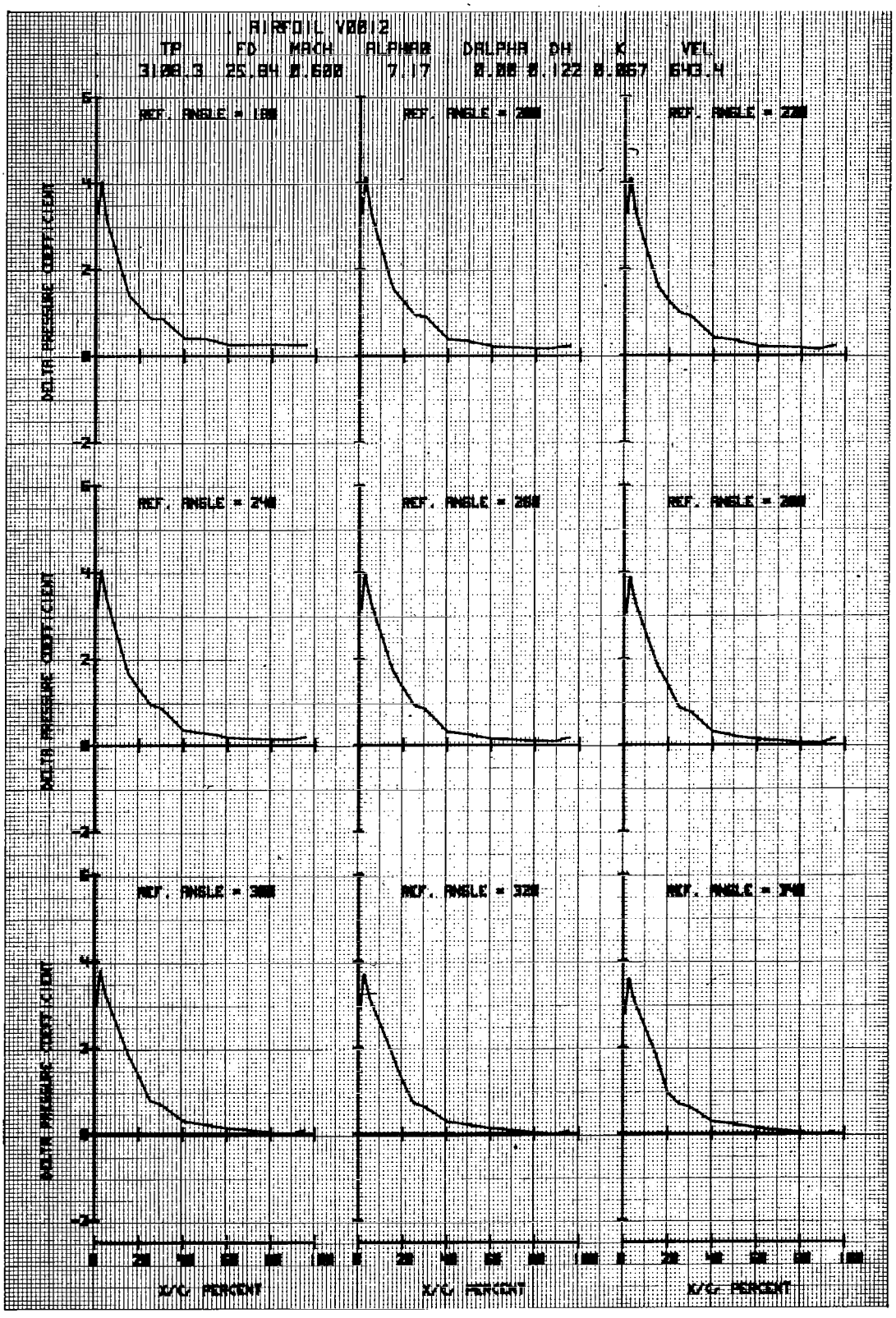

Figure 44e. Airfoil V0012 in Vertical Translation

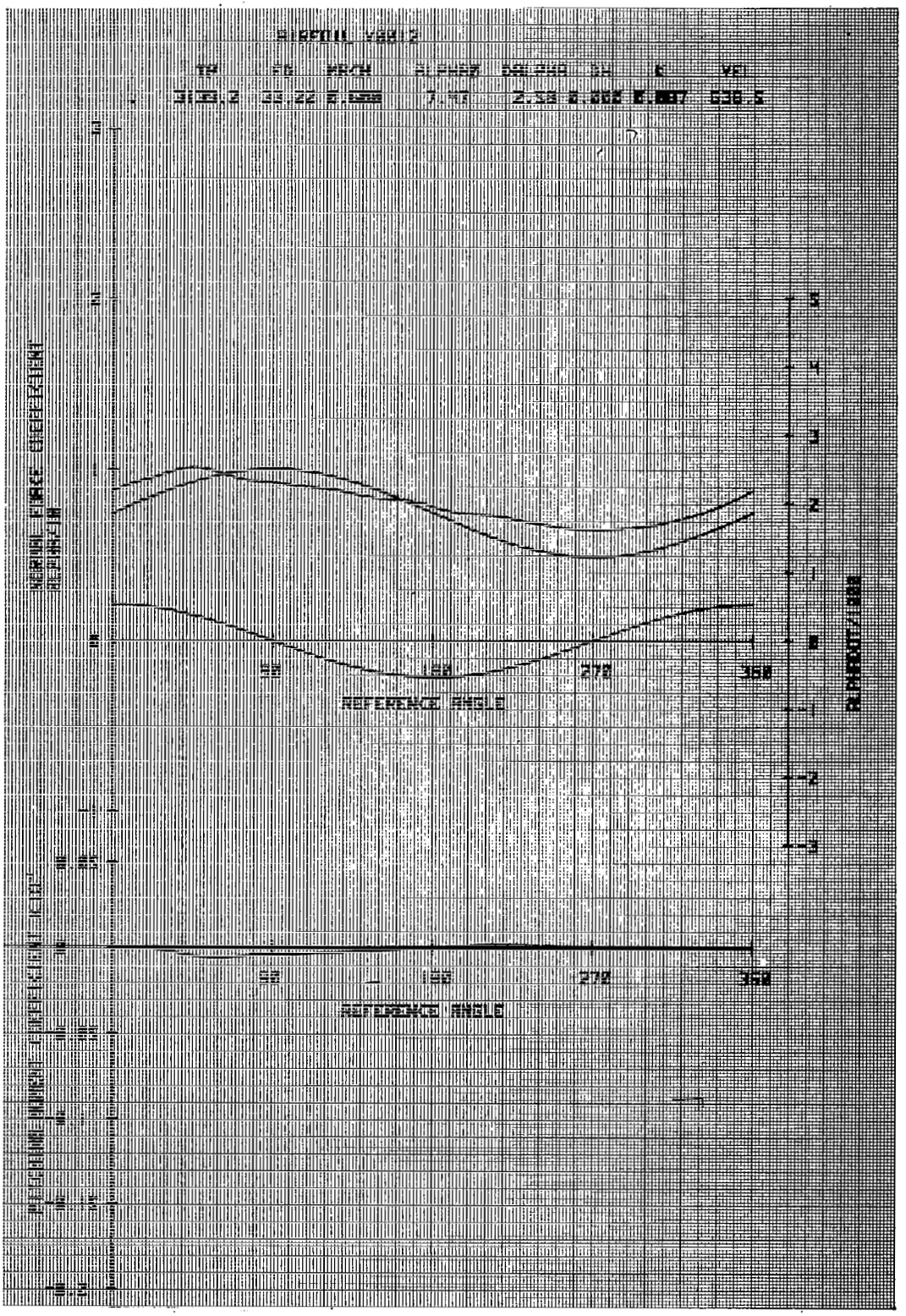

Figure 45a. Airfoil V0012 in Forced Pitch Oscillation

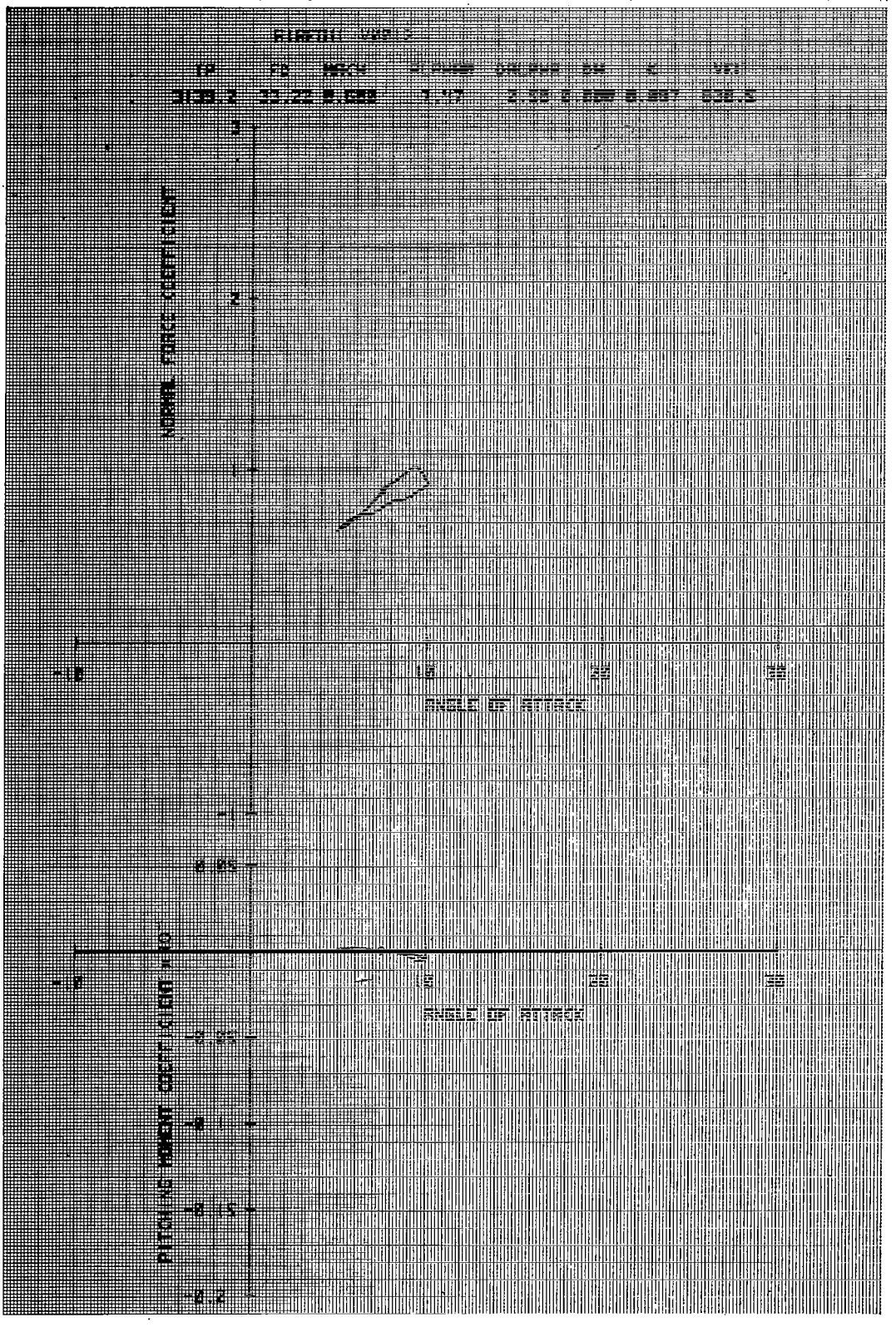

Figure 45b. Airfoil V0012 in Forced Pitch Oscillation

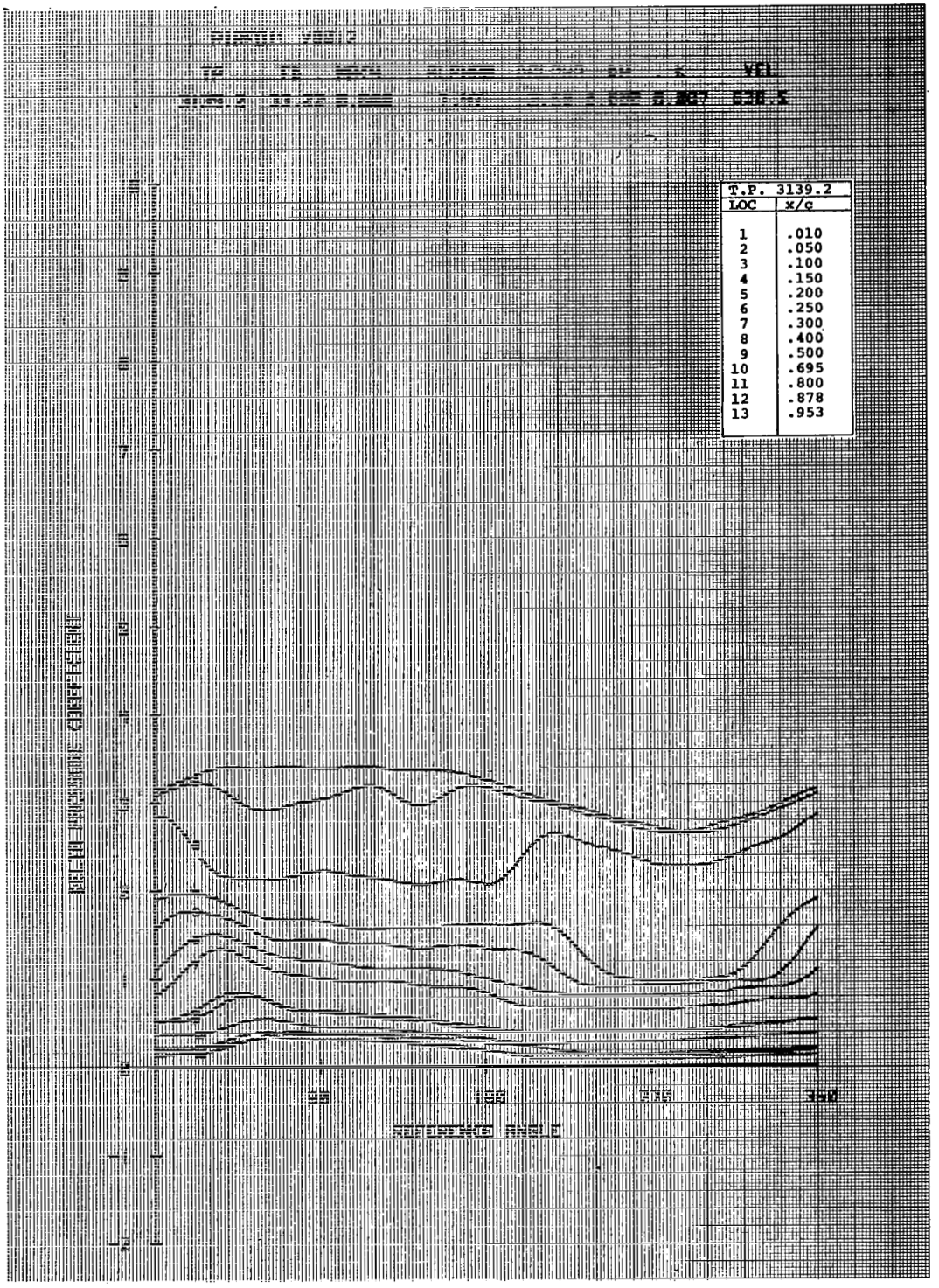

Figure 45c. Airfoil V0012 in Forced Pitch Oscillation

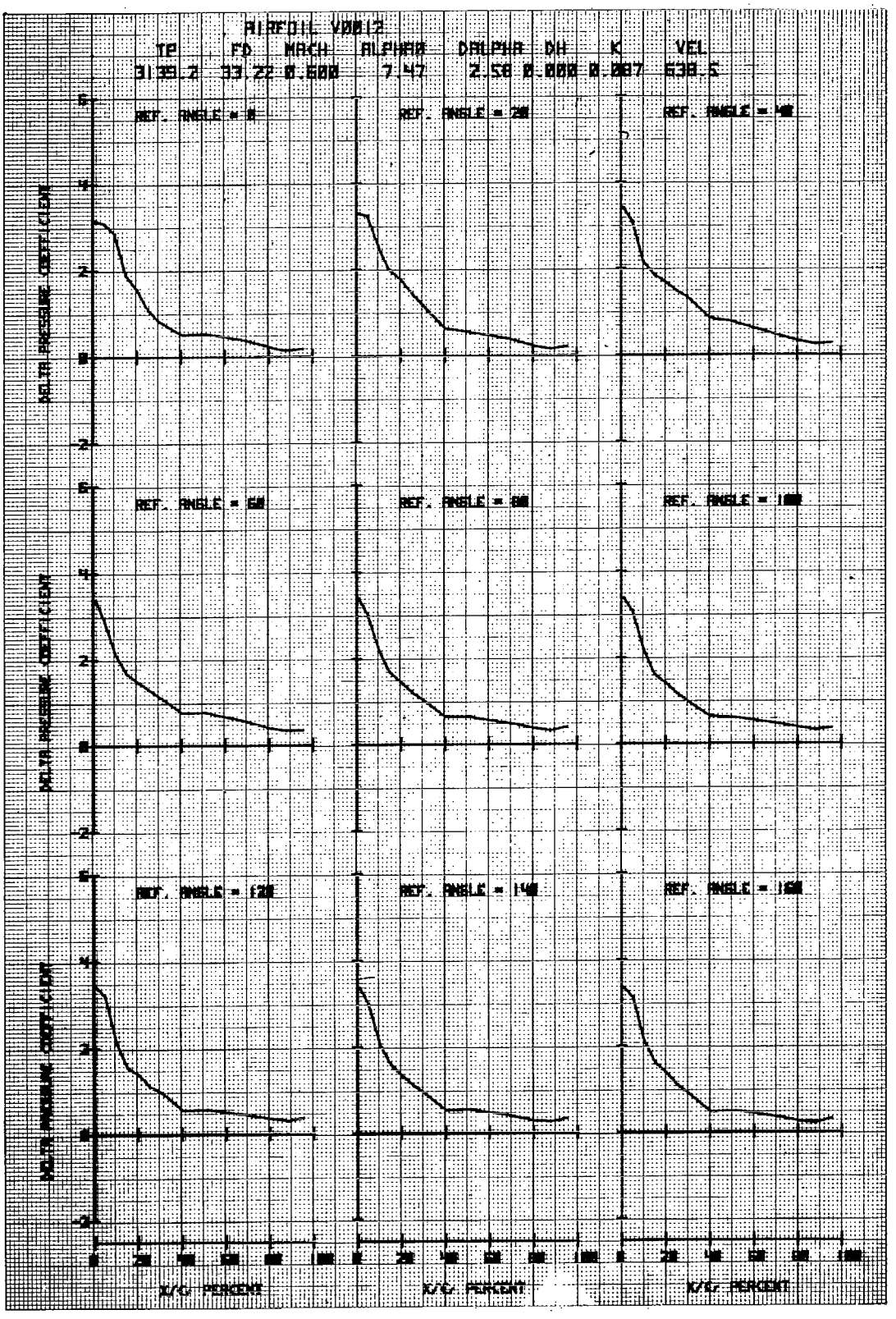

Figure 45d. Airfoil V0012 in Forced Pitch Oscillation

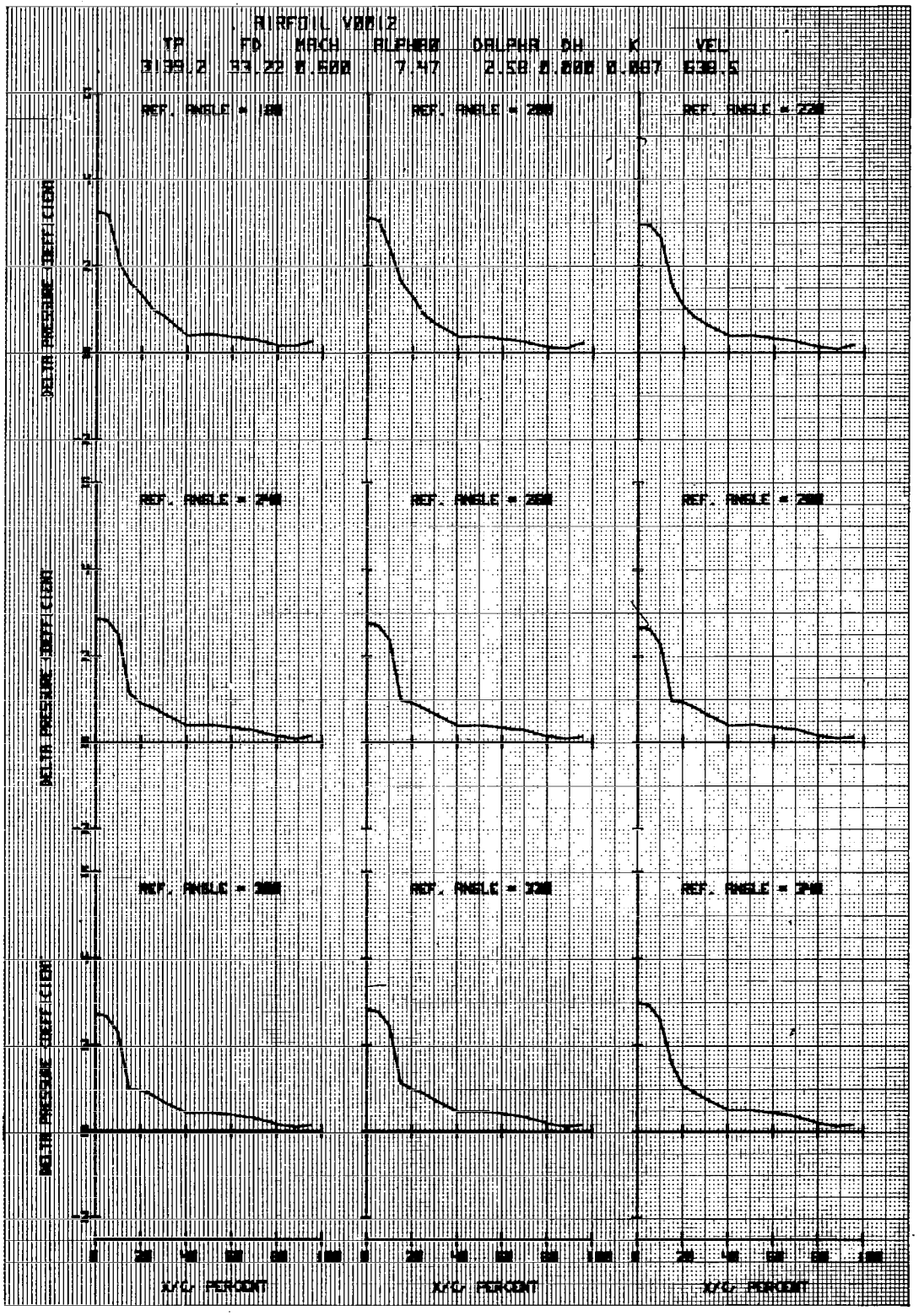

Figure 45e. Airfoil V0012 in Forced Pitch Oscillation